Fundamental investigation on inkjet printing of reactive nylon materials

Fundamental Investigation on Inkjet Printing of Reactive Nylon Materials

By

Saeed Fathi

BSc MSc

(Mechanical and Manufacturing Engineering)

Doctoral thesis submitted in partial fulfilment of the requirements of the award of Doctor of Philosophy of Loughborough University

January 2011

Abstract

Several additive manufacturing processes have been developed for plastic parts. However, there is an ongoing interest to increase the functionality of these parts which are mainly considered as prototypes due to the material and process limitations. This research investigated a novel additive approach for producing a functional engineering plastic, nylon 6. The idea was to combine inkjet printing technology and anionic polymerisation of caprolactam by depositing mixtures of caprolactam with activator and catalyst on top of each other under the appropriate conditions.

Some of the main material processing aspects were explored to provide a fundamental understanding of the parameters involved in the process development. Several mixtures of activator and catalyst were characterised in addition to caprolactam to investigate their jetting possibility. An experimental setup was integrated based on two identical jetting assemblies with pneumatic and thermal control, synchronised with a deposition system for the reaction of the mixtures upon radiation heating. Different offline material characterisation and inline process monitoring methods were employed to obtain an understanding of the material behaviour at each stage of the research. These included the use of high speed imaging, fluorescent microscopy, particle tracking and image analysis tools.

The physical properties of the molten materials important for jetting were investigated in addition to the melt supply behaviour in the system to choose the appropriate mixtures compositions and melt supply conditions for the jetting trials. It

was found that the surface tension and viscosity of all materials were within the range suitable for inkjet technology. However, with the catalyst mixtures, microcrystals of undissolved salt of the catalyst complex were found which had a high tendency to agglomerate. This influenced the melt supply behaviour by blocking the filtration unit. Using alternative catalyst mixtures, similar effect was observed; however, with a commercial sodium caprolactamate-based catalyst mixture at 20% concentration, there was a melt supply of over 6 ml before complete filter blocking and also enough concentration of the microcrystals beyond the jetting system to undertake the jetting trials.

The stability of jet(s) was monitored and the suitable ranges of jetting parameters were found. The mixtures had a narrower range of stability compared with caprolactam. The mechanisms behind jet instabilities, most commonly in form of developing jet trajectory errors, were investigated. This however could occasionally result in failure of the jet(s) and as a consequence, failure of the jets array in a behaviour similar to falling dominos. Within suitable range, higher level of instability was observed with the catalyst mixture which was assumed to be due to the microcrystals. This initiated an investigation of the interactions between the melt and the nozzle plate during a jetting period. A complex flow field was visualised on the nozzle plate using particle tracking velocimetry which showed the instability could be due to attraction of the particles within the melt towards the oscillating meniscus.

The research of droplet characteristics studied the shape and kinetics of droplets in addition to the nozzle wetting behaviour and droplet formation instabilities for the recommended range of jetting parameters. The result was to choose the optimum jetting conditions for deposition. With all droplets, a tail was formed which disintegrated into satellite droplets when using a high voltage. An additional 5 V was

required with the mixtures to obtain similar droplet shape and kinetics to caprolactam due to the mixtures having a 50% higher viscosity. Droplet formation characteristics were found unaffected by the jetting frequency. However, it affected nozzle wetting behaviour. The wetting was also found to be a source of jet instability when developed around the nozzle asymmetrically due to presence of contamination.

Droplet/surface interactions and mixing of droplets were of the aspects investigated in the deposition stage. It was found that with the chosen jetting parameters from the previous stages, there was spreading upon droplet impact onto dry surface and also onto previously spread droplets. A consistent content and dispersion of the microcrystals was also seen within the individual droplets deposited at different catalyst melt supply levels. By moving substrate, a stable bead was obtained with a cold surface whereas formation of bulges was observed with the heated surface. From this research stage, an accumulative drop-on-drop deposition into a DSC pan was chosen for the research of reaction. Therefore, dye tracing was used to observe the mixing outcome for the chosen approach. The consecutive impingement and also surface tension resulted in good mixing of the two mixtures inside the pan.

The research into reaction investigated formation of nylon upon using different radiation heating conditions. Samples were monitored before and after the drop-on-drop deposition and radiation heating, and then assessed by thermal analysis to find the appropriate conditions for the reaction. It was found that although some monomer conversion was achieved, the rates were much less than with the bulk polymerisation approach. Jetting of thousands of tiny droplets in air could have resulted in a very high monomer deactivation. This highlighted the importance of the environment as a more significant parameter for jetting of nylon 6 compared with the conventional method.

Acknowledgement

I praise God, the merciful and the passionate, for providing me the opportunity to step into the world of science and engineering, and granting me the capability to proceed successfully.

My sincere gratitude to my supervisor, *Prof. Phill Dickens*, for his support and contributions throughout the course of my PhD. It has been such an honour to research under his supervision and to receive his precise and valuable comments on my thesis. Special thanks to *Prof. Marianne Gilbert* and also *Prof. Richard Hague* for their support on my research work.

Thanks to Innovative Manufacturing and Construction Research Centre (IMCRC) of Loughborough University for covering all of my university tuition fees and living expenses and also granting financial support in attending several international conferences. I acknowledge Xaar plc (UK and Sweden) and Brüggemann Chemical GmbH (Germany) for kindly providing a number of equipments and materials.

This research was undertaken at the Additive Manufacturing Research Group (AMRG) of the Wolfson School of Mechanical and Manufacturing Engineering, and I am thankful for the support of members of the research group and also the technicians and staffs of the department.

I would like to express my deepest appreciation to my beloved wife, *Soudabeh*, for being such a powerful source of encouragement to me. I am very thankful to my parents for their never-ending support.

Saeed Fathi

January 2011

Table of Contents

List of Figures

List of Tables

Chapter 1. Introduction

1.1 Area of Research

This research investigated a new way of manufacturing plastic parts in nylon 6, which is one of the main engineering plastics in use today. The research involved inkjet technology and anionic polymerisation of caprolactam to give a new additive manufacturing process which could replace the conventional cast and injection moulding of nylon 6, remove the high cost of associated tooling and enable more design freedom in the manufactured parts. The main techniques currently used for layer manufacturing of end use plastic parts are described in Chapter 2.

Since the introduction of inkjet printers in the 1970s, inkjet technology has seen huge progress thanks to its commercial potential in the graphics industry. Many companies have made large investments in research to develop their inkjet technology for a faster and cheaper printer. This resulted in printheads capable of depositing materials which have been employed recently for many non-graphic applications such as printed electronics. The progress has reduced the droplet size and increased the deposition resolution, throughput and operating temperature where a wider range of functional materials could be deposited onto various surfaces. These have made the technology capable as a manufacturing tool for many applications.

Anionic polymerisation of caprolactam is a technique which synthesises nylon 6 with good mechanical properties to satisfy many engineering applications. The technique

requires mixing caprolactam, an activator and a catalyst at elevated temperatures to convert caprolactam into nylon. There are a number of forming processes that employ anionic polymerisation to produce nylon 6 parts including cast nylon process. In this process, the precursors of the anionic polymerisation are kept as two reactive parts and are premixed before injection into a heated mould at around 150℃. This results in manufacturing nylon parts.

1.2 Research Motivation

With the existing additive manufacturing processes for plastic parts, there are still a number of limitations as they were originally conceived as methods to make prototypes. The plastics involved in existing additive manufacturing processes are generally limited to photosensitive polymers or powdered nylons. High resolution could be achieved via printing of low viscosity photosensitive polymers, however, as they are usually based on epoxy, they tend to be brittle and suffer from absorption of moisture. Higher viscosity photopolymers used in Stereolithography also have limited mechanical properties. With lower resolution processes such as laser sintering, the porosity of sintered nylon parts also reduces mechanical properties. Although inkjet-based processes may have low throughput compared with the other techniques, they have the potential to be much faster as many thousands of jets could be used via multiple printheads.

1.3 Research Concept

There is a need for an additive technique to produce parts from a functional polymer with high resolution and good surface finish. Inkjet technology could fill this gap with nylon 6, however, nylon 6 in the melt state has such a high viscosity that it cannot be

jetted. As it can be polymerised from mixtures of low viscosity caprolactam at elevated temperatures, the idea of “Jetting of Nylon” could be a possibility.

The polymerisation concept would be similar as in the cast nylon process but instead of premixing of the two reactive compounds consisting of caprolactam and activator as *A* and catalyst as *B*, they could be deposited via inkjet printing. By depositing a layer of the two reactive mixtures on top of each other onto a substrate, the two mixtures were expected to mix and start the reaction under appropriate conditions. This could produce nylon 6 as a solid layer before fabricating the next layer in an additive approach. Then, it would be possible to produce solid nylon parts with fine resolution and with acceptable build speed.

1.4 Structure of the Thesis

Chapter 2 reviews the literature on additive manufacturing, inkjet technology and anionic polymerisation for nylon 6. This will be followed by introducing the features, challenges and objectives of this research. The methodology is detailed in *Chapter 3* which mainly describes the design and development of the experimental setup.

Chapters 4 to 8 present the results and discussions of this research. Characterisation of the materials for jetting is discussed in *Chapter 4* which includes the physical properties of the materials and their melt supply behaviour in the jetting system. In *Chapter 5*, the results of jetting trials for caprolactam and reactive mixtures are presented. Instabilities during jetting are discussed to propose conditions for jet stability. *Chapter 6* reports on the characteristics of individual droplets upon formation and their interactions with the nozzle. Meniscus oscillation, droplet shape evolution and kinetics of droplets and jet instabilities due to nozzle

wetting are assessed to conclude the optimum jetting conditions for deposition of materials.

Chapter 7 reports on the deposition aspects including droplet/surface interactions and drop-on-drop mixing. The outcome was to limit the number of deposition process parameters to proceed to the drop-on-drop reaction stage presented in *Chapter 8*. This chapter discussed first the heating approach for reaction followed by analysis of samples produced by drop-on-drop reaction at different heating conditions. *Chapter 9* concludes the research outcomes and proposes the future work.

Chapter 2. Background and Literature Review

2.1 Additive Manufacturing

This section introduces additive manufacturing briefly and more details of the technology, applications and trends can be found (Gebhardt 2003, Hopkinson *et al.* 2006, Wohler 2007, and Gibson *et al.* 2009).

2.1.1 Rapid Prototyping to Additive Manufacturing

The technology was introduced as Rapid Prototyping (RP) and has been in use to date for design prototypes. Although the first commercial process was introduced in the late 1980s, the concept can be traced back to the 1890s when manually added wax patterned layers were used to make topographical relief maps. A detailed history of RP including the relevant patents was reported by Beaman (1997).

Progress in the additive layer techniques and the consequent increase in the functionality of parts resulted in the concept of Rapid Manufacturing (RM) (Hopkinson *et al.* 2006). Other terminologies have also been in use since the introduction of RP such as Solid Freeform Fabrication (SFF) and Digital Direct Manufacturing (DDM). However, most recently, the term “additive manufacturing” was recognised by American Society for Testing and Materials (ASTM) to standardise terminologies commonly used for different varieties of additive approaches (ASTM 2009).

2.1.2 Basic Concepts

There are several techniques applied in additive manufacturing, however, the main concepts are almost the same. Figure 2-1 gives a schematic of a RP process chain. As the first step, the part is modelled by computer software in a three dimensional (3D) CAD file. A surface tessellated (STL) version of the CAD file is then exported from the software and sent to the RP machine. The machine interface software slices the STL file into several layers with a required thickness along the Z direction. The direction of slicing is important as the mechanical properties could be different between XY and Z directions (Hopkinson *et al.* 2006).

Additive manufacturing processes are capable of producing net-shape parts with great complexity. In most cases, there are some sections of the part that overhang and need a support material. The support needs to be easy to remove in a post-process stage without damaging the part's surface finish. Therefore, the support can be either the same as the part material (but with weak scaffold structure) or a different material (Hopkinson *et al.* 2006).

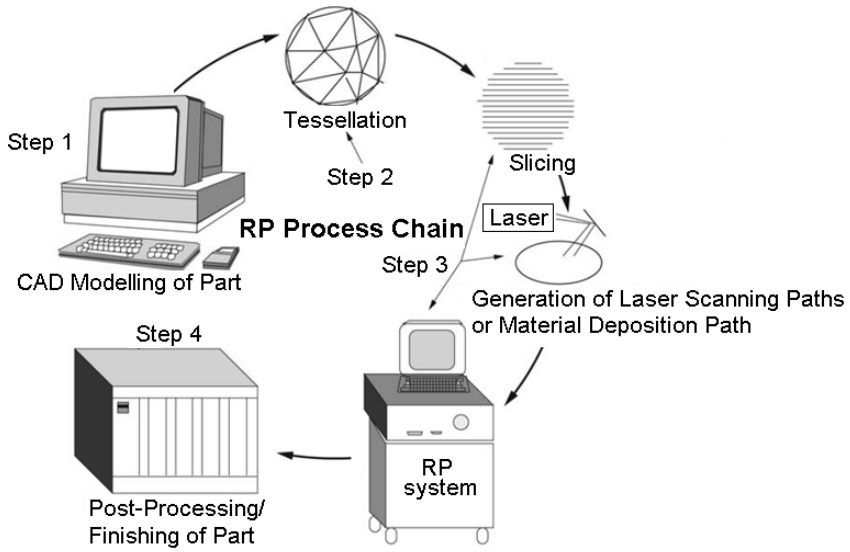

Figure 2-1 An RP process chain (Pandey *et al.* 2003)

2.1.3 Features

Additive manufacturing technologies have undergone significant development since their introduction in the late 1980s (Wohlers 2007). This has been as a result of interesting features such as design freedom and short design to reality cycle.

Today's market requires a fast and flexible process chain to make deliveries to customers. Additive manufacturing processes aid this. A revision in design is simple and fast while it may take more than a month for conventional processes. More importantly, the concept of adding layers has made the technology capable of manufacturing parts with great complexity. In addition, the design complexity would not considerably affect the cost of fabrication in these processes. However, the overall cost of manufacturing in conventional tool-based processes is directly affected by the complexity of a part.

The design freedom potential of additive manufacturing has also had an impact on design for manufacture (DFM) and design for assembly (DFA) typically by part consolidation (Hopkinson *et al.* 2006). Decreasing the number of parts by consolidation, additive manufacturing could reduce assembly steps and the associated cost of tooling. In addition, with the additive approach, it is possible to fabricate products based on each customer's requirements. Therefore, customisation is another capability of additive manufacturing.

There are situations in which parts have a limitation of geometry while a higher functionality is required. Functionally graded materials in the structure may be a solution for this (Hopkinson *et al.* 2006). Additive manufacturing, thanks to its layer-wise concept, could fabricate each layer with multiple materials to make a graded structure in the part.

2.1.4 Techniques

Several additive manufacturing techniques have been commercialised since the late 1980s which are really RP process rather than RM. These were categorised into liquid-based, powder-based and solid-based processes (Hopkinson *et al.* 2006) depending on the state of the material being processed during layer fabrication.

Stereolithography (SL) was the first commercial RP process patented by Chuck Hull in 1986 and first sold by 3D Systems in 1987 (Beaman 1997). Photo-curable resin is used in the process which applies an ultraviolet (UV) laser spot to polymerise the resin selectively (Hopkinson *et al.* 2006). After layer solidification, the substrate is lowered a step to cover the surface with fresh liquid resin and the consequent layers are fabricated. Figure 2-2 shows Streolithography process schematically.

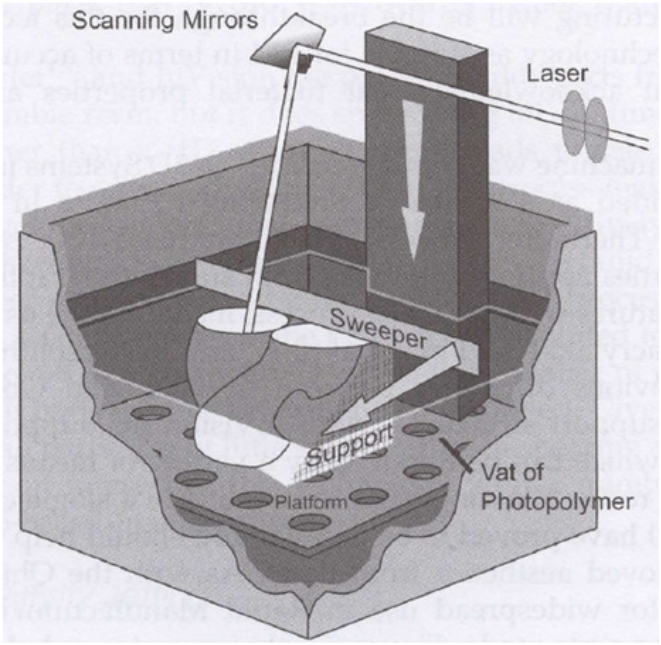

Figure 2-2 Schematic of Stereolithography (Hopkinson *et al.* 2006)

Selective Laser Sintering: The concept of sintering powders by a laser became the Selective Laser Sintering (SLS) process which was commercialised by DTM

Corporation (Beaman 1997). The process has similar concepts to SL in laser scanning and supplying fresh material. However, powdered raw material is used which is pre-heated to below the melting point for a scanning laser which then heats up the material selectively. This initiates fusion of powders and consequently a layer is fabricated (Hopkinson *et al.* 2006). A schematic of the SLS process is seen in Figure 2-3.

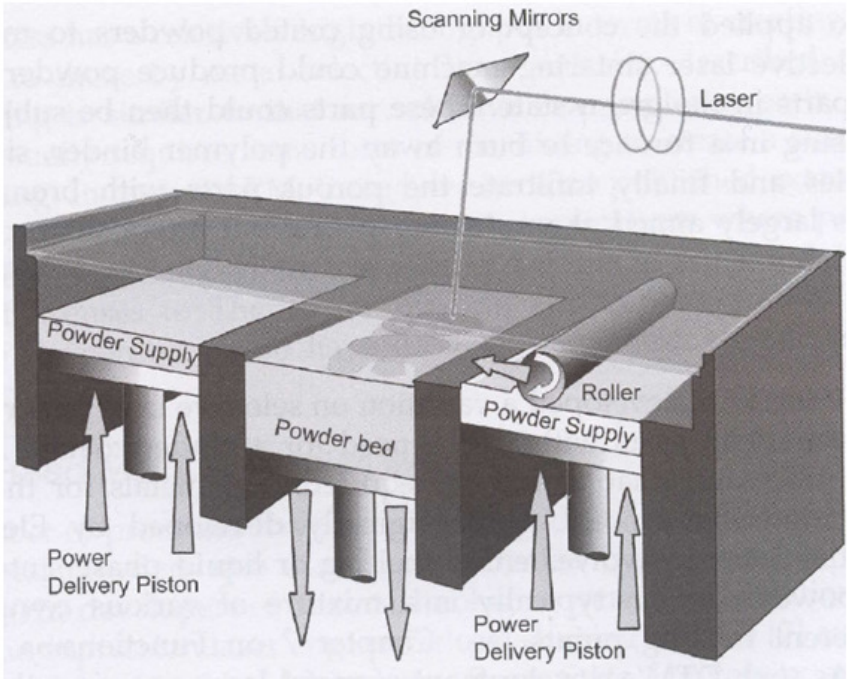

Figure 2-3 Schematic of Selective Laser Sintering (Hopkinson *et al.* 2006)

Fused Deposition Modelling: The concept of extruding a polymer in the molten state through a small nozzle to produce a layer was patented in 1991, by Scott Crump, the founder of Stratasys Inc. (Beaman 1997). Fused Deposition Modelling (FDM) extrudes two polymeric materials, one for the part and the other for supports as shown schematically in Figure 2-4 (Hopkinson *et al.* 2006).

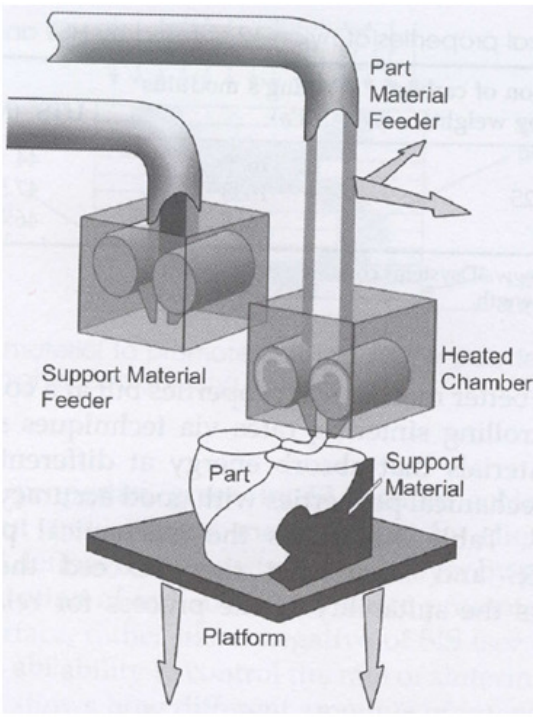

Figure 2-4 Schematic of Fused Deposition Modelling (Hopkinson *et al.* 2006)

Three-Dimensional Printing: Three-Dimensional Printing (3DP) was introduced in 1991 (Beaman 1997). The process has one or more inkjet printheads to deposit a polymeric binder onto a bed of powder (polymer, metal or ceramic) to pattern a layer. As with SLS, a platform is lowered to give a new layer of fresh powder (Hopkinson *et al.* 2006). Figure 2-5 shows a schematic of the 3DP process.

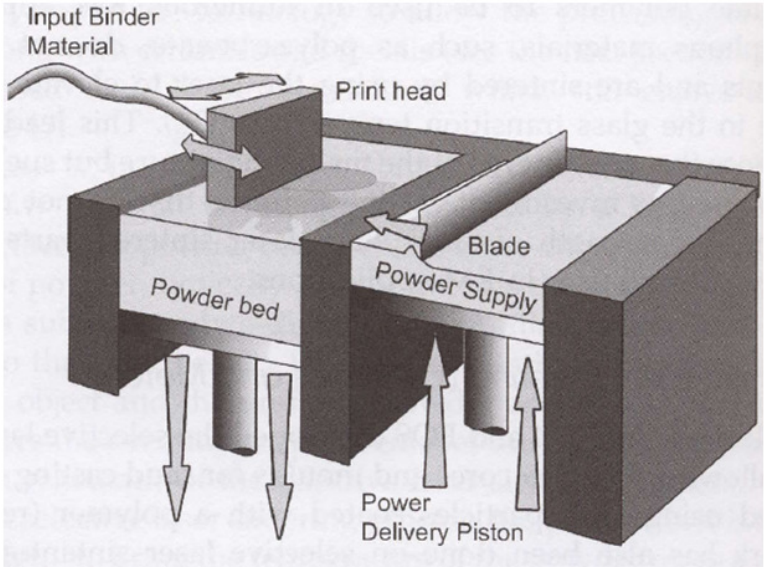

Figure 2-5 Schematic of Three-Dimensional Printing (Hopkinson *et al.* 2006)

2.1.5 Applications

The unique features of additive manufacturing processes have made them successful in many industries. Although the main application areas were prototyping of models, the recent focus has been on increasing the functionality of the parts and reducing the machinery and material costs. The most active industries for additive manufacturing have been aerospace, automotive, medical, architecture and games, although there are several successful cases in many other areas such as sport, military, art, construction and education (Hopkinson *et al.* 2006).

2.2 Inkjet Technology in Manufacturing

2.2.1 Inkjet Technology Development Path

The formation of uniform droplets from a stream of liquid which had been jetted through a small orifice was noted as early as 1833 by Savart (Pique and Chrisey 2002). Rayleigh described mathematically the break-up mechanism in a continuous jet (Rayleigh 1878). Much later, in 1948, Elmqvist of Siemens in Sweden patented

the first jetting-based machine, a *medical strip-chart recorder* (Kelly and Lindblom 2006). In early 1960s, Dr. Sweet of Stanford University demonstrated how a pressure wave pattern could break up a continuous stream of liquid into uniform droplets for printing applications (Le 1998). Dr. Sweet's achievements led to the birth of the world's first commercial inkjet printers which were introduced to the market in the late 1960s. IBM, in 1976, produced the first computer-printer interface and licensed the inkjet technology for use in printers.

Another jetting technique was developed independently by Professor Hertz's team in Lund Institute of Technology (Sweden) which was known as greyscale-based inkjet printing (Le 1998). The invention, which was commercialised later, was based on controlling the number of droplets deposited for each pixel to create the desired grey tone. The complexity of droplet charging and unreliability of circulating systems in continuous inkjet technology encouraged researchers to develop a new jetting concept based on generating droplets where needed during the deposition (section 2.2.2). This system was first used commercially by Siemens in 1977 (Le 1998).

Canon developed an inkjet system based on the growth and collapse of a water vapour bubble which was called Bubble Jet technology (Le 1998). The simplicity and low-cost production of this inkjet system led Hewlett-Packard (HP) to develop the same concept in their printers. The technology was known as Thermal Inkjet after HP's commercialised printer, ThinkJet in 1984. The cost of production of these printers was low enough for the birth of disposable inkjet printheads by HP which solved the problem of reliability in inkjet technology. Hot-melt inkjet, which was also known as solid inkjet, was first developed in packaging application by Dataproducts (Gregory 1991).

2.2.2 Inkjet Printheads

Inkjet technology has been classified into two main techniques based on the jetting head used: continuous mode and drop-on-demand (DoD) mode. These modes will be discussed briefly and additional information can be found in the literature (Le 1998, Pique and Chrisey 2002, Hon *et al.* 2008).

Continuous Mode

A continuous train of droplets is made in continuous mode inkjet printheads by pressurising the liquid through a feeding system and then vibrating a piezoelectric element inside the printhead. The feeding system has a pump driven circulation from the material reservoir and sends the material to the jetting head by pressure. A piezoelement in the jetting head is continuously vibrated via a signal generation system which stimulates the element to vibrate at a preset frequency and amplitude. By vibrating the element, a pressure wave is produced in a liquid filled chamber. The pressure from the feeding system sends out the fluidic material through a small nozzle and a continuous stream of the liquid material is formed. On the other hand, the pressure wave generated by the vibrating element breaks down the stream into tiny droplets. A train of droplets is made consequently to either impinge onto a substrate or enter into a circulation system (a gutter) by two deflection plates (Le 1998). The plates are a part of a deflection system wherein droplets are selectively charged electro-statically. This principle provides control to the jetting head to deposit material onto the substrate where it is needed. Figure 2-6 shows the principle of the continuous mode jetting heads.

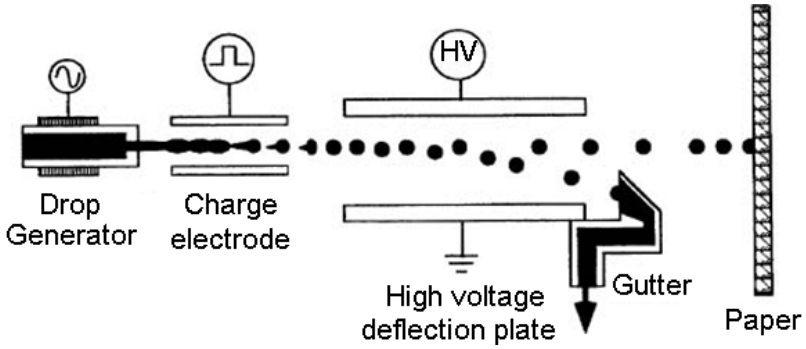

Figure 2-6 Continuous mode inkjet head principal (Le 1998)

Drop-on-Demand (DoD) Mode

In a DoD mode inkjet head, a voltage signal is sent to a transducer that forces liquid material through a nozzle and a droplet is generated to hit the substrate. The voltage signal is sent when a droplet is needed to be deposited. Therefore compared with the continuous mode, in DoD mode, there is no need for the droplet deflection and ink recirculation units resulting in a less complex system. However, the transducer in a DoD mode jetting head requires three or more times greater actuation energy to generate a droplet (Pique and Chrisey 2002).

Several actuation systems have been developed in which the thermal and piezoelectric systems are the widest used (Le 1998). In a thermal actuation system, shown schematically in Figure 2-7, a resistive layer element, installed close to the nozzle, receives a current and transforms it to heat. The water-based ink used in the thermal inkjet system becomes superheated and a bubble is nucleated on the heater. An increase of the temperature leads to the growth of the bubble which finally forces the ink to be jetted out of the orifice. At a certain volume, the bubble collapses which consequently produces a capillary wave to refill the nozzle area with ink for the next actuation.

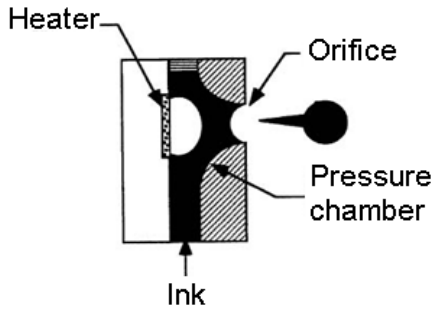

Figure 2-7 Principal of a thermal inkjet system (Le 1998)

In piezoelectric systems, the actuator contains a piezoceramic element which is pre-polarized in a specific direction. When a voltage signal is applied, an electrical field is induced in the piezoceramic element. The field can be either parallel or perpendicular to the polarization direction. Depending on this, the piezoceramic is deformed and displaced by engaging (bonding) one or two sides of the element to the printhead frame. Based on this concept, four main types of piezoelement actuation have been developed namely squeeze, bend, push, and shear modes as schematically shown in Figure 2-8.

A *squeeze mode* actuator comprises a tube of piezoelectric ceramic which is polarized radially and supported at both ends (see Figure 2-8(a)). Electrodes are provided at the inner and outer sides of the cylinder. When a voltage is applied to the electrodes, the tube is squeezed which results in an expansion and contraction of the tube (Bogy and Talke 1984, Lee *et al.* 1984). This radial displacement causes a pressure wave to be formed which generates a droplet.

A *bend mode* actuator has a piezoceramic plate installed in one side of the pressure chamber which has a diaphragm as shown in Figure 2-8(b). By receiving a voltage, the contraction of the piezoceramic bends the diaphragm inward to the pressure chamber and makes a pressure wave to generate a droplet.

A *push mode* actuator has a piezoceramic rod as shown in Figure 2-8(c). A droplet is expelled through the nozzle when a voltage is applied to the rod. Both bend and push mode designs have a thin diaphragm which isolates the piezoelement to avoid its contact with the ink. This feature helps the inkjet head to withstand the chemical interaction between the piezoelement and the ink (Le 1998).

In a shear mode actuator, the polarization direction on the piezoceramic element is set perpendicular to the applied electrical field which makes it different with the other modes. This feature produces a shear deformation as shown in Figure 2-8(d). Shear mode has been used in Xaar type inkjet printheads which is explained with more details in the next section.

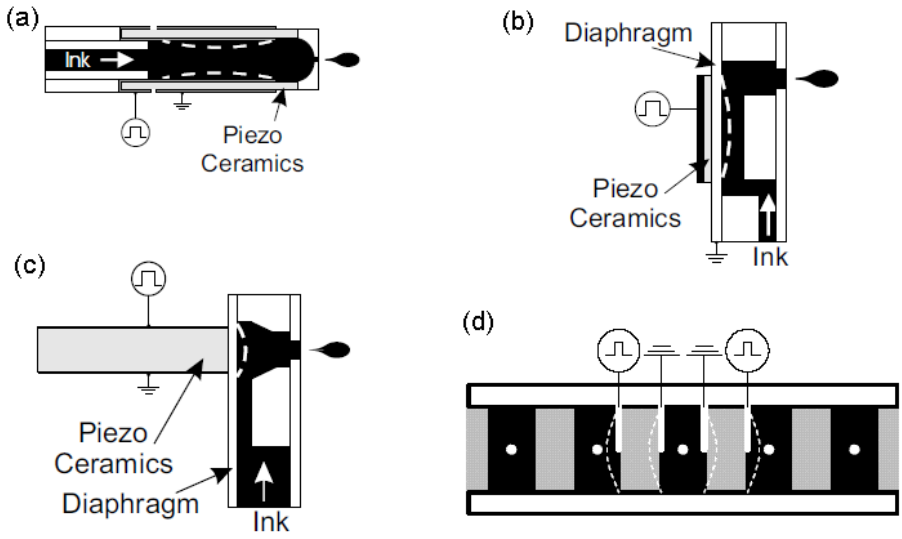

Figure 2-8 Schematic design of different modes of DoD piezoelectric printheads, (a) squeeze mode (Lee *et al.* 1984), (b) bend mode, (c) push mode, and (d) shear mode (Brunahl 2003)

2.2.3 Xaar-type Inkjet Printheads

Xaar patented its inkjet print head based on a shear mode piezoceramic actuator (Michaelis *et al.* 1989). Figure 2-9 shows the standard type of the Xaar inkjet head. It consists of a channel plate of poled lead zirconate titanate (PZT) ceramic. Thin long

parallel walls form channels which are bonded to electrical wires at one end, and to the nozzle plate at the other. Metallic electrodes are coated on the upper half of both sides of each wall. A cover plate is bonded rigidly on top of the walls with an inlet through which ink is fed into the channels.

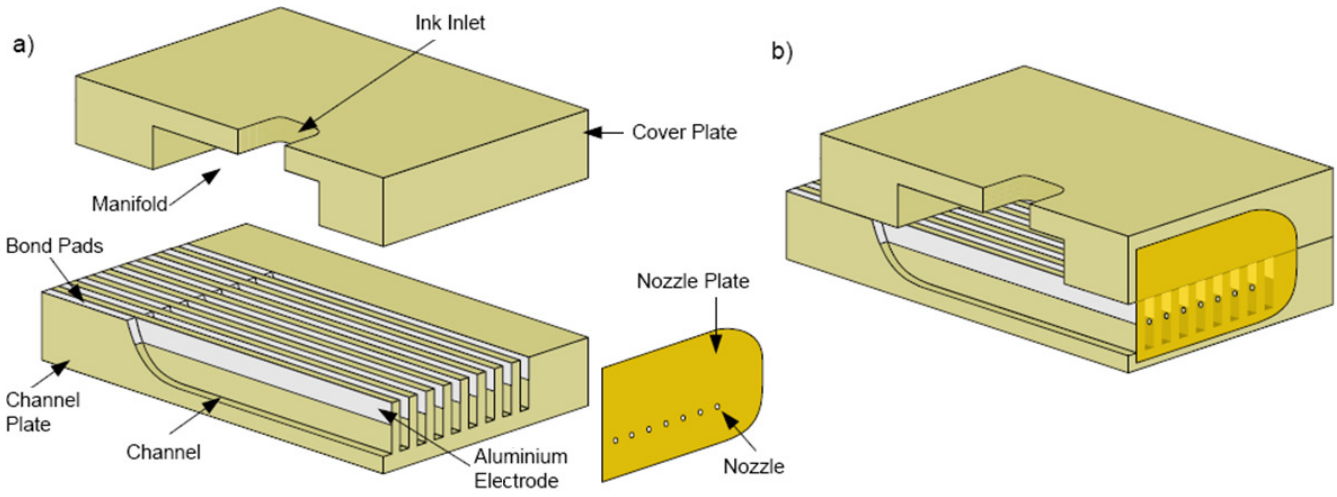

Figure 2-9 Xaar-type shear mode printhead a) components and b) assembled actuator (Brunahl 2003)

When applying a voltage to the electrodes, an electric field is induced perpendicular to the polarization direction of the walls. Consequently, as shown in Figure 2-8(d), the top half of the wall deflects in shear mode and displaces the centre of the wall as the top edge of the wall is rigidly bonded. The lower half of the wall is forced to follow the motion of the top half. Therefore, a chevron-like deformation in the cross-section of the wall is made as seen schematically in Figure 2-10. By applying an opposite electric field to the adjacent wall in channel 2, opposite displacement occurs in the adjacent wall which with the other wall's displacement decreases the volume of channel 1 and increases the volume of channel 2. The expansion and contraction of channel volumes generates an acoustic pressure wave in each channel. The pressure wave in the contracting channel forces ink out through the nozzle while the

wave in the expanding channel causes an intake of ink from reservoir. The channels and consequently the nozzles are grouped into two in which group one, typically, generates a droplet and group two drawn ink from the reservoir and vice versa.

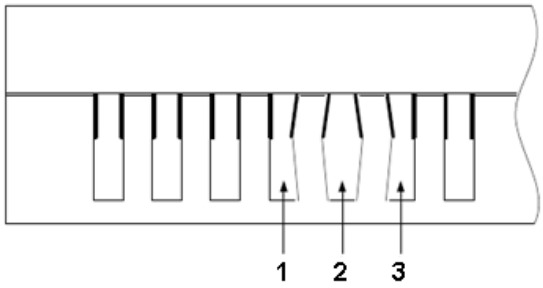

Figure 2-10 Cross section of ink channels upon actuation in Xaar shear mode actuator (Brunahl 2003)

2.2.4 Considerations for Inkjet based Manufacturing

The progress of inkjet technology has led to the development of jetting heads with high deposition speed as well as printing resolution by increasing the number of nozzles and decreasing the nozzle diameter (Pique and Chrisey 2002). However, to employ the technology for layer deposition in a manufacturing process, further attention should be given to a number of factors described briefly as follows.

Resolution and Layer Deposition

The number of droplets deposited onto a surface to make a line can vary based on the nozzles arrangement and density, jetting frequency and inkjet head/substrate relative motion. This value is known as resolution which is measured by the number of dots per linear inch (dpi). In graphical printing, invention of screen printing resulted in printing dots as “halftone” for text and images instead of a continuous tone for full covering of the printing area with ink. The concept was to print dots with small enough spacing, so that the human eye can no longer detect the dots and “smooth

out" the line or the image (Kipphan 2001). In colour halftoning, varying the space and the size of dots could vary the colour tone (recognised by eye) and therefore, limited colour inks could produce a range of light or dark colours (Kipphan 2001) as Figure 2-11 demonstrates.

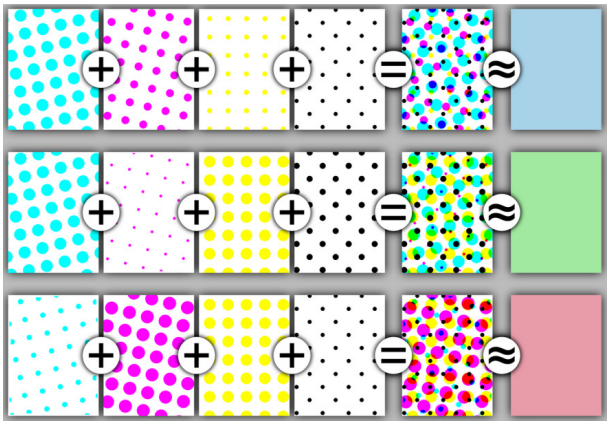

Figure 2-11 Colour halftoning (image retrieved from Wikipedia (2010) as an open source)

In most manufacturing applications of printing though, the need is to deposit a smooth fully covered area. This could be achieved with printing continuous lines known as beads, side-by-side, which would require high resolutions. The droplet spacing then would be a parameter which dictated the final geometry and stability of the bead and therefore the quality of deposition. The appropriate resolution should be defined based on the physical properties of the depositing material, the characteristics of the surface, the depositing speed and also kinetics of the droplet impact (Schiaffino and Sonin 1997, Duineveld 2003, Fathi *et al.* 2010).

In printing a fully dense 3D structure, the bead spacing should be set to have an overlap to give a smooth layer. The spreading and coalescence of the droplets is very important from a layer thickness and surface finish point of view. Proper droplet size and deposition parameters could be used for good exterior edge definition

(Calvert 2001). Controlling the material surface tension with a surfactant could assist in controlling the spread geometry and therefore provide better edge definition. Extremely narrow channels of less than 100 nm have been produced between two deposited beads in this way for electronic applications ((Sirringhaus *et al.* 2000, Sele *et al.* 2005).

Droplet Placement Accuracy

The accuracy of each single droplet position determines the final accuracy of a built part and the roughness of its surface. This parameter is more important in printing electronics due to the multi-material deposition and the influence of placement inaccuracies on the functionality of the printed structure electronically (Sirringhaus and Shimoda 2003). An accuracy of better than ±5 µm is typically required in printing digital displays which could be obtained by proper system characterisation (Bruner *et al.* 2007). Deviation in positioning can be due to variation in material behaviour in droplet formation, inkjet head's wettability, inaccuracies in the dynamics of the system and aerodynamic fluctuations when the droplets are in flight toward the substrate (de Gans and Schubert 2003). Aerodynamic fluctuations can be caused by the printhead/substrate relative motion while jetting. The inaccuracy caused by this problem could be reduced by decreasing the printhead/substrate gap distance to typically less than 1 mm (Creagh and McDonald 2003, Bruner *et al.* 2007).

Material State Change

A state change is required from a liquid (by which the material is jetted) to a solid. In the additive manufacturing approach, there should be enough layer rigidity to fabricate the next layer. The state change can occur by heat transfer, radiation (e.g.

UV, infrared, microwave), solvent evaporation or chemical reaction (Calvert 2001). Rapid solidification of hot melt materials such as wax as in printing a 3D model or solder in printed electronics is achieved by maintaining a cold surface which has the advantage of controlling droplet spreading (Schiaffino and Sonin 1997, Waldvogel and Poulikakos 1997).

Layer Fabrication Speed

In inkjet based manufacturing processes, very tiny droplets (typical volumes of 10 to 100 pl) are jetted to build a part which makes the fabrication time an important consideration. Typical droplet generation rates for continuous inkjet mode are on the order of 80 kHz, while in DoD mode the rates are on the order of 8 kHz (Pique and Chrisey 2002). Multiple heads are used in some processes to compensate for the low throughput of an inkjet printhead (Bruner *et al.* 2007). Variable droplet size is another approach which could be used to increase the fabrication speed (Jeng *et al.* 2000). The exterior of a part is made by smaller droplets to give a fine surface finish while bigger droplets are deposited for the interior portion. This method could decrease the fabrication time by up to 40% (Jeng *et al.* 2000).

2.2.5 Inkjet-based Manufacturing Processes and Applications

There was a fast growth in employing inkjet printing for different non-graphical applications (Calvert 2001) as the technology can deposit a wide range of materials on almost every substrate in a precise and controlled manner (Le 1998). In addition, the digital nature of inkjet printing gives it an advantage as information can be flexibly chosen from a computer for printing. Reproducibility is another advantage of inkjet printing as fault recognition and quality monitoring is easy to achieve in this type of

printing. These resulted in a wide range of applications, and this section briefly describes the most common.

Printed Electronics

Inkjet printing has been applied to manufacture electronic components such as printed circuit boards (PCBs), organic light-emitting diodes (OLEDs), and organic thin film transistors (OTFTs), to increase the speed and flexibility of production and reduce the cost and environmental pollution (de Gans *et al.* 2004). In addition to jetting solder at elevated temperature, printing of conductive organic polymer solutions revolutionised the industry for the high demand market in both electronic and display technology (Sirringhaus *et al.* 2000). The trend is in miniaturisation of components in electronics and higher resolution in display technology (Sele *et al.* 2005). One of the promising areas is flexible electronic-paper (e-paper) displays which could replace normal paper. The e-paper has a typical thickness of 0.3 mm, a bending curvature radius of 15 mm and a pixel density of 96 pixel per inch (Chen *et al.* 2003). However, there are still challenges facing a successful employment of printing technology for electronics such as achieving sub-micron accuracy (Perelaer *et al.* 2010).

Additive Manufacturing

Although the majority of printed electronics employ a number of layers and therefore are a kind of additive process, additive manufacturing as an application of inkjet technology is more common when it employs printing for fabrication of mechanical parts where the layer is much thicker than those in electronic printing.

Inkjet technology was first used in additive manufacturing by Sachs *et al.* (1993) of MIT in the early 1990s resulting in commercialisation of the 3DP process by Soligen in 1993 (Wohlers 2007). The concept though was to deposit a binder solution to consolidate the powders as the build material. MIT's patent was later licensed to Z-Corp. which launched its first 3DP machine in 1996 (Wohlers 2007). Research into a powder-based additive manufacturing process using inkjet technology was undertaken by Hopkinson's team for High Speed Sintering (HSS) at Loughborough University. The process prints radiation absorption ink onto a bed of powder which then receives infra-red radiation to fuse the coated powders for layer fabrication (Hopkinson and Erasenthiran 2004, Majewsky *et al.* 2008).

Early research on the use of inkjet technology to deposit the build material in an additive manufacturing approach was undertaken by Prof. Sonin's team at MIT with printing 3D wax structures (Gao and Sonin 1994, Schiaffino and Sonin 1997). The first commercialisation of the concept was the *ModelMaker* process by Solidscape (later called Sanders Prototype) which was introduced in 1994. 3D Systems developed its wax 3D printing based process, *Multi-Jet Modeller (MJM)*, and introduced the *Actua 2100 3D Printer* in 1997 which was later replaced by the *ThermoJet* system which had a better printhead technology for a faster process (Wohlers 2007). Most recently, 3D Systems produced its latest generation of 3D printers, *ProJet CP 3000*, based on wax capable of fabricating layers with 328 x 328 dpi (XY) resolution and 36 µm thickness (3D Systems 2010).

Additive manufacturing processes were developed based on printing photopolymer resins where a UV light could cure and solidify the deposited pattern. The first commercialisation of such a technique was introduced with *PolyJet* technology of Objet Geometries in 2001 (Gebhardt 2003). The process could print two different

photopolymer resins (as build and support materials) followed by a UV light scanner to solidify the layers in an additive manner. The weaker support material was then removed by a water jet. The latest series of the PolyJet technology was capable of a layer thickness of 16 µm. 3D Systems also introduced its first photopolymer-based 3D printing system, *InVision*, in 2003, which used wax as the support material (Gibson *et al.* 2009). The latest series of 3D Systems's photopolymer 3D printer (*ProJet 5000*) has a relatively large build environment (550 x 393 x 300 mm), 38 µm layer thickness and 328 x 328 dpi (XY) layer deposition resolution (3D Systems 2010).

Bioprinting

An interesting application of inkjet technology can be direct assembly of biological materials into 3D structures. Detailed reviews on bioprinting have been published (Mironov *et al.* 2003 and 2006). One of the main challenges of the application has been the concern over the damage to living cells due to the high shear rates during droplet generation and deposition impact (Saunders *et al.* 2008). Successful application of the technology requires both material considerations in structuring 3D shapes such as improving scaffold materials (e.g. hyrogels) and maintaining high viability of the cells after the deposition (Mironov *et al.* 2006).

Other Applications

Several other applications of inkjet technology as a manufacturing tool have been reported (Hon *et al.* 2008, Singh *et al.* 2010). The printing of solar cells is a novel process which still has limited throughput compared with the other conventional techniques (Krebs 2009). Printing solar cells onto textiles (clothing) could power

personal mobile devices (Schubert and Werner 2006). In addition, optical lenses and waveguides are manufactured by printing of UV-curable resins (Pique and Chrisey 2002). In life science, printing of miniaturised drug delivery devices and synthesis of a DNA array is a typical application (de Gans *et al.* 2004). Batteries, micro-sensors and micro-actuators in biological micro-electro-mechanical systems (bio-MEMS) are other applications (Singh *et al.* 2010).

2.2.6 Printing of Functional Materials

Considering the fluid property restrictions, the variety of jetting materials is impressive and have been printed for different applications. This section briefly introduces some of the common jetting materials with a focus on those applied in additive manufacturing.

Jetting of Waxes

Waxes which are low molecular weight polymers have a low melting point typically 50~90℃ and low viscosity in the melt state typically 10~15 mPa.s at 130℃ (Chovancova-Lovell *et al.* 2006). In addition, they quickly solidify on a cold substrate. These features resulted in their application in the graphics industry (Le 1998).

Fundamental studies of wax jetting and drop/surface interactions such as contact angle and stability of wax beads for rapid prototyping applications were reported as early as 1994 (Gao and Sonin 1994). Waxes have been used as vehicles in printing colloidal suspensions in the additive manufacturing approach (Wang *et al.* 2004). One of the most recent applications was the fabrication of paper-based microfluidics as portable medical devices by printing wax patterns onto cellulose membranes (Lu *et al.* 2010).

Jetting of Ceramic Suspensions

Inkjet technology has been used to manufacture ceramic parts by jetting ceramic particle suspensions in a binder-solvent solution or wax (Tay *et al.* 2003). After printing the object, there is usually a post-processing stage to sinter the green part. The typical viscosity of the ink suspensions are 1~10 mPa.s (Tay *et al.* 2003) and particles are less than 1 μm in diameter. Volumetric concentrations of up to 35% have been jetted (Tay *et al.* 2003, Wang *et al.* 2004). However, a higher concentration of 60 vol.% was achieved in jetting of zirconia and polyvinylbutyral binder in solvent applying continuous mode jetting (Calvert 2001).

The process required a drying stage for each layer, and solvent was evaporated by either hot air or by a hot substrate. This requirement limits the process in terms of fabrication speed as well as surface finish. Therefore, most of the research activities have been for fabrication of small features (Tay *et al.* 2003, Lejeune *et al.* 2009). However, printing of thin features (of about 50 μm thick) and multi-graded ceramic composition structures was successfully achieved (Lejeune *et al.* 2009). Wax-based ceramic inks, on the other hand, do not require a drying stage as wax is removed by melting in a post-processing stage (Calvert 2001).

Jetting of Metals

The high melt temperature of metals is a restriction for jetting; however, solders with a melt temperature of about 200~300℃ have been jetted onto circuit boards for electronic applications (Calvert 2001). MicroFab Technologies Inc. has been a key player in solder printing with patents published since 1992 and then commercialising its *SolderJet* technology (Wallace and Hayes 1998). In 3D additive manufacturing,

Orme developed the Precision Droplet-based Net Form Manufacturing process (PDM) to jet molten aluminium via continuous jetting (Orme 1991). Investigations showed the process was repeatable and consistent in droplet generation which gave fully dense components with a higher hardness than the wrought metal (Liu and Orme 2001). The same jetting technology with the aid of an additional machining step was investigated for a wider range of metals (typically tin, zinc, aluminium and copper) and the process was known as Uniform Droplet Spray (UDS) (Kim *et al.* 2002). Higher melt temperature metals were studied in the laboratory with a custom made system and although a jetting temperature as high as 1200℃ was achieved, a frequency higher than 10 Hz could not be obtained (Xiang-hui *et al.* 2010).

Jetting of Polymers

Most polymers are too viscous in their liquid state to jet due to their entangled long molecular chains. However, they can be jetted as a dilute solution or a colloidal dispersion (Calvert 2001, de Gans *et al.* 2004). The latter has the advantage of presenting a high-molecular-weight polymer in a low viscosity form. The effect of higher molecular weight on drop formation was investigated for polymer light-emitting diodes (PLEDs) printing (de Gans *et al.* 2004). Formation of a tail in the break-up process was studied in depth to avoid satellite formation (de Gans *et al.* 2004, Reis *et al.* 2005).

The main developments in printing polymers have been in display and electronic applications as they have a high commercial potential (de Gans *et al.* 2004). Printing of photopolymer resins have been commercialised for RP application since 2001 (Wohlers 2007). Photopolymer resin solutions were also used for printing ceramic suspensions for RP applications (Tomeckova and Halloran 2010).

2.2.7 Printing of Reactive Polymeric Materials

The concept of printing reactive polymers was reported in patents as early as 1987 by Hewlett-Packard (HP) for graphical printing applications (Hackleman and Pawlowski 1987). The technique was to print two water-based inks containing a low concentration of reactants via two separate printheads onto each other. Upon deposition onto the paper, this would produce cross-linked polymeric lattices encapsulating the inks for increased print quality.

The idea of printing multiple reactive epoxy-based materials via separate printheads was first published as a patent by Johnson *et al.* (2003). Later, Elsner *et al.* (2010) of Voxeljet Technology GmbH filed a similar patent on the concept in 2005 and reported the printing of lines and multiple layers with this approach (Uhlmann and Elsner 2005). The concept was developed for 3D printing of epoxy-based materials. Three printheads were employed to deposit three reactive components onto each other. By selective deposition of different compositions and mixing ratios of the components, multi-graded structures with desired graduated mechanical properties could be printed (Uhlmann and Elsner 2005).

Fabrication of micron-size 3D features using reactive printing of polyurethane (PU) was also reported (Kröber *et al.* 2009). The reaction was based on cross-linking of printed initiator and catalyst agents deposited as micron-size lines (beads). Thermoset polyurethane (PU) materials performed on a glass substrate at 90℃ within three minutes.

2.3 Physical Phenomena during Jetting of Materials

This section reviews the most important physical aspects which should be understood for jetting a new material.

2.3.1 Phenomenon of Droplet Generation

In a DoD inkjet printhead, the periodic change of volume by the actuation system induces an acoustic pressure wave inside the ink chamber by either deformation of a piezoelement or growth of a bubble (in thermal inkjet systems). The pressure wave propagates towards the nozzle and interacts with the ink meniscus in the nozzle. The wave overcomes the viscous pressure loss in the nozzle and the surface tension force from the ink meniscus to generate a droplet (Le 1998). The pressure wave should be strong enough to expel the generated droplet towards the substrate for deposition.

2.3.2 Material Characteristics for Jetting

Several physical properties of a liquid contribute to the droplet formation process from pressure wave propagation inside the nozzle to break-up of a droplet. Viscosity, surface tension and density are the most critical properties for jettability of a material (de Gans *et al.* 2004). Particle size in liquid suspensions (de Gans *et al.* 2004) and molecular weight and concentration in polymer solutions (Xu *et al.* 2007) are other factors. Depending on the physical properties of a fluid and the applied shear rate by the actuation process, a droplet can be jetted either with or without a tail disintegrating into smaller satellite droplets (MicroFab Technologies$_1$ 1999, de Gans *et al.* 2004).

Viscosity

Viscosity should be low enough, typically 20 mPa.s or less (de Gans *et al.* 2004) in inkjetting as it resists in two ways the droplet formation process. Inside a DoD inkjet printhead, it dampens the acoustic pressure wave made by the actuation which travels towards the nozzle in the ink pressure chamber (MicroFab Technologies$_1$ 1999). Therefore, a higher drive voltage is required to generate a fixed droplet velocity in higher viscosity liquid. On the nozzle, the viscosity resists the break-up process which causes necking and formation of a tail attached to the droplet. However, as the shear rate in the break-up process is of the order of 10^5 s^{-1}, shear thinning may occur which decreases the viscosity (de Gans *et al.* 2004). As viscosity decreases with temperature, the temperature of the liquid in the orifice should also be considered.

Surface Tension

As with viscosity, surface tension which ranges from 20 to 70 mN m^{-1} in inkjetting (MicroFab Technologies$_1$ 1999) plays a role. After the pressure wave made by the actuation reaches the meniscus in the nozzle orifice, it overcomes the surface tension of the ink and moves the meniscus outward (Le 1998). The surface tension has a small influence on the required drive voltage of the inkjet head. However, a slight increase of the voltage is required to maintain the desired droplet velocity in a higher surface tension fluid (MicroFab Technologies$_1$ 1999). The nozzle material also plays a role in the pressure wave/meniscus interaction as the formed meniscus is a result of wettability of the nozzle (MicroFab Technologies$_1$ 1999, de Gans *et al.* 2004).

Generally the main role of surface tension is in the maintenance of the spherical shape of the droplet. In addition, upon separation of the droplet with a tail, the resistance by surface tension forces may finally disintegrate the tail into satellite droplet(s) travelling with the main droplet towards the substrate (de Gans *et al.* 2004, Xu *et al.* 2007) which in turn can decrease the final droplet size (MicroFab Technologies$_1$ 1999).

Density

Practically, the effect of density on droplet formation is minor compared to the properties above (de Gans *et al.* 2004). Its indirect effect on droplet formation is on the acoustic pressure wave speed as density varies the acoustic speed. With more dense liquids, the acoustic speed is higher and consequently the meniscus on the nozzle orifice is oscillated earlier. This is considered in defining the pulse width in the nozzle actuation.

Particle Size

In addition to different types of pigmented inks, suspensions of ceramics, metals and polymers have been jetted with a nozzle diameter range of 20 to 70 µm (de Gans *et al.* 2004, Reis *et al.* 2005). However, when it comes to jetting reliability, the particle size and dispersion should be taken into account as they may cause nozzle clogging as well as instability in droplet formation. Usually, particles on the order of 1 µm or less are used in ink formulation and those bigger should be filtered before entering the ink channel. Generally it is advised that particles with diameters higher than 5% of the orifice should be filtered (MicroFab Technologies$_1$ 1999, Pique and Chrisey 2002).

Molecular Weight and Concentration in Polymer Solutions

Many high molecular weight polymer solutions have been used in inkjet printing applications (de Gans *et al.* 2004). Polymer addition in a solution turns a Newtonian fluid to non-Newtonian by polymer viscoelastic behaviour. The viscoelastic behaviour of polymers with a molecular weight of above 500,000 M_w, results in formation of relatively long tails which connects the droplet to the nozzle during the droplet break-up stage (de Gans *et al.* 2004, Reis *et al.* 2005). This behaviour is not seen in pure Newtonian fluids as Figure 2-12 demonstrates. In the high shear rates of the droplet generation process (typically 10^4~10^5 s^{-1}), the viscoelastic behaviour increases the viscosity of the solution by the long polymer molecule chain (de Gans *et al.* 2004, Xu *et al.* 2007).

The variation of molecular weight and concentration of the added polymer in the solution results in different regimes of tail disintegration behaviour (Hutchings *et al.* 2007, Xu *et al.* 2007). At a very low molecular weight and/or concentration, the tail is disintegrated into several satellite droplets. Increasing the molecular weight and/or concentration decreases the satellite droplets and at a certain molecular weight/concentration, no disintegration occurs and the tail attached to the droplet travels towards the substrate. Higher molecular weight/concentration does not let the droplet be detached from the nozzle because of the viscoelastic nature of polymer (Xu *et al.* 2007).

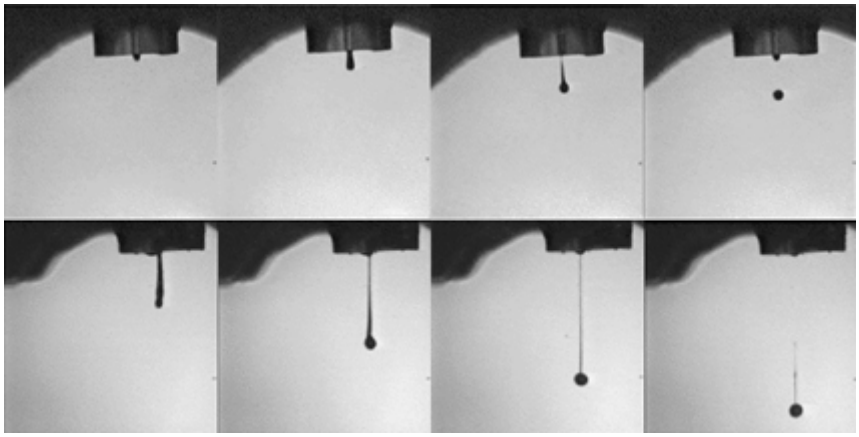

Figure 2-12 Effect of molecular weight on droplet formation by making a Newtonian fluid (upper images) a non-Newtonian fluid (lower images) by addition of small amount of a high molecular weight polymer (de Gans *et al.* 2004)

2.3.3 Actuation and Droplet Generation

All DoD inkjet printheads are driven by a voltage pulse with a waveform. The signal rises to a certain level where it is kept constant for a while. The constant time is called the pulse width after which the voltage falls to zero to return the actuator to a rest state. This sequence makes a trapezoidal waveform (MicroFab Technologies$_2$ 1999). The applied pulse provides a contraction and expansion of the ink channel volume to generate an acoustic pressure wave which propagates in the channel towards the ink meniscus. Fluid compressibility in pressure wave propagation and retraction of the wave from the meniscus oscillation results in acoustic resonances. This phenomenon implies an optimum pulse width and time delay in triggering the next pulse to maximise droplet velocity and/or mass at fixed amplitude (Bogy and Talke 1984, MicroFab Technologies$_2$ 1999). The effect of the fluid acoustic speed and ink channel length on optimum droplet formation was characterised by Bogy and Talke (1984) experimentally and theoretically. It was found that the optimum pulse width (for maximum droplet velocity), time delay in meniscus motion and period of

meniscus oscillation depend linearly on the value of ink channel length divided by the acoustic speed of the ink.

There is a threshold voltage amplitude after which a droplet is formed. This is because of viscous dissipation of the compressible ink. By increasing amplitude for a fixed pulse width, the displacement of the piezoelement increases resulting in stronger pressure waves. This consequently results in a bigger oscillation of the meniscus which means that a greater volume of ink occurs in droplet ejection which could form a long tail and subsequent satellite droplets. In addition, by jetting the droplet with higher kinetic energy, the droplet velocity increases. Therefore, an increase of amplitude in drive pulse increases both the total droplet volume and droplet velocity resulting in higher impact energy on the substrate.

Acoustic resonances made by the pressure wave propagation and retraction from the nozzle results in residual pressure waves inside the ink channel after ejection of the droplet. Triggering the actuation system before full damping of the residual pressure waves can be destructive to the newly generated pressure wave. This interference can cause instability in droplet formation (MicroFab Technologies$_2$ 1999). Therefore, the residual pressure wave should be damped to have reliable jetting. This requires a time delay (actuator rest time) between two consequent pulses which totally defines the jetting frequency of a DoD mode inkjet head. Surpassing the residual pressure wave makes the time delay shorter and increases the jetting frequency resulting in higher throughput of the inkjet head and consequent productivity. A negative voltage pulse can be applied for this approach (MicroFab Technologies$_2$ 1999, Kwon and Kim 2007). A complex two-pulse waveform design can increase the jetting frequency up to three times (Kwon and Kim 2007).

2.3.4 Ink/Nozzle Plate Interactions and Jet Instabilities

After appropriate jetting parameters are set, instability in the jet array could occur due to external sources causing a trajectory error or failure of a jet (de Jong *et al.* 2006, Wijshoff 2008). One of the main sources of external instability is contamination which could affect droplet formation by disturbing the oscillating meniscus. The contamination may come from the impurities in ink which is mainly filtered before supplying to the printhead, or from the surrounding environment. In the latter case, the contamination may sit on the nozzle plate of the printhead and cause asymmetric nozzle wetting (de Jong *et al.* 2006).

Ink Layer on the Nozzle Plate

Nozzle wetting is driven by the surface tension interactions of the ink and the nozzle plate. Many printhead manufacturers develop a non-wetting nozzle plate, however, in others, formation of a thin ink layer on the nozzle plate removes the concern of asymmetric nozzle wetting. The control of the ink layer thickness could be obtained by the back pressure of the ink reservoir. This is of importance as an increase in the ink layer thickness could result in air ingestion during the meniscus oscillation (de Jong *et al.* 2006). With higher ink layer thicknesses, no droplets may be expelled due to the higher pressure wave dissipation (de Jong *et al.* 2006).

Flow on the Nozzle Plate

The flow of the ink layer on the nozzle plate induced by a single nozzle actuation in a piezoelectric DoD printhead was studied by Beulen *et al.* (2007) and de Jong *et al.* (2007). In their study, some excess ink including tracer particles was placed on the nozzle plate around the actuating nozzle and particle tracking was used to visualise

the flow motion on the nozzle plate. It was found that the particles were attracted towards the actuating nozzles during jetting.

Two main origins of flow motion were identified as the meniscus oscillation and air motion induced by ejected droplets (Beulen *et al.* 2007). By applying jetting voltages low enough to have meniscus oscillation without expelling a droplet, fluid flow around the actuating nozzle was observed which showed the role of meniscus oscillation as the origin of the flow on the nozzle plate. The flow pattern was found to originate from a gradient in the surface tension of the ink across the thickness of the ink layer (de Jong *et al.* 2007).

Air Ingestion during Meniscus Oscillation

Air bubble entrapment during jetting is another source of jet instability which is initiated during meniscus oscillation (de Jong *et al.* 2006, Kwon 2009). After droplet break up from the nozzle, the consequent suction of the meniscus into the nozzle due to the channel contraction could entrap an air bubble. This was demonstrated by de Jong *et al.* (2006) for a single nozzle in a piezoelectric DoD printhead where the air ingestion could be triggered by incorrect ink layer thickness and also contamination. In the latter, contamination could be attracted to the actuating nozzle by the flow on the nozzle plate as discussed above and then trigger the air bubble entrapment during meniscus oscillation (Beulen *et al.* 2007). After hundreds of droplets were expelled, repetition of the air ingestion process could increase the bubble size as shown schematically in Figure 2-13. With a certain bubble size, the pressure wave (from the actuation) was dissipated too much when passing through the entrapped air bubble and could not oscillate the meniscus adequately resulting in the jet failure (Kim *et al.* 2009).

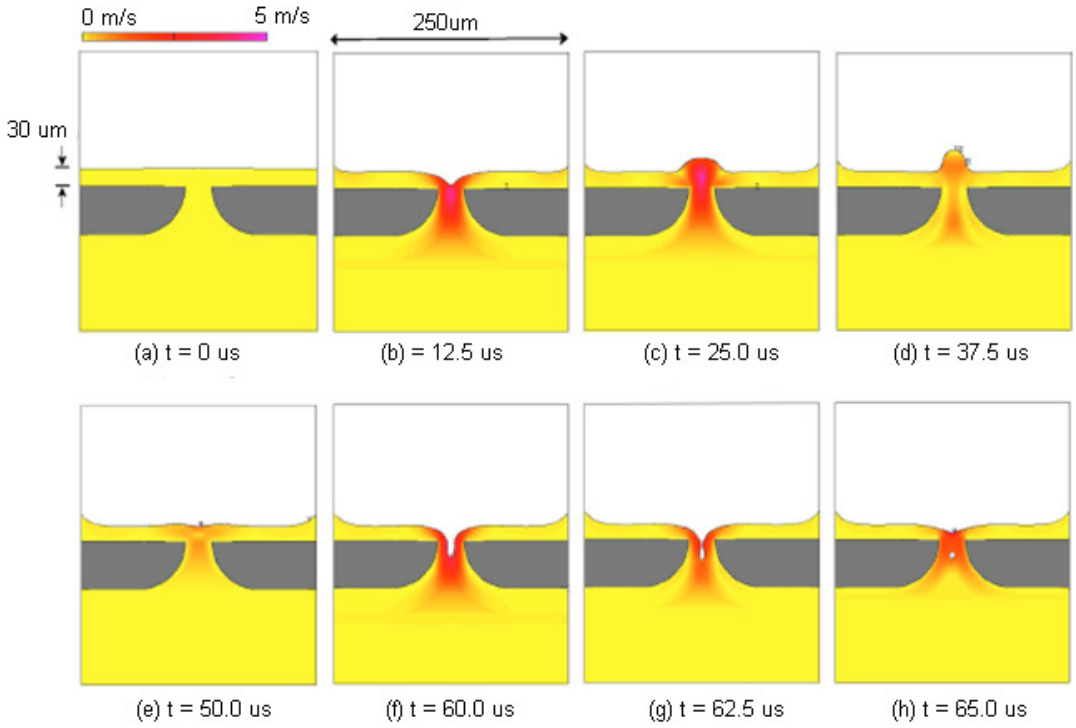

Figure 2-13 Modelling of air ingestion during meniscus oscillation in a DoD inkjet printhead (de Jong *et al.* 2006)

2.3.5 Deposition of Droplets

In inkjet-based manufacturing processes, it is important to understand the interaction between the droplets and the surface. However, the interaction includes a number of issues such as mechanical deformation as well as heat transfer or phase change which provide challenging on-going aspects of research in understanding the whole phenomena.

Droplet Impact Phenomena

Frohn and Roth (2000) and also Rein (2002) reviewed the extensive literature published on the impact behaviour of droplets on different static surfaces. More recently, Yarin (2006) reported that according to a droplet's physical properties and

the surface conditions, it may stick to the surface, bounce off or splash and split into smaller droplets as a general classification of the impact behaviour. In the case of a stationary surface, a droplet will impact and spread radially to form a liquid layer, usually known as *lamella*. Further phenomena after spreading depends on the physical and kinematic properties of the droplet mainly expressed by the dimensionless numbers of Weber (We), Reynolds (Re) and Ohnesorge (Oh) (Yarin 2006).

Droplet Impact and Mixing onto Liquid Surface

Impact of droplets onto different liquid surfaces (deep, shallow, similar and non-similar, etc.) have been researched (Rein 2002, Yarin 2006) and interactions were classified into floating, bouncing, coalescence and splashing as shown schematically in Figure 2-14 (Rein 1993). The latter two are the most common reported in the literature. With coalescence, a drop merges smoothly into the liquid surface without disturbing the surface and forms a vortex ring during penetration (Rein 1993). In contrast, splashing droplets produce a hollow sheet of the target liquid on the surface similar to a *crown* with secondary droplets upon impact (Rein 1993). To avoid splashing behaviour, the droplet kinetics should be lower than a threshold which has been formulated based on dimensionless numbers (Yarin 2006).

The vortex formation of impinging droplets into liquid surfaces has been the interest of scientists since the 1850s (Rein 1993). Visualisation of the vortex formation during droplet coalescence was reported by Anilkumar *et al.* (1991) for mixing of two drops and also for mixing of an impinging drop onto a liquid surface. During droplet penetration upon impact, the challenge between the droplet kinetics and the shear viscosity of the target liquid results in the vortex ring formation and the consequent

mixing (Rein 1993). The penetration depth could be greater than the size of the droplet diameter depending on the droplet kinetics (Anilkumar *et al.* 1991). Recent studies of droplet impact onto liquid films with different depths were reported by Pan and Law (2007) and Pan *et al.* (2008).

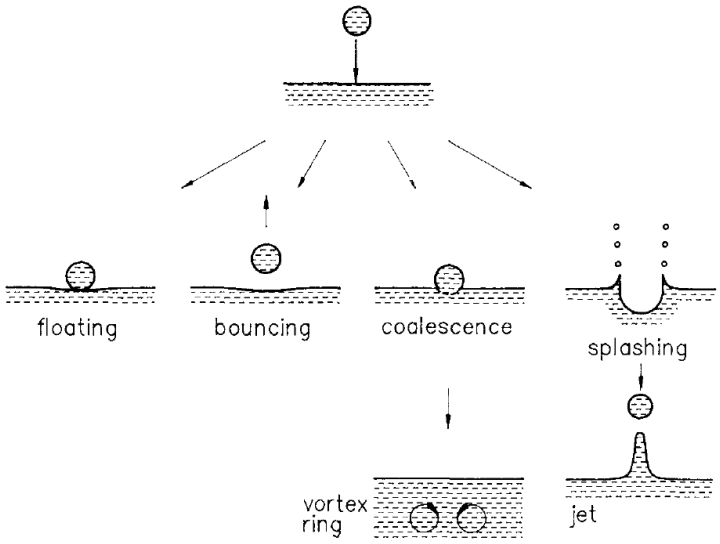

Figure 2-14 Droplet impact behaviour onto a liquid surface (Rein 1993)

Droplet Impact onto a Solid Moving Surface

Despite the many papers published for the case of droplet impact onto a stationary surface, few papers have reported the impact behaviour in the case of a moving surface. Mundo *et al.* (1995) studied droplet impact on a rotating dry disc to find the spreading–splashing threshold in correlation with different dimensionless numbers. Although there are a number of papers on the angled impingement (oblique impact) of a single aqueous droplet onto a surface (Leneweit *et al.* 2005, Okawa *et al.* 2008), there is little information on the independent effect of surface velocity. Courbin *et al.* (2006) showed qualitatively how the impact behaviour of individual droplets is affected by the surface motion where the spreading was shown to be asymmetric. All of these studies were accomplished with liquids having a viscosity lower than 3

mPa.s. There is a lack of literature on droplet train impact behaviour onto a moving surface, especially in applications where functional materials with higher viscosities are used.

In a jetting-based additive manufacturing process, the impact behaviour at the front of the bead being deposited by the droplet train and the surface motion is of importance for final layer geometry and surface finish. The bead front advances on the surface and it is of interest to study the formation of instabilities upon the advancing front. This was studied by Fathi *et al.* (2010) by investigating the impact behaviour of a train of micron size droplets of a bio-degradable resin solution. Deposition was undertaken using a continuous-mode inkjet printhead at various frequencies onto a glass surface with different linear velocities. The study categorised regimes of droplet impact at the advancing front of a bead being formed. Formation of large waves due to improperly set (unmatched) jetting frequency and surface velocity were observed and characterised at the advancing bead front. This could affect the surface of a deposited layer and after adding several layers, the surface could be bumpy affecting the fabricated part's quality and lead to a deterioration of the outer geometry.

Surface Characteristics

The droplet spreading behaviour depends on the droplet characteristics as well as the impinged surface. The characteristics of the surface such as surface energy, roughness and temperature can vary the impact behaviour of the droplets (Yarin 2006). For instance, the surface roughness could decrease the kinetic energy of the spreading droplet and subsequently result in a smaller diameter lamella compared with a polished surface (Hsiao *et al.* 2006). It was also shown that with a molten

metal droplet impinging onto a rough surface the possibility of droplet bouncing would be increased (Hsiao *et al.* 2006).

Surface energy and temperature interact during droplet spreading. Increasing the surface temperature could decrease the surface energy and consequently increase the wettability of the surface (due to lower contact angle). On the other hand, bouncing-off of a droplet could occur at surface temperatures higher than the Leidenfrost temperature where the surface temperature is much higher than the liquid's boiling temperature. This could form a vapour cushion between the spreading droplet and the surface as a result of very fast evaporation of the liquid droplet surface (Frohn and Roth 2000).

Stability of Beads

The deposition of a train of droplets results in formation of separate droplets or a continuous bead depending on the relative printhead/surface speed. This depends on the droplet and surface characteristics and also impingement frequency (Derby 2010). The droplet spacing will define whether two droplets overlap and consequently coalesce. The contact angle has a considerable importance in the stability of the bead (Davis 1980, Schiaffino and Sonin 1997, Duineveld 2003). Early analytical study of the bead stability was reported by Davis (1980). Schiaffino and Sonin (1997) investigated Davis's predictions experimentally for printed molten wax beads. Duineveld (2003) studied the bead stability to propose prediction models of bead instabilities based on process parameters. Figure 2-15 shows different behaviours during bead formation. The optimum spacing should be set depending on the printing material and process parameters.

Research on this area is still ongoing to define the appropriate deposition conditions for bead stability due to its critical role in the development of inkjet-based manufacturing processes (Derby 2010). A recent study was reported by Stringer and Derby (2010) who proposed a bead stability window for printing a nano-particulate ink system as a function of printhead/substrate relative velocity, droplet spacing and the bead contact angle.

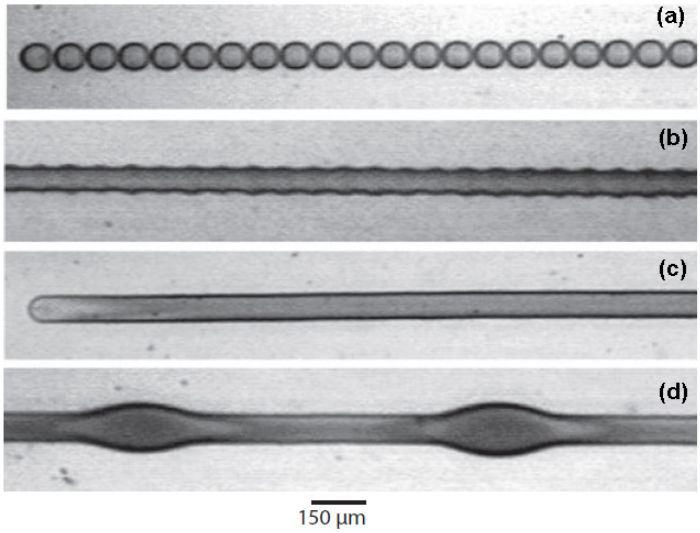

Figure 2-15 Deposited bead behaviours: (a) individual drops, (b) scalloped, (c) uniform, and (d) bulging. Drop spacing decreases from top to bottom (Soltman and Subramanian 2008)

2.4 Anionic Polymerisation of Caprolactam

Various methods have been described for the polymerisation of caprolactam among which anionic polymerisation provides the possibility of producing polymers with a well defined structure and the desired molecular weight distribution (Kohan 1995). This section introduces briefly the materials, processes and some recent research relevant to anionic polymerisation of caprolactam and its use in additive manufacturing. Comprehensive information and a detailed literature review on the

chemistry, kinetics and process parameters of anionic polymerisation can be found in the literature (Frunze *et al.* 1979, Kohan 1995, Khodabakhshi 2011).

2.4.1 Nylon 6

DuPont patented anionic polymerisation of caprolactam in 1939 as a process for producing high monomer conversions in a short reaction time (Hanford and Joyce 1948). The commercialised polymer was known as *Nylon* by DuPont in 1948 for moulding and extrusion processes which was later known as Nylon 6 or Polyamide 6 (PA6). Shortly after, by introducing a nylon suitable for spinning and drawing to produce nylon fibre, a fast growth in its production occurred (Kohan 1995).

Nylon 6 produced by anionic polymerisation (AP-Nylon) is a semi-crystalline polymer, suitable for many engineering applications as it provides a combination of high mechanical strength, heat resistance and chemical stability (Kohan 1995). It is processed by different extrusion and moulding techniques for a wide variety of applications such as moulded automotive components, extruded tubing and wire coating, and rotationally moulded tanks.

2.4.2 Caprolactam and Anionic Polymerisation

Nylon 6 is made from caprolactam ($C_6H_{11}NO$) which has six carbon atoms as a ring. It is white and solid at room temperature and melts at about 68 ℃. When molten, it is transparent and has a dynamic viscosity of lower than 10 mPa.s at 80℃ (Ritz *et al.* 2005). Detailed characteristics and production methods of caprolactam were reported by Ritz *et al.* (2005).

The synthesis method is called anionic due to the use of an anion to initiate the caprolactam ring opening and the consequent polymerisation. Production of nylon 6,

however, for non-engineering applications (mainly fibre industry) is dominated by the condensation polymerisation method which is used for large scale production of low molecular weight nylon (Kohan 1995). Therefore, the term AP-Nylon avoids such confusion between different nylon 6 grades as it is the nylon purely produced by anionic polymerisation.

Frunze *et al.* (1979) shows that the anionic polymerisation of caprolactam has been undertaken in presence of activator and catalyst compounds such as N-acetylcaprolactam (N-AcCL) and Sodium Hydrate (NaH). It was reported as early as 1970 that a reaction temperature of 130°C with such a combination resulted in a reaction time of over an hour whereas at 180°C, AP-Nylon was reacted with a high monomer conversion within less than 10 min (Frunze *et al.* 1979).

Anionic polymerisation takes place in three stages when mixing the reactants (compounds) and caprolactam at elevated temperatures. First, a catalyst reacts with caprolactam rapidly to form a catalyst complex (caprolactamate). In the second stage, the catalyst complex attacks the monomers with the aid of an activator complex to initiate the polymerisation. Finally, this procedure continues to grow the polymer chains. The process could be undertaken over a wide temperature range from about 130 to 180°C, varying the polymerisation time and monomer conversion rate considerably (Frunze *et al.* 1979).

Figure 2-16 shows the chemical structure of caprolactam, activator and catalysts complexes commonly used for synthesis of nylon 6 via anionic polymerisation. N-AcCL is the most commonly used activator complex. The most common catalyst compound is sodium hydrate (NaH). However, the use of magnesium bromide ($MgBr_2$) was also reported (Udipi *et al.* 1997) due to its higher stability in relation to the environment. A fast reaction within less than two minutes was also reported

using caprolactam magnesium bromide as the catalyst complex (Dave *et al.*[1] 1997). In addition, when increasing the reaction temperature to over 160℃, the reaction time decreased to less than 1 minute during which the viscosity of the polymer exceeded 10^3 mPa.s (Dave *et al.*[1&2] 1997).

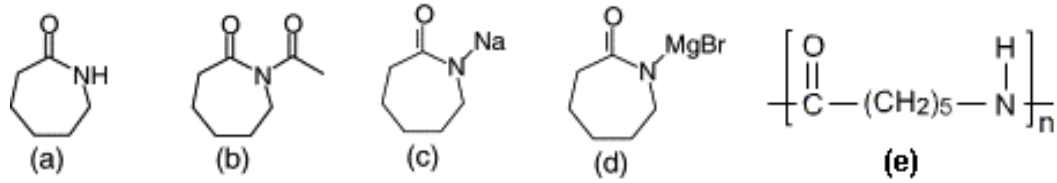

Figure 2-16 Chemical structure of (a) caprolactam, (b) N-acetylcaprolactam (N-AcCL), (c) sodium caprolactamate (NaCL), (d) caprolactam magnesium bromide (CLMgBr) and (e) Nylon 6

2.4.3 Cast Nylon Process

Reaction Injection Moulding (RIM) is a family of processes developed for two-part reactive polymers such as polyurethanes, polyesters, epoxies and nylons. The RIM process to produce moulded nylon 6 parts via anionic polymerisation is known as *Cast Nylon* and gives the highest mechanical properties in the group of reactive polymers used for RIM (Kohan 1995). The process involves supplying two reactive mixtures in the molten state to a mixer just before injection into a mould as shown schematically in Figure 2-17. Polymerisation occurs inside the mould which is pre-heated at the required reaction temperature. This solidifies the part before de-moulding after about 10 min (to avoid part warpage by early de-moulding) (Crawford 1998).

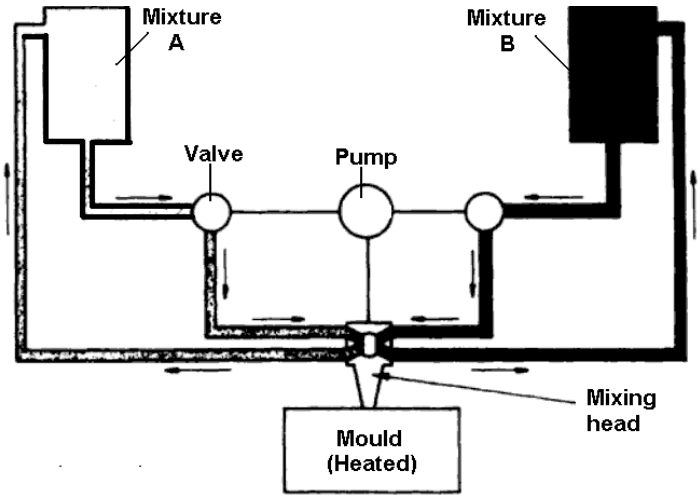

Figure 2-17 Schematic of reaction injection moulding process (Crawford 1998)

Some companies such as Brueggemann Chemical GmbH develop two-part reactive mixtures for the cast nylon process. Sold in form of a highly concentrated master-batch, the concentrate mixtures are diluted with molten caprolactam before the moulding process. This process is used for producing semi-finished and finished moulded parts for customers across different industries such as aerospace, transport, mining, agriculture, medical and packaging. Specific examples of cast nylon products are from small gears, pulleys and rollers for material transport to large parts such as support legs for machines, levelling plates for building machinery, and gear blanks up to 1100 kg (Ensinger 2010). Table 2-1 lists some of the mechanical and thermal properties of a commercially available cast nylon.

Mechanical			Thermal		
Tensile strength at yield	84	MPa	Crystalline melting point	> 216	°C
Elongation at break	40	%	Glass transition temperature	40	°C
Modulus of elasticity in tension	3400	MPa	Max. service temperature		
Hardness	80	Shore D	short term	130	°C
Impact strength 23º C (Charpy)	7.3	KJ/m²	long term	100	°C
Co-efficient of friction p = 0,05 N/mm²v=0,6 m/s on steel, hardened and ground	0,12		Thermal conductivity (23º C)	0,24	W/(K·m)
Wear p = 0,05 N/mm²v=0,6 m/s on steel, hardened and ground	< 0,1	µm/km	Coefficient of thermal expansion (23-55ºC)	9	10^{-5}1/K

Table 2-1 Typical properties of a commercial cast nylon, TECAGLIDE Green by Ensinger (2010)

2.4.4 AP-Nylon in Additive Manufacturing

AP-Nylon in Commercial Additive Manufacturing Processes

There is no known commercialised additive manufacturing process which involves the use of in-situ anionic polymerisation of caprolactam as a part of the manufacturing technique. Das *et al.* (2003) used powdered nylon 6 in a commercial SLS machine to fabricate small biomedical scaffolds. Commercial additive manufacturing processes are mainly dominated by other grades of nylons such as nylon 11 and nylon 12 using the powder-based SLS process (Gibson *et al.* 2009).

AP-Nylon in Research of Novel Additive Manufacturing Processes

Lombardi and Calvert (1999) reported an additive manufacturing approach for parts by emerging reactive extrusion and FDM processes fabricating AP-Nylon. The concept was to mix the two reactive compounds of AP-Nylon in a similar approach as RIM and then instead of injection into a heated mould, the two-part mixed component was extruded onto a heated aluminium surface to pattern a layer similar to the FDM process. By setting the substrate at 165℃, the deposited 1 mm thick

layer could obtain enough strength by initial polymerisation in air to receive the next layer in a few minutes time. A tensile test bar was formed by depositing multiple layers. The part was then placed into an oil bath at 165℃, for an additional four hours for further monomer conversion as a post-processing step. The final nylon 6 tensile test bar had mechanical properties near to bars made by the cast nylon process (Lombardi and Calvert 1999).

Despite the good mechanical properties obtained, the above approach had a number of major limitations as an additive manufacturing technique in addition to low resolution and surface finish (Lombardi and Calvert 1999). Each deposited layer required several minutes to solidify for the next layer. In addition, the number of layers that could be produced was limited due to the heating approach used for the reaction as the substrate heat eventually could not reach the top layers. This would also induce a gradual variation of the mechanical properties across the Z direction.

2.4.5 Bulk Polymerisation for Synthesis of Nylon 6

Fouchal and Dickens (2006) and then Khodabakhshi (2011) investigated various aspects of anionic polymerisation of caprolactam at Loughborough University. The aim was to investigate appropriate conditions and compositions of activator and catalyst mixtures for a fast anionic polymerisation in the presence of air which could also produce nylon 6 with sound mechanical properties. The outcome of this research could enable the concept of “Jetting of Nylon” with acceptable layer fabrication speed without the need of an inert gas.

The main process parameters investigated were the type of activator and catalyst compounds, their concentration and ratio in caprolactam, the reaction temperature and the environment. The reaction time and physical properties of the nylon

produced were investigated during and after the anionic polymerisation reaction (Khodabakhshi 2011). From the range of available activator and catalyst compounds, N-AcCL was used as the activator and Sodium Hydrate (NaH) and Ethylene Magnesium Bromide (EtMgBr) were used to synthesise two catalyst mixtures respectively as sodium caprolactamate (NaCL) and caprolactam magnesium bromide (CLMgBr) (Khodabakhshi *et al.* 2008).

An experimental setup was developed to investigate the reaction time as schematically shown in Figure 2-18. The reaction was undertaken inside a glass beaker which was placed into a thermally controlled aluminium chamber (labelled as "reactor") set at the required temperature (Fouchal and Dickens 2006). The chamber could have either a blanket of air or nitrogen, supplied from a cylinder. The glass paddle was rotated by an actuator. In addition to providing appropriate mixing, this was to monitor the voltage variation when maintaining the glass paddle rotation speed. Therefore, the melt viscosity variation made by polymerisation was monitored. After the catalyst compound was added to the molten caprolactam, monitoring started with addition of the activator compound when the reaction temperature was set at typically 150℃. Each trial produced a sample of about 30 ml. These were used for post-analysis of the physical properties. The monomer conversion, molecular weight and crystallinity of the nylon samples were analysed to investigate the optimised polymerisation conditions.

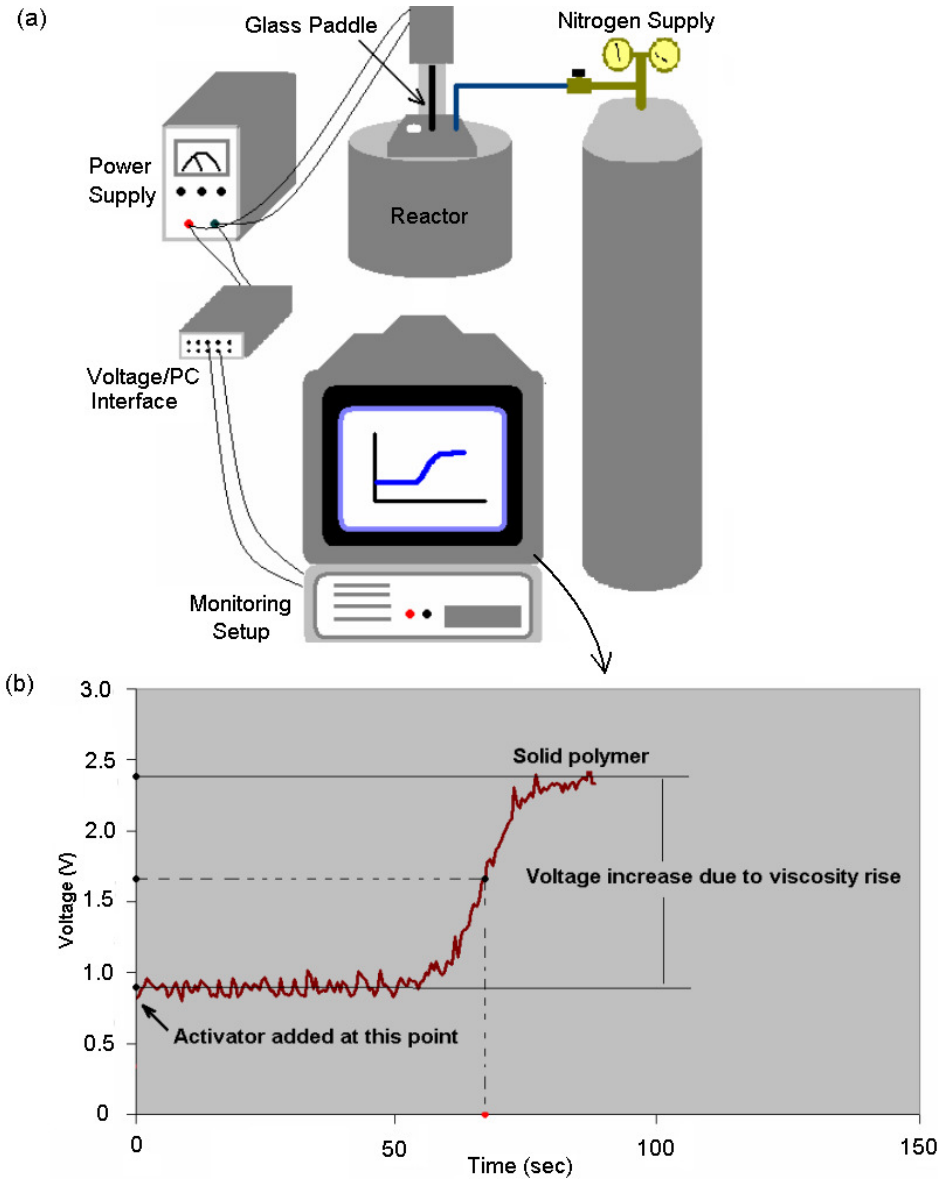

Figure 2-18 Experimental setup for research on optimising anionic polymerisation conditions of nylon 6 (Khodabakhshi *et al.* 2008)

Results showed that the influence of environment on the reaction time was considerable when using NaCL as the catalyst complex compared with CLMgBr. The reaction time in samples with CLMgBr were little influenced by the environment whereas samples with NaCL synthesised in air had much longer reaction time (Khodabakhshi 2011). Treating the nitrogen by additional chemicals (for reducing the moisture content) also shortened the reaction time when using NaCL (Khodabakhshi

2011). Table 2-2 shows typical results of the polymerised nylon when using (untreated) nitrogen. The polymerisation half-time was calculated as half the duration from onset to end of the reaction as shown in Figure 2-18.

A concentration of 10% (by weight) of both the activator and catalyst compounds and a reaction temperature of above 150℃ could provide high monomer conversion (typically above 95%) in a short period of time (Khodabakhshi 2011). The molecular weight and crystallinity were similar to commercial cast nylon when using both the catalyst systems in nitrogen. The variation in the results was much less when using nitrogen than air. The reaction time for most trials was below 2 min when using CLMgBr in air and less than 1 min in nitrogen. With NaCL though, a slower reaction occurred in both environments.

Response Prameter	Optimised Values	
	NaCL	**CLMgBr**
Reaction Half-time (sec)	30±5	11±5
Nylon Melting Point (C)	218±5	223±5
Monomer Conversion (%)	95±1	98±1
Molecular Weight	45,000±10,000	51,000±10,000

Table 2-2 Typical optimised results for anionic polymerisation of caprolactam with optimised conditions using the synthesised catalysts (NaCL and CLMgBr) and the activator (N-acetylcaprolactam) complexes (10% conc., reaction temperature: 150 to 165℃, nitrogen) (Khodabakhshi 2011)

2.5 Conclusions from the Literature Review

2.5.1 Novelty of the Research Concept

From the literature review, it was concluded that the concept of “Jetting of Nylon” was novel. In addition, few reports have been published on the concept of employing

polymerisation of a functional polymer during an additive manufacturing approach. The most relevant activities to the research concept were the reports by Uhlmann and Elsner (2005), Lombardi and Calvert (1999), and Fouchal and Dickens (2006). Although the work by Uhlmann and Elsner (2005) looked at two-part inkjet printing of reactive materials, the cross-linked polymer produced by this approach had limitations in functionality.

Although the concept of extrusion freeforming of nylon 6 (Lombardi and Calvert 1999) employed in-situ polymerisation of nylon 6, the approach had limitations such as low resolution and surface finish. In addition, premixing of the two reactive mixtures to extrude via a single nozzle could result in nozzle clogging and also the exothermic nature of the reaction could diminish the melt flow control during extrusion (Lombardi and Calvert 1999).

The work at Loughborough University on anionic polymerisation of caprolactam showed that using the correct mixtures of caprolactam, catalyst and activator and processing conditions, the solidification time of nylon 6 could be reduced to about 1 minute for large quantities (30~50 ml) (Fouchal and Dickens 2006, Khodabakhshi 2011). In addition, the physical properties of caprolactam were found to be within the range for the available inkjet printhead technologies (Fouchal and Dickens 2006). However, it was not investigated whether caprolactam mixed with a catalyst or an activator would have properties suitable for jetting.

2.5.2 Features and Challenges of the Research Concept

Developing an additive manufacturing technique capable of producing dense nylon 6 parts with high resolution would have a great commercialisation potential. Although the low viscosity of caprolactam is an advantage for deposition techniques such as

inkjet printing, it could be a drawback for techniques such as extrusion reported by Lombardi and Calvert (1999).

Researching the concept of “Jetting of Nylon” for an additive manufacturing process required overcoming several challenges. The main requirements were to investigate the possibility of jetting the two reactive mixtures and their deposition in a controlled manner so that droplets of the two mixtures could be mixed to initiate the reaction upon appropriate thermal and environmental conditions.

2.5.3 Research Objectives

This research was initiated by a list of questions as followings.

1) Were the molten caprolactam and the reactive mixtures jettable via an available ink-jet printhead? What were the parameters in terms of jettability for the mixtures and how would they affect the jetting process?
2) How reliable a jet array could be developed in terms of stability? What were the parameters affecting the jet stability? What were the jet instability mechanisms and could they be controlled?
3) What were the droplet formation characteristics when varying the jetting parameters? What would be the optimised parameters for the deposition?
4) How would droplets of the two mixtures interact with each other upon deposition?
5) Would nylon be produced and what temperatures would be required? How would the environment affect the jetting of nylon? What were the characteristics of the nylon compared with conventional cast nylon?

This research aimed to answer these questions which would contribute towards developing a new additive manufacturing process based on the concept of “Jetting of Nylon”.

Chapter 3. Methodology and Experimental Setup

3.1 Research Approach

The research stages are introduced here briefly.

Stage 1: Characterisation of materials for jetting

Pure caprolactam and a number of reactive mixtures were characterised for jetting. The physical properties of the materials, namely the surface tension, the dynamic viscosity and the particle content (just in the reactive mixtures) were investigated at different temperatures. In addition, by developing an experimental setup for jetting of nylon, the behaviour of the materials in the melt supply unit was investigated. This was to define the appropriate mixture compositions and supply conditions for jetting.

Stage 2: Jetting of caprolactam and the reactive mixtures

This stage was to investigate jetting of molten caprolactam and the reactive mixtures with a single nozzle and an array of nozzles. It began with jetting of pure caprolactam to obtain an understanding of the role and the range of parameters affecting the jetting behaviour. The process window for jet stability was the main focus. Investigation of the instabilities and their origin were undertaken. Different phenomena associated with jet instability and failure of jets were investigated at this stage.

Stage 3: Droplet formation characterisation

The droplet formation characterisation was to achieve the highest consistency and optimal droplet condition for deposition. The focus was to study the droplet formation process including the meniscus oscillation, droplet shape evolution after ejection and the kinetics of droplets for pure caprolactam and the reactive mixtures within the process parameter window obtained in stage 2. High speed imaging with microscopy was used to observe droplet/nozzle plate interaction and droplet characteristics. Image analysis was undertaken to extract information of different phenomena associated during droplet formation. This stage was to help further narrow down the jetting parameters for the deposition stage.

Stage 4: Deposition of materials

This stage was initially to research whether the range of the jetting parameters recommended in stage 3 were appropriate in terms of the deposition aspects. The interaction between the droplets and the surface during deposition was one of the criteria at this stage which employed high speed imaging and image analysis. This could assist in finding appropriate conditions for the reaction stage.

Mixing of droplets was another aspect of the deposition stage. This could define whether the droplets of the two mixtures were mixed upon deposition to start the reaction with the appropriate thermal and environmental conditions. Dye tracing and in-situ fluorescent microscopy was used as a tool for observing this.

Stage 5: Drop-on-drop reaction

Reaction of nylon was investigated when droplets of the two reactive mixtures were deposited on top of each other. The heating approach was developed and assessed

for reaction temperature and also evaporation. After drop-on-drop deposition of samples, they were exposed to different heating conditions. Using thermal analysis, the outcome of the reaction was analysed.

3.2 Design of Experimental Setup

The physical properties of caprolactam reported in literature were considered as the starting point to find the appropriate printhead and the design of the experimental setup.

3.2.1 Jetting Materials

Caprolactam (produced by Sigma Aldrich GmbH) was provided as granules in sealed containers. It is white in the solid state but melts at 68°C in atmosphere and is colourless when molten (Ritz *et al.* 2005). The dynamic viscosity of molten caprolactam was measured over a range of temperatures (Fouchal and Dickens 2006). Figure 3-1 shows the dynamic viscosity of caprolactam. It decreases rapidly with an increase in temperature. Therefore, with the high shear rates of jetting in the order of 10^4 (de Gans *et al.* 2004), the caprolactam had a viscosity below 10 mPa.s at temperatures higher than 75°C.

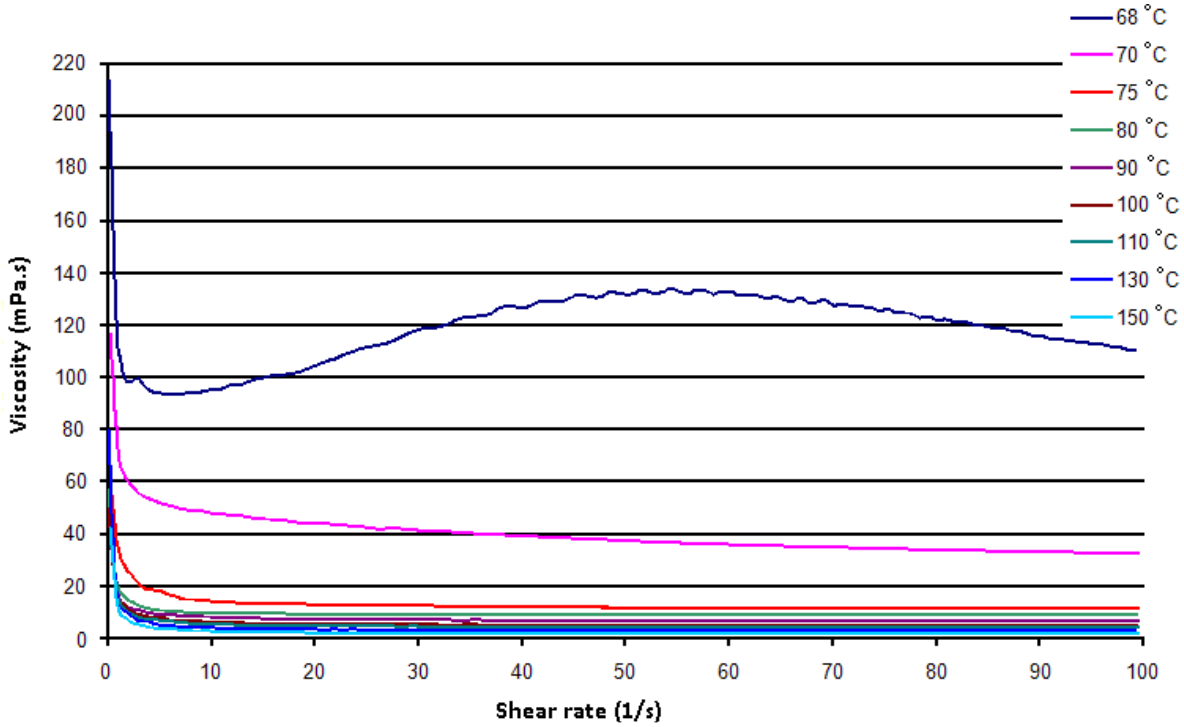

Figure 3-1 Viscosity versus shear rate at different temperatures for molten caprolactam (Fouchal and Dickens 2006)

3.2.2 Jetting Device

From observation of the characteristics of molten caprolactam and reviewing the available jetting technologies, it was expected that an industrial printhead could be employed in the jetting system if an operating temperature above 75℃ could be tolerated. A Xaar 126/80 drop-on-demand (DoD) printhead (Figure 3-2) was provided by Xaar Plc. (Cambridge, UK) for this research. With 126 nozzles (50 µm diameter) in an array of 17.2 mm width, the printhead was capable of jetting with a maximum frequency of 5.2 kHz. Table 3-1 presents the specifications of the printhead.

Figure 3-2 Printhead Xaar 126/80 (Xaar plc 2008)

Physical Attributes	Xaar 126/80	Unit
Active nozzles	126	-
Print swathe width	17.2	mm
Nozzle pitch	137.3	μm
Nozzle density (nozzles per inch)	185	npi
Printhead weight (dry)	22	g
Dimensions (WxDxH)	45 x 43 x 11.8	mm
Drop volume*	80	pl
Typical firing frequency*	5.2	kHz

* Depending on the ink used and jetting parameters

Table 3-1 Specification of the Xaar 126/80 printhead (Xaar plc 2008)

The Xaar 126/80 could jet non-aqueous fluids with a viscosity between 8 to 13 mPa.s, and the printhead's nozzle plate had a surface tension of 40 mN/m (reported by the manufacturer). Operating temperatures as high as 85℃ could be used with the printhead. However, from the physical properties of the molten caprolactam, a jetting temperature of 80℃ seemed to be reasonable to use as the viscosity at this temperature would be low enough.

Operation of the printhead was undertaken through a controller known as a XUSB (by the manufacturer). Figure 3-3 shows how the printhead was connected to its peripherals. The XUSB was powered by a power supply unit (PSU) and controlled by

software (XUSB software from Xaar Plc) on a windows based computer. A head personality card (HPC) transferred the signals generated from the XUSB to the printhead. A single nozzle or an array of nozzles could be actuated by the software.

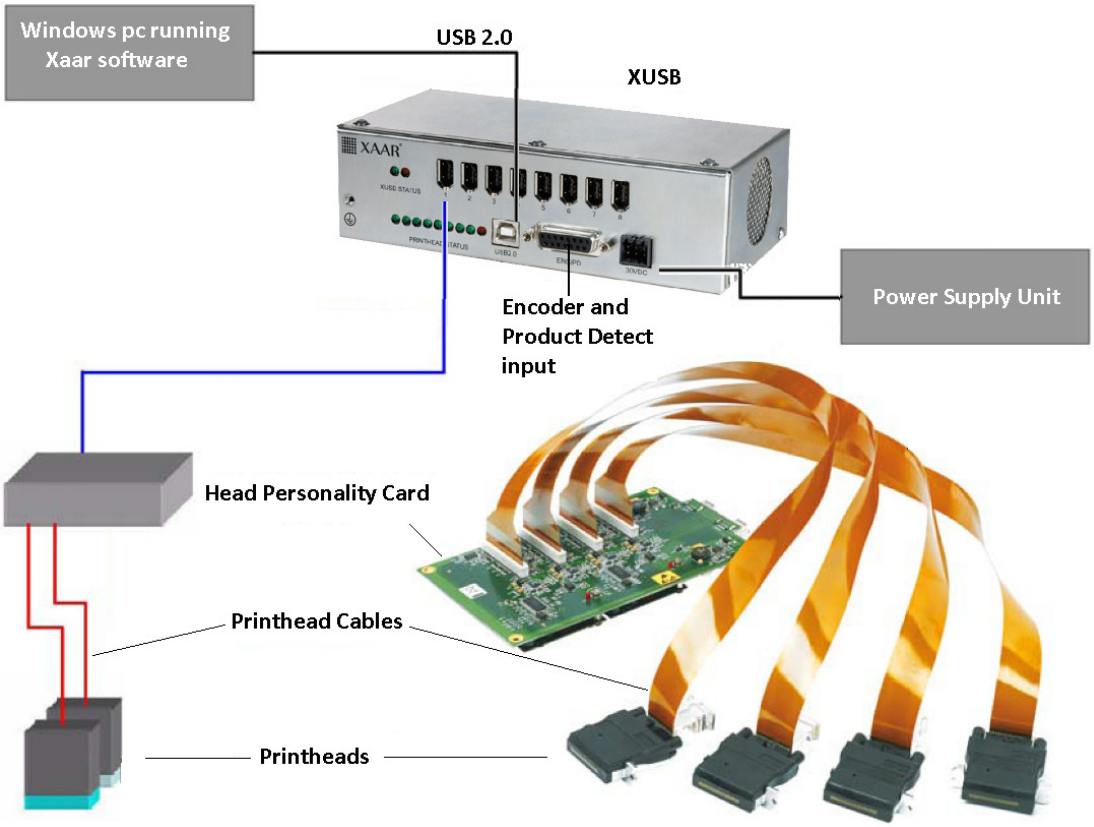

Figure 3-3 Setup for Xaar 126/80 printhead

3.2.3 Process Design Considerations

Many features were taken into account in designing the experimental setup. These were mapped as shown in Figure 3-4 and covered four main aspects of jetting-based process development.

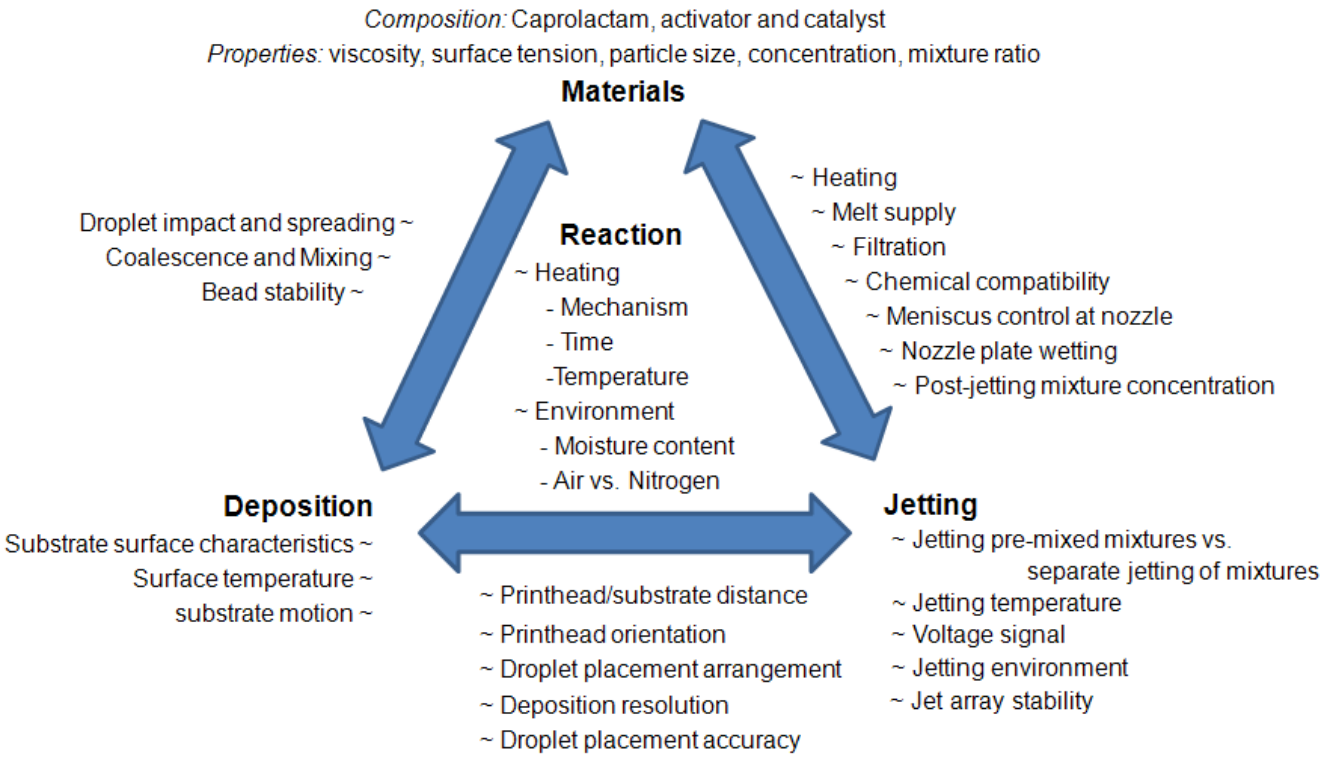

Figure 3-4 Design considerations for the experimental setup

The result of parallel research by Khodabakhshi (2011) showed that the two mixtures when brought together, could react at temperatures as low as 80℃ and form nylon. This meant that pre-mixing of the reactive materials for jetting via one single printhead could result in blocking of that printhead. Therefore, the approach was to jet the reactive mixtures separately via two separate but identical jetting assemblies. The mixtures could be cast in bar cartridges similar to a printer ink cartridge to insert into a melt supply unit equipped with a filtration unit. The melt supply unit could control the flow and temperature of the mixtures for jetting in each of the jetting assemblies. A pneumatic system could control the flow of melt in the melt supply system and form the appropriate meniscus at the nozzles for droplet generation.

By generating jet(s) of the two reactive mixtures, they could be deposited on top of each other, onto a heated surface to spread and mix. This could be achieved via synchronisation of the deposition using a linear motion system and a heated

substrate. Moving the deposited mixtures under a reaction unit, they could receive further heat to control the reaction. Upon reaction, monomer conversion was expected to occur to form nylon.

3.3 Jetting Assemblies

The jetting assembly was the main part of the experimental setup and the thermal and fluidic control over the melt was key for a consistent and reliable supply for jetting.

3.3.1 Printhead-Caprolactam Compatibility

The nozzle plate of the printhead was made from a heat resistant polyimide thin film (Upilex-S from UBE Industries Ltd.) that was 50 µm thick. Any change in the nozzle geometry could cause inconsistency in droplet separation from the nozzle plate and consequent problems such as droplet placement inaccuracy. Therefore, it was important to know if the thin film swelled in the presence of caprolactam.

Six samples of the film (10 mm x 10 mm) (supplied from Xaar plc) were placed in separate glass tubes filled with granulated solid caprolactam. After 5 minutes of placing the tubes inside an oven at 90^{o}C, the samples became immersed in molten caprolactam. Samples were removed from the oven after 1, 3, 8, 24, 64, and 104 hours and then washed with water to remove caprolactam from the surface. After drying, each sample was observed under an optical microscope to detect any microscopic change on the surface and the edges. No geometrical and dimensional changes were found from swelling or surface deterioration in all samples. This showed that molten caprolactam would not affect the nozzles in continuous operation of the printhead.

3.3.2 Melt Supply Unit

For each mixture, a melt supply unit was developed as a part of the jetting assembly. Figure 3-5 shows the unit attached to the printhead. It consisted of an aluminium syringe with 25 ml capacity, a flexible rope heater and a filtration unit attached to the syringe with a luer type connection. The rope heater was wrapped spirally around the syringe and the filtration unit, and was insulated with cotton in a cylindrical polyacrylic holder. The connection on top of the syringe cap, as shown in Figure 3-5, allowed a pneumatic tube to provide pressure or vacuum for melt flow control, and so the cap was sealed to the syringe by an O-ring. Figure 3-6 shows the contents of the unit and Figure 3-7 shows the unit when installed in the setup. Thermal control of the rope heater was achieved via a controller and a T-type thermocouple attached to the syringe at its conical end. The unit was also equipped with a cut-off switch attached to the syringe to cut the main power supply in case an unpredicted fault in the heating system occurred and the temperature rose above 100^{o}C.

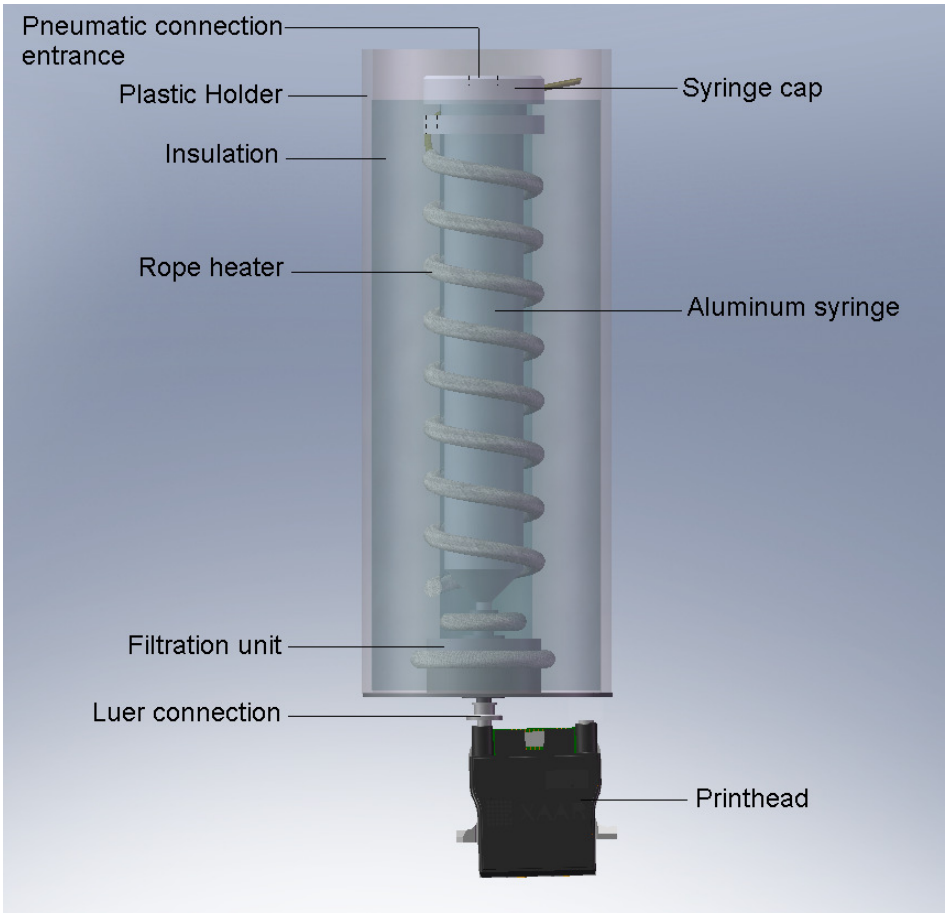

Figure 3-5 Melt supply unit with luer connection joined to the printhead

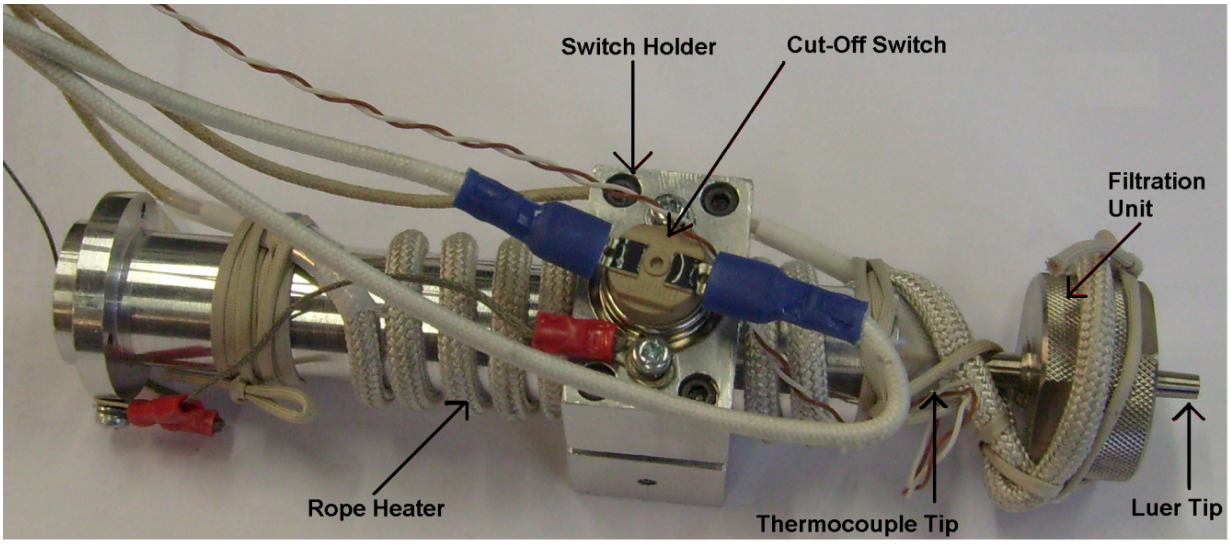

Figure 3-6 Contents of the melt supply unit

(a)  (b) 

Figure 3-7 Melt supply unit attached to a Z-stage linear motion slide (a) without insulation, (b) insulated with pneumatic connections at the top

The filtration unit was capable of operating at temperatures as high as 250℃. It consisted of a metallic holder (Microsyringe Filter Holder from Millipore Corp.) and a 25 mm diameter filter membrane (Mitex from Millipore Corp.). A polytetrafluoroethylene (PTFE) membrane with a pore size of 5 µm (Mitex Membrane Filter, LCWP02500, from Millipore Corp.) was used. The filter made of PTFE was to stop contamination entering the printhead which would otherwise clog the nozzles and diminish the jetting consistency and subsequent deposition reliability. There was also an internal filter within the printhead with a 5 µm pore size.

3.3.3 Heating the Printheads

Each printhead was heated by two 25 watt (W) resistors (HS25 from Arcol UK Ltd.) attached via two aluminium holders. Figure 3-8 shows the heating assembly for one of the printheads. The resistor holders were designed to be assembled with the printhead so that their bottom surface was level with the nozzle plate. This was to

ensure an even heat transfer from the resistors to the printhead. In addition, a T-type thermocouple (RS Components Ltd.) was embedded inside the holders near the printhead's nozzle plate to feedback the temperature for resistor control.

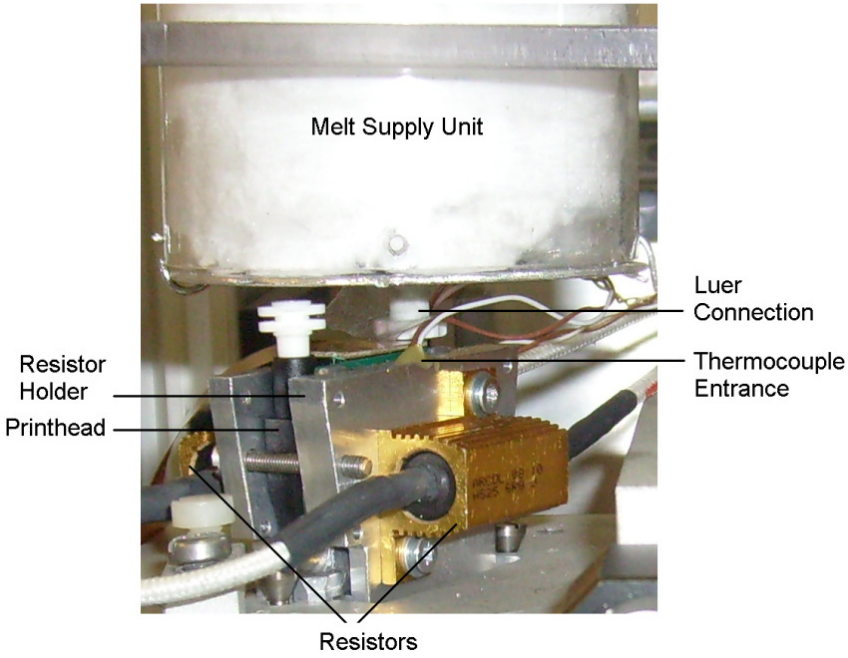

Figure 3-8 Heating assembly for the printhead

3.3.4 Jetting Assemblies Adjustment Mechanism

A fixture was developed to hold the jetting assembly and give adjustment to the printheads. Figure 3-9 details the adjustment mechanism of the fixture. The fixture was attached to the Z-stage of the motion system via a work holder. The adjustment was applied using a micrometer with 1 µm accuracy to set the relative linear position of the printheads as shown in Figure 3-9. To set the position of both printheads relative to the substrate, the mini-adjustment facility on the Z-stage, was used.

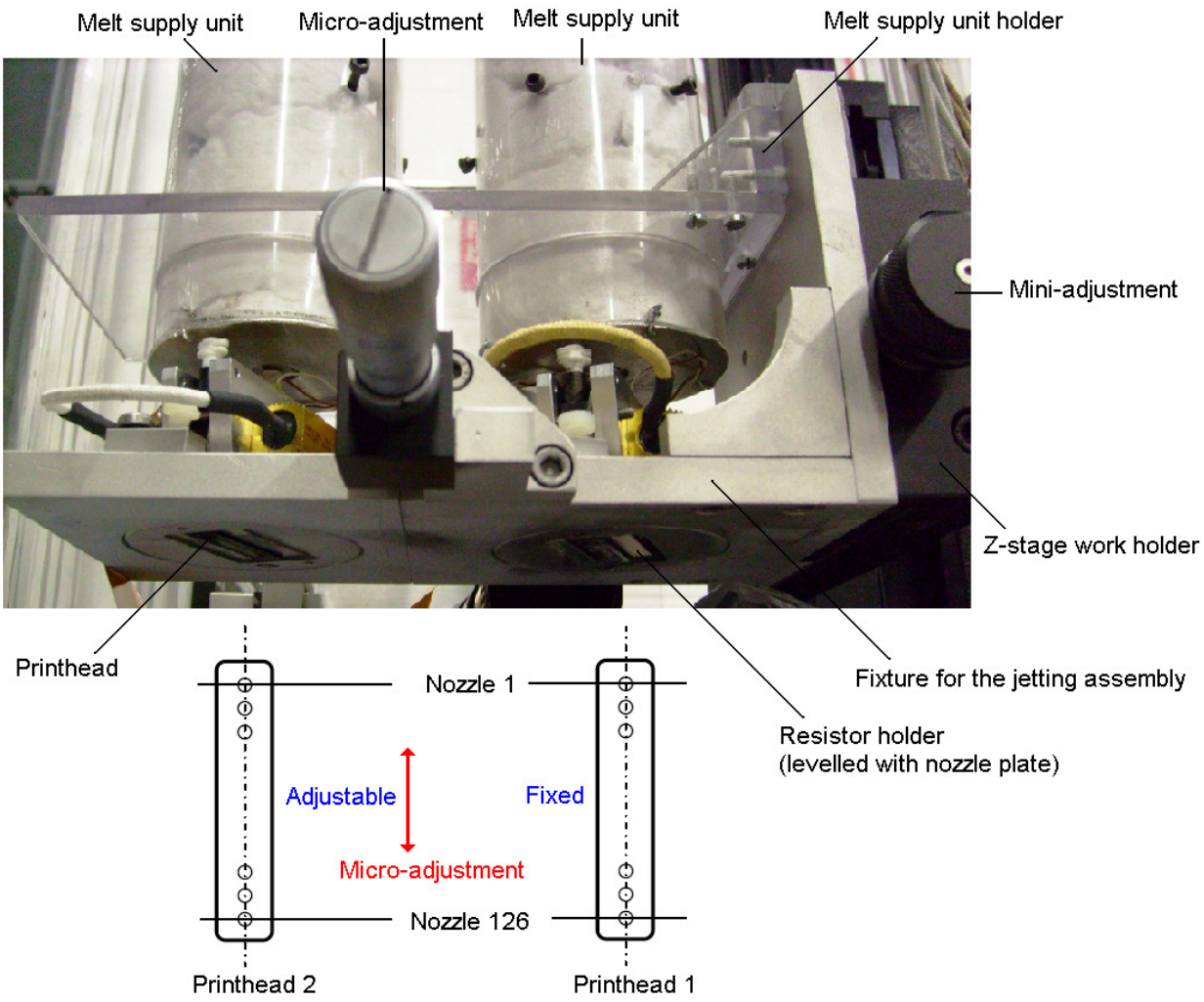

Figure 3-9 Fixture mechanism for printheads adjustment

Figure 3-10 shows the adjustment mechanism to vary the printhead nozzle array orientation, relative to the substrate motion (swathe path). This gave the possibility to set the deposition resolution of the printheads. Figure 3-10(b) shows schematically how the deposition resolution increased from 185 to 200 droplets per inch (dpi).

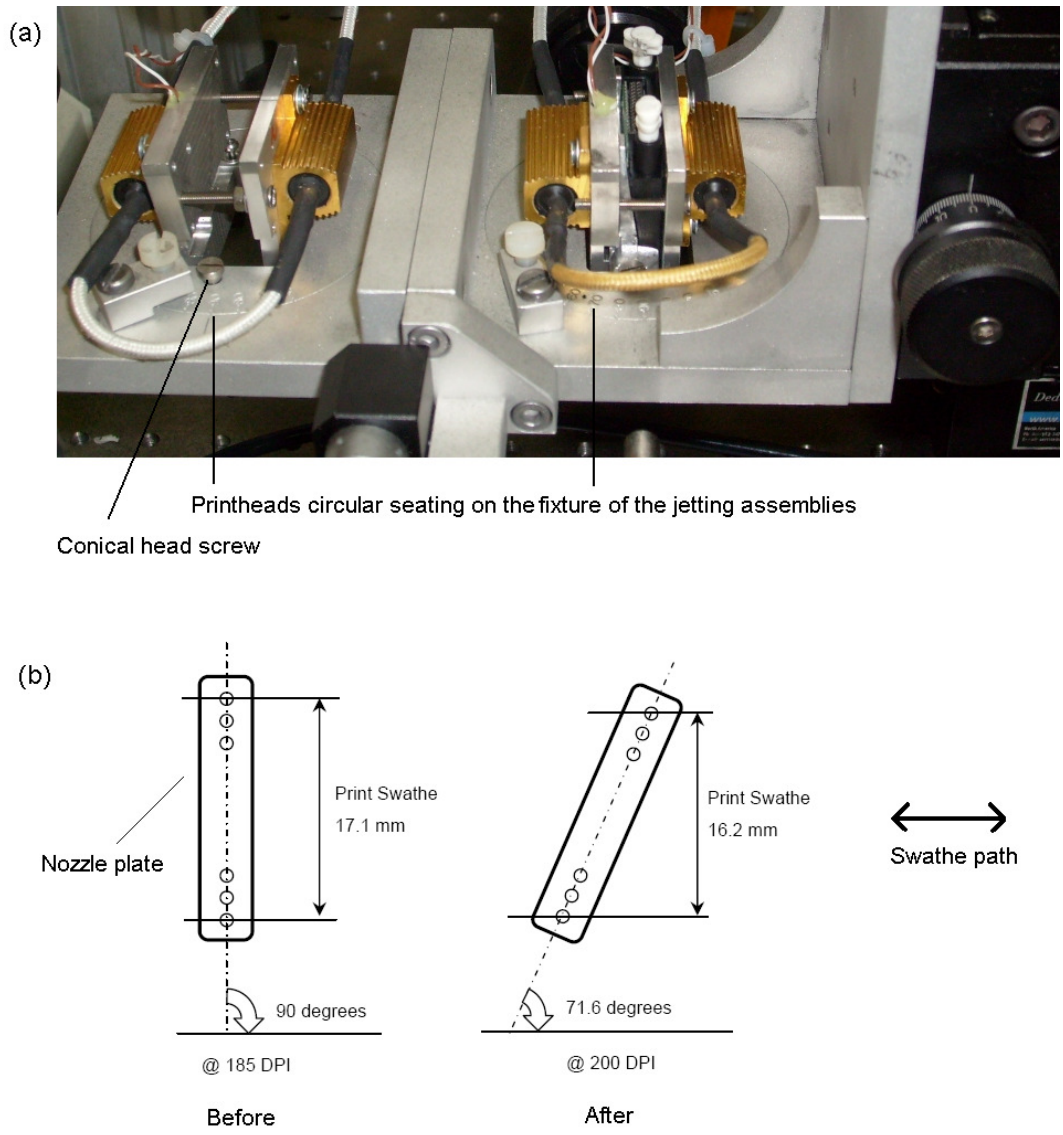

Figure 3-10 Deposition resolution adjustment by orienting the printhead, (a) Circular seating design, (b) Schematic view of nozzle plate oriented for higher resolution

3.4 Melt Supply for Jetting

3.4.1 Solid Mixture Cartridge for Jetting

The jetting materials were cast into an aluminium mould to form cartridges which would fit into the syringe of the melt supply unit. Figure 3-11 shows the cartridges that were cast in the aluminium mould, packed and sealed inside a plastic bag under vacuum to prevent moisture absorption.

Figure 3-11 Cartridges of the jetting materials

3.4.2 Thermal Management in the Jetting Assemblies

Four controlling channels were used for thermal management of the jetting assemblies by a 7-channel controller (CN1507-TC1 by Omega Engineering Inc.). The feedback was via the T-type thermocouples installed in different positions of the assemblies. A thermistor was also embedded inside the printhead (by manufacturer) with its reading displayed by the XUSB software on the computer.

Figure 3-12 shows the positions for the temperature measurements. Position 1 monitored the temperature at the syringe nozzle which was used to control the power given to the rope heater. In position 2, the thermocouple was attached to the exterior of the plastic luer connection joining the melt supply unit to the printhead. With no heating source allocated for this location, a short connection was key for a safe (hot) delivery of the melt mixture to the printhead, otherwise it could freeze and block the melt supply. The temperature inside the printhead could be read via the thermistor in position 3. The XUSB software used the temperature reading of

position 3 for adjusting the voltage signals to the printhead. Varying the temperature could vary the melt viscosity, therefore, the amplitude of the voltage signal was adjusted automatically by the software to keep the jetting conditions set to the melt viscosity. In position 4, a thermocouple was embedded inside the aluminium resistor holder. This position was about 2 mm from the nozzle plate, which was the closest possible for controlling the resistors heating the printheads.

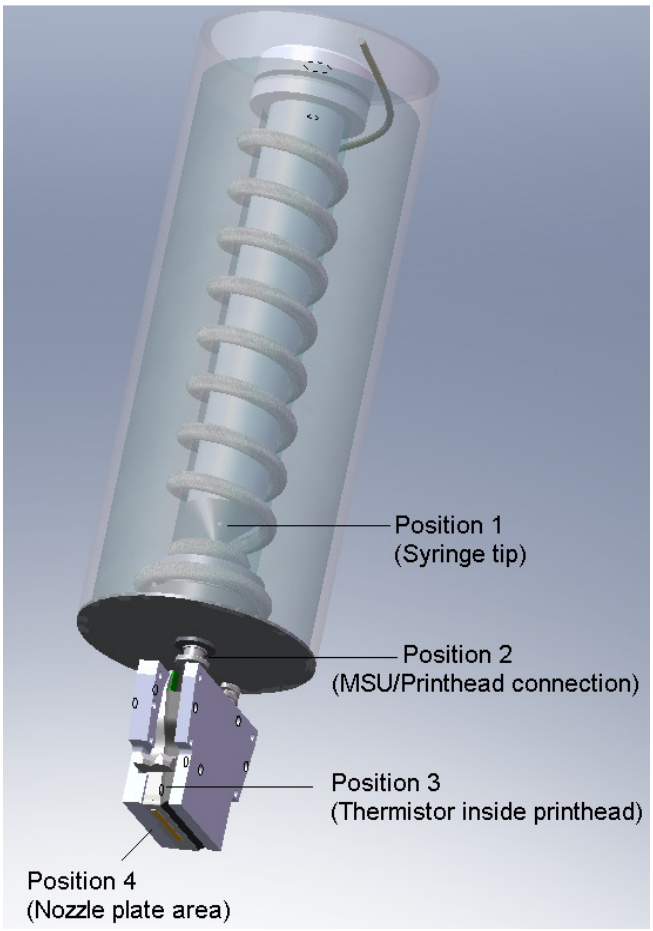

Figure 3-12 Temperature reading positions for each jetting assembly

The controller used a ramp and soak temperature profile for all the heating elements of the Jetting assemblies. It was set to reach the jetting temperature of 80℃ in 45 minutes through two soaking times of 5 and 10 minutes at 50℃ and 70℃

respectively. The temperature profile was to ensure that no heat shock would damage the jetting assembly, especially the printhead. High temperature fluctuations of the jetting assemblies during the process could affect the jetting behaviour. Therefore, the thermal behaviour of the Jetting assemblies was monitored.

Figure 3-13 shows the results of the thermal monitoring from the four positions along with the applied ramp/soak profile. A similar thermal behaviour was recorded for both the jetting assemblies. All the heaters were switched off after 60 minutes. Position 2 (at the melt supply unit/printhead luer connection) had a temperature difference of 6℃ from the set temperature of 80℃. The connection was initially 20 mm long and the resulting temperature of 62℃ led to freezing of the melt supply. Therefore, a shorter connection of 10 mm was developed which avoided this problem.

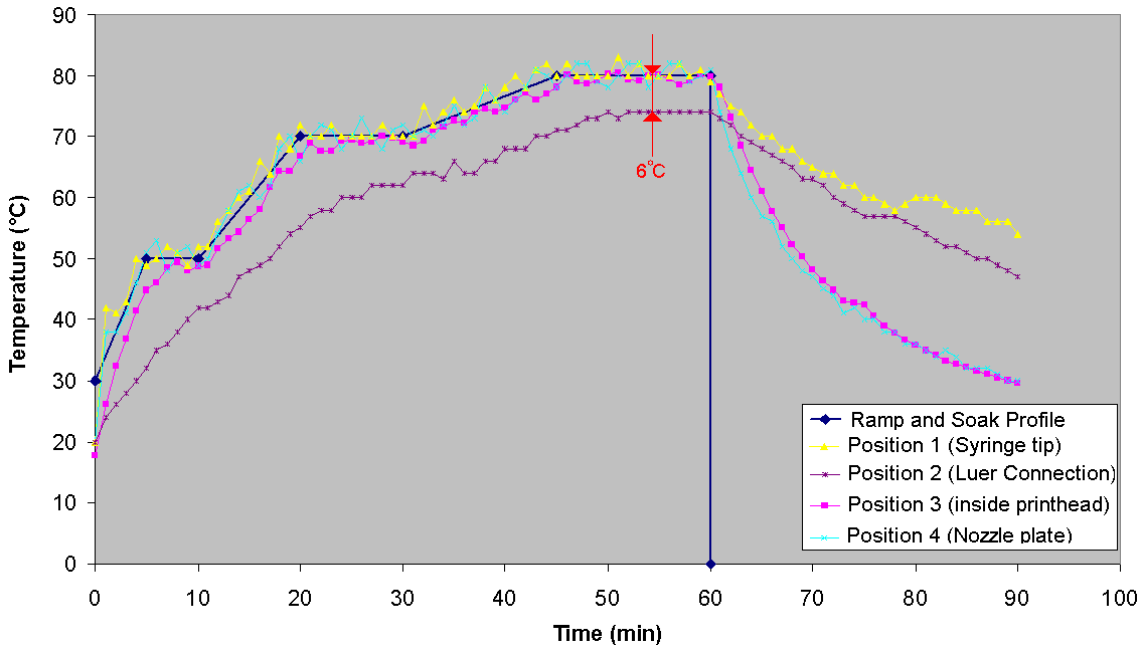

Figure 3-13 Thermal behaviour of jetting assembly with the set ramp and soak temperature profile

3.4.3 Pneumatic Control over the Melt Flow

With the heating system of the jetting assemblies set at 80℃, the molten caprolactam would need to be purged through the filter membrane into the printhead and then a vacuum would be required to control the melt flow. Therefore, a pneumatic system supplying both pressure and vacuum was developed. Pressure and vacuum were regulated by a digital manometer (FCO16 from Furness Controls Ltd.) working with 1 mbar resolution in a range of ±1000 mbar. An in-line venturi-type vacuum generator (GV2 from Vuototecnica Srl) supplied a vacuum by exhausting pressurised air.

Air could be trapped in the melt supply to the printhead when changing the cast bar cartridge in the jetting assembly. Due to the micro-scale channels of the printhead, there could be some air bubbles trapped and not removed by purging of the melt through the nozzles. Therefore, a bleeding tube was subsequently made to remove trapped air from the jetting assemblies before the trials. Figure 3-14 shows the two bleeding tubes used in the jetting assemblies. The internal structure of the printhead is seen in Figure 3-15 which demonstrates how the air bubbles could be extracted. After purging the melt into the printhead a vacuum could be applied by the syringe through the bleeding tube to extract the air bubbles with some melt bleeding out from the outlet which then solidified and sealed the port.

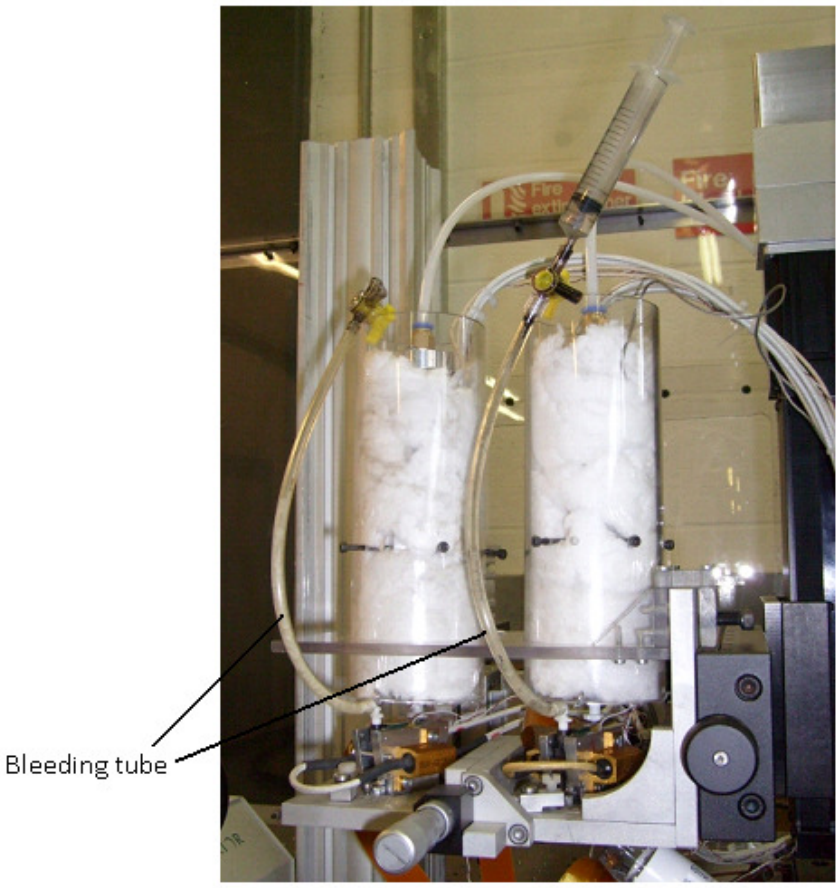

Figure 3-14 Bleeding tube setup in the jetting assemblies half filled with melt which has then solidified

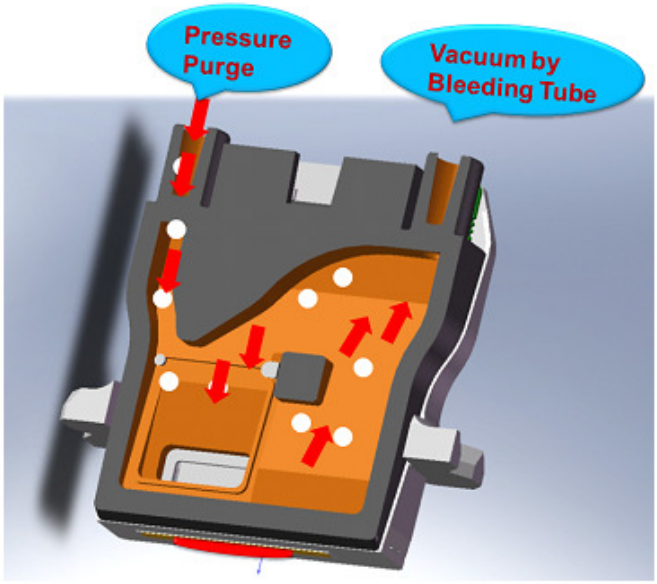

Figure 3-15 Technique for air removal from the printhead (image shows the cross-sectional view)

3.5 Material Behaviour Monitoring

Material behaviour at different stages of the process, from droplet formation to the impact of droplets onto the surface, was monitored with image and video recording as part of the setup. The objective was to study different phenomena in the jetting and deposition stages by qualitative and quantitative image analysis.

3.5.1 In-Situ Microscopy

A digital microscope camera (Dino Lite AM211 from ANMO Electronics Corp.) was used for local monitoring of the nozzle plate during jetting trials. Both video and photographs could be taken with an adjustable magnification (of 10, 50 or 200 times at different imaging distances). There was a ring light source inside the camera for direct lighting. Figure 3-16 shows how the microscope camera was positioned for monitoring the nozzle plate. A second digital microscope camera with fluorescent imaging capability (Dino-Lite Pro AM413T-FVW from ANMO Electronics Corp.) was also installed in-line with the deposition setup (which is described in Section 3.6). The second digital camera, switchable between normal (white light) and fluorescent imaging, was used to study material behaviour after the droplet deposition. It was equipped with ultraviolet light emitting diodes (UV LEDs) of 400 nm wavelength.

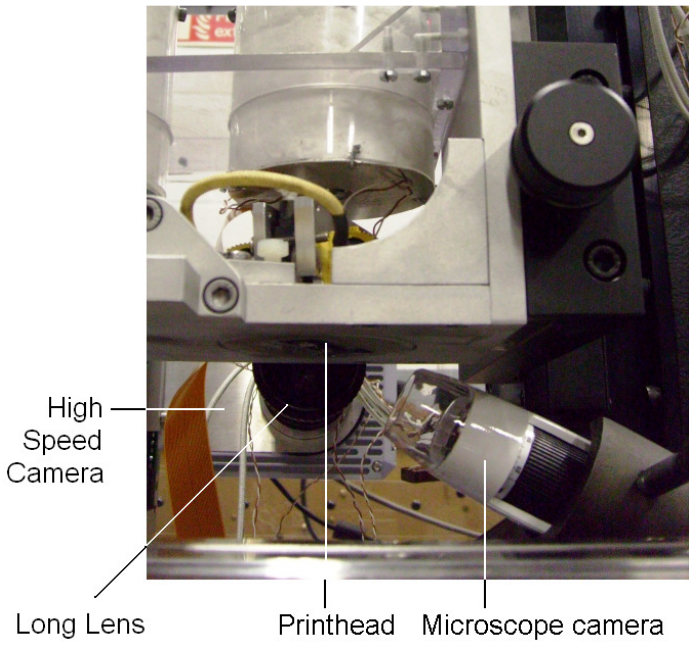

Figure 3-16 Digital microscope camera and high speed camera positions

3.5.2 High Speed Imaging

The droplet formation and impact onto the surface required high speed imaging. A high speed camera (FASTCAM APX-RS from Photron Inc.) with a long lens (12X Zoom from Navitar Inc.) was used in combination with an intensive light source (ELSV-60 from Everest VIT) placed opposite to the camera lens for backlight imaging as Figure 3-16 shows. The high speed camera was set with a working distance of 86 mm to magnify the nozzle plate and the deposition area on the substrate.

The camera was set at an imaging rate of 10,000 frames per second (fpm) and an exposure time of 4 μs to capture the droplet during formation and impact. Two lens settings for different magnification were used throughout the study. Figure 3-17 presents two images captured by the imaging system for the magnification calibration. The left image shows the nozzle plate with lens set 1 giving a matching

pixel size of 6.7 µm (micron per pixel) and the right image shows the lens set 2 with matching pixel size of 1.6 µm. Rods with standard diameter of 2000 µm and 250 µm respectively were used for calibration and scaling purposes. Images from the high speed camera were analysed quantitatively with software (measureIT from Olympus UK Ltd.).

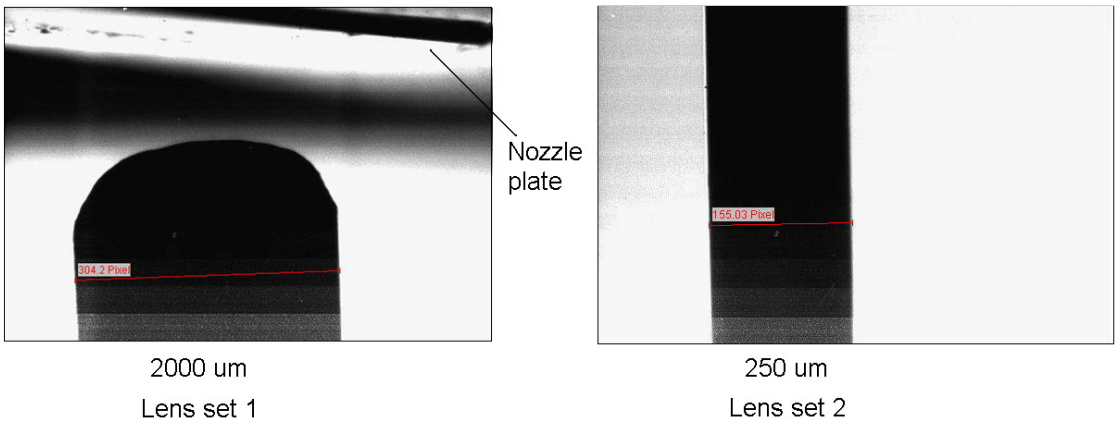

Figure 3-17 Calibration magnification of the high speed imaging in the two lens settings

3.6 Deposition Setup

3.6.1 Requirements for the Deposition

The two mixtures were required to be deposited on top of each other and receive heat to initiate the polymerisation. Therefore, the substrate needed to have a heated surface and be synchronised with the printhead for accurate placement of droplets. Other factors to consider in deposition would be the substrate surface properties, deposition speed and the gap between the printhead and the substrate.

3.6.2 Substrate

The substrate was designed to hold either DSC pans or a glass slide. In both cases, they needed to be easy to insert onto a heated surface and remain attached to a

moving carriage (X stage). Aluminium plates were used to fabricate the substrate, sandwiching two flexible silicon rubber heaters (SRFG-203/10 from Omega Engineering Inc.) to heat an area of 100 mm X 150 mm. There was an insulating sheet between the heaters and the bottom aluminium plate to avoid heat transfer to the carriage on the X stage. The top aluminium plate had two different designs for the two deposition surfaces. A T-type thermocouple was embedded 0.5 mm from the top surface to control the temperature. One aluminium top-plate was designed to hold a microscope glass slide (Gerhard Menzel GmbH) of 76 mm length, 26 mm width and 1 mm thickness. The other top-plate was to hold five DSC pans in blind holes of 6 mm diameter and 1 mm depth, with 22 mm spacing (Figure 3-18). The thermal control of the substrate was achieved via the 7-channel controller. The substrate temperature was set to 80℃. The surfaces were cleaned with lint-free cloth to remove any contamination.

3.6.3 Substrate Motion Control for Deposition

Positioning of the substrate was achieved by a 3D motion system. It consisted of three stages of X, Y and Z each with 1 μm resolution. The X stage was to position the heated substrate horizontally (LMA-264R-1000 from Aerotech Inc.) whereas the jetting assemblies, attached to the Z stage (ATS125-100 from Aerotech Inc.), could be moved vertically. The Y stage (ATS125-100 from Aerotech Inc.) moved the jetting assemblies to the front or rear of the machine. All of the stages were controlled by a computer programme which could define the position and speed of the substrate.

Figure 3-18 Heated substrate on the X stage carriage for deposition into DSC pans

3.7 Reaction Unit

The deposited mixtures required enough heat to initiate the nylon polymerisation. The appropriate temperature for the reaction was about 150℃ (Khodabakhshi *et al.* 2008). Deposition of samples in small volumes onto the hot substrate at this temperature gave a high rate of evaporation (which is reported in Chapter 8). Therefore, an alternative heating mechanism was developed using radiation to heat up the deposited samples from 80℃ to about 150℃.

The surface radiation heating system used two 150W/230V halogen linear lamps (DEQ-K12 from General Electric Co.) in parallel, inside a cast aluminium box. Figure 3-19 shows the cast box fixed to a stand besides the digital microscope camera,

along the X stage. A rectangular slot of 10 mm x 50 mm, in the middle of the box lid, allowed the thermal radiation to be exposed to the deposited samples. The required distance to the deposition surface could be set as shown in Figure 3-19. Different power settings of the radiation heating are seen in Table 3-2. This could vary the radiant heat flux to give different reaction temperatures. The heating time onto the samples could be controlled by programming the substrate motion.

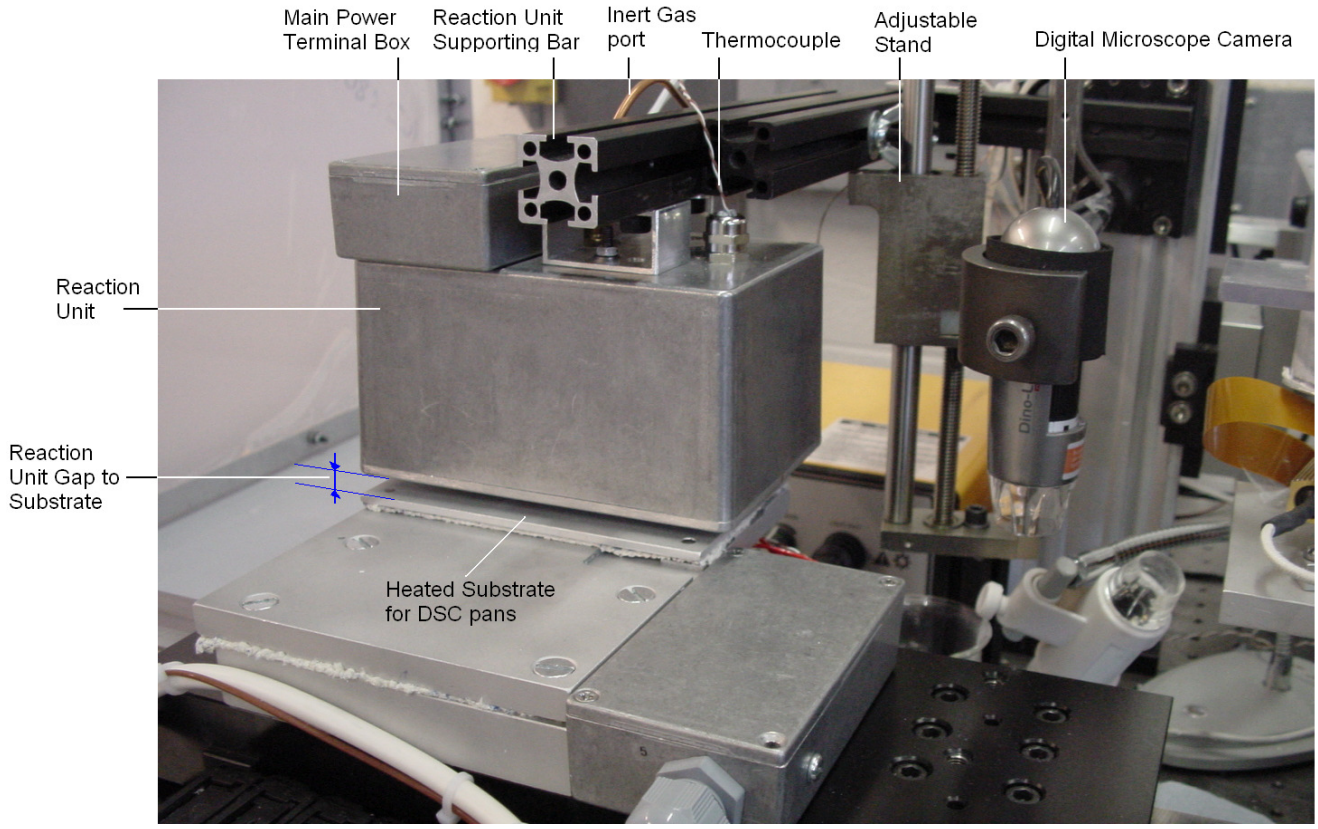

Figure 3-19 Reaction unit

Setting	Voltage (V)	Power (W)
1	82	140
2	120	220
3	160	280
4	194	340
5	216	360
6	228	370

Table 3-2 Power settings for the radiation heating of the reaction unit

3.8 Environmental Effects and Control

3.8.1 Process Environment and Need for Control

There were two situations requiring control of the process environment; jet stability and the polymerisation reaction. The trajectory of a single jet or an array of jets could be affected by the surrounding environment, leading to deposition instabilities. Air movement could cause this. In addition, the polymerisation reaction is sensitive to moisture. Therefore, the process was enclosed in a glove box, fabricated from polycarbonate sheets as Figure 3-20 shows. Two windows in the front and back provided access.

3.8.2 Air Motion in the Jetting Area

Air motion was observed around the jetting area (nozzle plate). The cooling fans of the head personality card for the printheads and the intensive light source for high speed imaging, were found to be the air motion sources. To minimise the air motion originated by fans, their positions were changed. Also, with these sources switched off, there was still some air motion when the jetting assemblies were heated up. The heat dissipation from the jetting assemblies, and hence convection could be another source of air motion.

Figure 3-20 Glove box to control process environment

Chapter 4. Material Characterisation for Jetting

This chapter reports on the jetting materials, their physical properties and characteristics during the melt supply for jetting.

4.1 Requirements and Approach

The activators and catalysts could be used at different concentrations. The criteria for composing the appropriate sets of mixtures were their ability to jet and also their fast reaction after deposition on top of each other. The reaction of the mixtures was investigated in parallel research (Khodabakhshi 2011) (section 2.4.5) which proposed a number of compositions for jetting.

The surface tension, dynamic viscosity and particle content of the proposed compositions were investigated. Then, they were supplied to the jetting system to study the melt flow behaviour and consequently their ability to be supplied to the printhead in a controlled manner.

4.2 Materials for Jetting of Nylon

4.2.1 Base Material

The main material used was caprolactam with a molecular weight (MW) of 113.16, supplied from Sigma-Aldrich GmbH ($C_6H_{11}NO$, 99% pure ε-caprolactam).

4.2.2 First Set of Mixtures

The first set of reactive mixtures were synthesised by Khodabakhshi *et al.* (2008) using chemical compounds and molten caprolactam. The catalyst mixture was made by mixing ethyl magnesium bromide (in diethyl ether supplied from Sigma-Aldrich GmbH) with molten caprolactam. This produced the complex of caprolactam magnesium bromide (CLMgBr) in caprolactam (CLMgBr-CL). As the activator mixture, N-acetylcaprolactam (N-AcCL) (99% purity, MW = 155.19 supplied from Sigma-Aldrich GmbH as a liquid solution) was mixed into molten caprolactam (N-AcCL-CL). Khodabakhshi *et al.* (2008) aimed to develop compositions for a faster reaction where the mixtures were synthesised at 10% concentration. Therefore, this composition was also investigated in this research.

4.2.3 Second and Third Sets of Mixtures

Initial characterisation of the first set of mixtures showed that the catalyst mixture would not pass through the melt supply properly (this will be discussed in section 4.6). Therefore an alternative catalyst mixture was used. It was thought a commercially synthesised catalyst mixture would result in better melt supply behaviour. Brueggemann Chemical GmbH provided two catalysts mixtures (C1 and C10, both in flake form), with one recommended matching activator mixture (C20P, in pellet form).

As the second set of mixtures, C1 was used with C20P. C1 was a composition of 10-25% caprolactam magnesium bromide (CLMgBr) in caprolactam (Brueggemann Chemical GmbH 2009) and therefore was similar to the synthesised catalyst mixture in the first set. C20P was made of blocked diisocyanate in caprolactam with approximately 17% free isocyanate content as reported by the supplier

(Brueggemann Chemical GmbH 2009). The C1 and C20P concentrates were diluted to the required concentration with caprolactam to form the second set of mixtures respectively known as C1-CL and C20P-CL in this thesis. It was found that the second catalyst mixture had issues in the melt supply similar to the first, and therefore, a third catalyst mixture was used.

The third catalyst mixture (C10) was selected to have a sodium caprolactamate based catalyst complex which is commonly used in anionic polymerisation (van Rijswijk *et al.* 2006). The C10 concentrate consisted of 17-19% of sodium caprolactamate (NaCL) in caprolactam. Therefore, C10 was diluted with molten caprolactam (C10-CL) at the required concentration and was used with C20P-CL as the third set of mixtures.

The work of Khodabakhshi (2011) indicated for the commercial mixtures that the catalyst and activator concentration should be between 5% and 20%. As with the work on the first set of mixtures (synthesised), 10% concentration was initially used for the second and third sets of mixtures for the experiments regarding the melt supply. However, after initial results, a higher concentration of 20% was selected. This was due to concerns over the effect of filtering in the melt supply on the final concentration of the materials (before the jetting system) which will be discussed in section 4.6. Therefore, the results of physical properties tests with the commercial mixtures were reported for the higher concentration (20%) in section 4.3.

4.3 Surface Tension

4.3.1 Procedure

The surface tension of the molten caprolactam and all the mixtures were measured at a temperature of 80℃ using the pendent drop method (OCR 20 by DataPhysics

Instruments GmbH). The instrument was equipped with a temperature controlled hot chamber. Images of the pendent drop were captured by the monochrome camera in the instrument after the temperature was stabilised. To calculate surface tension, the density of the materials was taken as 1.02 g/cm^3 at 80℃ (reported by the supplier).

4.3.2 Results for Surface Tension

Table 4-1 shows the result of the surface tension measurement for all the materials. Caprolactam and the mixtures had a similar surface tension, all ranging from 34 to 38 mN/m which was slightly lower than the nozzle plate surface tension of 40 mN/m. This suggested that the nozzle plate would be wet by caprolactam and the reactive mixtures.

Figure 4-1 shows the pendent drop of caprolactam and the first set of reactive mixtures (N-AcCL-CL and CLMgBr-CL) at 80℃. A clear pendent drop is seen in Figure 4-1(a) and (b) for the molten caprolactam and activator. This impression was made by the light passing through the middle of the drop. With the catalyst mixture, the drop was less clear as seen in Figure 4-1(c), making it darker in the middle. The catalyst mixture seemed to contain an agglomeration of fine particulates which could be seen to be moving while the pendent drop was being formed. Similar behaviour was observed in all pendent drops of the catalyst mixture during the experiments.

Material	*Concentration (% in weight)*	*Surface Tension*	
		Mean Value (mN/m)	*Standard Deviation*
Caprolactam	-	34.9	0.29
N-AcCL-CL	10	36.0	0.06
CLMgBr-CL	10	34.9	0.23
C20P-CL	20	36.2	0.56
C1-CL	20	35.3	0.08
C10-CL	20	37.1	0.03

Table 4-1 The results for the surface tension measurement at 80℃

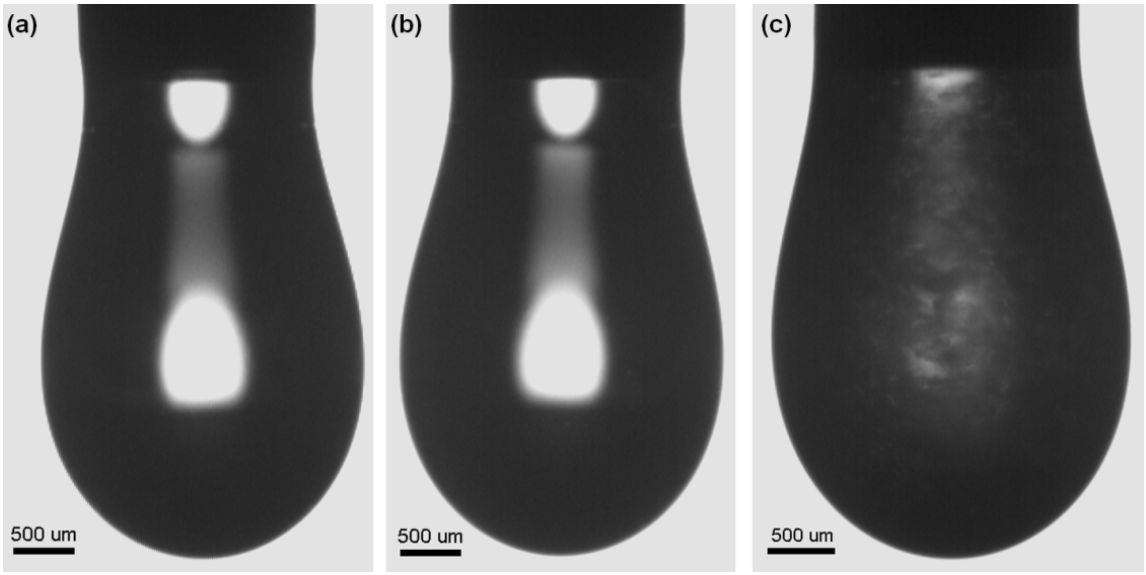

Figure 4-1 Images of pendent drop of materials at 80℃, (a) caprolactam, (b) N-AcCL-CL, and (c) CLMgBr-CL (set 1 of the mixtures)

There was a question of whether an increase in temperature would affect the presence of particulates. Therefore, it was decided that the molten pendent drop should be studied over a thermal cycle of 80-100-80℃ at 1℃/min (temperatures over 100℃ could initiate considerable evaporation in the chamber).

Figure 4-2 shows images of a pendent drop of the first set of catalyst mixture (CLMgBr-CL) at different temperatures. Interestingly, by increasing the temperature from 80℃ to 90℃, as seen in Figure 4-2(a) and (b) respectively, the particulate state

and therefore the transparency of the molten mixture changed. The particle agglomeration seemed to be dispersed which darkened the drop by light scattering. However, this changed again when increasing the temperature to 100℃ as seen in Figure 4-2(c). The particles seemed to disappear, making the drop clear and allowing the light to pass through. The drop was still less clear compared with the molten caprolactam or the activator mixture as seen in Figure 4-1(a) and (b). More interestingly, when reducing the temperature from 100℃ to 80℃ (Figure 4-2(d)), the (same) drop returned to its original state as in Figure 4-2(a). This reversible behaviour was observed in repeated experiments which suggested a thermo-physical evolution in the catalyst mixture. It was thought that this could be due to dissolving of the particles in the molten caprolactam. Therefore, hot stage optical microscopy was to be used for further understanding which will be discussed in section 4.5.

Despite the changes observed in the drop transparency in Figure 4-2, the results for the surface tension measurement during the thermal cycle showed little difference. Table 4-2 shows only a slight decrease of surface tension as the temperature increased.

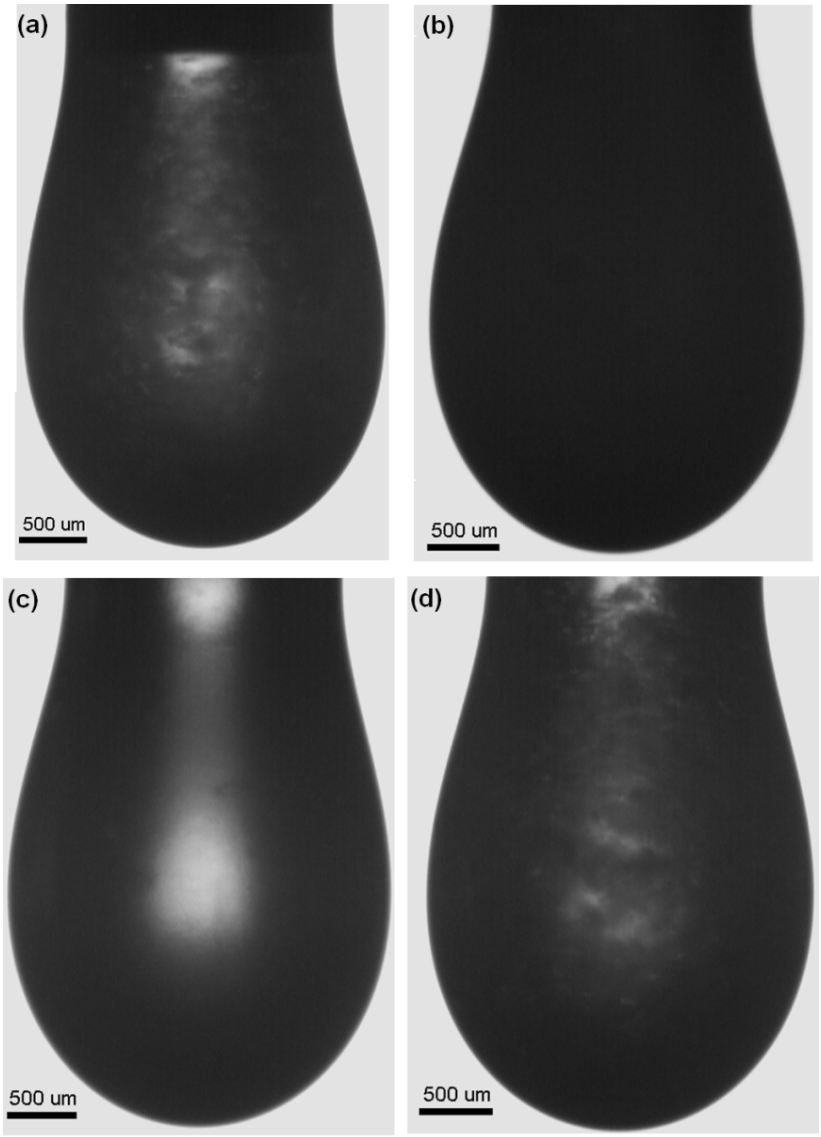

Figure 4-2 Pendent drop of the synthesised catalyst mixture (CLMgBr-CL) during the surface tension measurement in a thermal cycle, (a) 80℃, (b) 90℃, (c) 100℃, (d) 80℃

Material	*Melt Temperature (℃)*	*Surface Tension*	
		Mean Value (mN/m)	*Standard Deviation*
CLMgBr-CL	80	34.9	0.23
	90	34.8	0.79
	100	32.7	0.76
	80	34.4	0.22

Table 4-2 Surface tension of the synthesised catalyst mixture during a thermal cycle corresponding to the images in Figure 4-2

4.4 Dynamic Viscosity

4.4.1 Experiments

The dynamic viscosity was measured using a rheometer (Physica MCR101 by Anton Paar GmbH). The resistance of the materials in the molten state to shear flow between a rotating stainless steel plate (25 mm diameter) and a heated surface (fixed) was monitored when using a gap setting of 500 µm (recommended by the instrument manufacturer).

First Set of Mixtures

For the first set of mixtures (synthesised), the effect of temperature on the viscosity was investigated at a fixed shear rate of 1000 s^{-1}. Previous work (see Figure 3-1) had shown that the viscosity of caprolactam dropped to a minimum at shear rates well below 1000 s^{-1} and then remained stable. The temperature was controlled over a cycle of 80-100-80°C (with 1°C/min change) to correspond with the surface tension tests (Figure 4-2). It was found that the catalyst mixture behaved differently to the caprolactam and the activator mixture. Therefore, further viscosity experiments were carried out on the catalyst mixture. These were:

(1) the shear rate was varied from 1 s^{-1} to 1000 s^{-1} at a fixed temperature of 80°C. This was to ensure the validity of the assumption above.

(2) a wider thermal cycle range of 80-150-80°C to determine if a higher temperature was necessary to eliminate the particles. This would help to determine if a different printhead was necessary.

(3) a reduced gap distance of 100 µm in an attempt to more closely simulate the conditions in the jetting head.

Table 4-3 summarises the viscosity experiments undertaken on the first set of mixtures.

Experiment	*Material*	*Temperature (℃)*	*Shear Rate (s^{-1})*	*Gap (µm)*
1	Caprolactam (CL)	80-100-80	1000	500
2	N-AcCL-CL	80-100-80	1000	500
3	CLMgBr-CL	80-100-80	1000	500
4		80	1-1000	500
5		80-150-80	1000	100, 500

Table 4-3 Viscosity experiments for caprolactam and the first set of mixtures (synthesised)

Second and Third Set of Mixtures

The commercial concentrates were diluted with caprolactam at 20% concentration to compare with the undiluted concentrate mixtures (100% conc. of C20P, C1 and C10) in the viscosity experiments. This comparison was to give a better understanding of the role of the catalyst and activator complexes in the molten caprolactam on the viscosity variation and consequently droplet formation characteristics. In addition, the results could be used for prediction of the viscosity of a different concentration (if required later).

During the melt supply experiments with the first set of mixtures (Table 4-3), a temperature drop from 80℃ to 75℃ was occasionally noticed in the jetting assembly. Therefore, in further experiments (with the commercial mixtures) the viscosity was measured over a thermal cycle of 75-100-75℃. The gap setting of 100 µm and 500 µm was to ensure the validity of the viscosity results. Table 4-4 lists the experiments for the catalyst and activator mixtures of the second and the third sets.

Experiment	*Mixture*	*Concentration (% in weight)*	*Temperature (°C)*	*Shear Rate (s^{-1})*	*Gap Setting (μm)*
6	C20P	20, 100	75-100-75	1000	100, 500
7	C1	20, 100	75-100-75	1000	100, 500
8	C10	20, 100	75-100-75	1000	100, 500

Table 4-4 Experiments for the second and third sets of the mixtures

4.4.2 Results for First Set of Mixtures

Figure 4-3 shows the results for the dynamic viscosity of the molten caprolactam and the first set of reactive mixtures during two cycles of 80-100-80°C. The viscosity of the activator mixture was similar to the molten caprolactam. At 80°C, both materials had a dynamic viscosity of about 9 mPa.s which dropped linearly to about 5 mPa.s at 100°C. However, a big difference was seen with the catalyst mixture (CLMgBr-CL). The viscosity of this mixture was about three times higher. At 80°C, it was slightly below 30 mPa.s in the first cycle. It was also noticeable how viscosity varied during the two thermal cycles for this catalyst mixture. The viscosity was lower during the heating stage of the 1st cycle compared with the second cycle.

The higher viscosity of the synthesised catalyst mixture could be due to the existence of the particles observed in the pendent drop, as seen in Figure 4-2 (and also discussed in section 4.5). The particles could resist flow during shear induced by the rotating plate of the rheometer. Figure 4-4 shows the result of varying the shear rate where the viscosity did not change much for rates higher than 400 s^{-1}. Thus, the shear rate setting at 1000 s^{-1} was appropriate for this catalyst mixture.

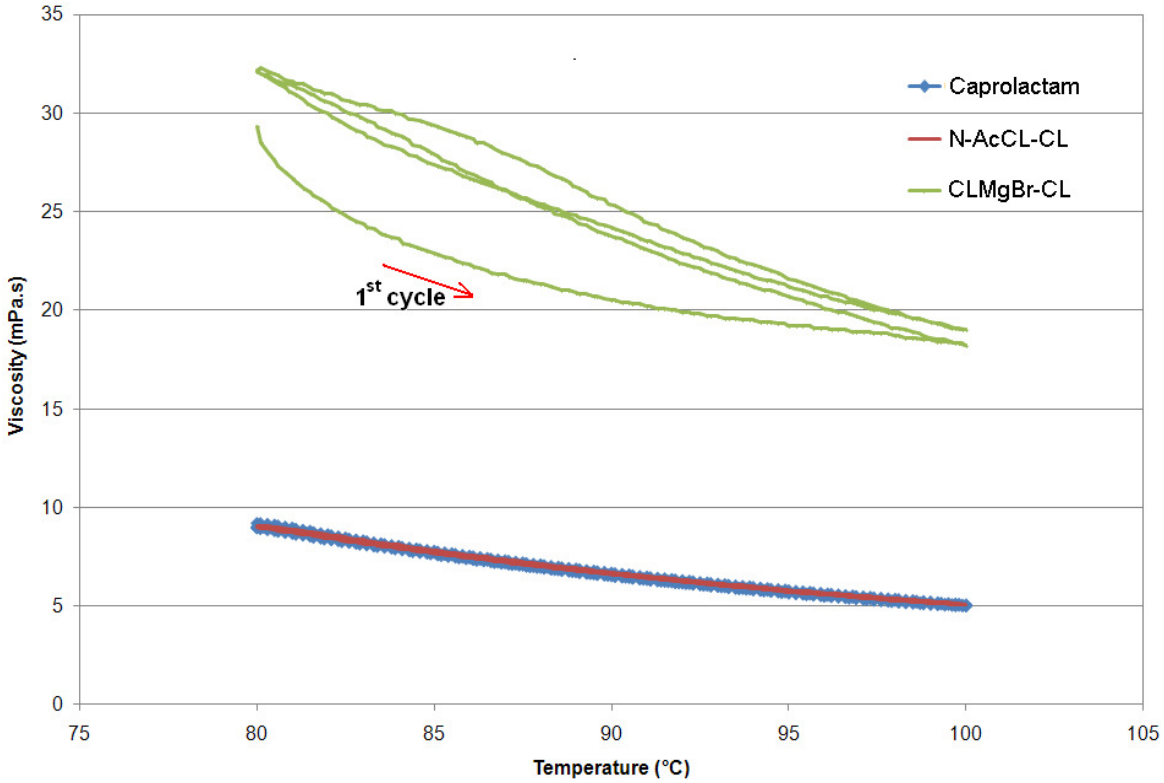

Figure 4-3 Dynamic viscosity of the molten caprolactam and the first set of the reactive mixtures in two thermal cycles (Experiments 1, 2 and 3 in Table 4-3)

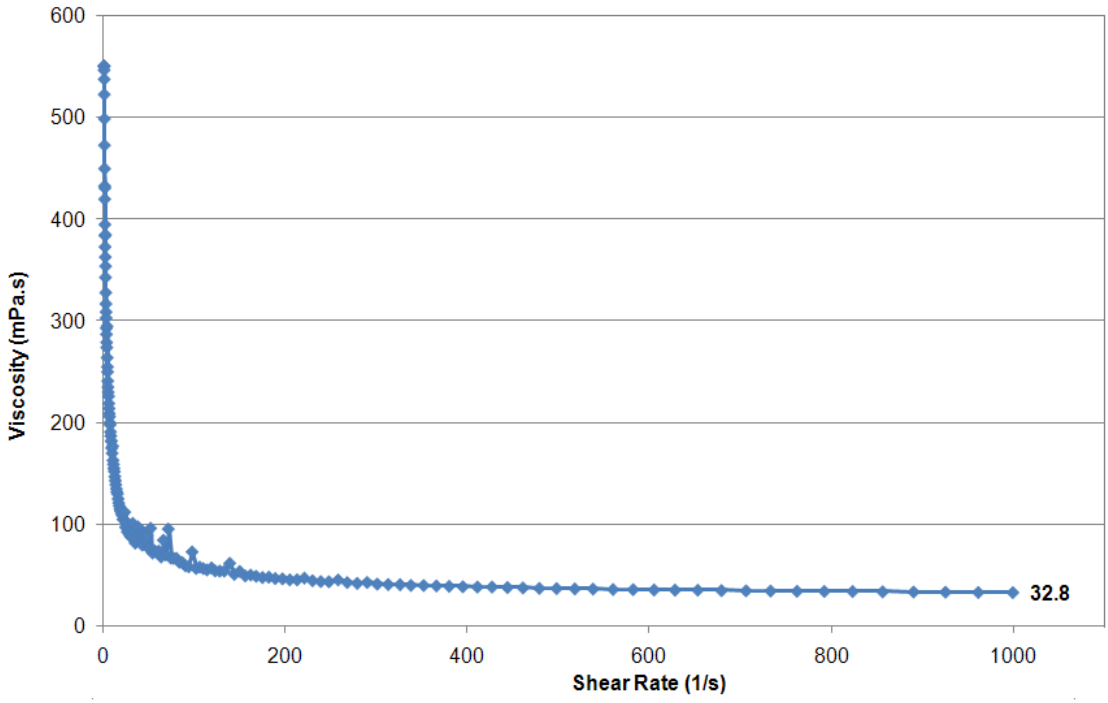

Figure 4-4 Dynamic viscosity of the synthesised catalyst mixture (CLMgBr-CL) at 80℃ with different shear rates (Experiment 4 in Table 4-3)

Figure 4-5 shows the results for viscometry of the synthesised catalyst mixture (CLMgBr-CL) in two cycles of 80-150-80℃. Variations of the viscosity are seen over time (top axis) with temperature (bottom axis) and with the two gap settings. The viscosity with a 500 µm gap was generally repeatable whereas fluctuations occurred in both thermal cycles with a 100 µm gap. The fluctuations started in the first cycle when the temperature was dropping from the maximum of 150℃.

Figure 4-6 shows the rotating (top) plate and the heated surface in the rheometer just after the viscometry trial. By removing the top plate, it was observed that the caprolactam had evaporated completely and traces of agglomerated particles were left on the heated surface. The sample volume was much smaller with the smaller gap setting (100 µm). This resulted in evaporation and left the agglomerated particles on the top plate. The accumulation of the particles as seen in Figure 4-6 was probably responsible for the relatively high fluctuations seen with the 100 µm gap in the second thermal cycle. These results confirmed the need for a proper particle content study for the catalyst mixture at different temperatures.

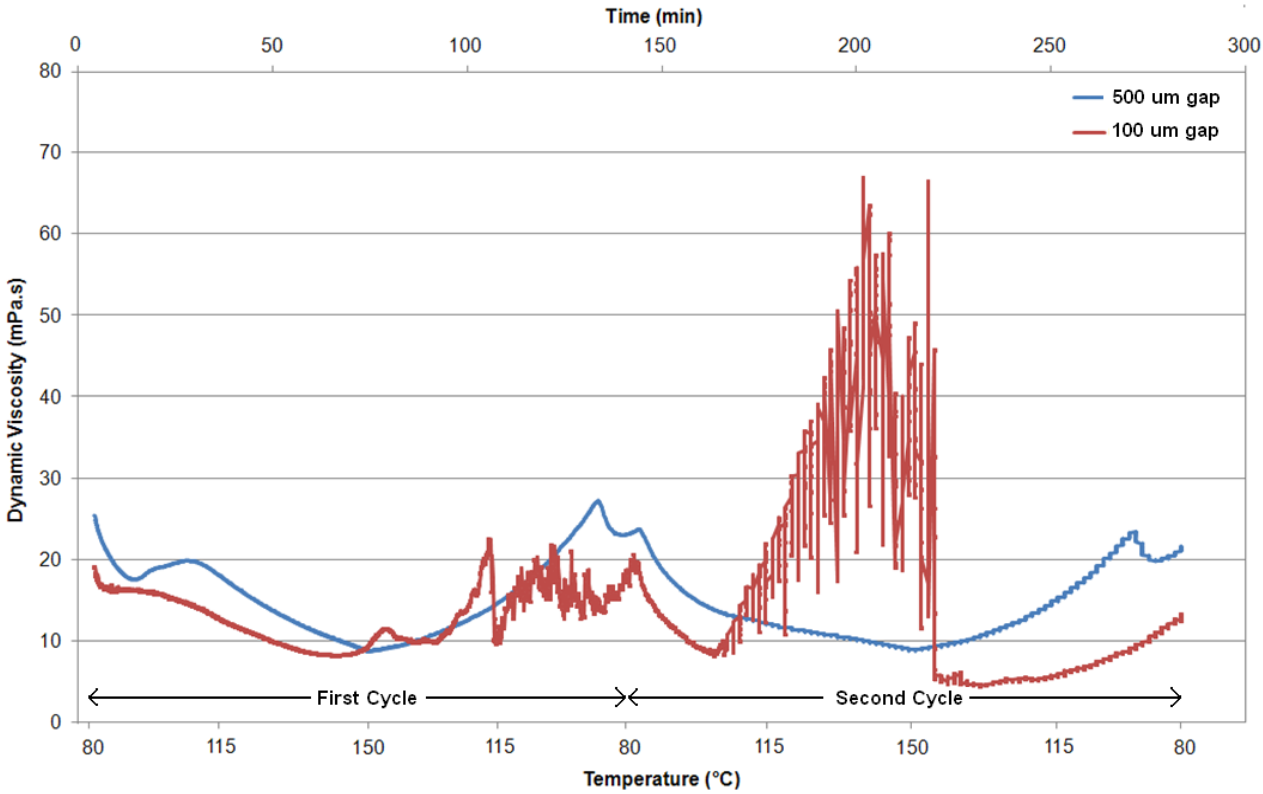

Figure 4-5 The effect of temperature variation and gap setting on the viscosity of the synthesised catalyst mixture (CLMgBr-CL) in two cycles of 80-150-80℃ (Experiment 5 in Table 4-3)

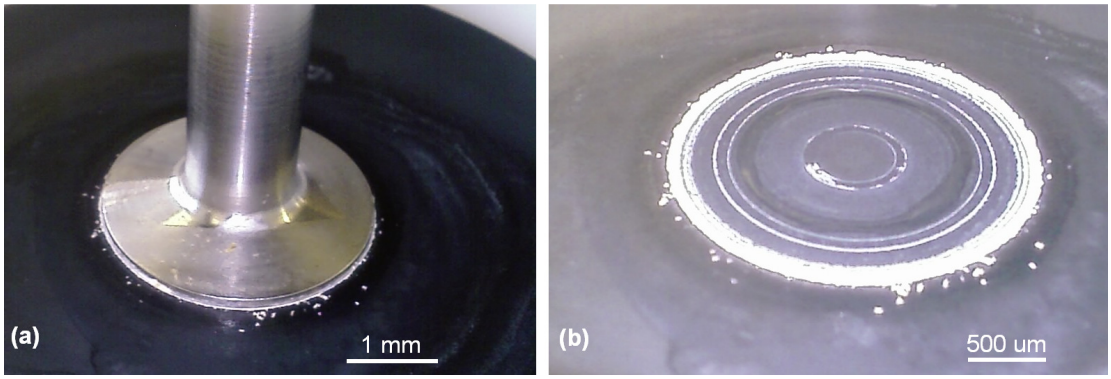

Figure 4-6 Images of the rheometer at 100 µm gap setting after a test with the synthesised catalyst mixture (CLMgBr-CL) over two thermal cycles of 80-150-80℃ during 5 hours (Experiment 5 in Table 4-3), (a) hot (bottom) surface before removing the top plate, (b) traces of particles on the hot surface

4.4.3 Results for Second and Third Sets of Mixtures

The results of viscosity tests for the activator mixture used in both the second and the third sets are shown in Figure 4-7. Figure 4-8 and Figure 4-9 show the results for the two catalyst mixtures used in the second and third sets. Each figure contains four graphs to correspond to the settings shown in Table 4-4 (two concentrations and two gap settings).

It is seen that the undiluted mixtures had a much higher viscosity than the 20% concentration. This was especially noticeable at around 75℃ which resulted in elevated viscosities. There were no significant fluctuations seen with these catalysts (compare Figure 4-5 with Figure 4-8 and Figure 4-9). This could be due to a difference in the particulate nature between the synthesised and commercial catalyst mixtures.

All the mixtures (C20P-CL, C1-CL and C10-CL) at 20% concentration behaved very similar and viscosity decreased almost linearly from 15 mPa.s at 80℃ to 8 mPa.s at 100℃. This was however about 50% higher than the molten caprolactam ranging from 9 to 5 mPa.s for temperatures between 80 to 100℃ (Figure 4-3).

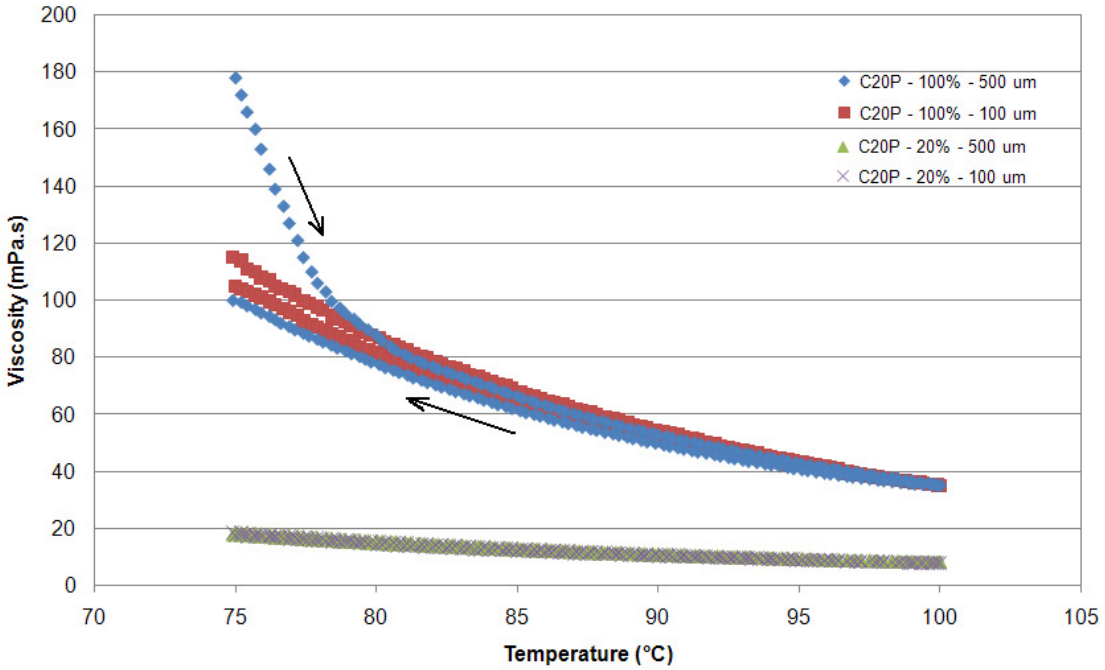

Figure 4-7 Viscosity variation of the second set of activator mixture (C20P-CL) with temperature (Experiment 6 in Table 4-4)

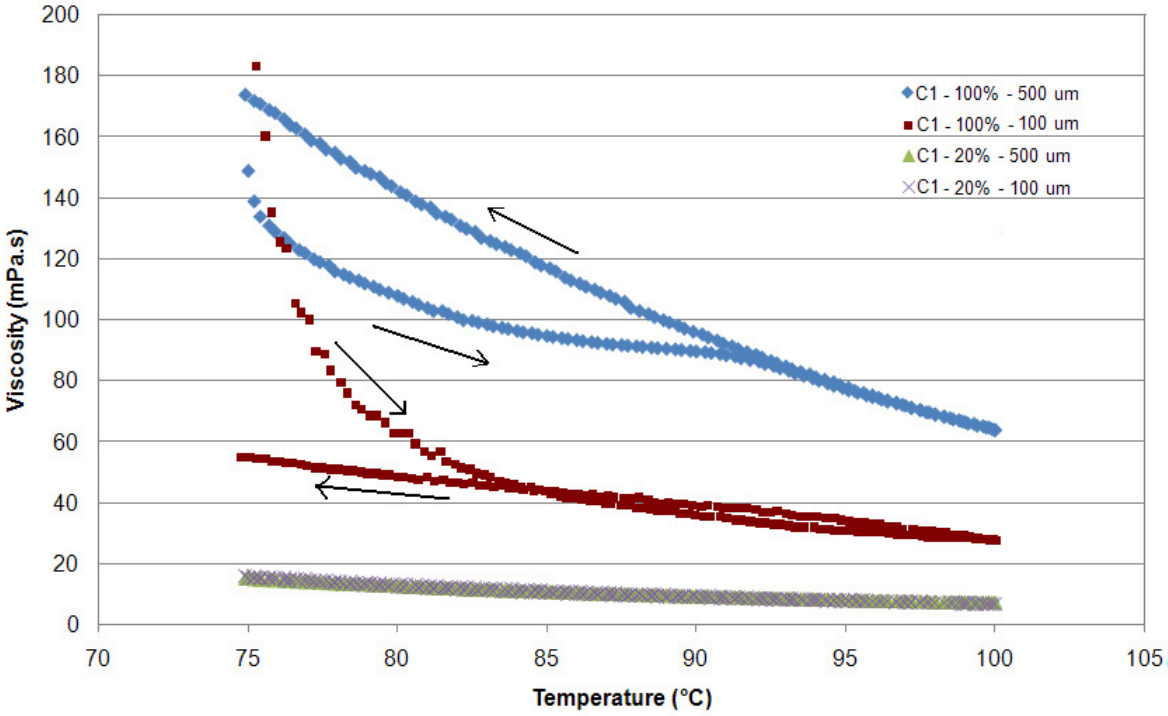

Figure 4-8 Viscosity variation of the second set of catalyst mixture (C1-CL based on caprolactam magnesium bromide) with temperature (Experiment 7 in Table 4-4)

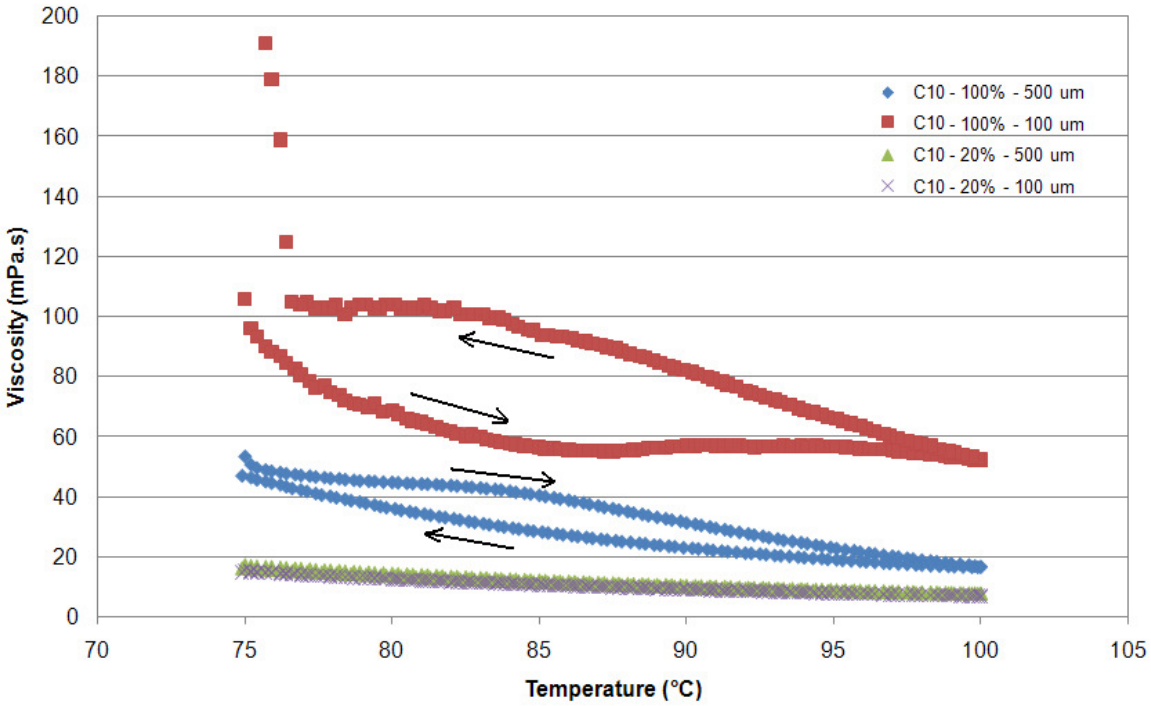

Figure 4-9 Viscosity variation of the third set of catalyst mixture (C10-CL based on sodium caprolactamate) with temperature (Experiment 8 in Table 4-4)

4.5 Particle Content

4.5.1 Particle Characterisation Procedure

An investigation of the particle content within the synthesised catalyst mixture in the first set of mixtures was carried out using an optical microscope (DFC 350 – Leica Microsystems GmbH) equipped with thermally controlled hot-stage (FP90 by Mettler-Toledo Inc.) to understand the particles nature and their distribution. Small samples of the catalyst mixture about 1 µl in size were placed on a glass slide fixed to the hot stage of the microscope. After melting, a cover slip was placed onto the molten sample to spread it before microscopy. Three different lighting setups were used: bright field, phase contrast and transmitted polarised light.

Greyscale images were processed with the *UTHSCSA Image Tool for Windows*, version 3.00, (The University of Texas Health Science Center at San Antonio, Texas,

USA). It could transform a 256-level greyscale image to a binary black and white image when a grey threshold level was used. This was to filter the spots in the microscopic images representing the particles by turning them into white pixels. Counting the white pixels gave a percentage of the total particulate area of the image. With this procedure, the particle content was characterised qualitatively and quantitatively over a range of temperatures to correspond with the observation of the pendent drop (Figure 4-2).

4.5.2 Observation of the Particles Nature

The particles could only be seen with the polarised light and as microcrystals with their sizes in the range of microns as Figure 4-10 shows. The caprolactam magnesium bromide (CLMgBr) is known to have a positive metal ion ($MgBr^{+}$) and a negative non-metal ion (CL^{-}) (Udipi *et al.* 1997) which could form a crystalline salt structure.

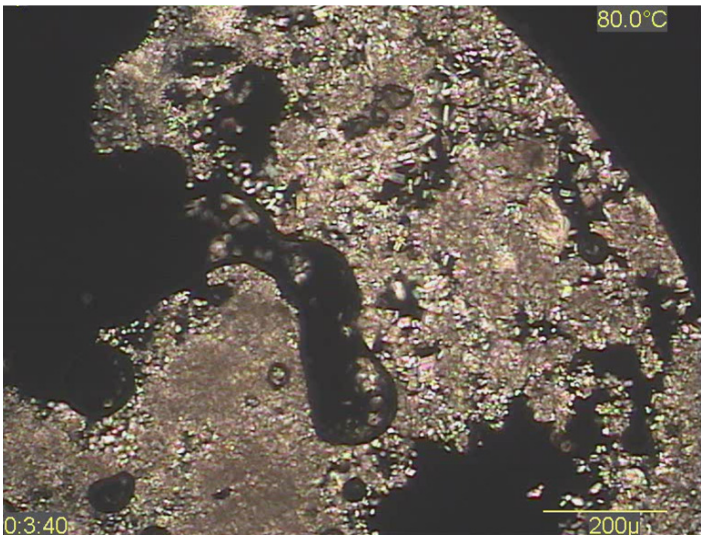

Figure 4-10 Polarised light microscopy revealing an agglomerated particle area of the molten synthesised catalyst mixture, CLMgBr-CL, at 80℃

4.5.3 Effect of Melt Temperature on Particles

The effect of temperature on the particle behaviour in the synthesised catalyst mixture was also investigated in response to the observation in Figure 4-2. Figure 4-11 shows a sequence of images captured from a video of the catalyst mixture under the hot stage microscopy. The sample was kept at 80℃ for 5 minutes and then was heated to 150℃, with a constant heating rate of 10℃/min. The area of the microcrystals reduced with increasing temperature and at 150℃ there were no visible particles (the strip seen at the bottom of the images was external contamination).

The disappearance of the particles at elevated temperatures could be either by melting or dissolution. No report was found on the CLMgBr microcrystals dissolution behaviour as a colloidal complex in molten caprolactam. However, a report was published by Kriz *et al.* (2001) on the thermal properties of the caprolactam magnesium bromide (CLMgBr) particles. In their study, the catalyst complex was first filtered from caprolactam and then dried to obtain the remaining particles. The melting point of the particles was reported at 168.7℃ in the study. Therefore, the observations in Figure 4-2 and Figure 4-11 indicate that the microcrystals at temperatures between 80℃ and 150℃ were dissolving in the molten caprolactam. The images in Figure 4-11 were also analysed using the image processing software to obtain the proportion of the area covered by the microcrystals as an indication of the dissolution rate which is seen in Figure 4-12.

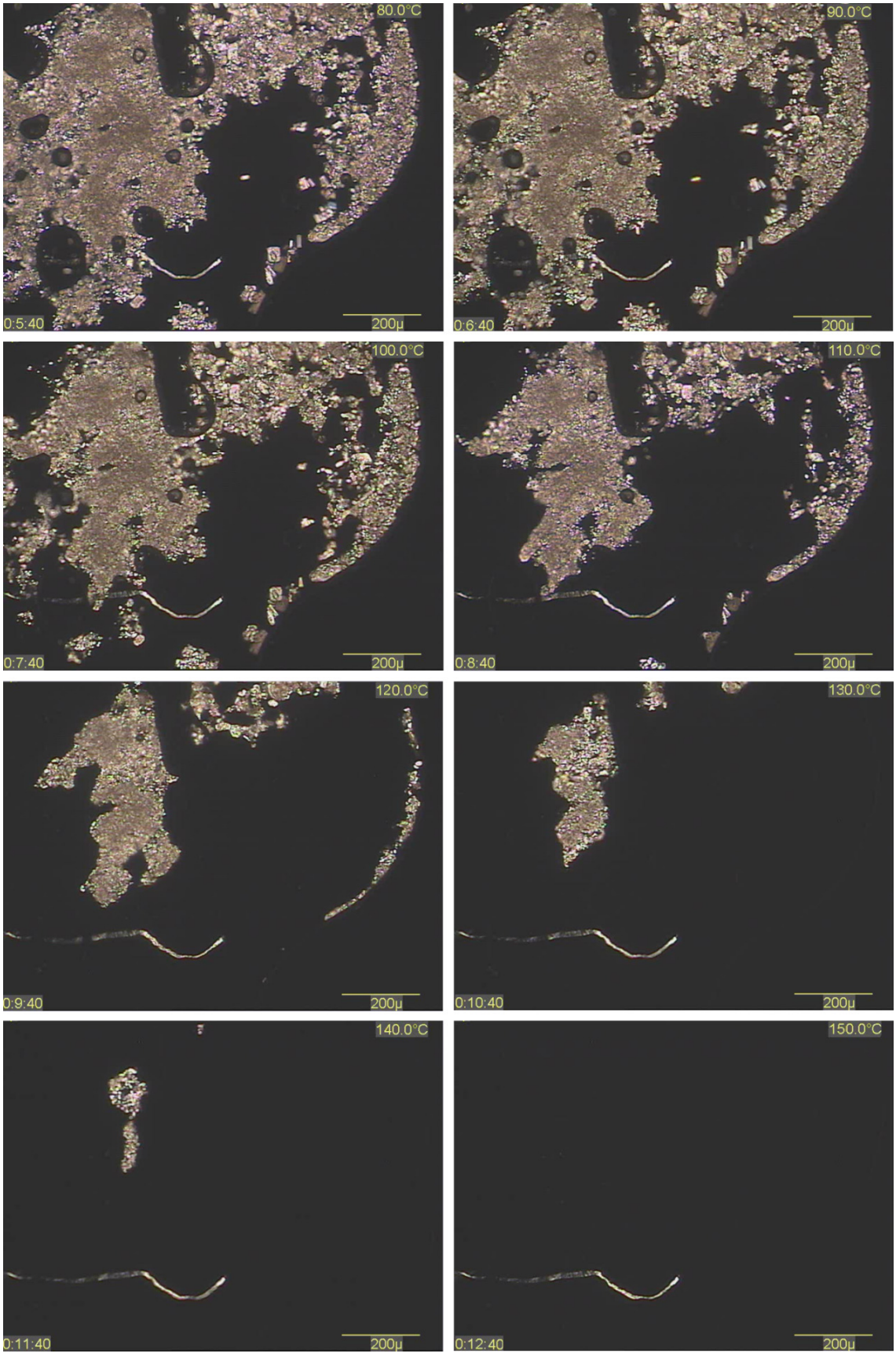

Figure 4-11 The effect of increasing temperature on the agglomerated area of microcrystals in the synthesised catalyst mixture during the hot stage polarised light microscopy

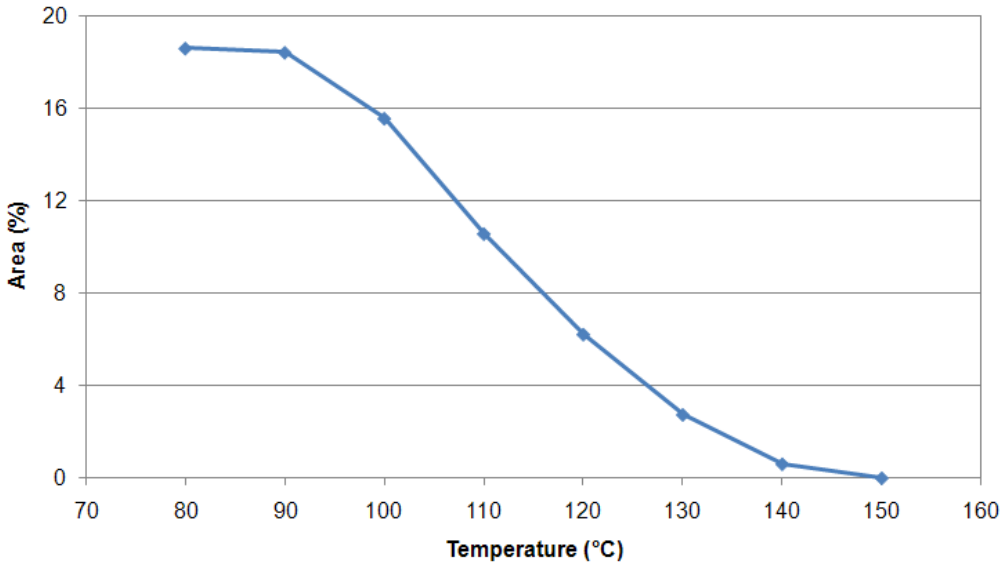

Figure 4-12 Dissolution of CLMgBr microcrystals with increasing temperature in the synthesised catalyst mixture during the hot stage polarised light microscopy (heating rate: 10℃/min)

4.6 Melt Supply for Jetting

This section describes how the molten caprolactam and different reactive mixtures behaved within the melt supply system.

4.6.1 Characterising Materials for Melt Supply

Melt flow behaviour during supply to the printhead was a critical characteristic of the mixtures for jetting. It was not known if the thermal and pneumatic control in the setup would provide a reliable supply for a process with a long operation time. The pneumatic pressure in the jetting assembly was to feed the printhead with melt. As soon as dripping of the melt from the printhead was observed, a vacuum was applied to control the meniscus on the nozzles.

To characterise the different materials in terms of melt supply, they were inserted into the jetting assembly in the form of solid cartridges, and then the aluminium

syringe of the melt supply unit was closed to provide a seal for the pneumatic control as described in section 3.3.2. After heating up the jetting assembly and melting the materials inside the supply unit, the temperature was monitored for 5 min to ensure it stabilised (at 80℃). Then, the nozzle plate was monitored with the digital microscope camera to observe the flow of melt through the printhead nozzles. The pressure, required to fill the printhead and obtain dripping of melt through the nozzles, and also the vacuum, required to stop dripping and control the meniscus shape on the nozzle plate, were monitored.

The melt flow rate was also measured during dripping of the melt. A beaker under the printhead collected the dripping melt and was weighed in-situ by a digital scale (PW01 by Technico). This was undertaken in two situations, (1) when only the head pressure (gravity) of the melt was in place which could provide up to 15 mbar with the maximum level of melt (25 ml) in the supply unit, and (2) when a pressure was applied.

4.6.2 Supplying Molten Caprolactam

The molten caprolactam did not initially fill the printhead under gravity as no melt was observed on the nozzle plate. This could have been due to the resistance of the melt to flow through the filter membrane. Therefore, an initial pneumatic pressure of up to 100 mbar was required. This filled the printhead and provided dripping of the melt via the nozzles. After removing the pressure though, the dripping continued at a lower rate. The flow rate due to the head pressure after initiation was found to be consistent at about 0.3 g/min (or about 0.3 ml/min) as Figure 4-13 shows. A vacuum of about 10 mbar could stop the dripping and retract the excess melt on the nozzle plate into the printhead. This experiment showed that supplying the molten

caprolactam for jetting required an initial pressure and then a vacuum to initiate the meniscus condition on the nozzles.

In some trials, air bubbles were trapped inside the printhead when supplying molten caprolactam as Figure 4-14 shows. These images were taken at the start and end of a pressure signal of about 100 mbar amplitude. Air could be trapped when inserting the bar cartridge and could affect the supply behaviour of the melt. Due to the micro size channels of the printhead, there could also be some air bubbles trapped and not removed by the pressure purging. A bleeding tube was used to ensure the removal of the trapped air from the melt supply before the jetting trials.

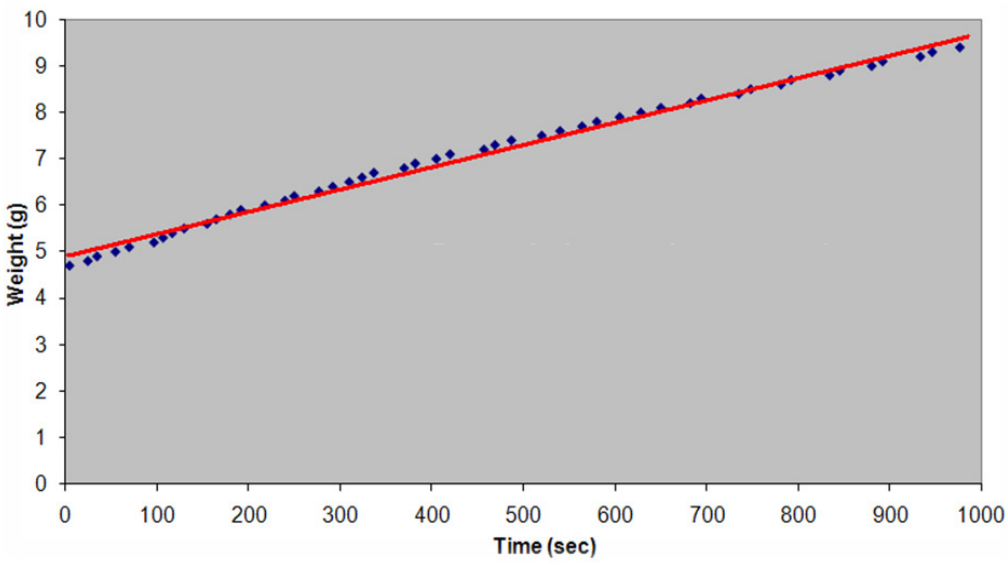

Figure 4-13 Molten caprolactam flow due to the head pressure from the melt supply level in the jetting assembly (after initiation by a pressure signal)

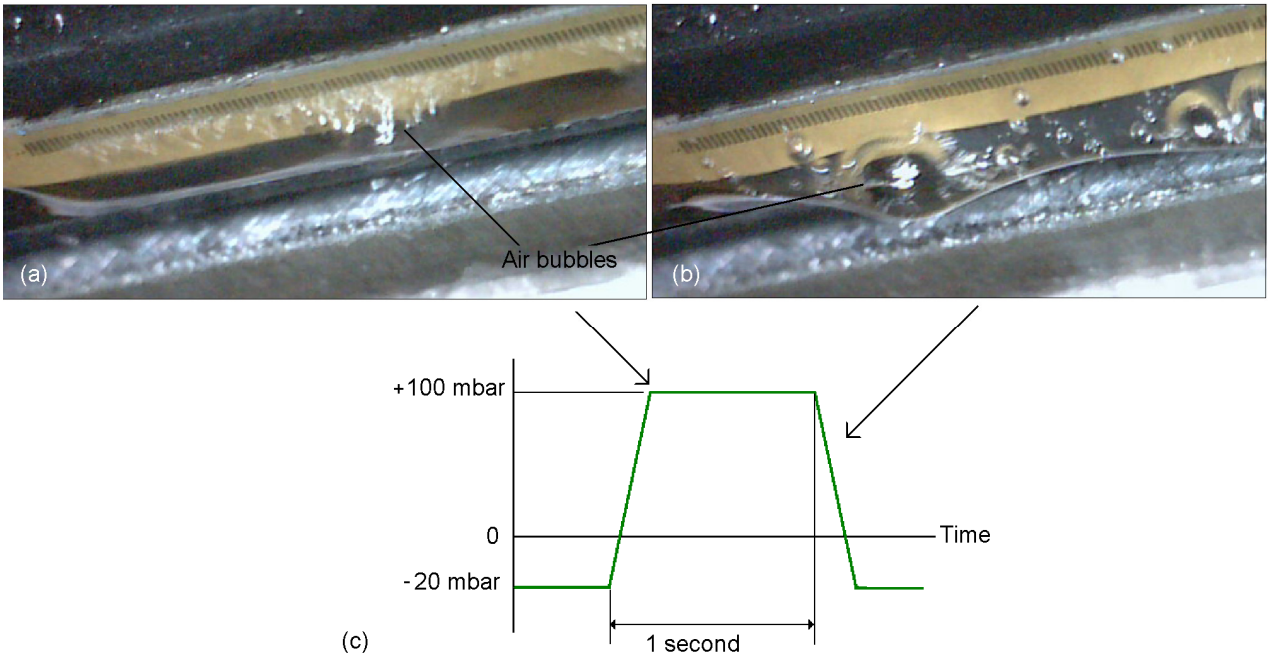

Figure 4-14 Air bubbles trapped in the printhead revealed by purging of the molten caprolactam, (a) start of the pressure signal, (b) end of the pressure signal, (c) the pneumatic purging signal

4.6.3 First Set of Reactive Mixtures (synthesised)

Similar conditions to the pure caprolactam were considered for feeding the melt supply unit with the reactive mixtures. With the synthesised activator, dripping was initiated with a starting pressure of up to 150 mbar. Similar to caprolactam, dripping for this activator mixture continued due to gravity, however, at a lower rate than pure caprolactam which could be controlled with vacuum levels above 5 mbar.

The synthesised catalyst mixture behaved very differently compared with the activator mixture. No dripping was observed with 150 mbar pressure. Even after increasing the pressure to 750 mbar (maximum possible in the setup), no melt was observed passing through the nozzles. In fact, the melt did not reach the printhead. This was found after removing the melt supply unit from the printhead. By applying a vacuum of 15 mbar, the melt could back up into the aluminium syringe, so that the filtration unit could be separated from the rest of the melt supply unit to check the

status of the filter membrane. Only a small amount of melt was observed beyond the filter membrane. However, without the filtration unit and when removing the vacuum holding the melt in the syringe, the melt purged out through the supply unit syringe tip under gravity which showed blocking of the filter membrane had occurred during pressure purging.

The test was repeated three times, each using a new filter membrane and fresh catalyst mixture cartridges. All trials encountered the same filter blocking problem. One possibility was the melt freezing in the filtration unit. Therefore, the temperature was monitored in the empty side of the filtration unit during operation and found to be about 75℃ at which the melt was still expected to flow. The melt supply temperature was increased to 90℃ in a new trial and similar blocking was observed. Therefore, it was assumed that the microcrystals of the catalyst mixture blocked the pores of the filter membrane. Without a filtration unit, the printhead would be blocked and need replacing. Although elevated temperatures as high as 150℃ could dissolve the microcrystals (as seen in Figure 4-11), this was not practical due to the thermal limitation of the printhead.

4.6.4 Filter Blocking and New Sets of Mixtures

The filter blocking with the synthesised catalyst in the first set of mixtures led to the use of new mixtures. The 25 mm diameter filter membrane with a 5 µm pore size had a thickness of 170 µm, a porosity of 60% and a tortuous pore structure (Millipore Corp. 2008). Blocking of the pores could occur by trapping individual large microcrystals. It was thought that commercial catalyst mixtures instead of the in-lab synthesised mixture would have smaller microcrystals or be better dissolved for resolving the problem with the melt supply. In addition, trapping the microcrystals

during filtration could lower the concentration of the catalyst mixture. If the supplied 10% concentrated mixture of the new set had a concentration below 5% after purging through the system, it could affect the reaction as discussed in section 4.2.5. Therefore, it was thought that increasing the catalyst mixture concentration within the recommended range for reaction, from 10% to 20%, could reduce the risk of failure of reaction. Therefore, 20% concentration was uses as well as 10% for the melt supply behaviour study with the new sets of mixtures.

4.6.5 Second Set of Reactive Mixtures

The commercial activator mixture at both concentrations (10% and 20%) behaved similar to the synthesised activator in the first set (N-AcCL-CL, 10%). Dripping was achieved with about 150 mbar at the start of the melt supply. This could then be controlled with a vacuum of above 5 mbar. The challenge though remained with the diluted catalyst mixture at both concentrations (10% and 20%). It behaved similar to the synthesised type (CLMgBr-CL) in repeated experiments. Using the highest possible pneumatic pressure of 750 mbar, the printhead was filled and a small amount of melt was observed on the printhead nozzle plate but no dripping occurred. The new catalyst mixture also blocked the filter. Therefore, the catalyst mixtures based on the caprolactam magnesium bromide were discontinued for future stages of the research.

4.6.6 Third Set of Reactive Mixtures

The sodium caprolactamate based catalyst mixture (C10-CL) was then used for the third set to study the melt supply behaviour. C10 was diluted with caprolactam at 10% concentration initially and was fed into the melt supply unit. An initial pressure

of 150 mbar did not provide dripping through the printhead. With increasing pressure, a small amount of melt was observed on the nozzle plate. A pressure of 750 mbar could provide dripping of the melt at a rate below 1 ml/min at the start of purging. However, the dripping rate was low and decreased over time until it stopped. This was before the whole amount of mixture from the supply unit was purged through the printhead. After separating the supply unit from the printhead, it was found that the filter membrane was blocked. This occurred after about 8 to 12 ml (of the 15 ml fed into the system) was purged in repeated trials. This showed that the catalyst complex of the third set of mixture possibly had a particulate nature too. The results of hot stage microscopy confirmed this (which will be discussed in section 4.7).

Before filter blocking occurred, there was a large meniscus on the nozzle plate which could be retracted with a vacuum of about 10 mbar. This showed that although purging the molten catalyst mixture initially required a high pressure to fill the printhead, a vacuum could provide appropriate meniscus control for droplet formation.

The 20% concentrated C10-CL catalyst mixture was used to study the melt supply behaviour. The test was repeated several times, and each time with a new filter membrane. The results showed that the filter membrane was blocked earlier than the 10% concentration and purging could provide 6 to 8 ml out of a total of 15 ml fed into the system.

There was dripping of melt with this higher concentration mixture when the purging pressure was set at 750 mbar. By applying this pressure continuously, the dripping rate was 0.6 ml/min at the start of purging which decreased to 0.2 ml/min after typically purging 5 ml of the molten mixture. When removing the pressure at this

stage, the dripping stopped and a large melt meniscus formed on the nozzle plate. It required about 10 mbar vacuum for up to 5 sec to retract the meniscus into the printhead completely. After applying the 10 mbar vacuum for 10 sec, the 750 mbar pressure was applied (continuously) again which resulted in dripping at a rate of 0.6 ml/min for the first minute. This however decreased to 0.2 ml/min in the third minute of reapplying the pressure. This may suggest that the filter was temporarily unblocked with the vacuum. Practicing this procedure did not work when the filter membrane was blocked completely and no further dripping could be obtained.

A supply of 8 ml would be sufficient for the later research. Therefore, it was decided not to search for a new catalyst mixture. Therefore, C10-CL as the catalyst and its matching activator mixture, C20P-CL, were preferred to be used at 20% concentration as the finalised set of reactive mixtures for the jetting trials rather than the 10% concentration due to the concern over the effect of filtration onto the reaction.

4.7 Microcrystals beyond the Jetting System

4.7.1 Filtration and Microcrystals Content

The concentration of the catalyst microcrystals could vary due to the filtration stage and this could be an important variable affecting the material behaviour during jetting, deposition and especially the drop-on-drop reaction. Therefore, a new process parameter would be how much melt was purged when a jetting trial was undertaken. This parameter was considered as “melt supply level” in this thesis.

It would be difficult to determine the concentration of the catalyst mixture after the jetting system at different melt supply levels as detection of the entire catalyst complex was not possible due to the limitations in the microscopy (magnification and

2D imaging). However, microscopy of the detectable microcrystals and quantifying their content could give an understanding of the possible variations made by the filtration within the supplied melt for jetting. Therefore, it was decided to undertake such investigation with the finalised catalyst mixture (C10-CL, 20% concentration).

4.7.2 Procedure

The catalyst mixture was purged through the jetting assembly using a continuous pneumatic pressure of 750 mbar which produced dripping of the molten mixture. The samples were collected at different melt supply levels by depositing two molten drops (about 0.2 ml) onto a microscope slide (at each melt level) which was then immediately packed into a sealed bag. The printhead required about 2 ml to fill and filter blocking occurred at a minimum melt supply level of 6 ml. Therefore, samples were taken after 2, 3, 4 and 5 ml of the melt being purged.

Polarised light optical microscopy and image processing were employed with the procedure as explained in section 4.5.1. From each (0.2 ml) purged sample at each melt level, a smaller sample of about 1 µl was taken from the solidified mixture and was placed onto a clean glass slide for the hot stage microscopy. When the sample was molten, a thin glass cover slip was placed on top. The chosen sample volume (1 µl) could cover the microscopy area of the slide (under the cover slip). For each melt level, this procedure for sampling was carried out three times and each time, the smaller (1 µl) sample was taken from a different place of the larger sample to investigate the repeatability of the microscopy results.

The monochrome camera of the optical microscopy could capture greyscale (256-level) images of about 1400 µm x 1000 µm in size. The molten sample area (under

the cover slip) was about 24 mm x 24 mm, therefore samples images were taken as shown schematically in Figure 4-15.

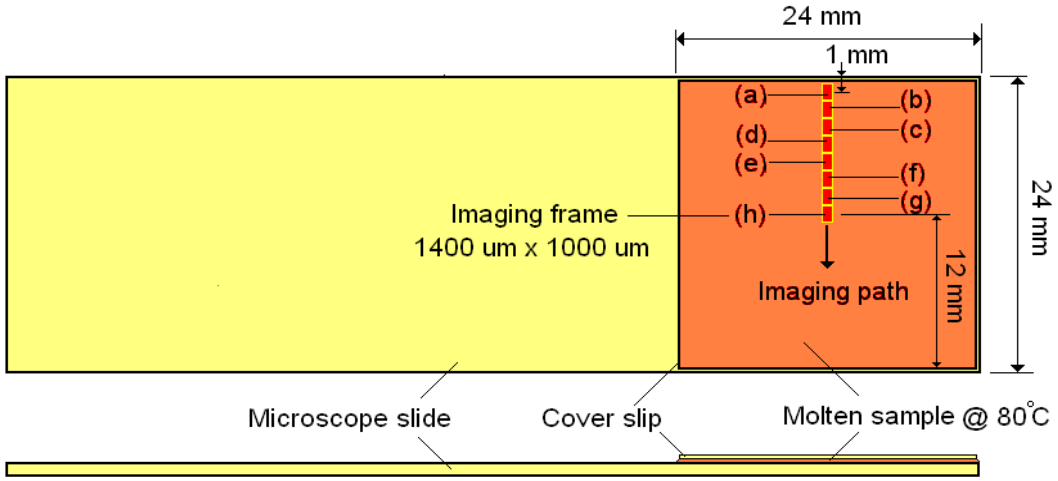

Figure 4-15 Arrangement for optical microscopy of the catalyst mixture for characterising microcrystals

In addition to the eight frames shown in Figure 4-15, intermediate frames were taken. Therefore, fifteen frames were captured which had 50% overlap area with adjacent frames. This was to give a more accurate quantification of the microcrystal content. Therefore, with microscopy of three samples at each melt level, 45 images were produced. In addition, the whole procedure was repeated (with a new mixture supply) to produce a second series of samples from which another 45 images were generated. Image processing was carried out using the grey-binary transformation at a threshold grey level of 128. The total of 90 images taken by the microscopy were processed for each of the four melt levels (2 to 5 ml).

4.7.3 Microcrystals Content and Behaviour

Figure 4-16 shows a set of images corresponding to the arrangement shown in Figure 4-15 (from *a* to *h*). The dark background represents the molten caprolactam whereas the brighter areas represent the microcrystals. Two conclusions could be drawn from the images. One that the microcrystals were agglomerated in different areas and did not disperse equally within the sample, and the other is that concentration of the microcrystals varied considerably. The variation was significant between some of the images (compare frame (a) with (f) in Figure 4-16). This was a typical example from a sample at the 4 ml melt level. This agglomeration behaviour and its variation were observed in all samples within different melt levels.

Figure 4-17 compares images of pure caprolactam, the activator mixture (C20P-CL, 20% concentration) and the catalyst mixture, prior to and after the image processing. The white pixels in Figure 4-17(f) represent the microcrystals in the catalyst mixture as originally seen in Figure 4-17(e). They did not exist in pure caprolactam or the activator mixture as seen in images from Figure 4-17(a) and (c). Some areas on the left of Figure 4-17(e) were not as bright as the areas on the right. However, both areas were transformed into white pixels by the imposed threshold grey level as seen in Figure 4-17(f). This difference in brightness could have been due to the agglomeration state of the microcrystals within the samples affecting polarisation of the light, and therefore the final light intensity. The white pixels were counted by the image processing software to quantify the total area of the microcrystals in relation to the image size.

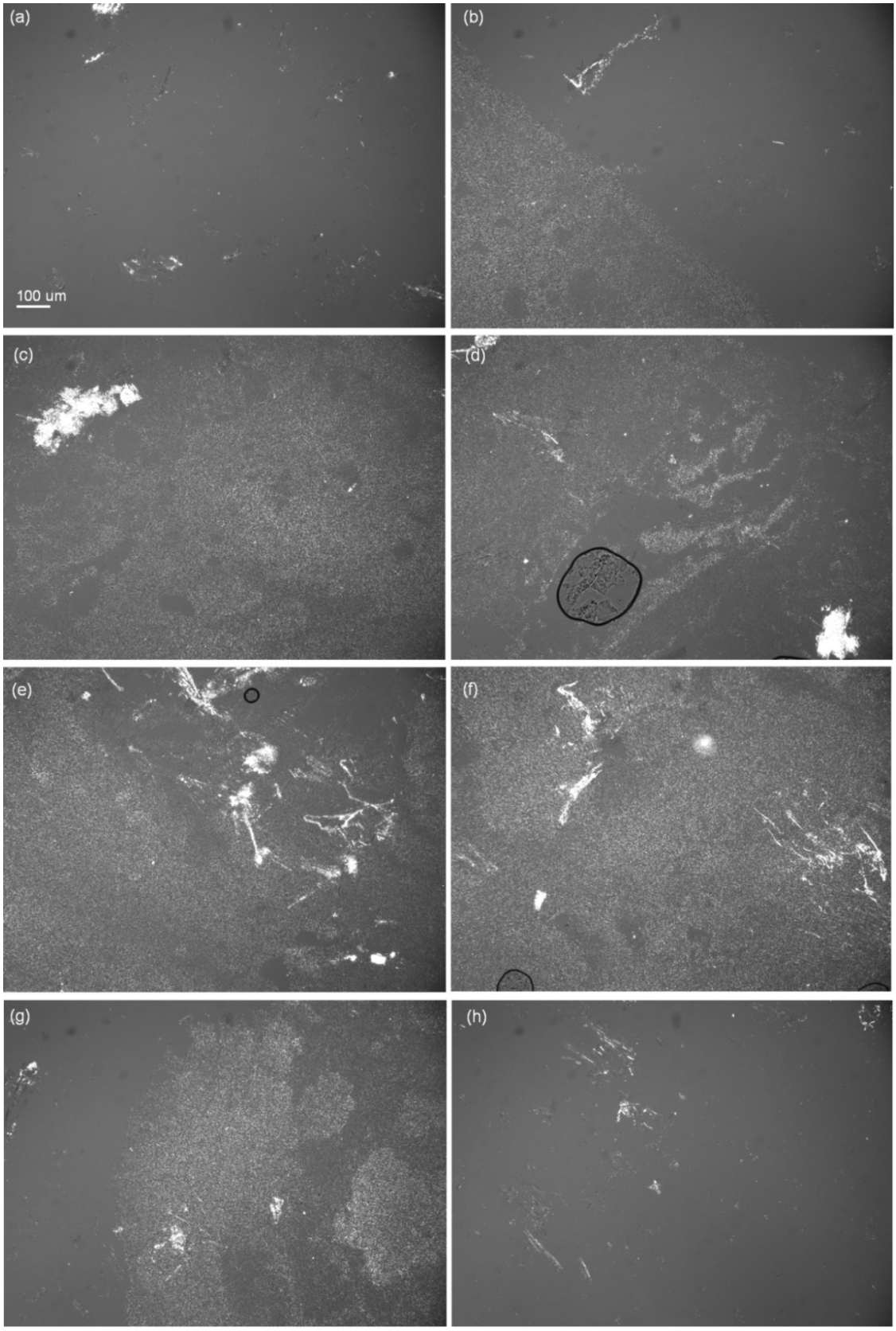

Figure 4-16 Polarised light microscopy images of the catalyst mixture (C10-CL, 20% concentration) from the 4 ml melt level at 80℃. Images in (a) to (h) correspond to the labels as shown in Figure 4-15.

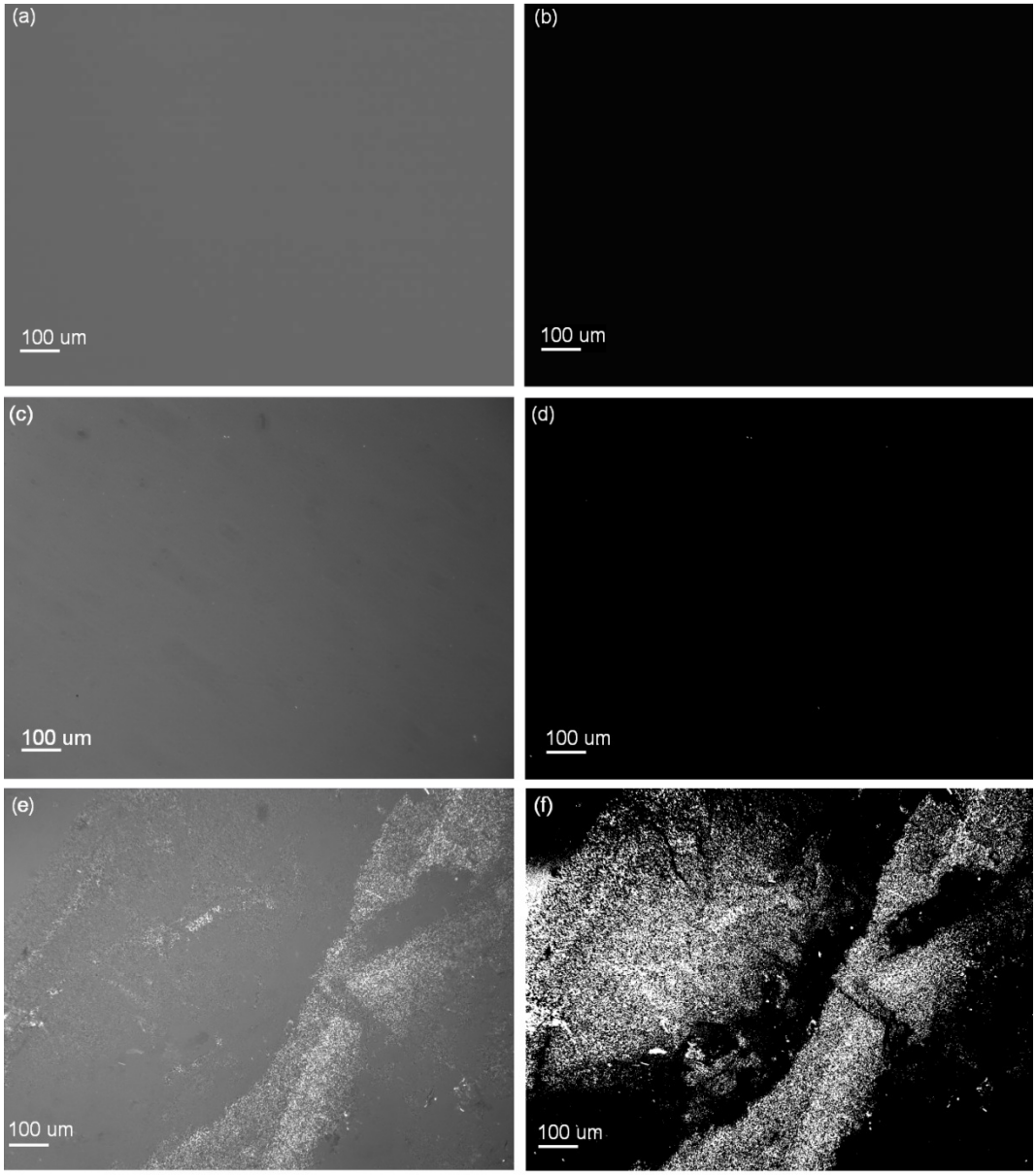

Figure 4-17 Images from optical microscopy using grey-binary transformation (grey threshold level of 128), for caprolactam: (a) original image, (b) processed image; the activator mixture (C20P, 20% conc., 2 ml melt level): (c) original image, (d) processed image; and the catalyst mixture (C10, 20% conc., 2 ml melt level): (e) original image, (f) processed image

4.7.4 Quantifications for Microcrystals

Figure 4-18 shows the results for the first series of samples with the catalyst mixture. For each melt level, it is shown that the concentration of the detected microcrystals

varied with location and also between the triplicate samples. This behaviour was also repeated in the second series of samples as seen in Figure 4-19. There was no relationship between the microcrystal content and the melt level as shown in Figure 4-20. However, the majority of samples had an average microcrystal area of about 15% and the total average of all 90 images from all the samples was 12.9%.

A lot of fluctuation is seen in the microcrystal content of the samples made by purging. The agglomeration could be a physical tendency of the microcrystals possibly due to their adhesion behaviour. Placing the cover slip onto the molten samples could further influence this as the consequent melt flow could further assist them to collide and agglomerate and consequently vary the dispersion of the microcrystals. These samples were produced by purging large volumes of melt through the nozzles whereas the actual situation would be droplets deposited onto the surface. Therefore, for a better understanding of the microcrystal content of the jetted melt, individual droplets were deposited directly onto a glass slide to analyse with the polarised microscopy, for which a cover slip would not be needed as a droplet was expected to spread upon impingement, enough for microcrystal dispersion detection. This approach was investigated in the deposition stage and the results are reported in Chapter 7.

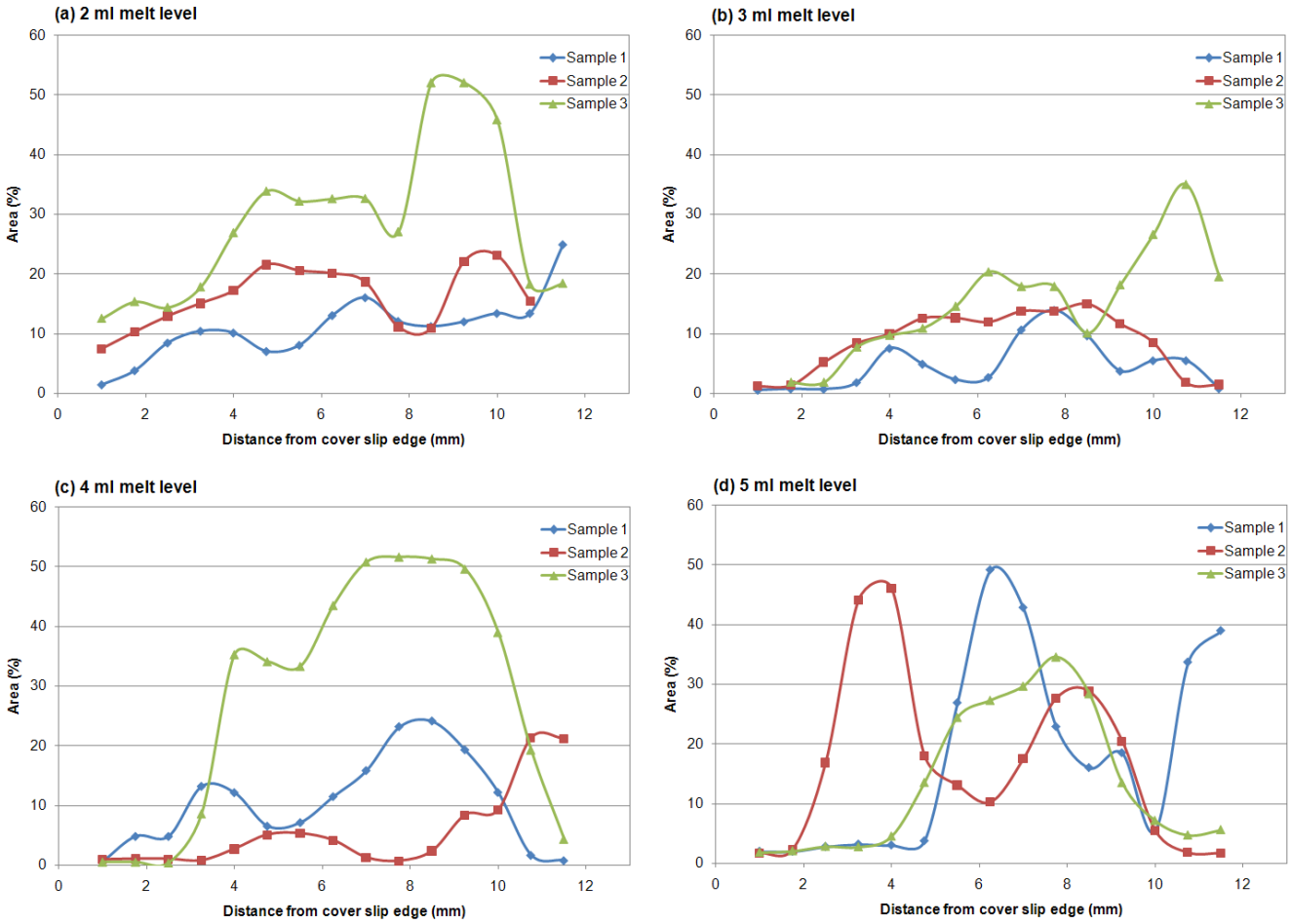

Figure 4-18 Microcrystal content as white pixel area at different imaging locations as shown in Figure 4-15 for different melt levels of the first series of samples

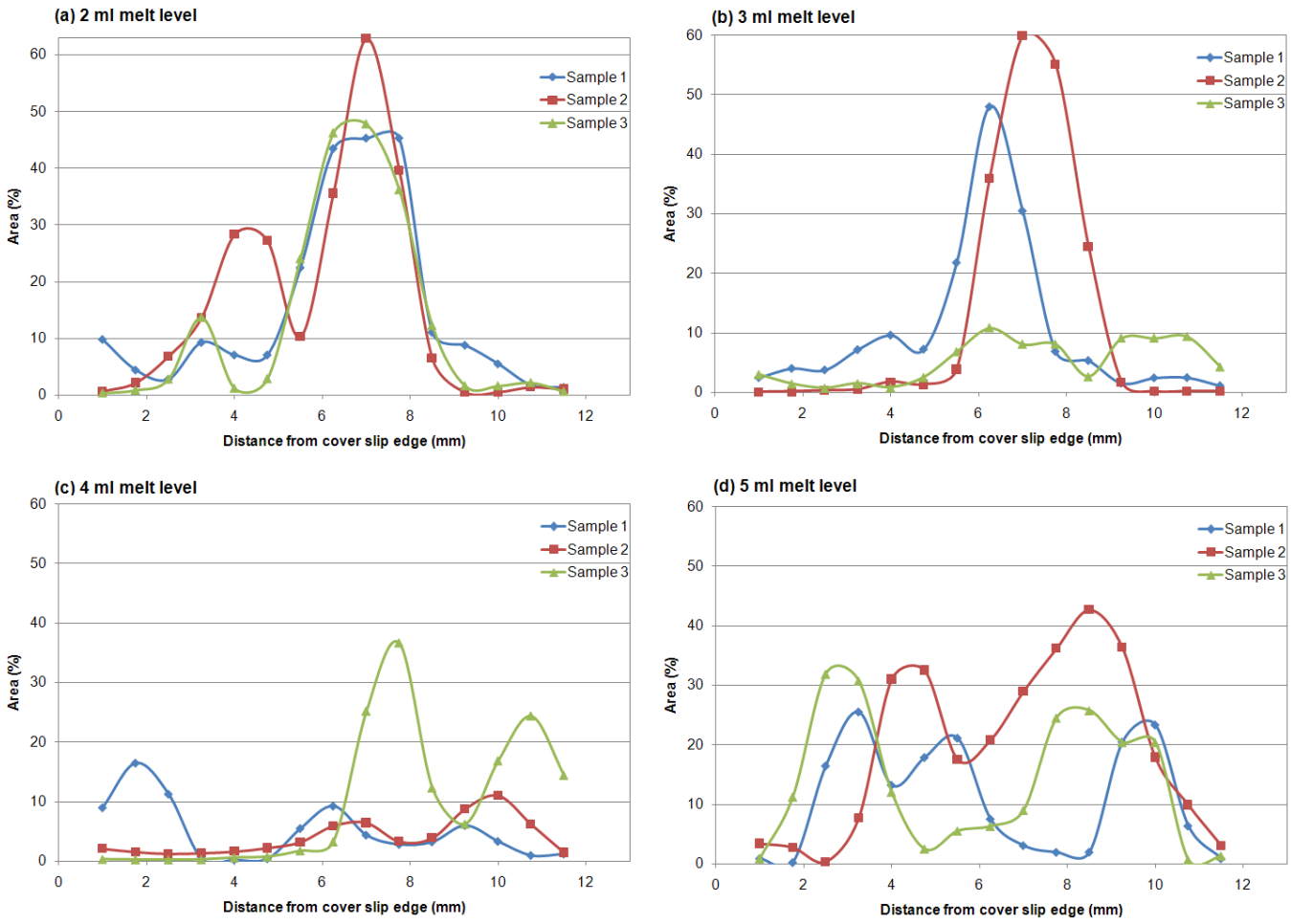

Figure 4-19 Microcrystal content for different melt levels of the second series of samples

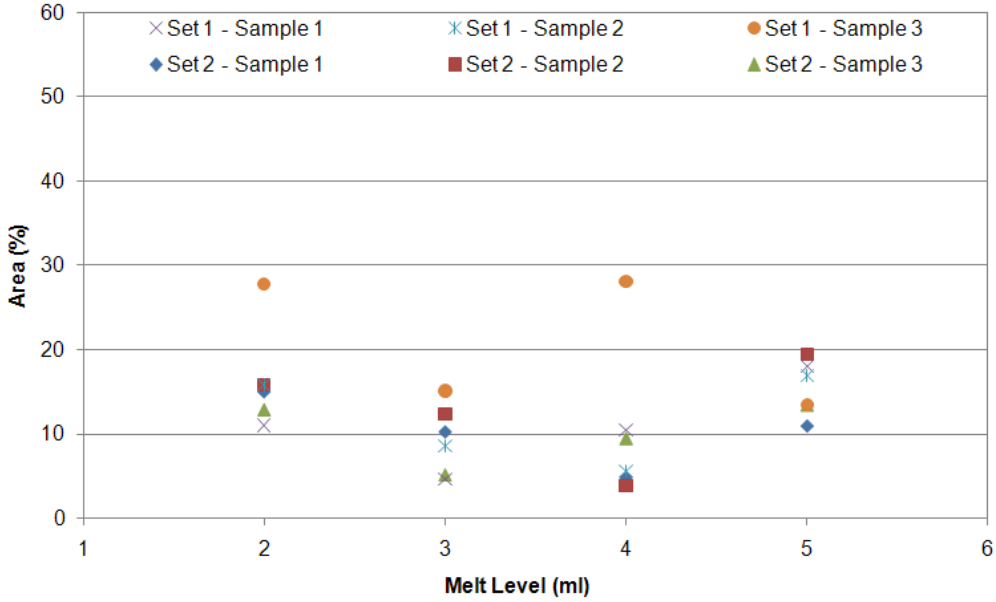

Figure 4-20 Mean values for microcrystal content area vs. melt level for the two sets of trials

Chapter 5. Jetting of Caprolactam and the Reactive Mixtures

This chapter presents the investigations into jetting of molten caprolactam and the reactive mixtures and in particular jetting stability and interaction between the jet array and the nozzle plate.

5.1 Procedure for Jetting Trials

5.1.1 Materials for Jetting Trials

The results of previous chapter suggested that C20P-CL and C10-CL at 20% concentration should be used for the jetting trials. However, initial jetting trials were undertaken with caprolactam to narrow down the process window for the reactive mixtures.

5.1.2 Jetting Parameters

Controllable variables for the jetting were the melt temperature, the voltage signal for droplet generation and the vacuum level. The melt temperature was set at 80℃ in the jetting assembly. For the voltage signal, the amplitude and frequency could be varied whereas the waveform and pulse width were fixed by the printhead manufacturer. The pulse amplitude and the signal frequency could be varied within 0 to 40.0 V and 0 to 5.2 kHz respectively. The vacuum level which affected the meniscus shape and therefore the droplet formation process, was varied from 5 to

50 mbar. The melt level was also considered as a process parameter for jetting of the mixtures and the trials were carried out after 2, 3, 4, and 5 ml of melt were purged through the system, to investigate its effect on the jet stability.

Before the melt supply system was developed for the caprolactam and the reactive mixtures, a normal graphical ink (Xaar 861, an oil-based ink) was used in a functionality test with the printhead. The test trials with the black ink were undertaken within the full range of 0 to 40.0 V and frequency range of 1 to 5 kHz. Droplet formation occurred with a minimum voltage of 15.0 V at all frequencies. This helped to design the experiments for the jetting trials.

Figure 5-1 shows the nozzle plate and the nozzle array after the functionally test. The black rectangular features containing the nozzles in the middle were made by removing material from the nozzle plate surface to ease the droplet separation.

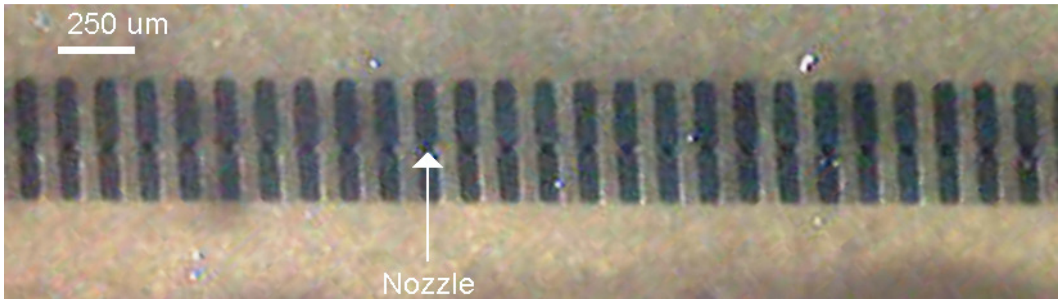

Figure 5-1 Nozzle array on the printhead

5.1.3 Start-up Strategy for Jetting Trials

The start-up strategy ensured a supply of the melt to the printhead before nozzle actuation. Figure 5-2 shows a start-up strategy with 5 pressure/vacuum conditions. State 1 was just after the jetting assemblies reached 80℃. No melt was observed on the nozzle plate with atmospheric pressure. Therefore, pneumatic pressure was applied to purge out the melt through the nozzles which provided dripping, seen as

State 2 in Figure 5-2. The dripping continued after removing the pressure signal as seen in State 3. In this state, the nozzle plate was cleaned with a lint-free cloth in order to remove any contamination within the excess melt on the nozzle plate. In State 4, a vacuum was applied to stop the dripping and retract the large meniscus. To obtain the appropriate meniscus on the nozzles for droplet generation, the applied vacuum level was increased to more than 10 mbar which provided a thin layer on the nozzle plate as seen in State 5 in Figure 5-2.

From the functionality test of the printhead with the black graphical ink, some particles were left inside the printhead during subsequent trials with molten caprolactam. This enabled better observation of the thin molten layer in State 5 via movement of the black particles on the nozzle plate as shown in Figure 5-3. The black particles were then removed by purging the melt and cleaning the nozzle plate with lint-free cloth.

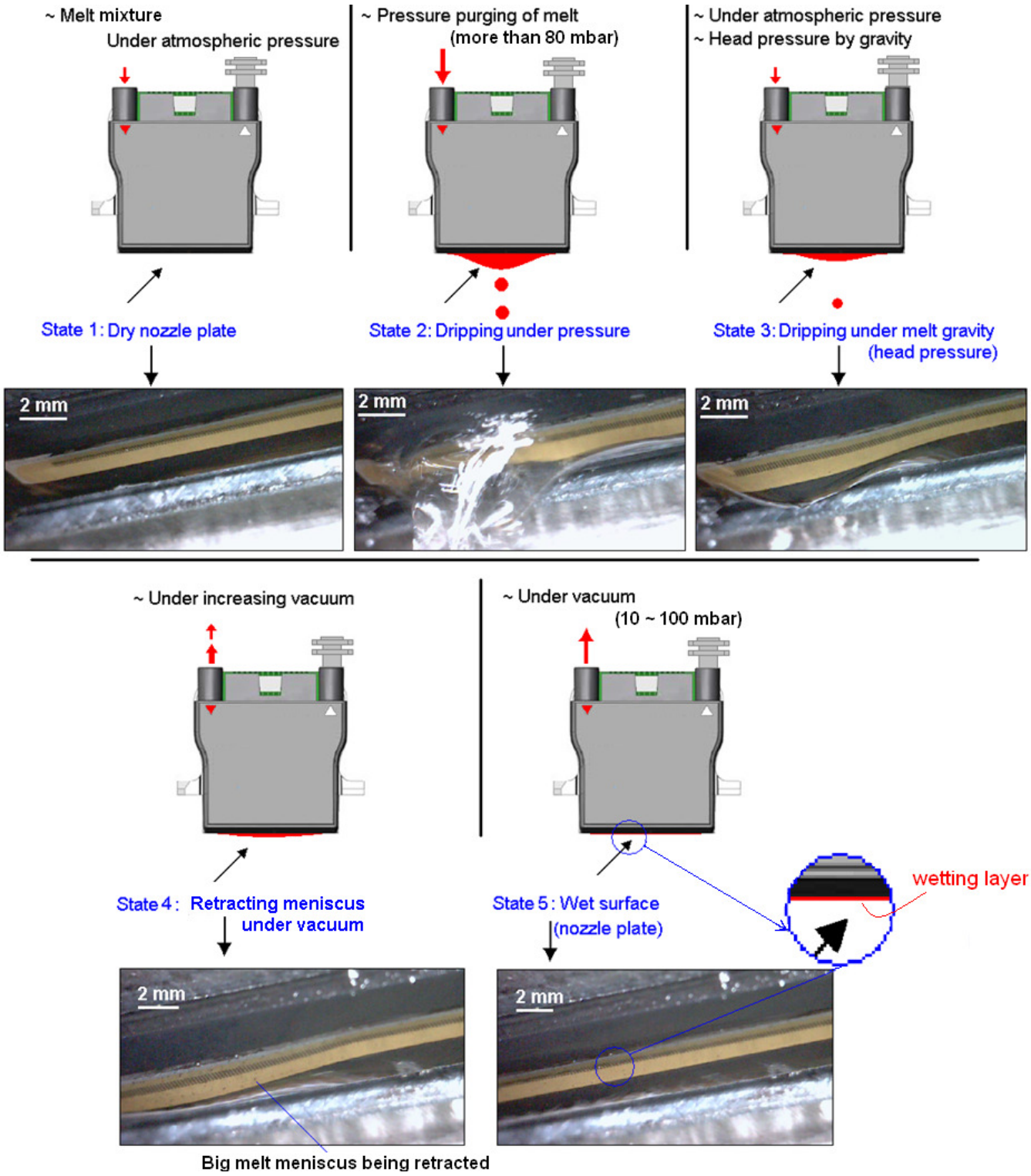

Figure 5-2 Sequence of the start-up for jetting trials

Figure 5-3 Black particles in the thin molten layer on the nozzle plate with a vacuum level of 20 mbar

5.2 Jetting of Caprolactam

5.2.1 Jetting Trials for Caprolactam

Table 5-1 lists the sets of experiments undertaken for jetting of molten caprolactam. All the trials were repeated three times and for at least 10 seconds each. Set 1 was to find the appropriate vacuum level which could control the melt flow and the melt meniscus on the nozzle. With the microscope camera, the nozzle plate was monitored when varying the vacuum level. It was found that a minimum vacuum level of 10 mbar was required to control the meniscus. In other sets of experiments, jettability and jet stability of molten caprolactam were studied. Both single jet and multiple jets were studied in the experiments.

Set 2 was to investigate if a stable jet could be developed when varying voltage and frequency. This was with two vacuum levels. The range of voltage and frequency was selected based on the experience from trials with ink. It was found that frequency did not affect the jet stability and the chosen voltage increments did not make a visible change for trials with 15.0 V and over. Therefore, investigations continued with a new set of experiments in Set 3, where jetting frequency was fixed at 5 kHz and voltage increments increased to 5.0 V. In this set of experiments, the vacuum level was varied over a wider range to observe any significant effect on the

jet array stability. At higher vacuum levels, with high voltage, jet failure was observed in the jet array by air ingestion. Therefore, a new set of experiments (Set 4) was undertaken to investigate the effect of voltage and vacuum level on the jet failure especially at high values. A finer voltage increment and a wider range of vacuum level were used to observe the stability behaviour.

Set	Experiments Objective	Jetting Status	Voltage (V)		Frequency (kHz)		Vacuum (mbar)	
			Range	Inc.*	Range	Inc.	Range	Inc.
1	Meniscus control	No jetting	-	-	-	-	0 ~ 20	5
2	Jet stability	Jetting	10.0 ~ 20.0	2.5	1 ~ 5	1	15, 25	-
3	Jet array stability	Jetting	15.0 ~ 25.0	5.0	5	-	5 ~ 35	10
4	Air ingestion	Jetting	12.0 ~ 26.0	2.0	5	-	10 ~ 50	10

** Increment*

Table 5-1 Experiments undertaken for jet stability study of molten caprolactam

5.2.2 Jet Stability Observation

One of the main objectives of this research was to investigate whether molten caprolactam could be jetted with a normal graphical industry printhead. This was confirmed initially by triggering one nozzle of the printhead in Set 2 of the experiments. A single jet of molten caprolactam was achieved as seen in Figure 5-4 with voltage, frequency and vacuum level set at 17.5 V, 4 kHz and 15 mbar respectively. Multiple jets of caprolactam were also produced as seen in Figure 5-5 (with 126 jets) with 17.5 V, 5 kHz and 25 mbar and all jets were stable. However, within the trials some instability occurred especially when jetting an array as seen in Figure 5-6. As the instability could have originated externally by contamination or air motion, the trials with instability were repeated after a purging period (for a further three times). This was to check if the instability occurred due to improper setting of parameters.

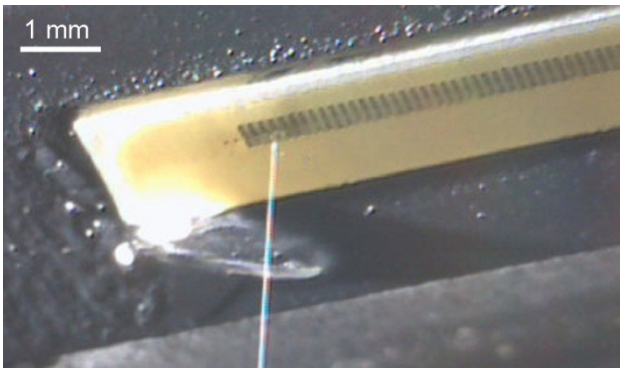

Figure 5-4 Single jet of caprolactam (17.5 V, 4 kHz, 15 mbar, Set 2)

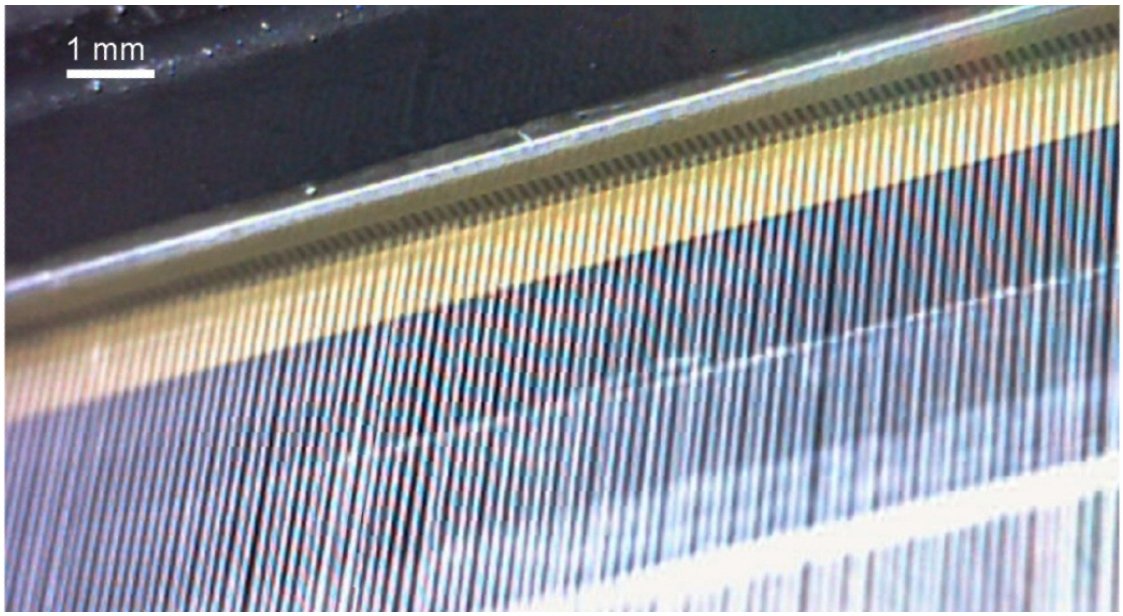

Figure 5-5 Jet array of melt caprolactam (17.5 V, 5 kHz, 25 mbar, Set 2)

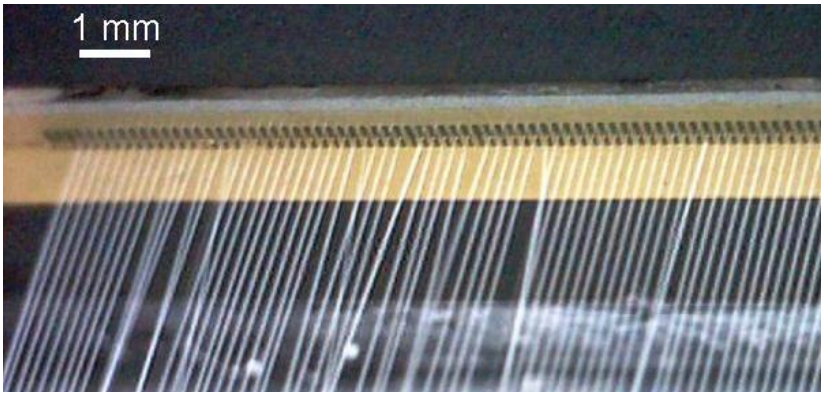

Figure 5-6 Jet instabilities during trials with molten caprolactam

Figure 5-7 shows the results for Set 2 experiments. Similar stability behaviour was seen irrespective of the jetting frequency or vacuum level used for both single and multiple jets. Decreasing jetting voltage, however, resulted in instability and no jet was developed with a low voltage of 10.0 V. The effect of jetting voltage and vacuum level on the jet stability is shown in Figure 5-8 which presents results for Set 3. No jet occurred with 5 mbar vacuum level and instability occurred when using low jetting voltage and a 10 mbar vacuum. Also, a combination of high values of these two parameters resulted in unstable jets. Results from Set 4, shown in Figure 5-9, give a better understanding of the instability behaviour when varying voltage and vacuum levels. Some jets failed in the jet array with the vacuum set at 50 mbar at all jetting voltages at the very start of the trial. All the remaining jets failed within seconds which indicated a time-dependent phenomenon responsible for the jet failures.

Figure 5-7 Stability of single jet and jet array in Set 2 (15 and 25 mbar)

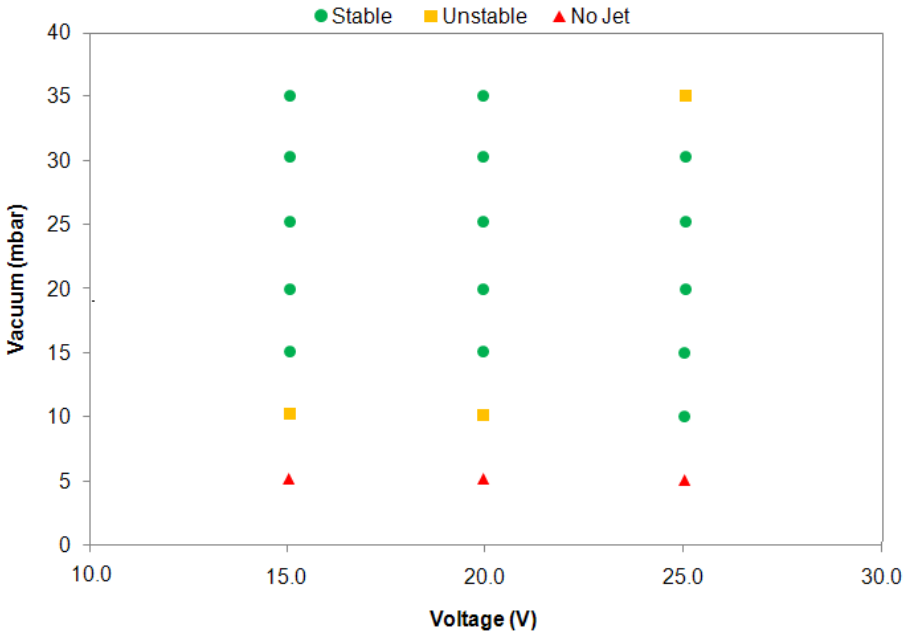

Figure 5-8 Stability of single jet and jet array in Set 3 (5 kHz)

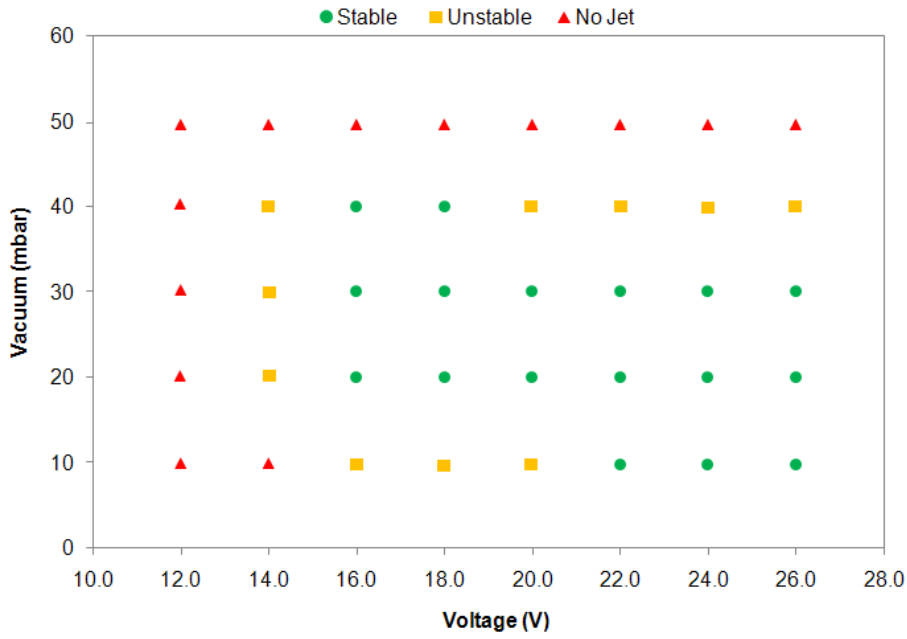

Figure 5-9 Stability of single jet and jet array in Set 4 (5 kHz)

5.2.3 Jet Instability Classification

Instabilities occurred in the form of individual jet trajectory which could lead to single jet failure and occasionally jet array failure where all jets in an array failed. In most

cases, this started from a single jet failure. Figure 5-10(b) illustrates the instability types in individual jets. In Figure 5-10(a), the front and side view schematics of the jet array depict the types of instabilities, and Figure 5-10(b) shows the actual situation. The jetting plane was considered as the plane normal to the nozzle plate passing through the line of jets. As a jet with an off-plane error did not reflect light the same as the others, it was easily recognised as in Figure 5-10. The side trajectory error was defined as still on the jetting plane but angled towards an adjacent jet. A failed jet is also shown in Figure 5-10.

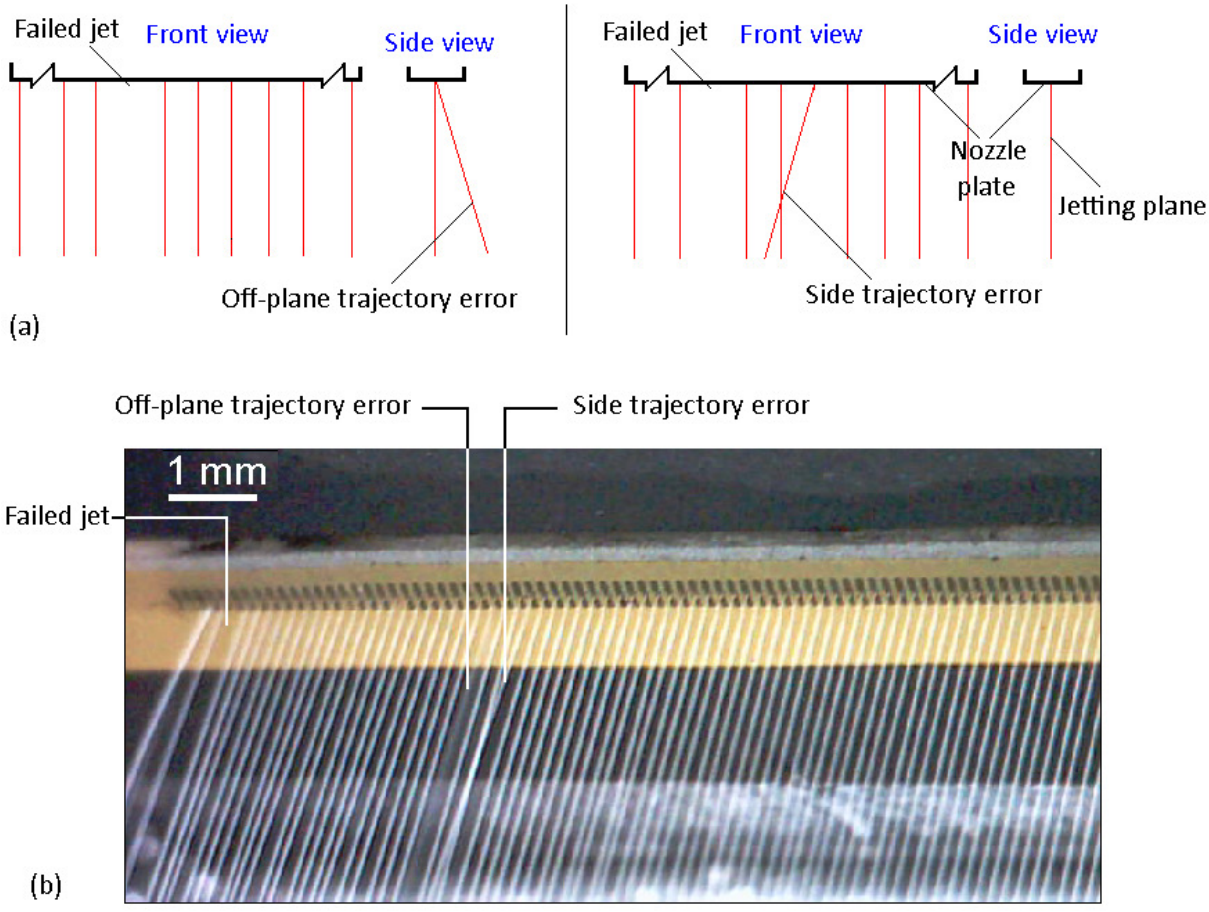

Figure 5-10 Instabilities of individual jets in the jet array (a) schematic (b) actual situation (15.0 V, 5 kHz, 30 mbar)

5.2.4 Instabilities due to the Parameter Settings

With the start-up strategy, the risk of air entrapment in the melt supply was eliminated but there were still instabilities in individual jets or in the array of jets in some experiments. Jet instability was observed when the jetting voltage and vacuum level were low. No jet was produced for jetting voltages below 10.0 V and with vacuum levels as low as 5 mbar. In such a case, the pressure wave generated by the nozzle actuation inside the melt channel was dissipated when propagating towards the meniscus on the nozzle as the melt layer on the nozzle plate was too thick.

With jetting voltages below 15.0 V with all vacuum levels or 20.0 V and vacuum levels equal to or below 10 mbar, a trajectory error occurred as seen in Figure 5-11. The cause of the instability was the combination of low voltage and vacuum resulting in inadequate meniscus oscillation amplitude. This situation was also recorded as shown in Figure 5-12. From the first ejected droplet in Figure 5-12(a), a trajectory error of 8 degrees is seen. The trajectory error increased to 12 degrees after 0.8 ms of jetting (Figure 5-12(b)) and then to 45 degrees after about 335 ms (Figure 5-12(c)). This continued until the jet was parallel to the nozzle plate (Figure 5-12(d)). When the droplets touched the nozzle plate, it led to failure of the jet after about 1 sec. This shows how the individual jets could become unstable when using inadequate jetting voltage and vacuum level.

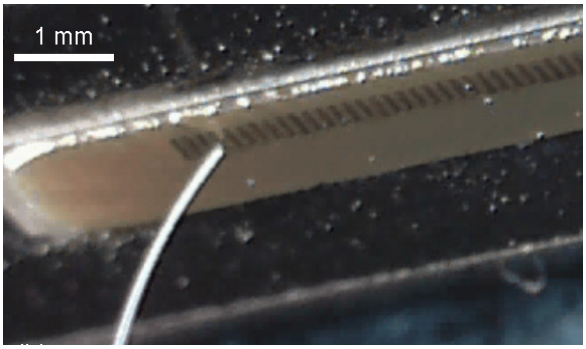

Figure 5-11 Single jet of caprolactam with trajectory error due to low jetting voltage (13.0 V, 4 kHz, 15 mbar)

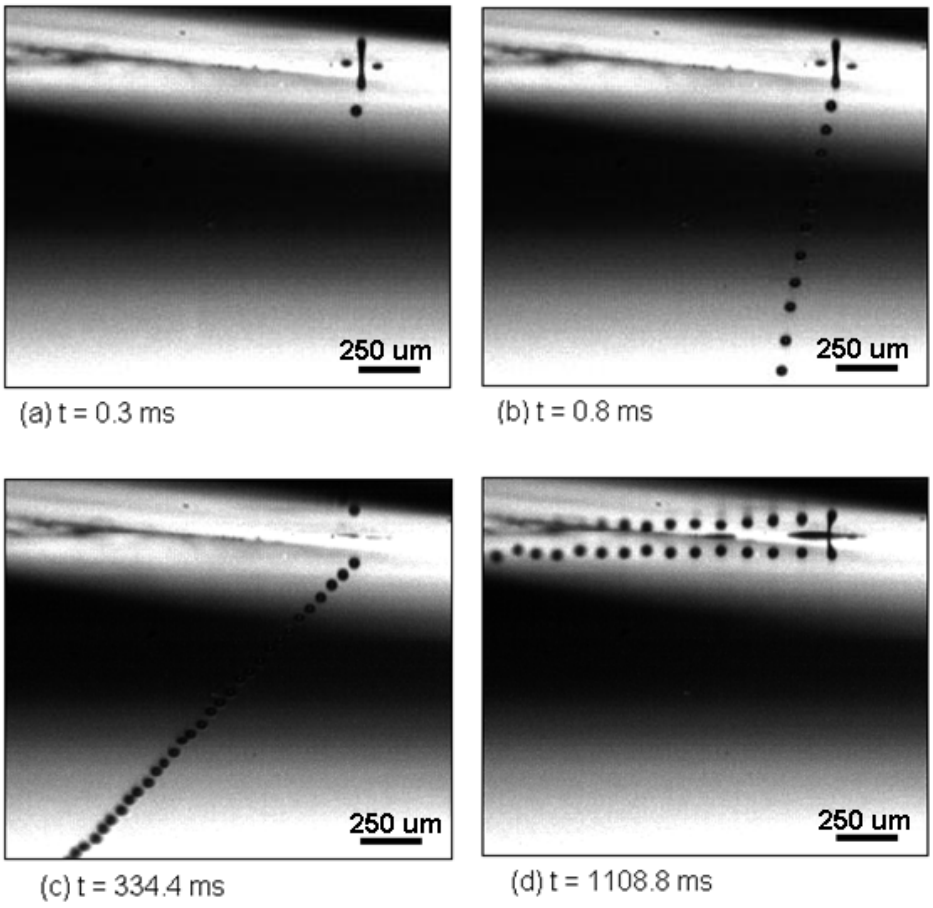

Figure 5-12 Jet trajectory alteration by air motion in a trial with a combination of a low jetting voltage and vacuum level (13.0 V, 5 kHz, 25 mbar)

Figure 5-13 shows jet instability in an array which originated from the jetting parameters being set too low. However, as Figure 5-13 shows, more jets exhibited

instability with low jetting voltage (Figure 5-13(a)) than with low vacuum level (Figure 5-13(b)). Increasing the jetting voltage from 12.0 to 15.0 V increased the number of stable jets significantly despite the decrease of vacuum level from 20 mbar to 10 mbar. This behaviour was repeatable within the trials which suggests jet stability was influenced by voltage more than vacuum level.

Droplets with less kinetic energy were generated with low jetting voltages or low vacuum levels due to the pressure wave dissipation in the meniscus oscillation. Therefore, air motion around the nozzle plate could affect the droplets and alter the jet trajectory. Although the jetting system was enclosed in a glove box to control the surrounding air motion, the temperature gradient between the nozzle plate (kept at 80℃) and the jetting environment (around 20℃), could cause air motion due to heat convection.

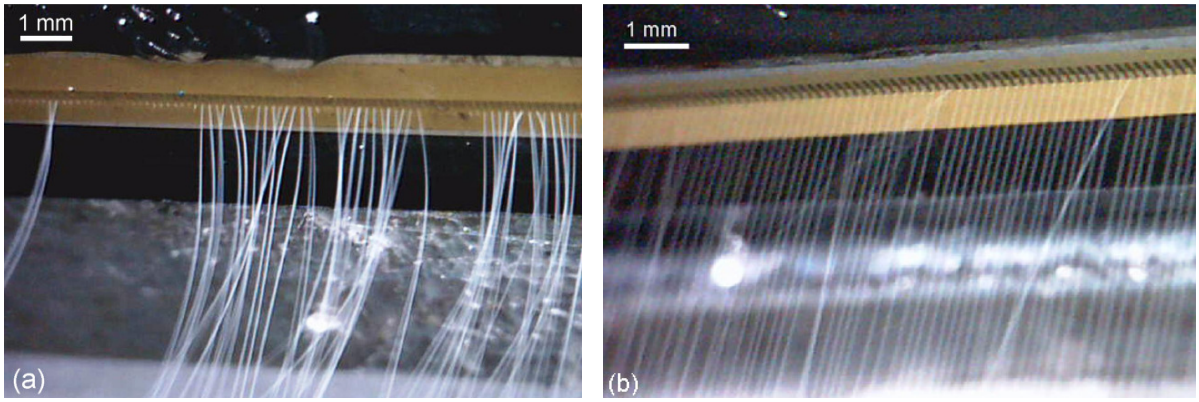

Figure 5-13 Instability in jet array with (a) low jetting voltage (12.0 V, 5 kHz, 20 mbar), and (b) low vacuum level (15.0 V, 5 kHz, 10 mbar)

Jet instability was also observed at high vacuum levels as seen in Set 4. Individual nozzles failed during the trials as shown in Figure 5-14 typically with a vacuum level at 50 mbar. When next applying a pressure signal to the nozzle plate, molten caprolactam was purged through all the nozzles. Air bubbles were found in the melt

coming from the failed nozzles. Trials with the initial purging were repeated to ensure the removal of previous air entrapment. However, air bubbles were formed again as soon as the jetting trial started causing repeated nozzle blocking. In trials with jetting voltages and vacuum level equal or below 25.0 V and 30 mbar no nozzle blocking by air bubbles was observed. However, when increasing the vacuum level, air entrapment occurred at lower jetting voltage than 25.0 V as seen in Set 4. In such a case, with increasing voltage at high vacuum levels (higher than 40 mbar), the number of air bubbles extracted by pressure purging increased.

It was found that air ingestion generated the air bubbles. The air ingestion was due to the meniscus oscillation while expelling a droplet. Upon droplet separation from the nozzle, the consequent suction of the melt meniscus into the nozzle by the channel contraction could entrap an air bubble. Similar situation was reported by de Jong *et al.* (2006) for a single nozzle jetting with a piezoelectric DoD printhead as discussed in section 2.3.4.

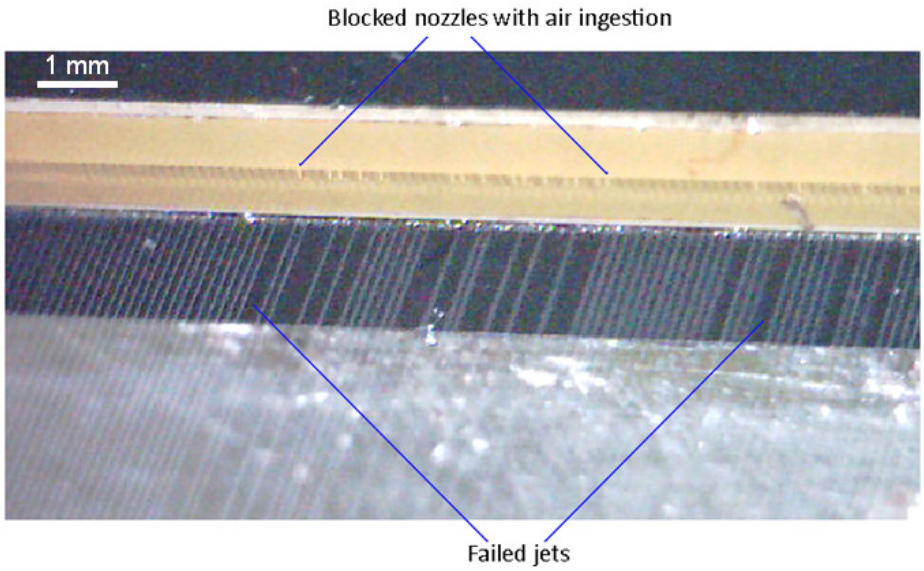

Figure 5-14 Individual jet failure with high voltage and vacuum level (24.0 V, 5 kHz, 50 mbar)

5.2.5 Recommendations for Stable Jetting

Figure 5-15 gives a general guideline for setting the two parameters of voltage and vacuum in relation to each other for stable jetting of molten caprolactam. Jetting stability was sensitive to jetting voltage and vacuum level whereas jetting frequency did not play a significant role. As a combination of high voltage and high vacuum level led to air ingestion and consequent nozzle blocking, it is recommended that at higher jetting voltage, the vacuum level is decreased and vice versa.

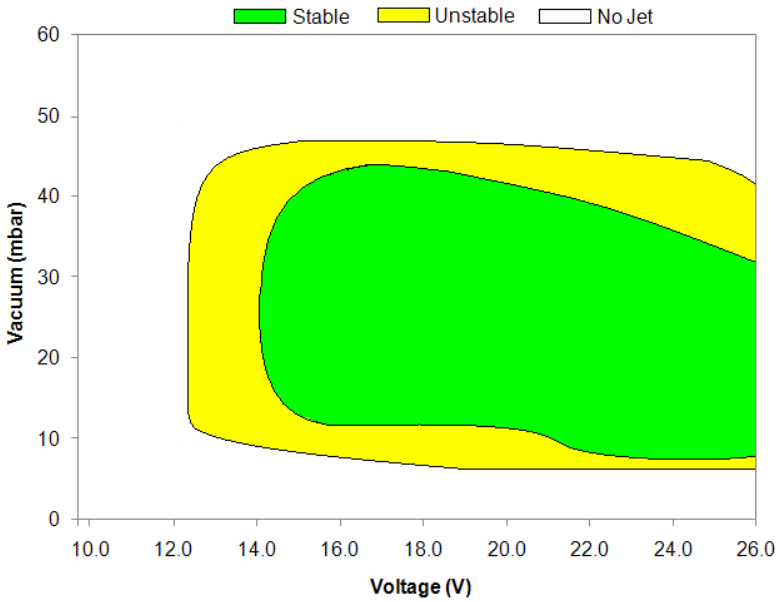

Figure 5-15 Guideline jetting parameters for caprolactam at 80℃

5.3 Instability Behaviour within the Stable Range

When a stable jet array of molten caprolactam was developed, there were cases where instability occurred in the form of jet trajectory, single jet failure and jet array failure even with suitable parameters. External sources such as contamination and air motion could initiate the instability.

5.3.1 Jet Trajectory Error

The jet trajectory error was one of the most common instabilities observed. In most cases, this was just a temporary instability. However, there were situations where a jet trajectory error developed and then remained stable with a specific angle and Figure 5-16 shows such a case. Two periods of jetting occurred in the trial. In the first period after 0.1 sec, a trajectory error developed in one of the jets (Figure 5-16(a)) followed by another at t = 0.4 sec as shown in Figure 5-16(b). The two jets remained with the same trajectory (Figure 5-16(c)) until end of first period at t = 2.1 sec and continued after the second period started at t = 4.7 sec as seen in Figure 5-16(d). The continuation of the trajectory error could have been due to contamination that partially blocked the nozzle and which could not be removed by the jet automatically. The contamination could effectively change the nozzle geometry and alter the jet trajectory as long as contamination remained in place.

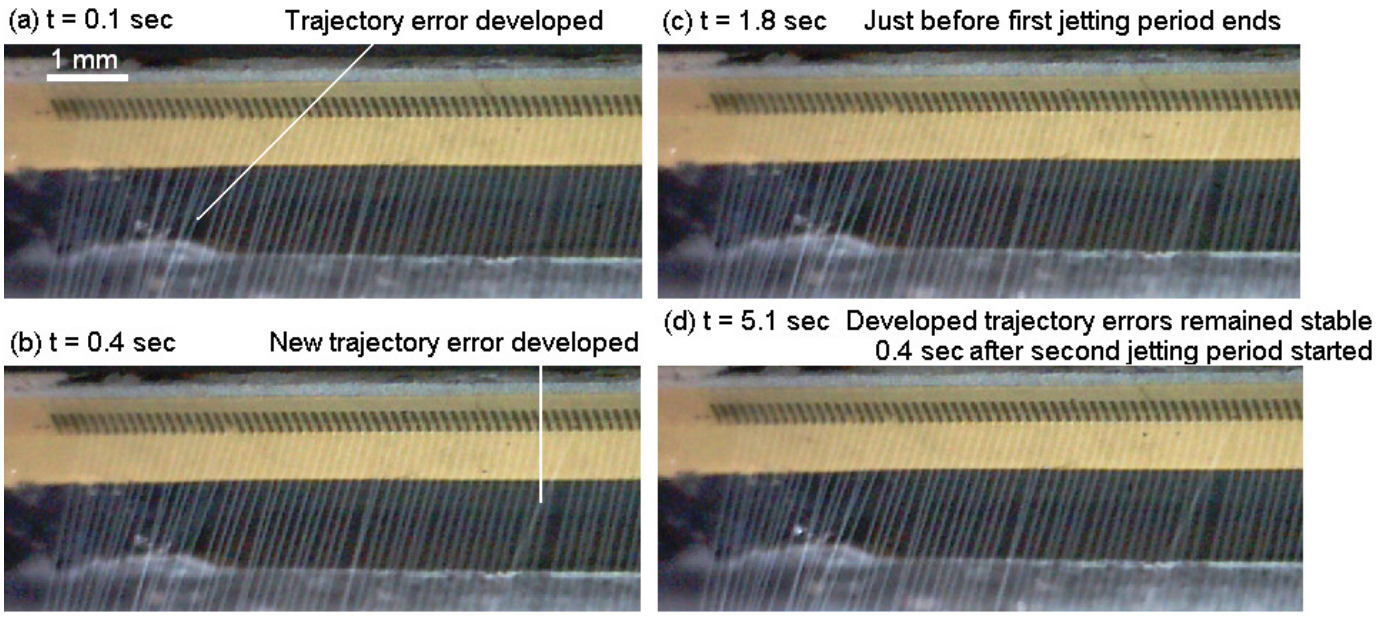

Figure 5-16 Stable jet trajectory errors (15.0 V, 5 kHz, 30 mbar)

5.3.2 Jet Failure

There were some trials where a jet trajectory error led to a jet failure and Figure 5-17 shows a typical situation. At t = 0.1 sec in Figure 5-17(a), a trajectory error occurred (J1). After a further 2 seconds (Figure 5-17(b)) a trajectory error also occurred in three other jets (J2, J3 and J4). J2 failed at 2.5 sec and failure of J3 occurred at 2.6. The bleeding through a failed jet could affect the molten layer thickness locally affecting the adjacent nozzles droplet formation. The possibility of a jet failure could increase with contamination or air bubbles entrapped inside the nozzle. This could make a jet sensitive to bleeding from an adjacent nozzle and its consequent molten layer thickness variation. Therefore, the failure of J3 in Figure 5-17 could have been a result of bleeding from the nozzle of failed J2, where the jets between J2 and J3 could have less sensitivity to the bleeding.

The jet instability behaviour in an array was different amongst the jets. A trajectory error can result in jet failure or be temporary as with J4 which started at t = 2.1 sec (Figure 5-17(b)) and re-stabilised at t = 12.4 sec when a trajectory error then occurred for its adjacent jet (J5). The error in the trajectory of J1 was constant until t = 12.4 sec where it then started to increase (from Figure 5-17(f) to (h)) and finally caused failure of the jet (Figure 5-17(i)). This transition from a trajectory error to jet failure could be a slow process. In contrast, the failure of J2 occurred quickly (Figure 5-17(c)). The failure of J1 after a period of constant trajectory could be a result of bleeding from the nozzles of failed jets (J2 and J3) which could change the molten layer thickness locally.

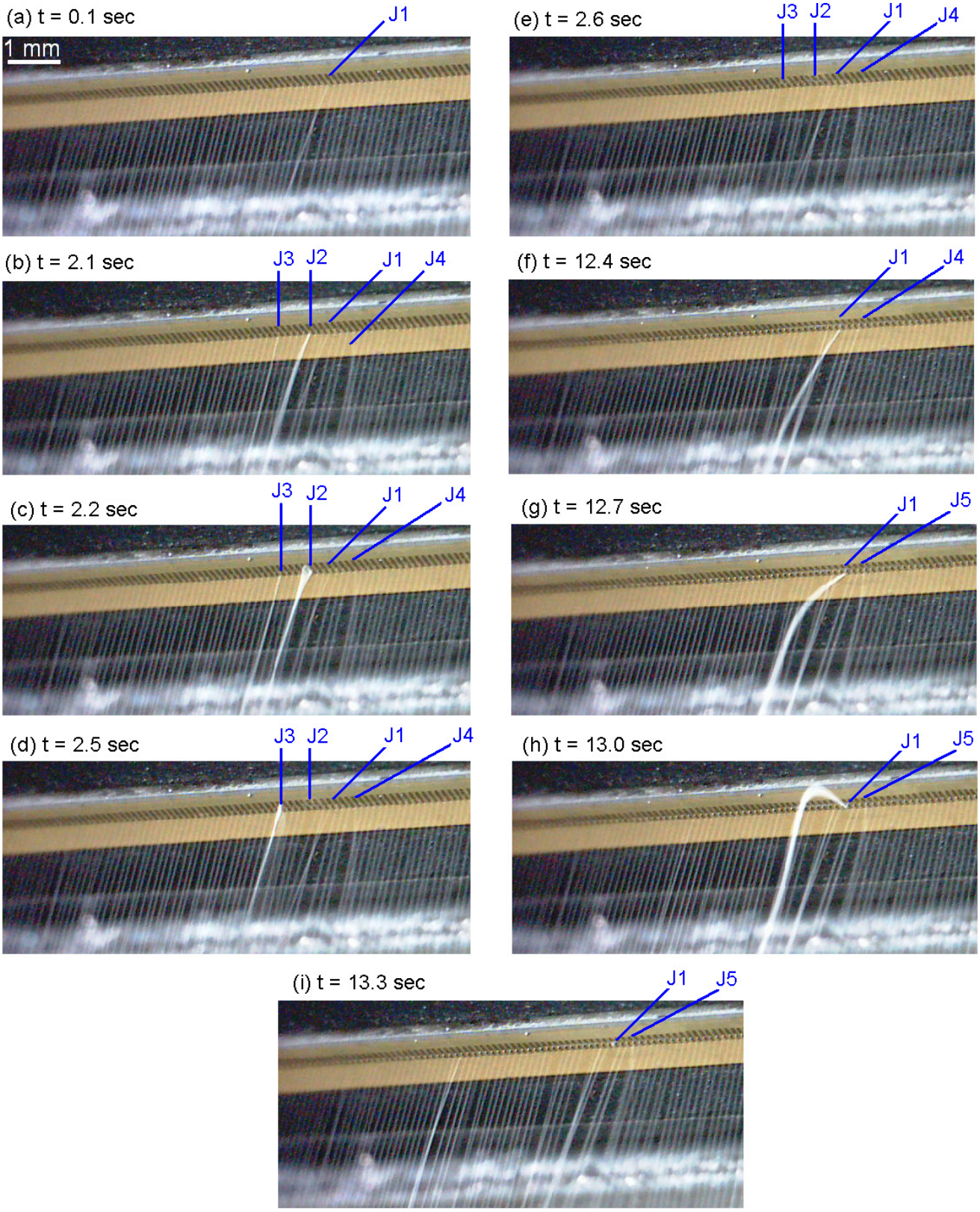

Figure 5-17 Trajectory error developing to a jet failure (15.0 V, 5 kHz, 10 mbar)

5.3.3 Jet Array Failure: A Domino Effect

The jet failures usually occurred after a trajectory error. In such cases, the error increased until the jet touched the nozzle plate and then failed similar to the case of J2 in Figure 5-17 (from (b) to (d)). Due to the applied vacuum level and the surface tension forces, the molten layer thickness was expected to be uniform across the nozzle array before jetting started. When a jet failed though, the actuating nozzle continued to operate and could purge excess melt onto the nozzle plate accumulating locally. Therefore, this could change the melt layer thickness in the bleeding area and consequently affect the stability of the adjacent jets.

Bleeding from a failed jet could propagate towards adjacent nozzles. The thicker melt layer due to bleeding could result in new jet failures leading to a complete jet array failure similar to falling dominos. This phenomenon is referred to as the "domino effect" in this thesis. Figure 5-18 shows a sequence where this occurred. After t = 0.25 sec (Figure 5-18(a)), a nozzle failed to jet. At t = 0.50 sec another jet failure occurred (Figure 5-18(b)). Nozzle bleeding from these two jet failures could cause the excess melt to enter onto the adjacent nozzles. However, it was not until t = 2.00 sec that the instability affected the other jets in the array when two new jets were affected by trajectory error (Figure 5-18(c)). More jets were involved in the instability as seen at t = 2.25 sec (Figure 5-18(d)). This finally caused the domino effect on the jet array which started at t = 2.50 sec (Figure 5-18(e)) from the left and propagating to the right.

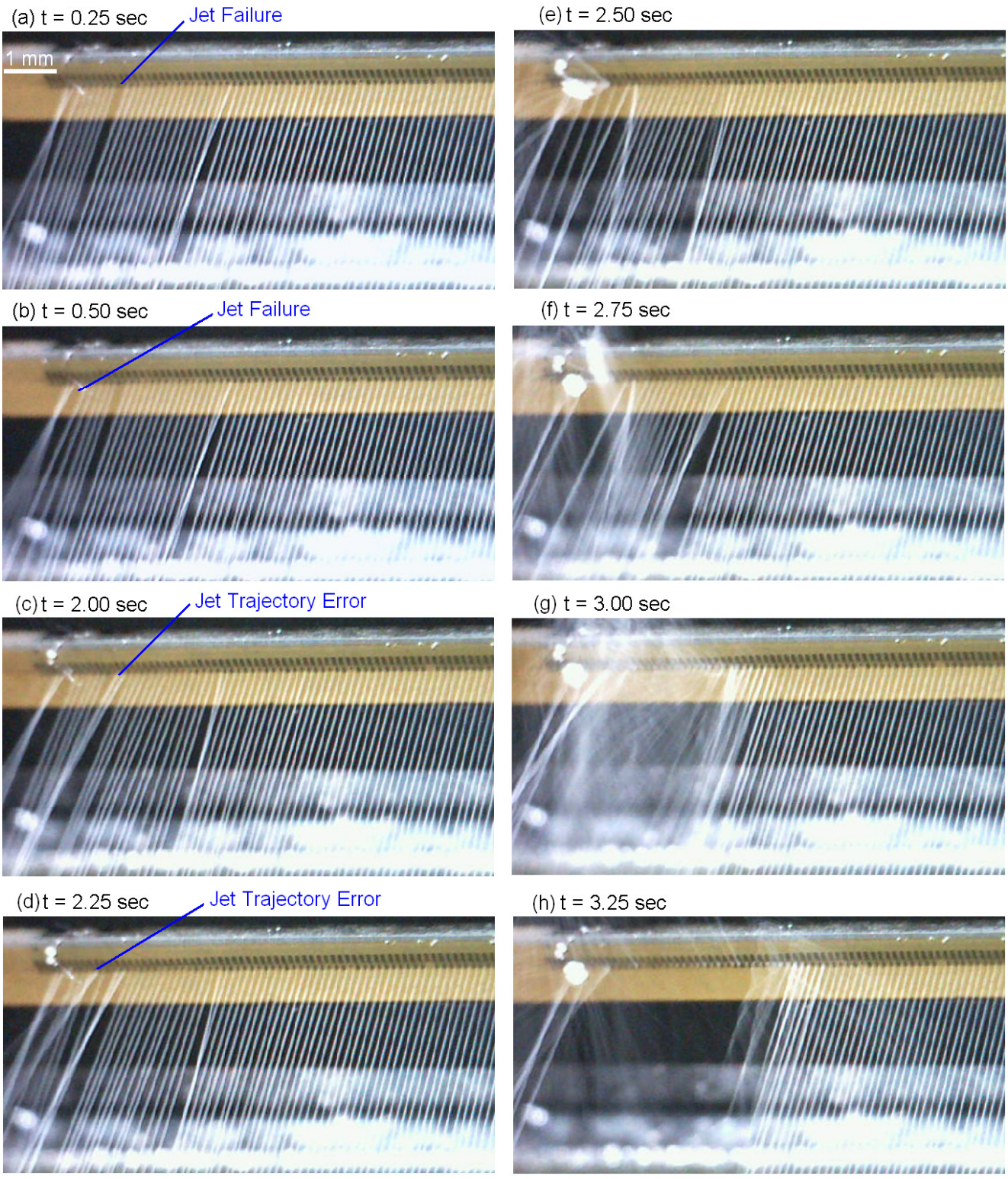

Figure 5-18 Jet array failure initiated by a single jet failure and propagated by the domino effect (15.0 V, 5 kHz, 30 mbar)

5.4 Jetting of the Reactive Mixtures

Although caprolactam dominated the reactive mixtures, systematic jetting trials with the reactive mixtures showed a different stability behaviour which is presented in this section.

5.4.1 Jetting Trials

The reactive mixtures were investigated for jetting based on the procedure explained in section 5.1. The jetting trials were carried out with a single jet and also an array (126 jets). The recommended range of parameters for stable jetting of molten caprolactam (Figure 5-15) could have been used for the reactive mixtures. However, a narrower window was selected to limit the number of experiments. This was 15.0 to 25.0 V for the voltage with 2.5 V increments, and 20 to 30 mbar for the vacuum level with 5 mbar increments. Two jetting frequencies of 3 and 5 kHz were also used to ensure the jet stability remained unaffected with frequency as with molten caprolactam. Each trial was undertaken three times, each for over 10 sec. When instability occurred in a trial, it was repeated another three times to ensure that the instability originated from the parameter setting and not an external source.

5.4.2 Jet Stability with a Single Jet

Figure 5-19 shows the results for the jet stability of the reactive mixtures. With both the activator and the catalyst mixtures at different melt supply levels, similar stable ranges of parameters were achieved for a single jet. However, with the catalyst mixture, there were instabilities in form of jet disturbance (temporary trajectory error) in a few trials within the stable range. On such occasions, further trials with the same

parameter settings showed stability with the single jet. This suggested that the instability was possibly due to an external source.

A jet was not developed with a voltage of 15.0 V and there was some instability with 17.5 V in the form of a trajectory error. Jetting was stable at 20.0 V and 22.5 V for all the vacuum levels and frequencies. With 25.0 V, jetting was stable when setting the vacuum level at 20 and 25 mbar. By increasing the vacuum to 30 mbar though, air ingestion occasionally occurred causing jet failure after a short time.

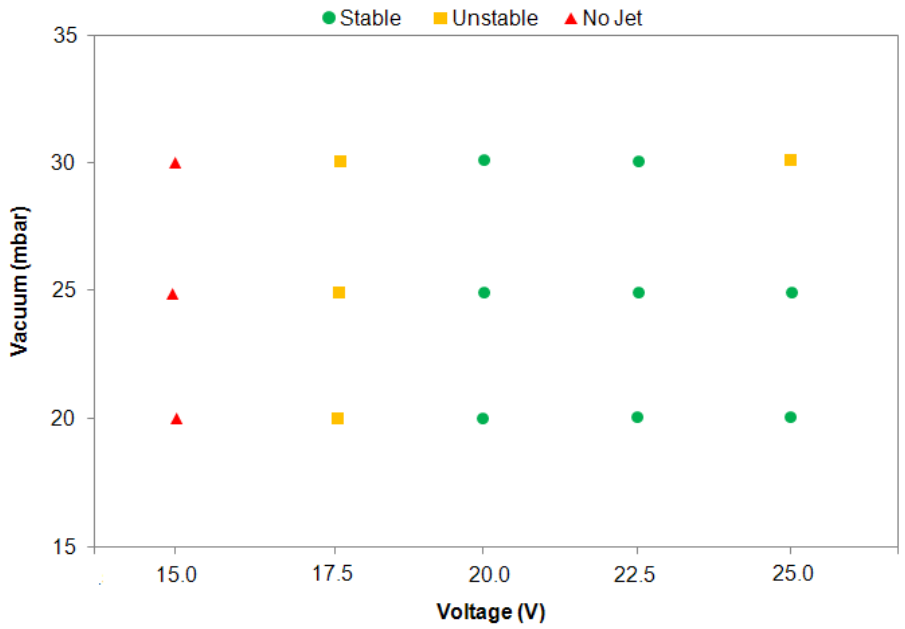

Figure 5-19 Stability status in single jet trials with the activator and catalyst mixtures

Caprolactam and the reactive mixtures did not have the same jetting voltage range for jet stability. The range was narrower with the reactive mixtures (20.0 ~ 22.5 V). A higher jetting voltage was required to develop a stable jet with the reactive mixtures. This means that greater pressure wave dissipation occurred with the mixtures compared with the molten caprolactam. This could be due to the higher viscosity of the mixtures (50% higher, see section 4.4.3). The molten caprolactam and the

reactive mixtures had similar surface tension values (section 4.3.2). However, for a fixed vacuum level, a thicker melt layer could occur with the mixtures on the nozzle plate compared with caprolactam, increasing the pressure wave dissipation and so the stability threshold value for voltage.

5.4.3 Stability with a Jet Array

The result of jetting stability with the array of jets for the activator mixture was similar to the results with the single jet. However, stable jet array trials with the catalyst mixture were not as repeatable as with the activator mixture. There were actually several trials which encountered a form of jet instability in one or more individual jets. The instabilities were in the form of a temporary jet trajectory error which either stabilised or developed towards a single jet failure and sometimes to a domino failure of the array. When repeating those trials, instability was observed again but different individual jets from the previous trials had instability. This behaviour was found to be random. In such cases, the nozzle plate was cleaned with a dry lint-free cloth, and then after dripping by applying a purging signal, the vacuum retracted the melt into the nozzles to form a fresh thin melt layer on the nozzle plate. However, the random failure of the individual jets in the array existed.

The random instability with the catalyst mixture was much higher compared with caprolactam and the activator mixture. However, with 126 jets of the catalyst mixture, the possibilities for a trial with instabilities increased considerably. The main difference with the catalyst mixture was the microcrystals. They could have agglomerated on the nozzle plate and disturbed the meniscus oscillation as reported in the literature for normal ink (de Jong *et al.* 2006, Beulen *et al.* 2007). Visualisation of these problems in this study was difficult. However, studying the influence of

nozzle actuation on the thin molten layer of the nozzle plate could give a better understanding of the jet instabilities originated by agglomerated microcrystals.

5.5 Melt Flow on the Nozzle Plate

5.5.1 Melt Flow Visualisation

Although this investigation was motivated by the above observation, it was actually seen in some initial jetting trials with caprolactam that the black particles on the nozzle plate (left from the functionality test) moved towards the actuating nozzles during jetting periods. This was used to visualise the melt flow on the nozzle plate. Interestingly, in such trials, jet instabilities were also observed concurrently with the particles movement. This was observed clearly in video clips captured from trials as in Figure 5-20 which shows moments before, during and after a jet instability during a five-jet trial (jet 1 of 5). Some of the particles on the nozzle plate are also shown in Figure 5-20(a). Movement and tracking of selected particles of this trial is shown with higher magnification in the following section.

5.5.2 Particle Tracking

The trial shown in Figure 5-20 was analysed to observe the melt flow. The trial was undertaken with five jets in an array with two non-actuating nozzles in between (making a jet spacing of 410 µm) to show the role of individual jets in the melt flow. The jetting parameter was chosen to be within the stable range of parameters (Figure 5-15). Five periods of nozzle actuation (jetting) were undertaken. Twelve (easier to track) particles were selected for the flow pattern visualisation and six of them are shown in Figure 5-22. Particle positions were studied in the video clip which monitored the nozzle plate for 25 sec. To protect the microscope camera

against depositing droplets, the viewing direction was angled with the arrangement shown in Figure 5-21. The first nozzle in the array (to the left) was the reference point with X and Y directions as shown in Figure 5-22. The exact positions of nozzles in the array were shown in Figure 5-1.

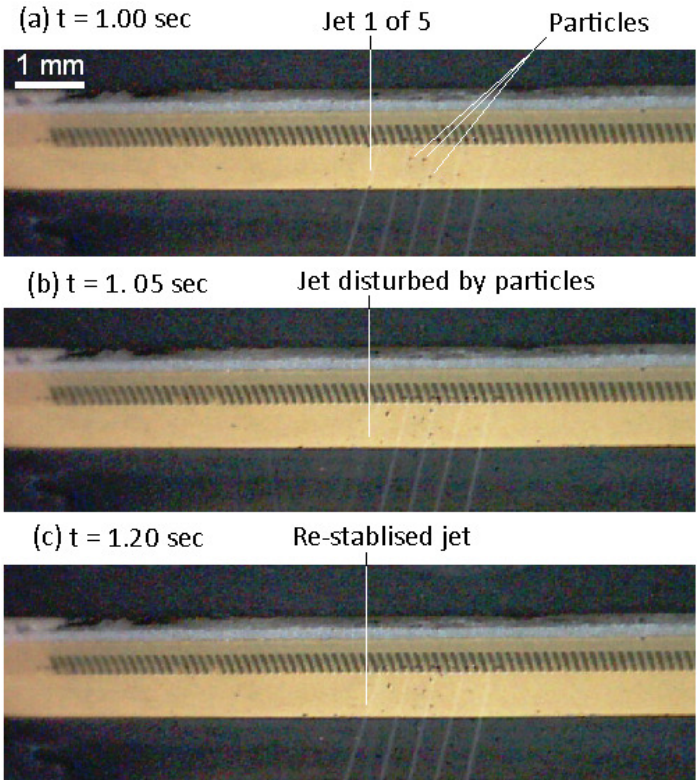

Figure 5-20 Jet instability during a jetting trial with caprolactam containing particles on the nozzle plate left from printhead functionality test (15.0 V, 5 kHz, 30 mbar)

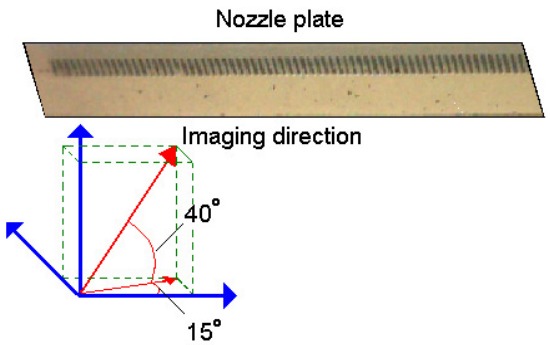

Figure 5-21 Viewing direction of the microscope camera in relation to the nozzle plate

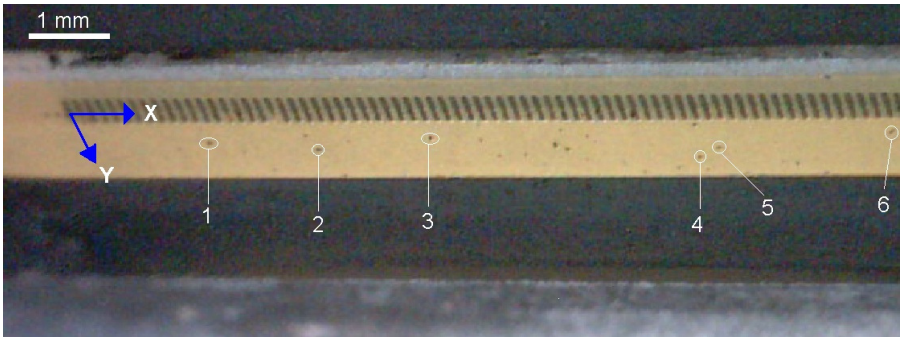

Figure 5-22 Coordinate system for particle tracking and some of the particles on the nozzle plate

Figure 5-23 and Figure 5-24 show images from the first and second jetting periods. As seen in Figure 5-23(a) and (b), particle 1 (P1), P2 and P3 had no displacement until the first jetting period started at t = 3.04 s. P3 was seen to move more than the other two during jetting. This could be because it was closer to the actuating nozzle for jet 1 (J1). At the end of the first jetting period, all the particles continued to move, possibly due to inertia as seen in Figure 5-23(g) to (h).

Figure 5-23 (frames *d* to *h*) also shows a particle (P8) being repelled from the actuating nozzles. This was while P1, P2 and P3 were being attracted. This repelling behaviour was also observed with P9 just before the end of the second jetting period when P1 and P6 were being attracted as shown in Figure 5-24. The simultaneous attraction and repelling behaviour were observed with the other particles during the third, fourth and fifth jetting periods as shown for some of the particles in Figure 5-25 and Figure 5-26 (Figure 5-29 shows such behaviour in a report by Beulen *et al.* (2007) which is discussed later in this section). P1 for instance was attracted towards the jets from far left side of the nozzle plate and reached the nozzles just after the end of the third jetting period (Figure 5-25(g)). Then, during the fourth and fifth jetting periods, P1 was repelled from the nozzles as shown in Figure 5-26 whereas P14 moved towards the nozzles at the same time. Plotting the particles paths during the five jetting periods helped to visualise the melt flow field on the nozzle plate.

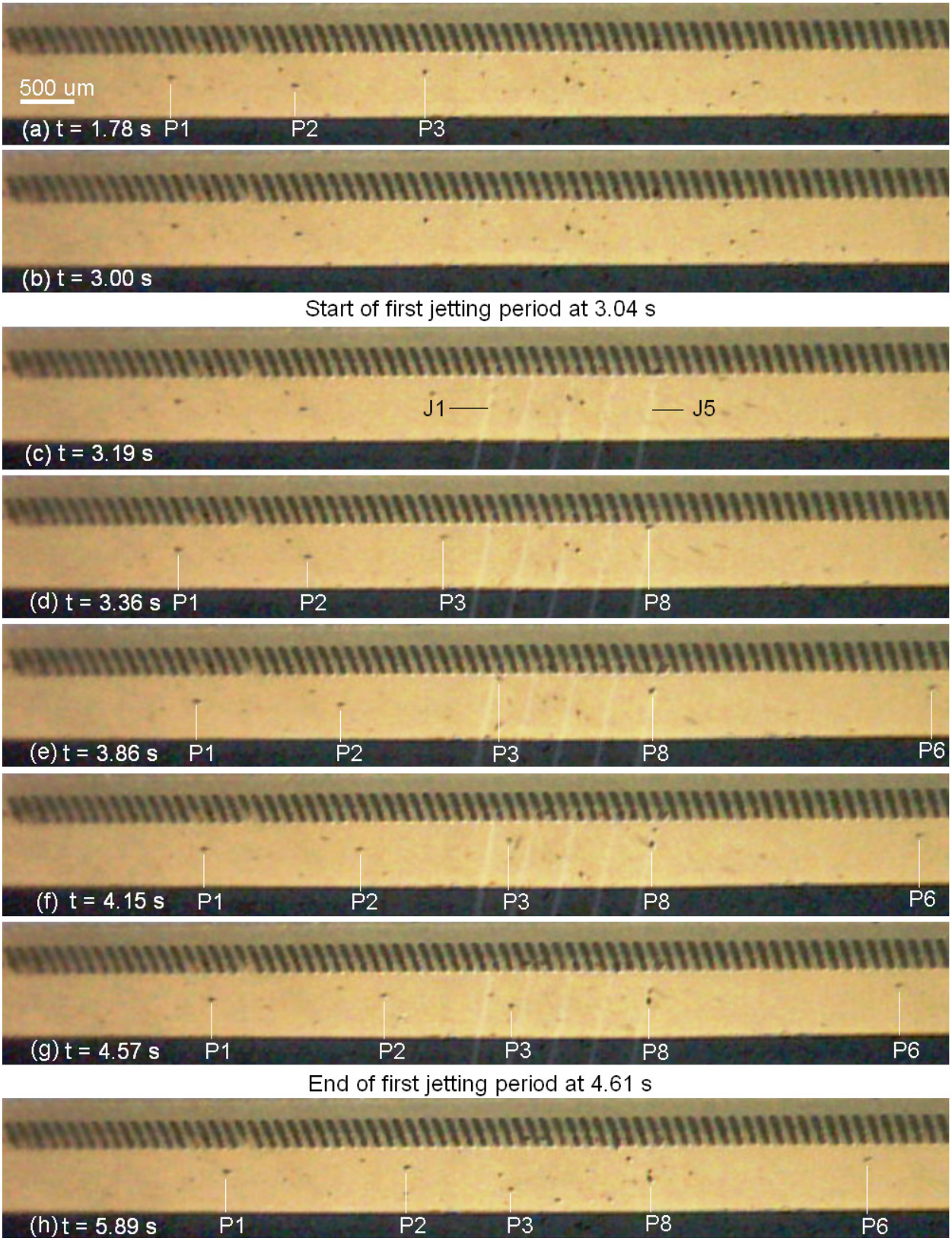

Figure 5-23 The first jetting period of the particle tracking trial with five jets of caprolactam (15.0 V, 5 kHz, 30 mbar)

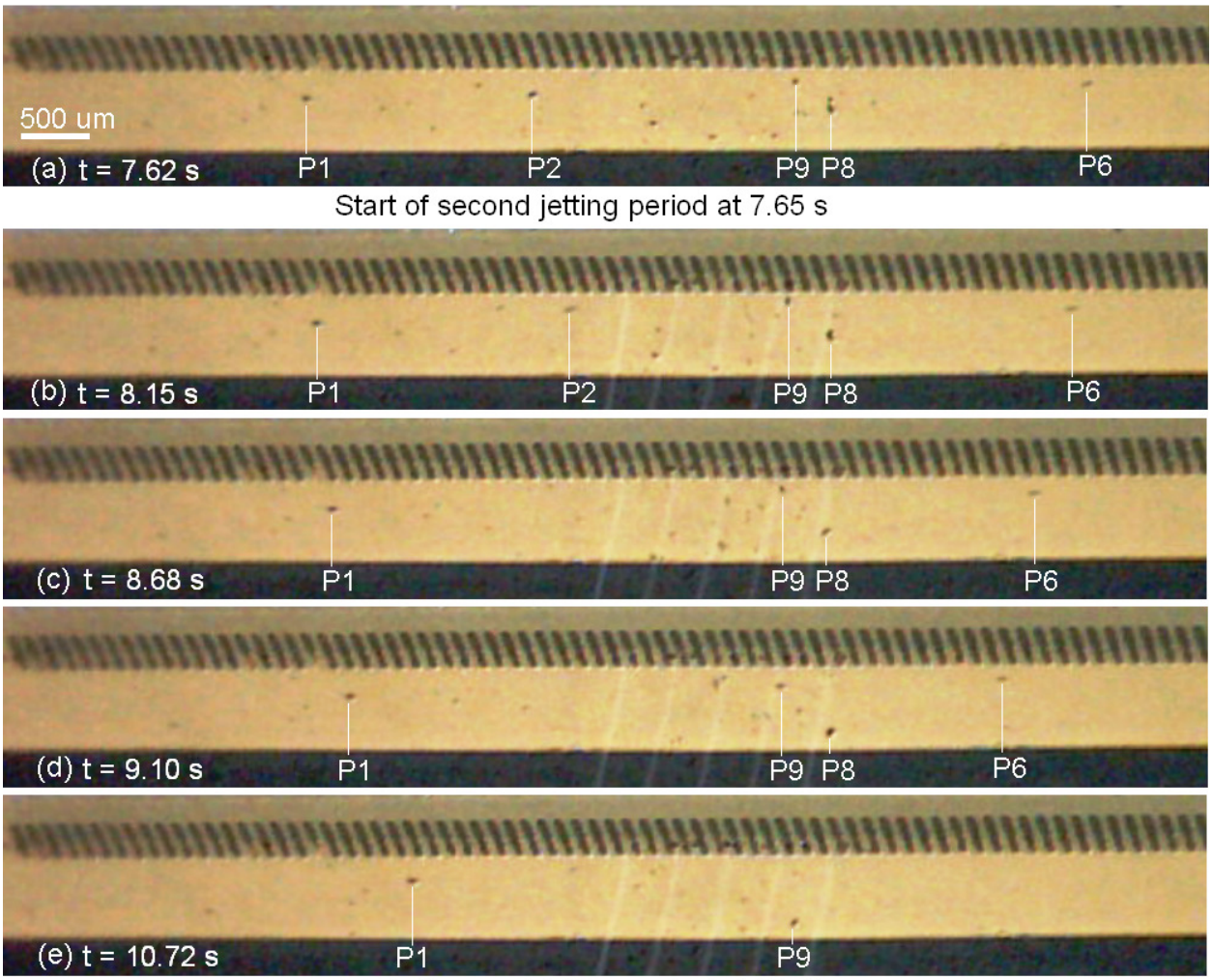

Figure 5-24 Particle tracking of the second jetting period

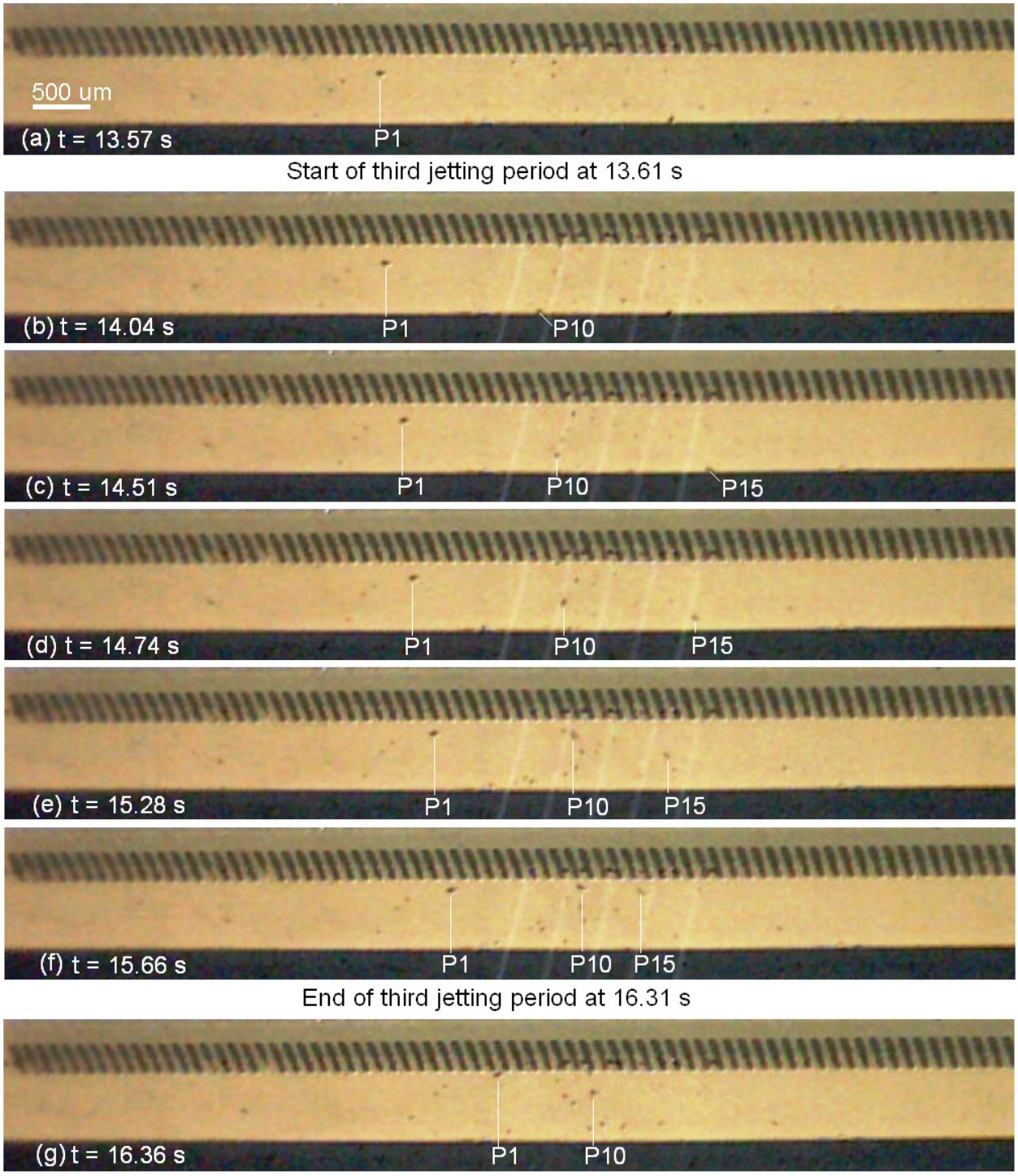

Figure 5-25 Particle tracking in the third jetting period

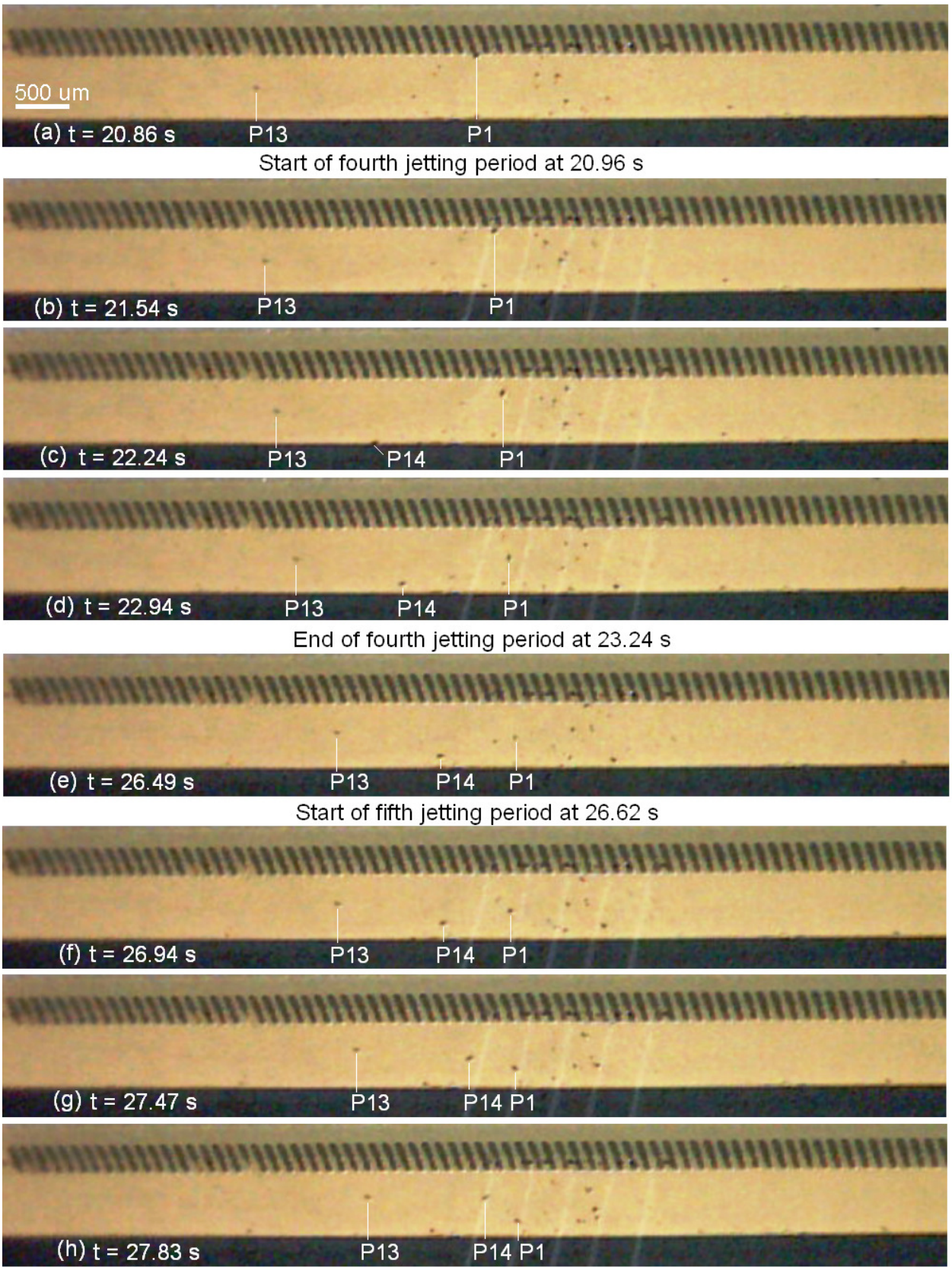

Figure 5-26 Particle tracking in the fourth and fifth jetting periods

5.5.3 Melt Flow Field

Figure 5-27 shows the results of the particle tracking during the five jetting periods to reveal the melt flow field. Only the actuating nozzles and the tracked particles are shown. The dots in the graph represent the centre position of the particles with ±50 µm accuracy for every 0.65±0.05 sec of the trial. Figure 5-28 shows the particle tracking velocimetry results corresponding to Figure 5-27 and it can be seen that the velocity was higher during the jetting periods. Overall, particle velocity was higher when they entered onto the nozzle plate from the side where a maximum velocity of 2 mm/s was recorded.

Figure 5-27 suggests that the particles moved in a radial pattern centred on the actuating nozzles. Some of the particles moved towards the actuating nozzles and then moved in the opposite direction. However, not all particles returned from the nozzles. Observing the movement of a number of particles at the same time was easy in the video clips and limited images were shown for this in Figure 5-23 to Figure 5-26. In addition, one could relate the particle positions and timings by observing Figure 5-27 and Figure 5-28 respectively, to find out how particles moved in relation to each other. It was found that attraction and repelling of some of the particles occurred at the same locations and times (e.g. Particle 7 to 12 in Figure 5-27). In addition, particles were recorded with different velocities as seen in Figure 5-28. This indicated a complex flow motion in the thin molten layer.

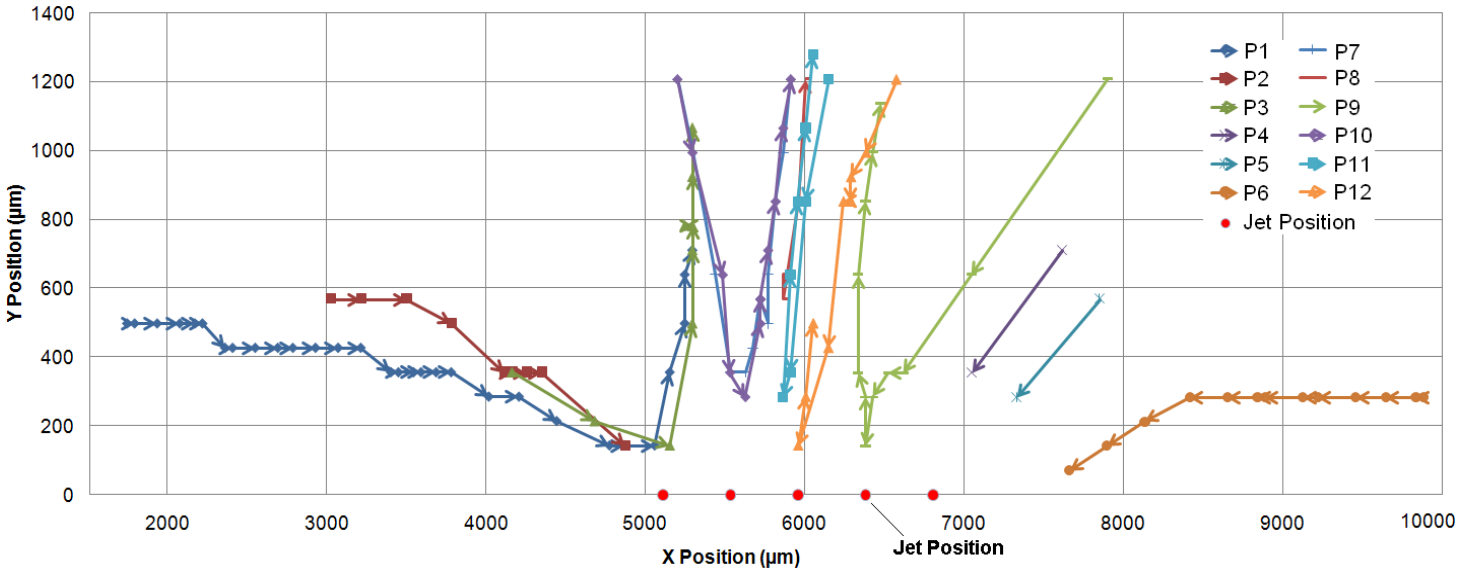

Figure 5-27 Particle tracking in a trial with five individual actuating nozzles in four jetting periods (15.0 V, 5 kHz, 30 mbar)

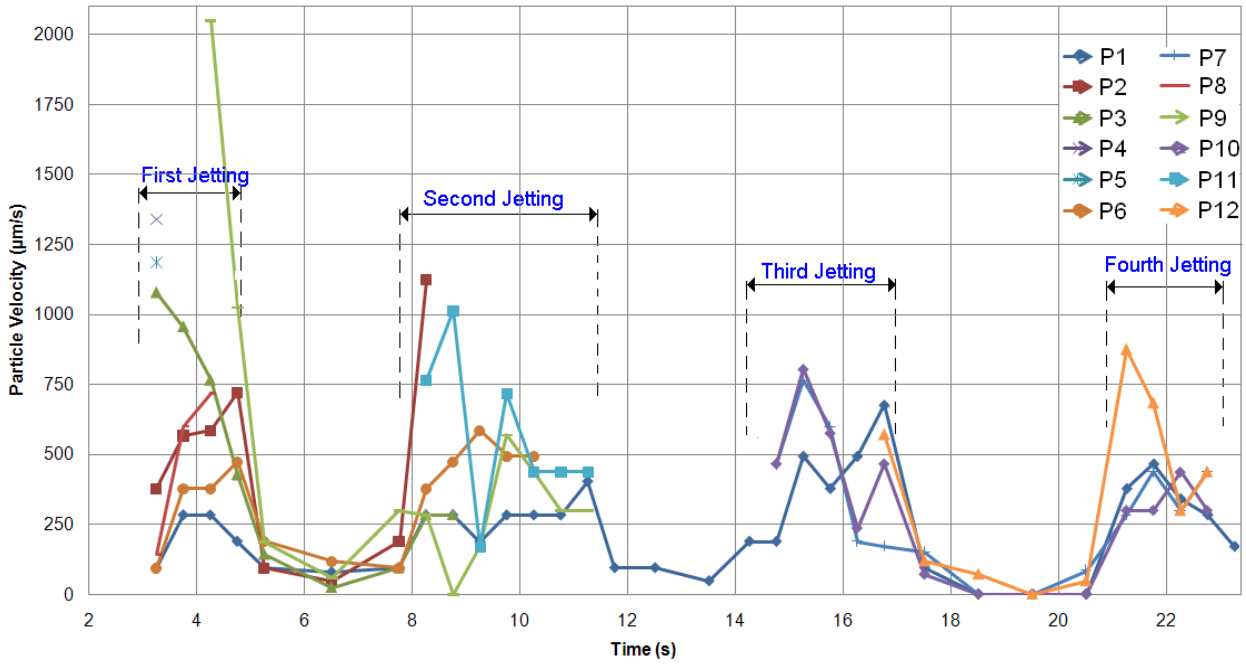

Figure 5-28 Velocity of particles in the trial shown in Figure 5-27 (15.0 V, 5 kHz, 30 mbar)

Beulen *et al.* (2007) also studied the flow pattern of a room temperature graphical ink layer on the nozzle plate of a DoD piezoelectric printhead. However, their particle tracking study was undertaken with a single jetting nozzle and provided details of

flow motion around the actuating nozzle including the velocity profile across the ink layer thickness. As shown in Figure 5-29, the ink at the ink-air interface moved towards the nozzle whereas the ink closer to the nozzle plates moved away from the nozzle.

Although a radial flow pattern and also particle motion in opposite directions at the same position on the nozzle plate were recorded with the molten caprolactam in the current study, the general melt flow field seems to be affected by the combination of multiple jets. This means that the interaction of the flow fields generated by each actuating nozzle could have affected the resulting whole flow field. This could have made a more complex velocity profile than that reported by Beulen *et al.* (2007) for a single jet. Therefore, the velocity profile across the melt layer thickness produced by an array of jets remains unexplored.

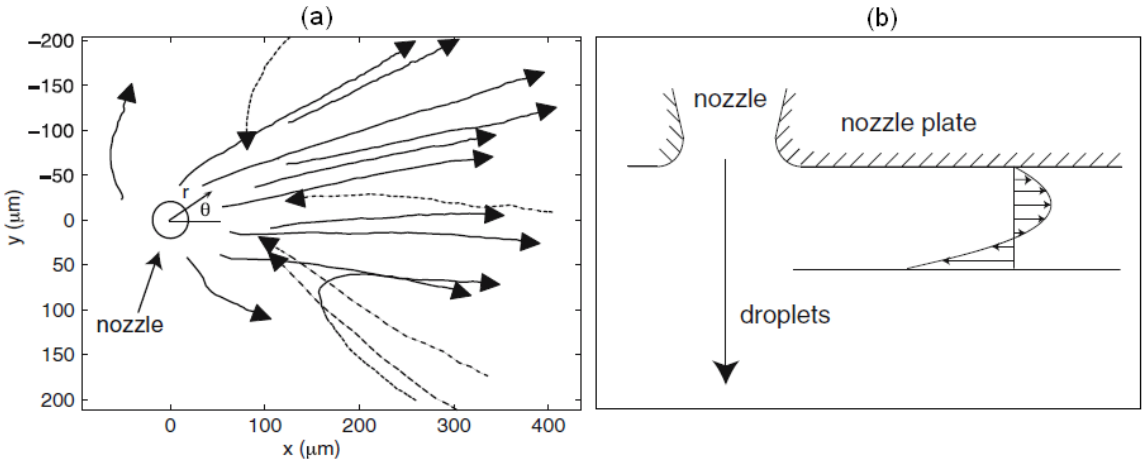

Figure 5-29 Ink flow pattern around an actuating nozzle studied by Beulen *et al.* (2007) on a DoD printhead. (a) particles moving towards the nozzle (dashed lines) and particles moving away from the nozzle (continuous lines) indicating a depth-dependent velocity in the ink layer, (b) velocity profile across the ink layer thickness

The particle tracking study with the molten caprolactam showed how the flow field on the nozzle plate could take particles to the actuating nozzle resulting in potential for disturbing the droplet formation process. Catalyst microcrystal agglomeration in combination with the melt flow on the nozzle plate could give such behaviour. With random agglomeration of microcrystals, the jet array instabilities with the catalyst mixture in the repeated trials as reported in section 5.4.3 may be better understood with the above discussion.

Chapter 6. Droplet Formation Study

The droplet formation characteristics of the molten caprolactam and the reactive mixtures were investigated. Oscillation of the melt meniscus on the nozzle, formation and separation of droplets from a single nozzle were studied by high speed imaging. Nozzle wetting, trajectory errors and some other instabilities were also investigated. This was to generate a more detailed understanding of the appropriate values for the jetting parameters to be used for deposition.

6.1 Experiments

6.1.1 Motivation

Droplet formation characteristics such as size, shape and velocity are important, as are the kinetics of droplets to indicate how they would interact with the surface upon deposition. In addition, the phenomena associated with the separation of a tail (ligament) attached to the droplet from the nozzle plate and its disintegration into satellite droplets was one of the criteria for choosing the appropriate jetting parameters. There was also a need to investigate any instability initiated by the interaction between the melt and the nozzle plate which could initiate a trajectory error and the consequent droplet placement inaccuracy.

6.1.2 Design of Experiments

Table 6-1 shows the sets of experiments for the droplet formation study for caprolactam and the reactive mixtures at 80℃. The nozzle plate was cleaned with a

lint-free cloth to remove contamination which also provided a dry nozzle plate for better observation of the meniscus oscillation and droplet formation. Set 1 was to give a general understanding of the role of the jetting voltage and frequency on droplet formation. The actuating nozzle was monitored with a high speed camera to show the interaction between the nozzle and molten caprolactam and to monitor any instabilities. In addition, the nozzle wetting behaviour during the first second of jetting was monitored.

The parameters ranges for Set 1 were selected based on the results of the jetting trials with caprolactam. It was reported in section 5.2.2 that no jet was observed with 10.0 V and 12.5 V when jetting caprolactam. However, it was not clear whether this was due to immediate jet failure which the normal camera could not detect. In addition, the effect of low voltages on meniscus oscillation and wetting of the actuating nozzle could be better understood when no jet was developed. Therefore, these two low voltages were also used in Set 1 to give an understanding of the role of low voltage jetting. Although it was found that the jetting frequency did not affect the jet stability, its effect on the droplet formation characteristics and also nozzle wetting were studied in this set. The vacuum level was chosen as being in the middle of the stable range.

Set 2 was to quantify the effect of jetting parameters on the droplet characteristics. The droplet shape, size and kinetics were characterised by processing the images obtained from the high speed camera. The jetting frequency increment was increased in this set to limit the number of experiments. The vacuum level was set at 25 mbar similar to Set 1.

In Set 3 and 4, the catalyst and activator mixtures were characterised for droplet formation behaviour. Although it was reported in section 5.4 that the jet stability of

the mixtures was not affected by the melt supply level, it was necessary to ensure that the droplet characteristics would be unaffected. Therefore, Set 3 was undertaken at three melt levels of 2, 3 and 4 ml. However, the results showed that there was no need to vary this parameter when investigating the droplet formation of the activator mixture and so Set 4 was kept at 4 ml.

The jetting voltage was varied from 17.5 to 25.0 V with 2.5 V increments with the mixtures in Sets 3 and 4. Although 17.5 V resulted in jet instability as reported in section 5.4.2, it was used to observe how instabilities formed on the actuating nozzle. Frequency was not varied with the mixtures because the experiments with molten caprolactam showed that the droplet characteristics were found to be independent of this parameter. It was maintained at 3 kHz for both the sets as this gave the most detail on the droplet shape evolution when the imaging rate of the high speed camera was at 10,000 fps with a 4 µs exposure time.

With the mixtures, the vacuum level of 25 mbar was used according to the stability results as reported in section 5.4.2. It was also interesting to know how the vacuum levels of 15 and 35 mbar would affect the droplet characteristics with the reactive mixtures. However, due to the time restriction in the research, this was only investigated with the activator.

The high speed imaging was set according to the description in section 3.5.2. The camera enabled the system to capture about 3 seconds of each experiment. The printhead was triggered for jetting after imaging started to record the formation of the first few droplets as well as the development of the wetting area around the nozzle. The images were analysed to characterise droplets after 600, 1800 and 3000 droplets were ejected for all the jetting materials. The main error in the image analysis was from the droplet edge definition which gave ±1 pixel accuracy (the

matching pixel size was enhanced from 6.7 µm for caprolactam to 1.6 µm for the mixtures due to the different lens settings used).

Set	Jetting Material	Melt Supply Level	Voltage (V)		Frequency (kHz)		Vacuum (mbar)	
			Range	Inc.	Range	Inc.	Range	Inc.
1	Caprolactam	-	10.0 ~ 25.0	2.5	1 ~ 5	1	25	-
2	Caprolactam	-	15.0 ~ 25.0	2.5	1 ~ 5	2	25	-
3	Catalyst Mixture	2, 3, 4	17.5 ~ 25.0	2.5	3	-	25	-
4	Activator Mixture	4	17.5 ~ 25.0	2.5	3	-	15, 25, 35	-

Table 6-1 Sets of experiments for droplet formation characterisation

6.1.3 Characterisation Procedure

From the image analysis the droplet size and velocity were measured. For the droplet velocity, the distance that the droplet centre travelled was extracted from two consecutive images for which the elapsed time was known from the imaging frequency. Other characteristics such as droplet kinetic energy, Weber and Reynolds numbers were calculated from droplet size, velocity and the physical properties. The evolution in the shape of the droplet from separation to the tail disintegration was quantitatively analysed. As the distance between the substrate and the nozzle plate was recommended by the printhead manufacturer as 1 mm, the droplet characterisation was undertaken at this distance (±100 µm, depending on the position of the droplets in the image frames).

6.2 Meniscus Oscillation and Droplet Formation (Set 1)

6.2.1 Meniscus Oscillation on the Actuating Nozzle

Oscillation of the melt meniscus was observed at the actuating nozzle even with jetting voltages as low as 10.0 V and with all frequencies as Figure 6-1 shows. It is

also seen in the figure that the oscillating meniscus (seen as a dark spot) had a reflection on the nozzle plate. Another feature of the figure is that no spot was seen for the adjacent nozzles. Considering the viewing direction and the magnification, the image was expected to cover at least five nozzles in the frame (the nozzle spacing was 137 µm). This suggests that the meniscus for the adjacent nozzles was inside due to the vacuum level used. The image shown in Figure 6-1 was taken after hundreds of nozzle actuations and the dark strip around the oscillating meniscus was the wetting area which occurred for all experiments in Set 1.

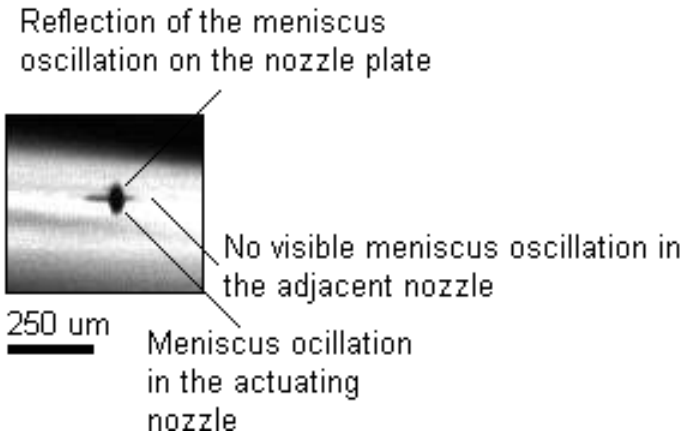

Figure 6-1 Meniscus oscillations in the actuating nozzle at a low jetting voltage (10.0 V, 5 kHz, Set 1)

The high speed microscopic imaging showed that the meniscus oscillation with 10.0 and 12.5 V did not form a single caprolactam droplet at all jetting frequencies. Therefore, the lack of jet in the trials discussed in section 5.2 was not from an immediate jet failure with these voltages. It was assumed that the pressure wave generated by the actuation was not adequate to overcome the surface tension forces on the melt meniscus to expel a droplet.

Jetting voltages equal to and higher than 15.0 V formed a train of droplets at all jetting frequencies in Set 1. Figure 6-2 shows a droplet of the molten caprolactam

being ejected. Before the droplet separated from the nozzle, a tail formed which was attached to and travelled with the droplet. This was the same for all jetting parameters which could generate droplets in Set 1. The tail attached to the droplet disintegrated into small satellite droplets with voltages higher than 17.5 V. The tail evolution will be discussed further in section 6.3.1.

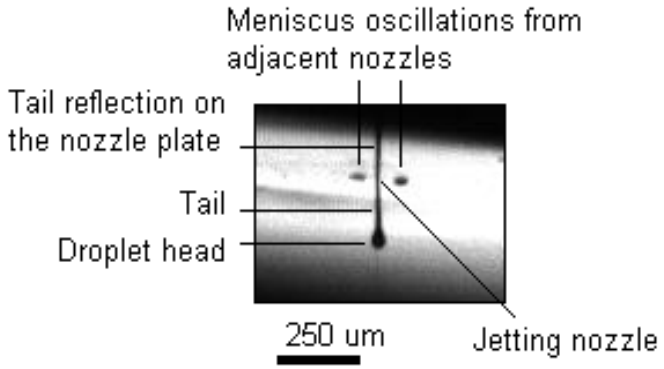

Figure 6-2 High speed imaging of a droplet being ejected from a nozzle (15.0 V, 3 kHz, Set 1)

Two small spots around the actuating nozzle are also seen in Figure 6-2. They were meniscus oscillations on the adjacent nozzles made by the actuation. From the adjacent nozzle positions and the reflection of the tail on the nozzle plate, the exact position of the actuating nozzle was determined.

6.2.2 Meniscus Oscillation on the Adjacent Nozzles

Figure 6-3 shows how the meniscuses of the adjacent nozzles behaved during droplet formation with a high voltage of 25.0 V at 3 kHz. The situation prior to nozzle actuation is seen in Figure 6-3(a) where all channels were at rest (t = 0 ms). Figure 6-3(b) is after jetting started when the meniscus of the adjacent nozzles vibrated before the droplet was expelled. In the next frame (after a further 0.1 ms in Figure

6-3(c)), there is a droplet with a long tail separated from the nozzle. Figure 6-3(d) shows the jetting and adjacent nozzles having returned to their initial (rest) form. The meniscus oscillation to the droplet separation took less than 0.2 ms as seen in Figure 6-3.

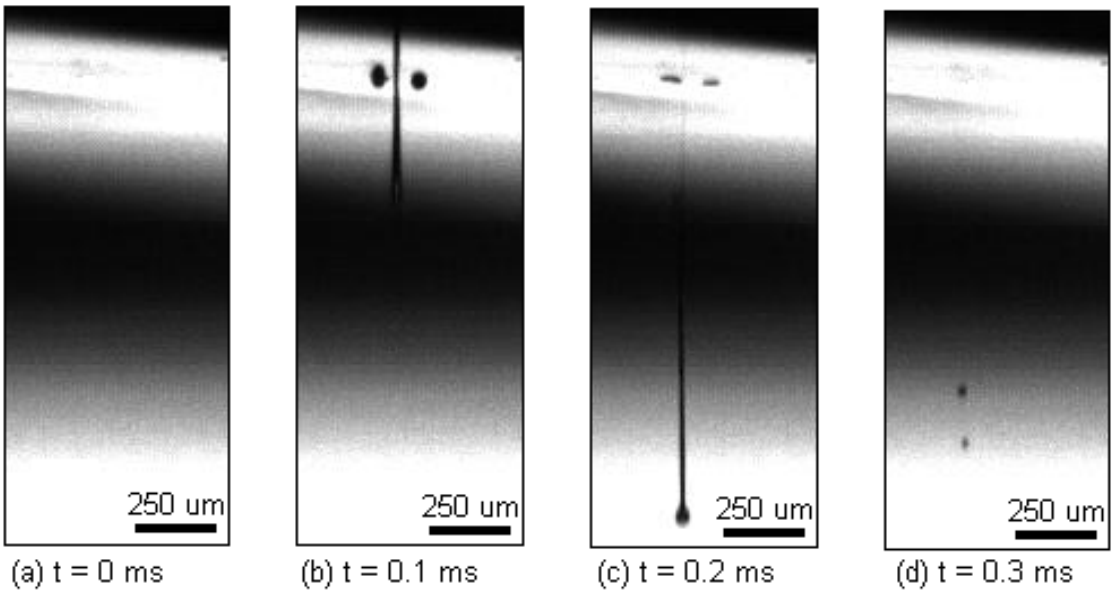

Figure 6-3 Meniscus oscillation in the adjacent actuating nozzles due to the shared wall technology used in the printhead (25.0 V, 3 kHz, Set 1)

The structural design of the printhead shared each channel's walls with the adjacent channel. This technology was patented and known as "shared wall" by Xaar plc (Le 1998). With a voltage signal, the channel walls of an actuating nozzle vibrated to expand and contract the melt channel to generate a droplet. With the shared wall technology, the adjacent channels were also affected making a partial expansion and contraction. This consequently resulted in the meniscus oscillation on the adjacent nozzles as seen in the form of dark spots around the jetting nozzle in Figure 6-3(b) and (c). The meniscus oscillation made by the partial actuation is also known

as “crosstalk” (Raman 1999) which could affect the jet stability by influencing wetting (to be discussed in section 6.5). With higher voltages, the meniscus oscillation on the neighbouring nozzles from the partial actuations increased in size, however, no droplet was expelled with the partial actuation. Figure 6-4 summarise the observations made in Set 1 of the experiments.

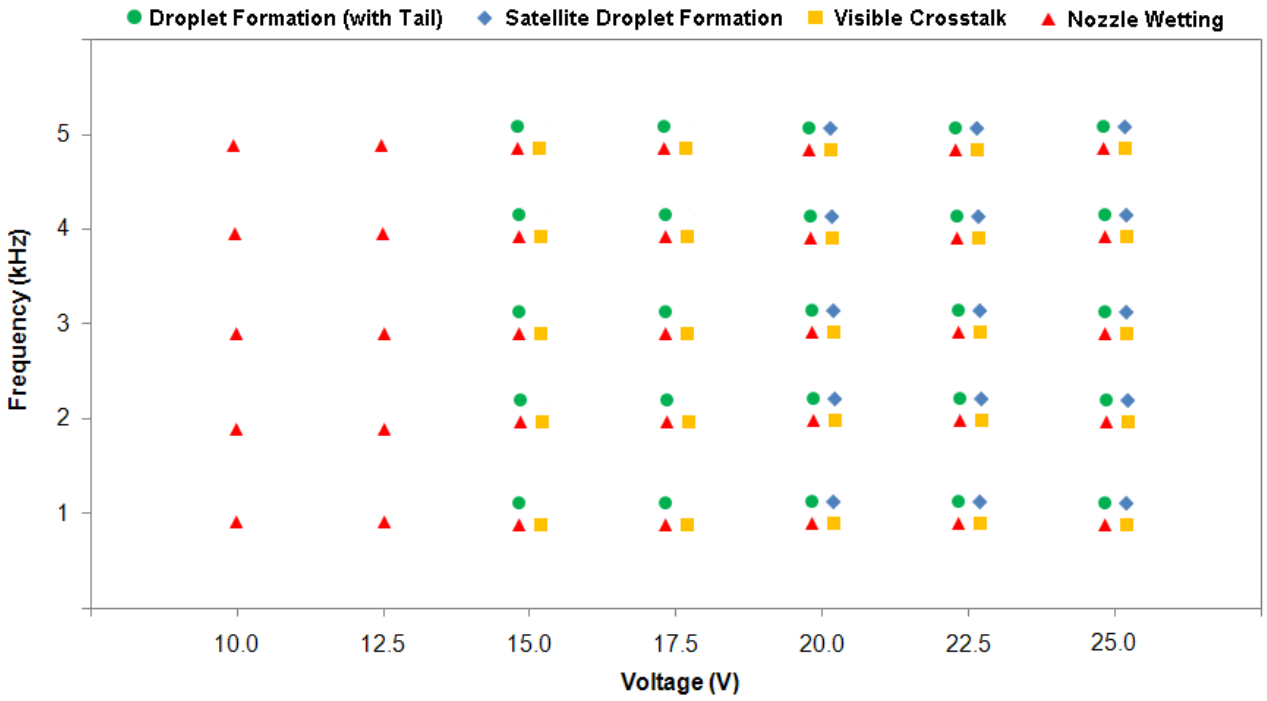

Figure 6-4 Summary of observations in Set 1 of the experiments

6.3 Droplet Characteristics of Caprolactam (Set 2)

6.3.1 Evolution of Droplet Tail

Within the range of parameters in Set 2, all droplets of molten caprolactam were accompanied with the formation of a tail. Analysis of the high speed imaging showed that varying jetting frequency did not affect the droplet shape or the tail size. However, the tail formation characteristics varied with the jetting voltage.

Figure 6-5 shows the tail length for low and high jetting voltages. As seen, the tail length was measured just after the separation from the nozzle. Results for tail length versus jetting voltage are shown in Figure 6-6. Increasing the voltage produced greater oscillation of the melt meniscus and therefore a larger amount of melt was ejected which resulted in formation of a longer tail with the droplet.

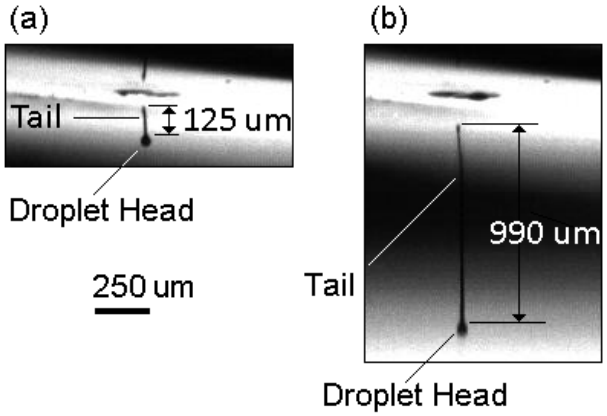

Figure 6-5 Tail length measurements after separation when jetting of molten caprolactam (a) 15.0 V, (b) 25.0 V, (3 kHz, Set 2)

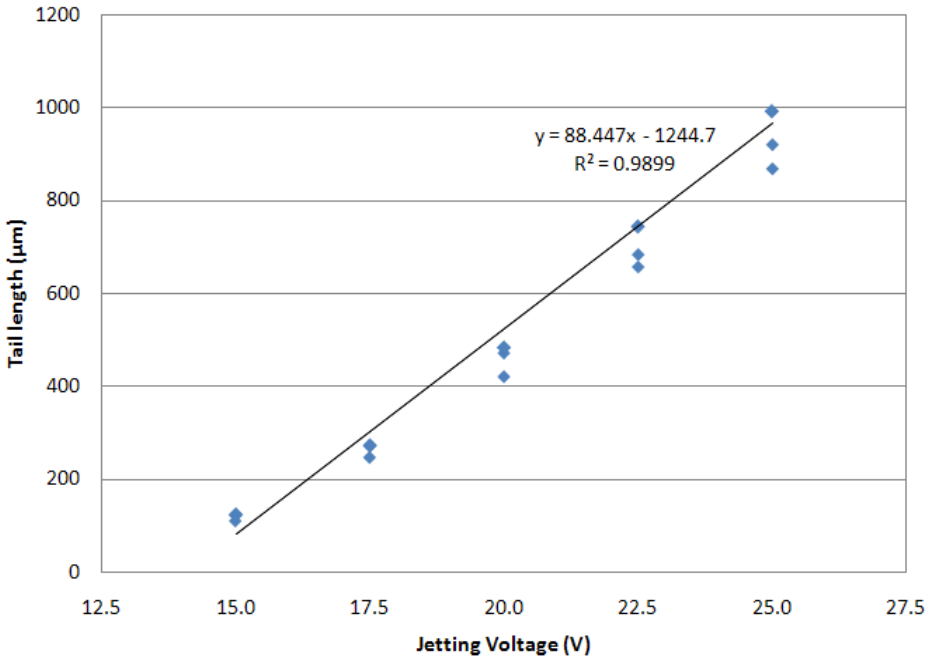

Figure 6-6 Tail length vs. voltage when jetting of molten caprolactam (3 kHz, Set 2)

Figure 6-7 shows the evolution of a droplet with a tail and also demonstrates the meniscus oscillation in the adjacent nozzles. In Figure 6-7(a) and (b), the meniscus oscillations from the partial actuations are seen. After 67 µs, as seen in Figure 6-7(c), two further adjacent nozzles on both sides of the ejecting nozzle were also partially actuated. Figure 6-7(c) also shows the situation just before the tail separated from the nozzle. It is seen that the tail end became thinner than the nozzle diameter (50 µm) due to necking just before separation. This supports the discussion in section 6.2.1 that the meniscus was inside the nozzle. It is also seen that the tail thinning was deflected to one side which could have been the result of separation from the rest of melt inside the nozzle and then touching the nozzle edge. A similar situation was reported by Hutchings *et al.* (2007) when graphical ink at room temperature was jetted. The deflected tail end can be seen in Figure 6-7(d). The tail end deflection was repeatable within the range of jetting voltages and frequencies in Set 2.

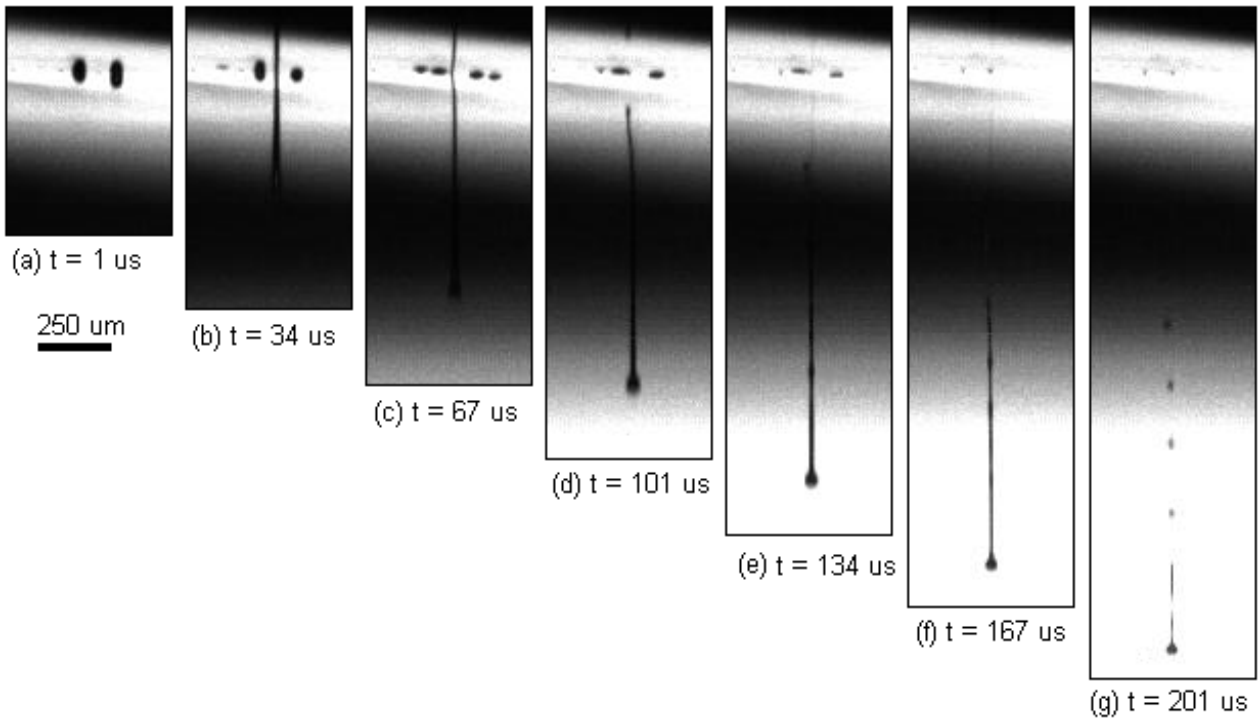

Figure 6-7 Evolution of a tail (formation and disintegration) in jetting of molten caprolactam (25.0 V, 3 kHz, Set 2)

The tail was attached to the droplet head in flight for about 100 µs when a high jetting voltage was used as seen in Figure 6-7(c) to Figure 6-7(f). Disintegration of the tail occurred after about 200 µs (Figure 6-7(g)), when several satellite droplets were formed. Figure 6-8 shows the distance of the main droplet centre against time for the trial shown in Figure 6-7. The linear trend line (regression) fitted well to the measurements and its equation represents the droplet head velocity (8.71 m/s). As inferred from Figure 6-8, the velocity of the main droplet was not affected by the tail disintegration at about (150 to 200 µs). The tail disintegration behaviour depended on the jetting voltage.

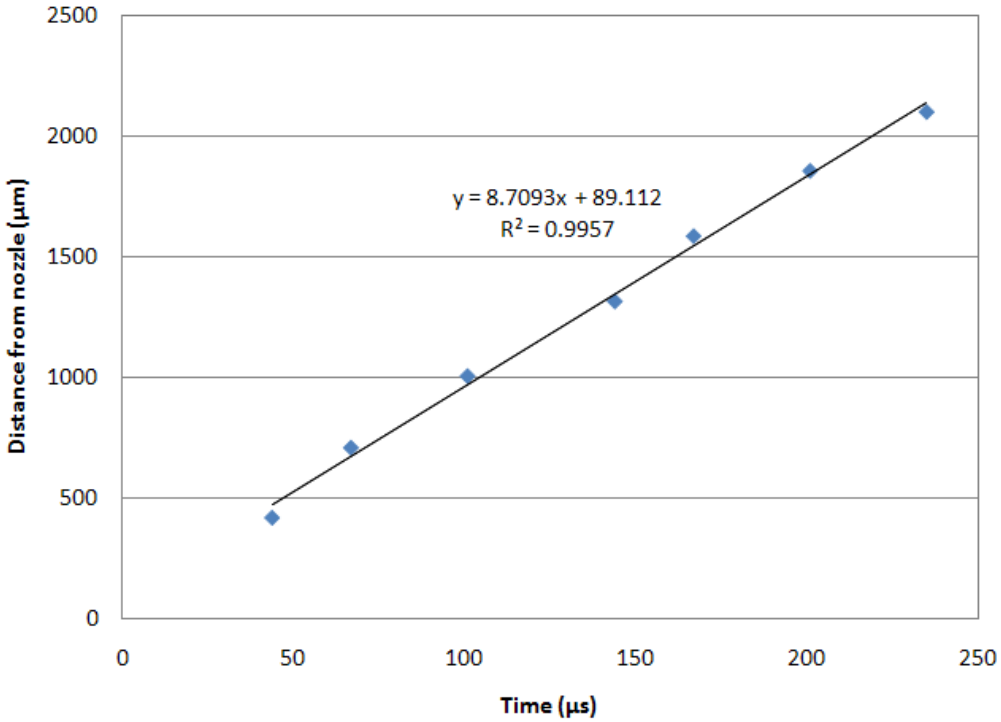

Figure 6-8 Tracking of the droplet head during the tail evolution (25.0 V, 3 kHz, Set 2)

Within the first 100 µs after separation from the nozzle, the tail either disintegrated into satellite droplets flying behind the main droplet (with higher jetting voltages) or rejoined the main droplet (with lower jetting voltages). This was driven by the competition between the surface tension forces and the inertial and viscous forces described by Rayleigh (1878) and is known as Rayleigh instability of a liquid jet.

The disintegration/rejoining behaviour and the distance it occurred are shown in Table 6-2 for different voltages when jetting molten caprolactam in Set 2. Droplets generated with 15.0 V had a short tail with no disintegration to form any satellite droplets. The rejoining of the tail to the main droplet for this voltage occurred at about 250 µm from the nozzle. The tail formed with 17.5 V jetting voltage also rejoined the main droplet without disintegration. However, the rejoining distance increased to about 550 µm. In contrast, with the jetting voltage higher than 17.5 V, the tail disintegrated into several satellite droplets. The disintegration distance

increased from about 900 µm at 20.0 V to 1550 µm at 25.0 V. The tail evolution from formation to rejoining or disintegration occurred within 200 µs of the nozzle actuation for all voltages. The table also suggests the appropriate jetting voltages were 15.0 and 17.5 V to avoid formation of satellite droplets.

Voltage (V)	15.0	17.5	20.0	22.5	25.0
Tail behaviour	Tail rejoining (no satellite droplet)		Tail disintegration (satellite droplets)		
Distance (µm) of droplet head from nozzle for rejoining or disintegration	~ 250	~ 550	900 ~ 950	1300 ~ 1350	1500 ~ 1550

Table 6-2 Tail behaviour versus the jetting voltages for caprolactam (3 kHz, Set 2)

6.3.2 Droplet Size

The size of droplets was considered to be the diameter of the main droplet (after the tail disintegration) or the droplet head (those still having the tail attached) at 1 mm distance from the nozzle. Figure 6-9 shows the variation of caprolactam droplet size with jetting voltage and frequency in Set 2 of the experiments. It was almost constant at around 50 µm which was also the nozzle size. This shows that the droplet size was not affected by the jetting parameters and was due to the nozzle size. As the droplets produced at 20.0, 22.5 and 25.0 V had satellites, the main droplet was a proportion of the whole material forced out. Therefore the results for kinetics energy, Weber number and Reynolds number would be based on the main droplet size which would be deposited onto the surface, independent from the satellite droplet kinetics.

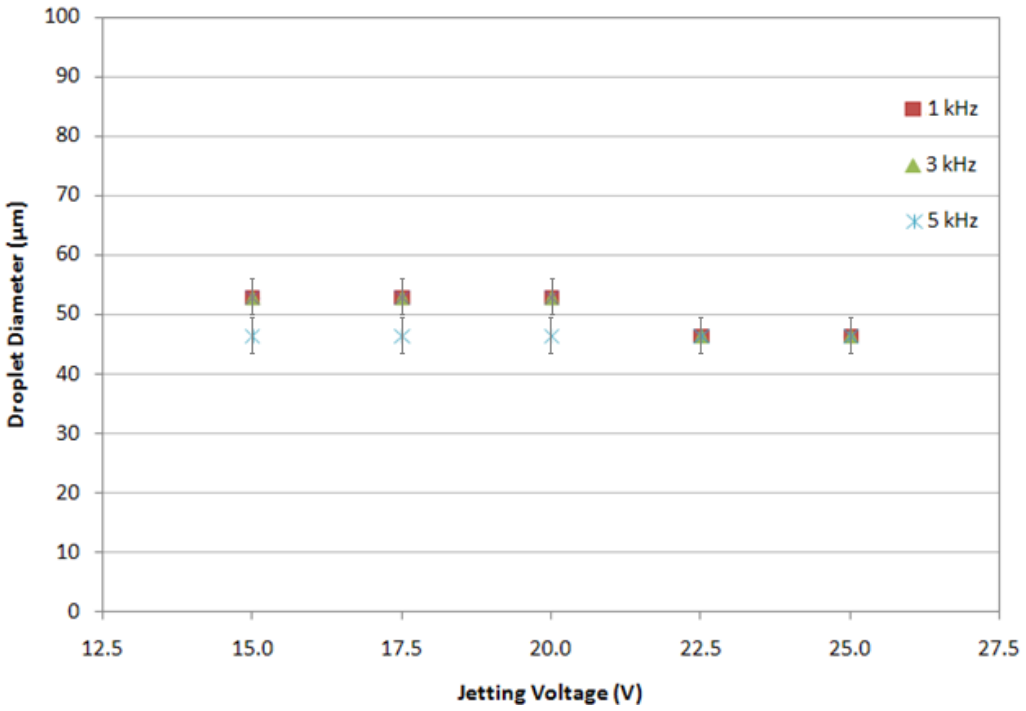

Figure 6-9 Droplet size vs. voltage at different frequencies for molten caprolactam (Set 2)

6.3.3 Kinetics of Droplets

The variation of the droplet kinetics with jetting voltage and frequency was quantified. Figure 6-10 shows that frequency did not have an effect on the droplet velocity. With a higher jetting voltage, a higher amplitude pressure wave was formed and propagated towards the meniscus giving the droplet a higher velocity. The velocity fluctuations and the linear regression of the curve show that the droplet kinetic behaviour was repeatable within the range in Set 2.

Figure 6-11 shows the droplet kinetic energy (E_k) when at 1 mm from the nozzle plate. The droplet kinetic energy which is equivalent to the impact energy, was calculated from equation (1) where m, the weight of a droplet was calculated from the density of caprolactam (1.02 g/cm^3) and the volume of droplets calculated from droplet size in Figure 6-9. The droplet velocity (V_d) used was from Figure 6-10.

$E_k = ½ mV_d^2$ (1)

E_k: Droplet kinetic energy in *nj*

V_d: Droplet velocity in *m/s*

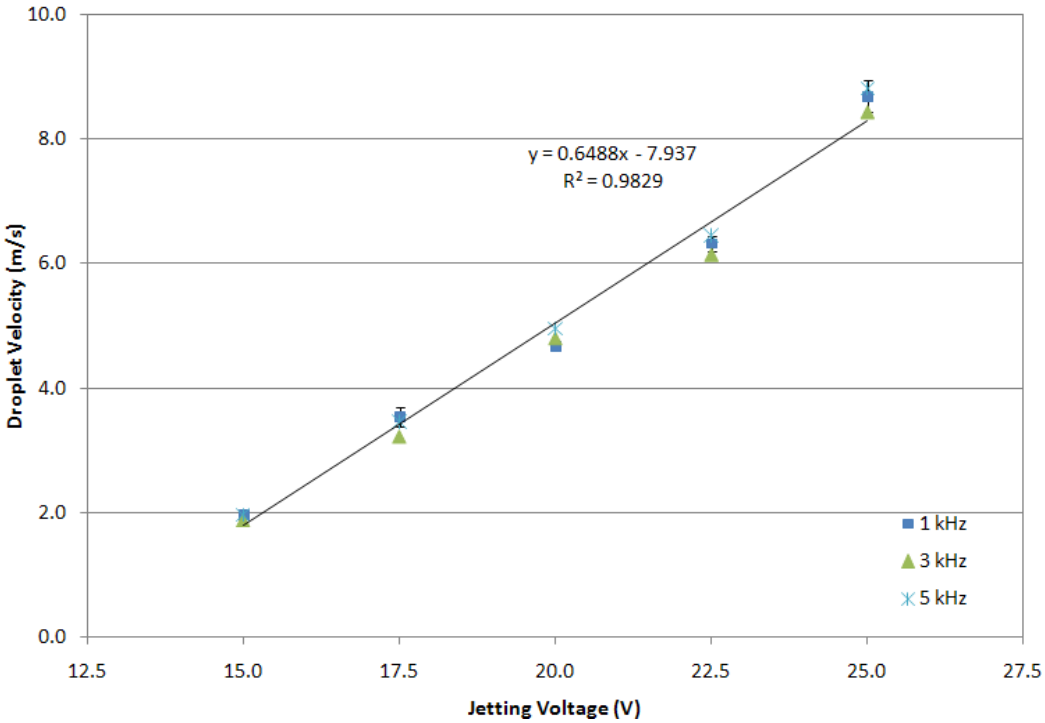

Figure 6-10 Droplet velocity vs. voltage at different frequencies for molten caprolactam (Set 2)

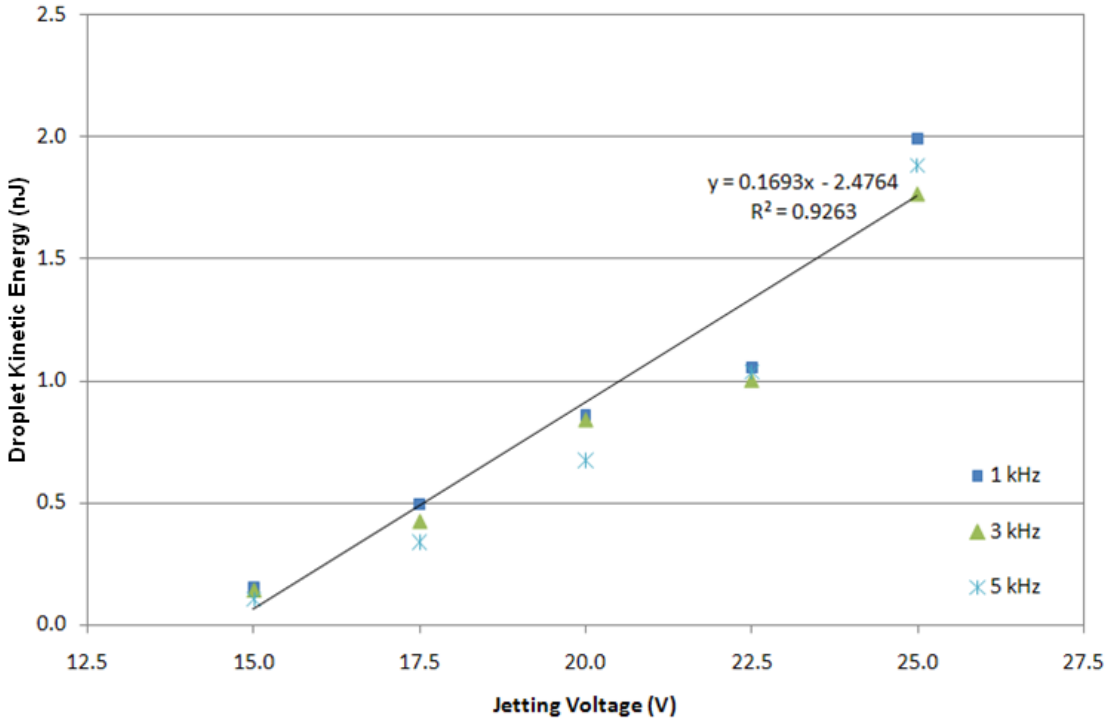

Figure 6-11 Droplet kinetic energy vs. voltage at different frequencies for molten caprolactam (Set 2)

Weber and Reynolds are the two main dimensionless numbers widely used to predict the impact behaviour of droplets (Yarin, 2006). These numbers are respectively defined as the ratio of inertial forces to surface tension and viscous forces. The equations are $We = \rho D V_d^2/\sigma$ and $Re = \rho D V_d/\mu$, respectively where V_d is the droplet velocity on impact, D is the droplet diameter, ρ , σ and μ are the molten caprolactam density, surface tension and dynamic viscosity respectively. Figure 6-12 shows the result for the Weber number and Figure 6-13 the Reynolds number. Both the Weber and Reynolds numbers were relatively low for all the settings which would indicate little tendency of molten caprolactam to splash on the surface during impingement (Yarin 2006). Therefore, it was expected that while depositing molten caprolactam, only droplet spreading would occur with no secondary droplets from splashing.

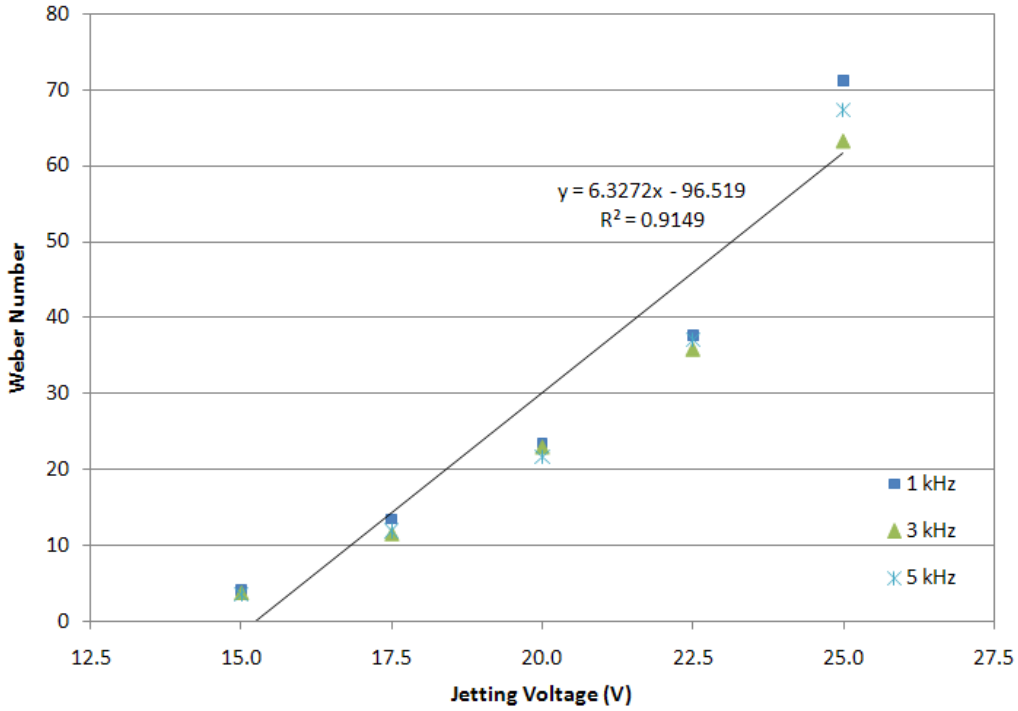

Figure 6-12 Droplet Weber number vs. voltage at different frequencies for caprolactam (Set 2)

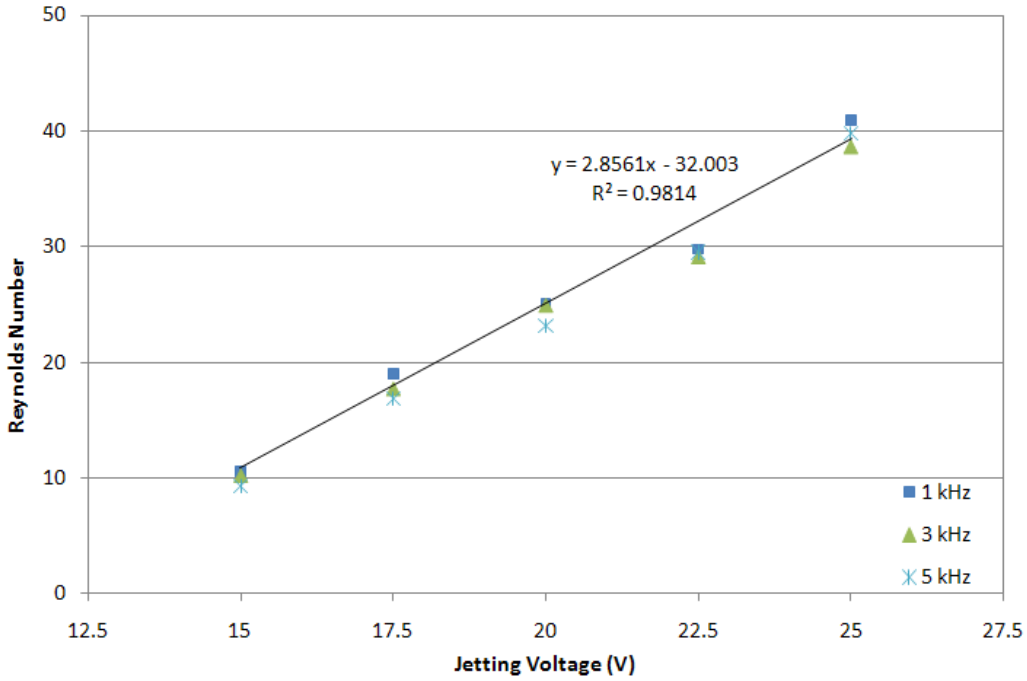

Figure 6-13 Droplet Reynolds number vs. voltage at different frequencies for caprolactam (Set 2)

6.4 Droplet Characteristics of the Reactive Mixtures (Set 3 and 4)

6.4.1 Droplet Tail

Qualitative analysis of the droplet shape from the results of Set 3 and 4 showed that the reactive mixtures had a similar droplet shape to the molten caprolactam. A tail was formed with the droplets at all settings in the two sets of experiments. However, the results for the tail length at different jetting voltages, shown in Figure 6-14, revealed a difference between the reactive mixtures and caprolactam (Figure 6-6). The tail length with the mixtures was much less than with caprolactam for the same voltage. Also, the rate of increase of tail length versus voltage was greater with caprolactam than with the mixtures. This could be due to the 50% higher viscosity of the reactive mixtures than the molten caprolactam. This could increase the pressure wave dissipation during the droplet formation with the mixtures, resulting in smaller meniscus oscillation and therefore less melt being ejected, forming a shorter tail.

Table 6-3 presents the tail disintegration behaviour for the catalyst and activator mixtures which were similar. The distance that the droplet travelled before the tail evolution (rejoining or disintegration into satellite droplets) occurred is also presented in Table 6-3. The tail disintegration into satellites for the mixtures occurred at a higher jetting voltage for the mixture compared with molten caprolactam (Table 6-2). However, the disintegration occurred for tails longer than 300 µm and at a distance of about 550 µm (from the nozzle) for both caprolactam and the reactive mixtures. This suggests that the disintegration into satellites depended on the tail length which was influenced by the melt physical properties and the jetting voltage. As a general conclusion, a higher jetting voltage was required with the reactive mixtures to reproduce a similar droplet shape to caprolactam.

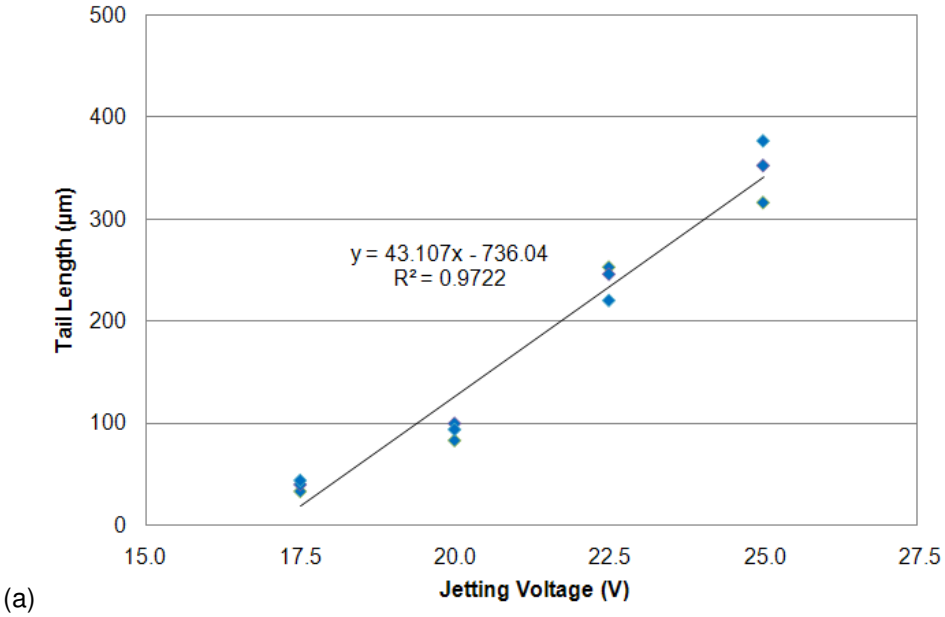

(a)

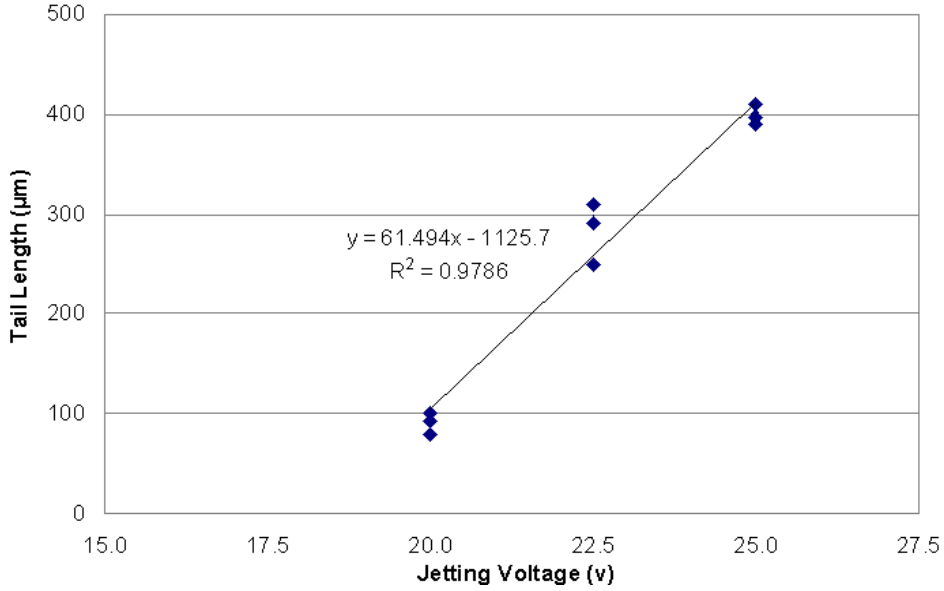

(b)

Figure 6-14 Tail length vs. voltage for (a) catalyst mixture (4 ml, Set 3) and (b) activator mixture (Set 4)

Voltage (V)	15.0	17.5	20.0	22.5	25.0
Tail behaviour	No droplet	Tail rejoining (no satellite droplet)			Tail disintegration (satellite droplets)
Distance (µm) of droplet head from nozzle for rejoining or disintegration	-	~ 100	150 ~ 200	500 ~ 550	850 ~ 950

Table 6-3 Tail disintegration behaviour vs. voltage for the two mixtures (4 ml, Set 3 and 4)

6.4.2 Droplet Size

Figure 6-15 shows the results for the catalyst mixture droplet size in Set 3 of the experiments where different melt supply levels were investigated. Figure 6-16 also shows the droplet size variation with voltage for the activator mixture in Set 4 of experiments at different vacuum levels. The results for all of these conditions in both sets were the same, with the droplet size almost constant in all conditions for both mixtures and were similar to the caprolactam (Figure 6-9) at around 50 µm. This suggests that the droplet size in all jetting conditions (in Set 2, 3 and 4) was mainly dependent on the nozzle geometry, and the physical properties and the jetting parameters had no significant effect.

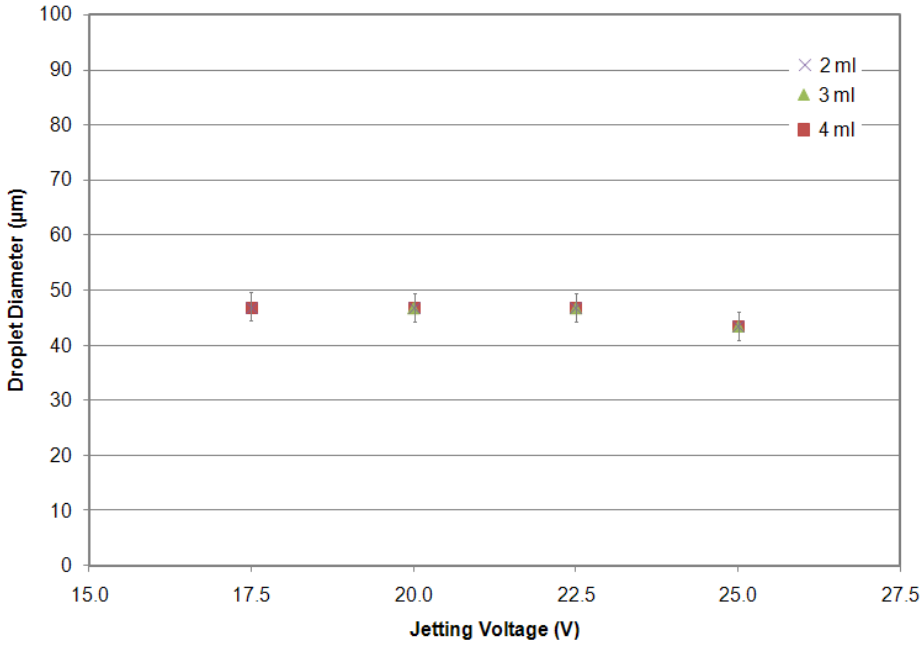

Figure 6-15 Droplet size vs. voltage when jetting catalyst mixture at different melt supply levels (Set 3)

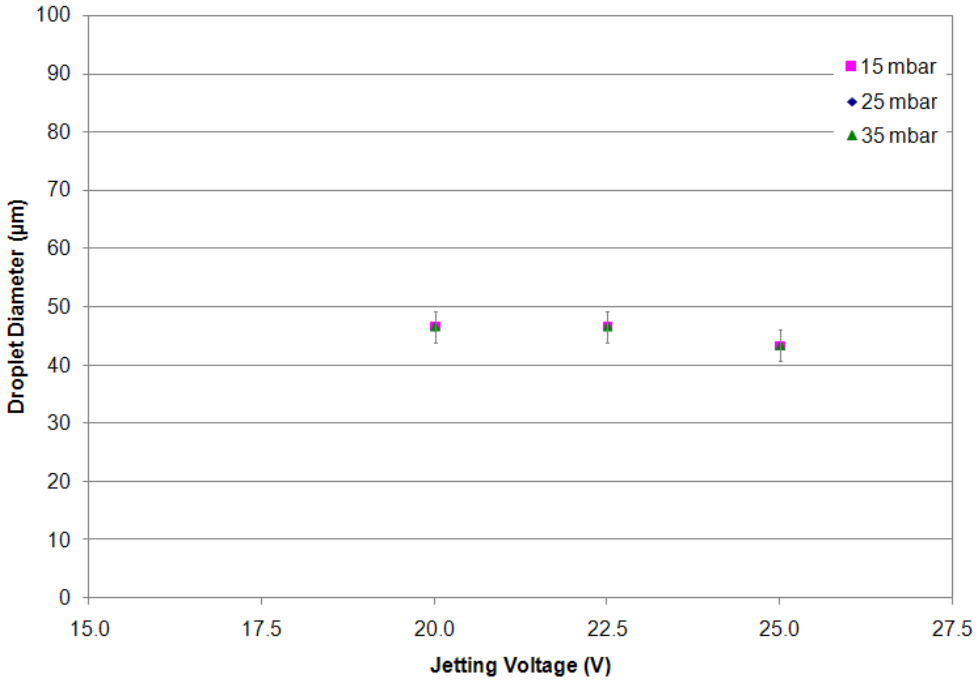

Figure 6-16 Droplet size vs. voltage with different vacuum levels when jetting activator mixture (Set 4)

6.4.3 Kinetics of Droplets

Figure 6-17 presents the results for the effect of jetting voltage on the droplet kinetics at different melt supply levels of the catalyst mixture in Set 3. The droplet velocity increased with the jetting voltage almost linearly. The melt level did not affect the droplet velocity considerably. No velocity results are seen for 2 and 3 ml melt levels at 17.5 V as the jet failed quickly after the start. However, there was a considerable difference between the results with pure caprolactam and the catalyst mixture when comparing Figure 6-10 and Figure 6-17. The velocity with the catalyst mixture was less than half the velocity of the caprolactam droplets, especially when jetting with lower voltages. It is seen from the results that jetting the catalyst mixture required an additional 5.0 V jetting voltage compared with the caprolactam to obtain a similar droplet velocity.

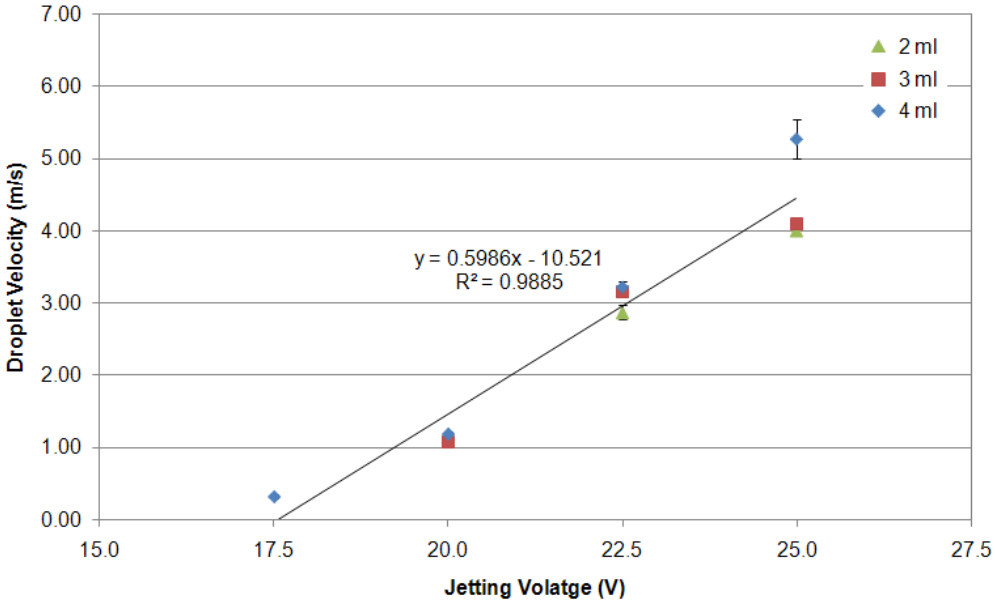

Figure 6-17 Droplet velocity vs. jetting voltage at different catalyst mixture melt supply levels (3 kHz, 25 mbar, Set 3)

A velocity difference between the first few droplets of the catalyst mixture compared with the rest of the droplets was noticed during the high speed imaging. Therefore, the first 10 droplets of each trial were characterised for the droplet velocity as shown in Figure 6-18. The figure compares the droplet velocity versus droplet number at different voltages and melt supply levels. In all settings, the velocity of the first droplet was up to about 20% higher than the rest of droplets. This could be due to the difference in the meniscus condition before and after the first nozzle actuation. The meniscus was at rest before generating the first droplet whereas with the other droplets, there could be some residual oscillations on the meniscus from previous actuations. The effect on first droplet was not investigated with the other materials due to time restrictions.

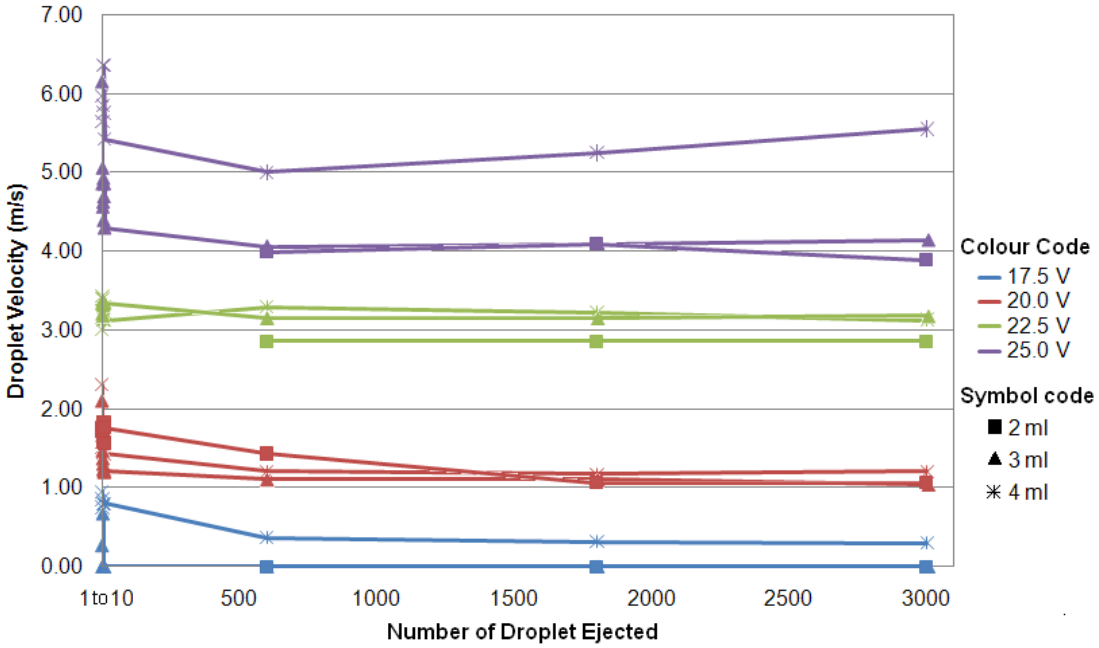

Figure 6-18 Droplet velocity variation after different number of catalyst mixture droplets were ejected when varying jetting voltage and the melt supply level (Set 3)

Figure 6-19 shows the droplet velocity against jetting voltage for the activator mixture in Set 4. The effect of vacuum level was also investigated in this set. Compared with the catalyst mixture in Set 3 with a similar vacuum level (25 mbar), droplet velocity was slightly lower with the activator mixture for jetting voltages higher than 20.0 V (comparing Figure 6-17 and Figure 6-19). Compared with pure caprolactam, the droplet velocity decreased with the activator mixture more than with the catalyst.

The effect of vacuum level on the velocity was clear as seen in Figure 6-19. Increasing the vacuum level from 15 mbar to 35 mbar decreased the droplet velocity by almost 1 m/s for all the jetting voltages. The vacuum level affects the meniscus shape and therefore the interaction between the pressure wave and the meniscus surface tension. Due to the higher surface tension of the nozzle plate than the jetting materials, the vacuum applied should form a concave meniscus inside the nozzle. Increasing the vacuum level could increase the surface area of the meniscus (Leu

and Lin, 2008). This means a higher total surface energy of the meniscus was competing against the pressure wave upon droplet generation. This could decrease the amount of energy being delivered to the droplet and subsequently cause the decrease in the droplet velocity when a higher vacuum was used as seen in Figure 6-19. This may also suggest why air ingestion occurred in the jetting trials with high vacuum levels where a highly concaved meniscus had more potential to entrap an air bubble.

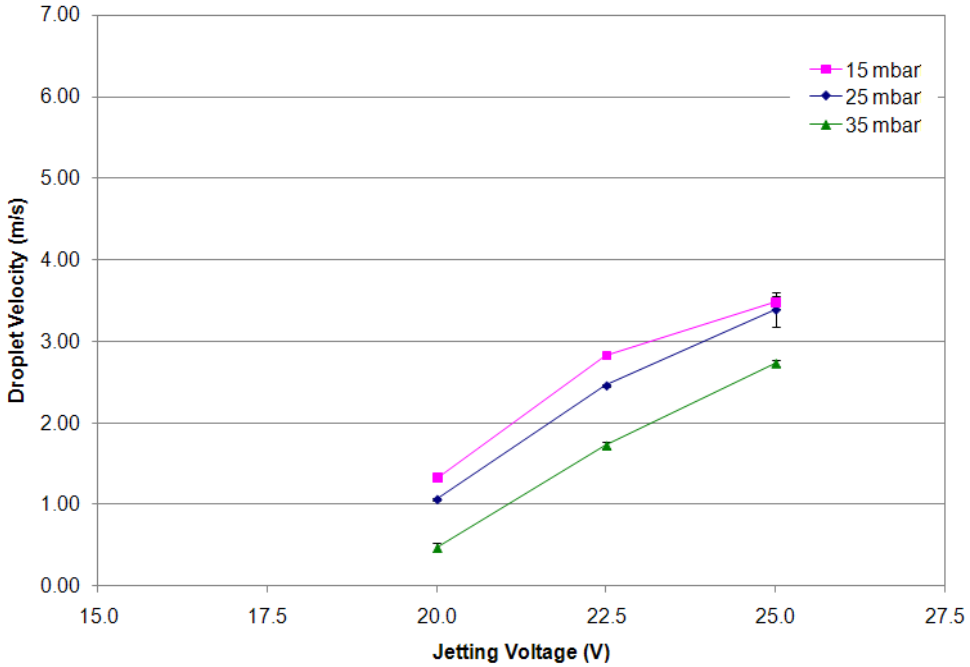

Figure 6-19 Droplet velocity vs. voltage with different vacuum levels when jetting the activator mixture (Set 4)

6.5 Nozzle Wetting

6.5.1 Wetting Behaviour

The wetting behaviour during the droplet formation process is important as it could interact with the jet stability. This was studied with molten caprolactam in Set 1 with a

range of jetting voltages and frequencies. With a dry nozzle plate, a wetting area developed over time around the actuating nozzle. This phenomenon was observed in all the parameter settings in Set 1 (within about 1 second of jetting). Figure 6-20 compares the actuating nozzle before and after the wetting area developed. Figure 6-20(a) shows the start of jetting with no residual melt on the actuating nozzle and only the meniscus oscillation of the adjacent nozzle visible. On the other hand, Figure 6-20(b) shows the wetting area after ejection of 3311 droplets at 25.0 V and 3 kHz. The wetting area is seen as a dark strip because the camera was slightly angled from the horizontal position (a side view) to capture this. Meniscus oscillation and the lower surface tension of the jetting materials compared with the nozzle plate were responsible for the development of the wetting area. With each actuation, a small amount of melt was left on the nozzle plate. This resulted in propagation of the wetting area and its expansion over time as seen in Figure 6-20(b).

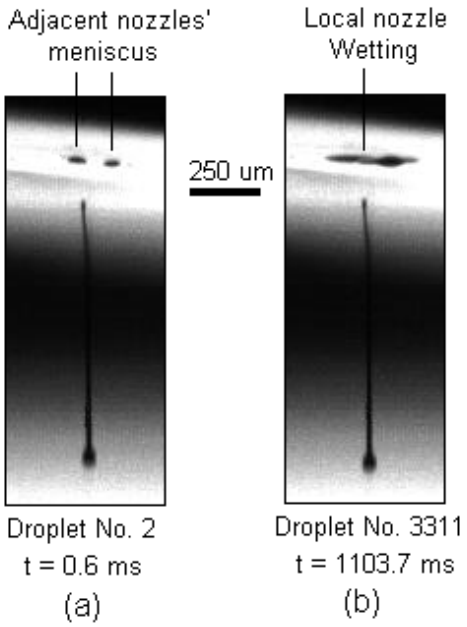

Figure 6-20 Nozzle wetting after jetting (a) 2 droplets, (b) 3311 droplets (25.0 V, 3 kHz, 25 mbar, Set 1)

6.5.2 Effect of Jetting Parameters

Voltage defines the amplitude of the meniscus oscillation, and frequency the number of droplets being ejected both of which could affect the wetting area development. This was investigated by monitoring the actuating nozzle over time. The wetting development rate was measured at different parameter settings when jetting molten caprolactam in Set 1. The high speed camera captured images for about 1.5 seconds from the first droplet ejection and so recorded generation of at least 1500 droplets when frequencies as low as 1 kHz was used. From the images, the width of the wetting area (as seen in Figure 6-20(b)) was measured after the first 1000 droplets were ejected for all the voltage and frequency settings.

Figure 6-21 shows the results for the wetting area development versus voltage and frequency when jetting caprolactam. At lower frequencies, wetting was generally greater. This was considerable with 20.0 V at 1 kHz with the highest wetting in the trials. The decrease of the wetting area development with increasing frequency suggests that wetting was a time dependent phenomena. With more time between droplet formation (i.e. lower jetting frequency), the wetting area developed further on the nozzle plate. Therefore, it was concluded that the wetting was not necessarily dependent on the number of droplets but the effect of jetting time was considerable.

At higher frequencies, the voltage did not affect the development of the wetting area significantly. This was below 100 µm with frequencies below 3 kHz in the first 1000 droplets. Therefore, the wetting area did not cover the adjacent nozzles. To deposit the required amount of material when using a dry nozzle plate, a higher jetting frequency would be preferred. This helps to avoid partial wetting of the adjacent nozzles which could lead to instabilities in their droplet formation.

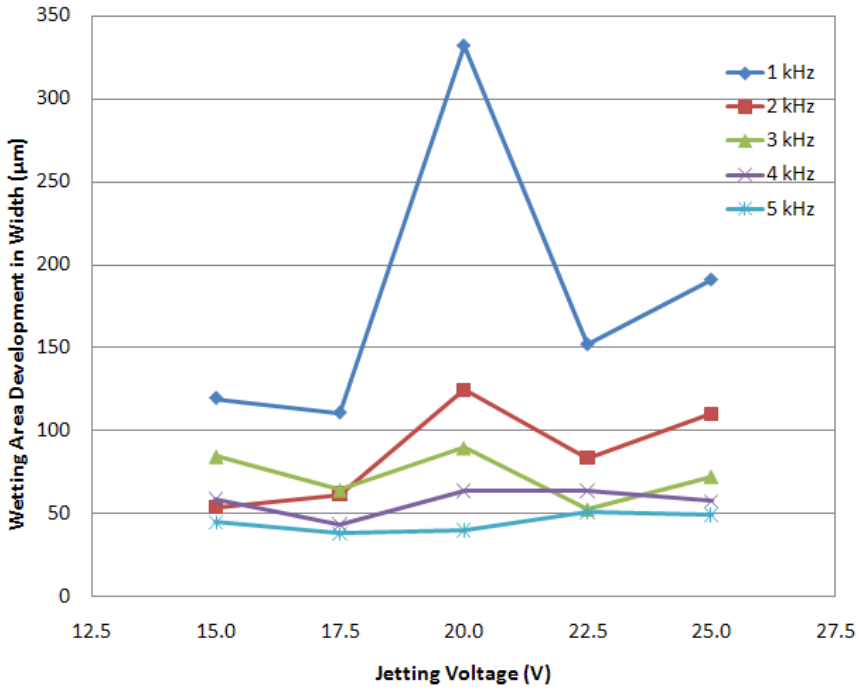

Figure 6-21 Nozzle wetting area development for first 1,000 droplets ejected vs. voltage at different frequencies in jetting caprolactam (25 mbar, Set 1)

6.6 Instabilities in Droplet Formation

The instabilities of the droplet formation process were monitored with high speed imaging to understand the detail of the formation process. The jet trajectory error and jet failure made by wetting, improper parameter setting and also air motion were studied.

6.6.1 Effect of Nozzle Wetting

Jet instability occurred in some trials after the wetting area developed around the actuating nozzle. In such a case, the wetting area was found to develop asymmetrically in relation to the nozzle position. An external source such as contamination or air motion could provide conditions for such asymmetry during the

wetting area development. Figure 6-22 shows how the presence of contamination near to the nozzle could lead to a trajectory error. In Figure 6-22(a), the position of the contamination to the left of the actuating nozzle is seen. The meniscus oscillations in the adjacent nozzles are also seen. Figure 6-22(b) shows a moment just after a droplet was ejected when there was no residual melt left around the nozzle. However, over time the wetting area developed as seen in Figure 6-22(c) and (d). The wetting development though was not symmetric to the actuating nozzle. The contamination could possibly attract the wetting area. The asymmetric wetting could affect the droplet separation by deflecting the tail towards the centre of the (asymmetric) wetting area (left of the actuating nozzle) as seen in Figure 6-22(d). This situation could lead the trajectory to be altered after ejection of 3,607 droplets within about 1 second.

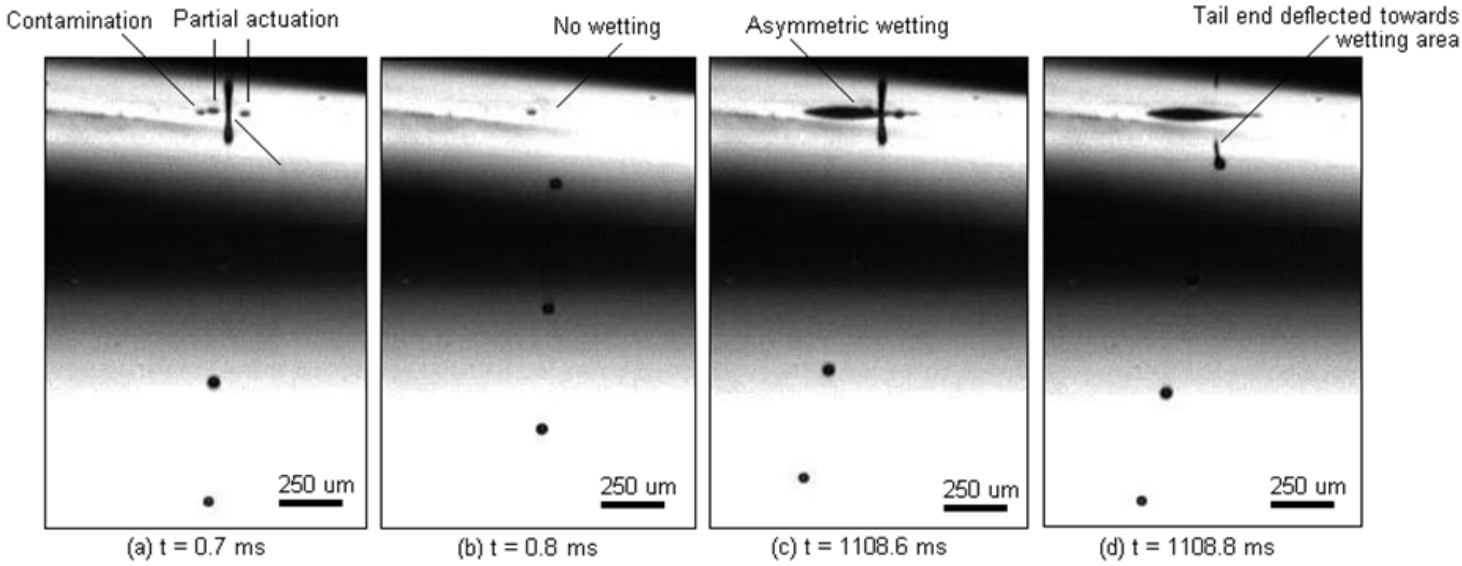

Figure 6-22 Jet trajectory error made by an asymmetric development of wetting around the nozzle due to a contamination on the nozzle plate (15.0 V, 4 kHz, 25 mbar, Set 1)

Figure 6-23 shows that the jet trajectory error with asymmetric nozzle wetting was also seen in a trial with the catalyst mixture in Set 3. Figure 6-23(a) shows the nozzle position during the meniscus oscillation. The nozzle position was 173 µm from the edge of the frame. In Figure 6-23(b), the final separation of the tail was made with 40 µm displacement from the nozzle position as seen in Figure 6-23(c). This process could lead to the trajectory error seen in this trial.

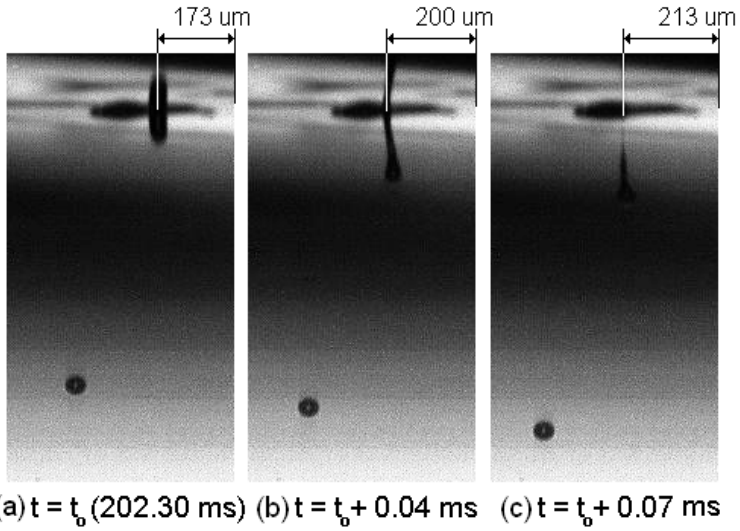

Figure 6-23 Trajectory error during tail separation in a trial with the catalyst mixture (3 ml, 20.0 V, 3 kHz, 25 mbar, Set 3)

Although the above discussion may explain the trajectory error after about 200 ms, it does not explain how the wetting area developed asymmetric to the nozzle when no contamination was found around the actuating nozzle. The air motion could alter the trajectory from ejection of the first droplet and result in tail separation occurring repeatedly to one side resulting in the asymmetric wetting area. Figure 6-24 shows a graph of the trajectory error development for the trial shown in Figure 6-23. From the

first few droplets, an error in the trajectory was made which increased to about 16 degrees within the first 200 ms and then remained constant (until the end of the trial).

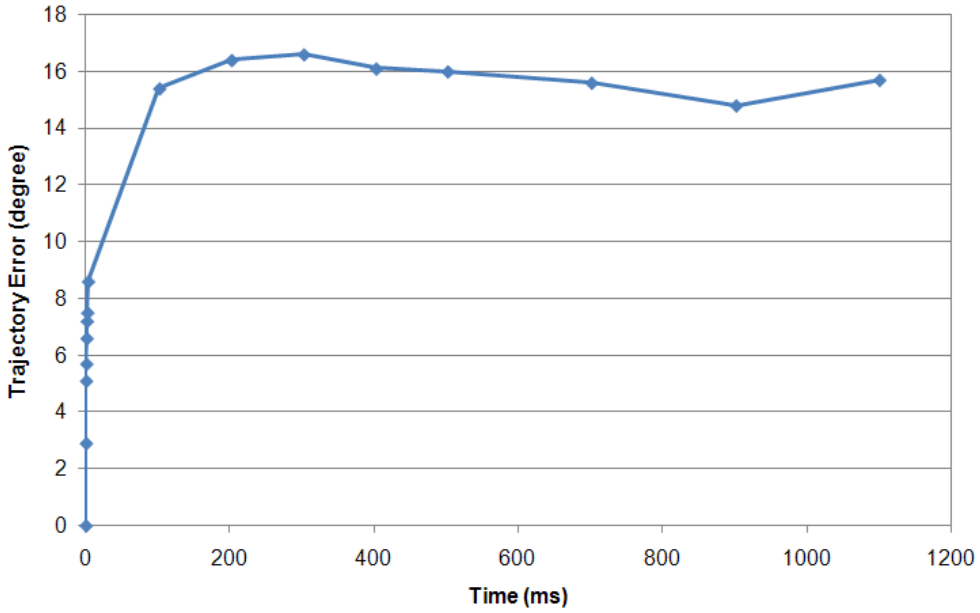

Figure 6-24 Increase of the trajectory error over time in a trial with the catalyst mixture as shown in Figure 6-23 (3 ml, 20.0 V, Set 3)

6.6.2 Effect of Improper Parameter Setting

The trajectory error development made by nozzle wetting was usually a slow process which could result in jet failure after some seconds. However, a faster development occurred due to a combination of sources. Figure 6-25 shows a trial with the catalyst mixture in Set 3 where a trajectory error developed quickly into jet failure within the first 5 ms. The error was plotted versus time as seen in Figure 6-26. From the first droplet a trajectory error of about 10 degree was recorded. This increased to about 90 degrees as seen in Figure 6-25 at t = 4.3 ms. The droplets touched the nozzle plate at t = 5.3 ms, wetting the nozzle plate. This was a rapid jet failure with no incorporation of the asymmetric wetting area discussed in the previous section.

However, due to the low jetting voltage, droplets were ejected with very low kinetic energy. This could allow the air motion to alter the trajectory of the low kinetic droplets in flight leading to jet failure.

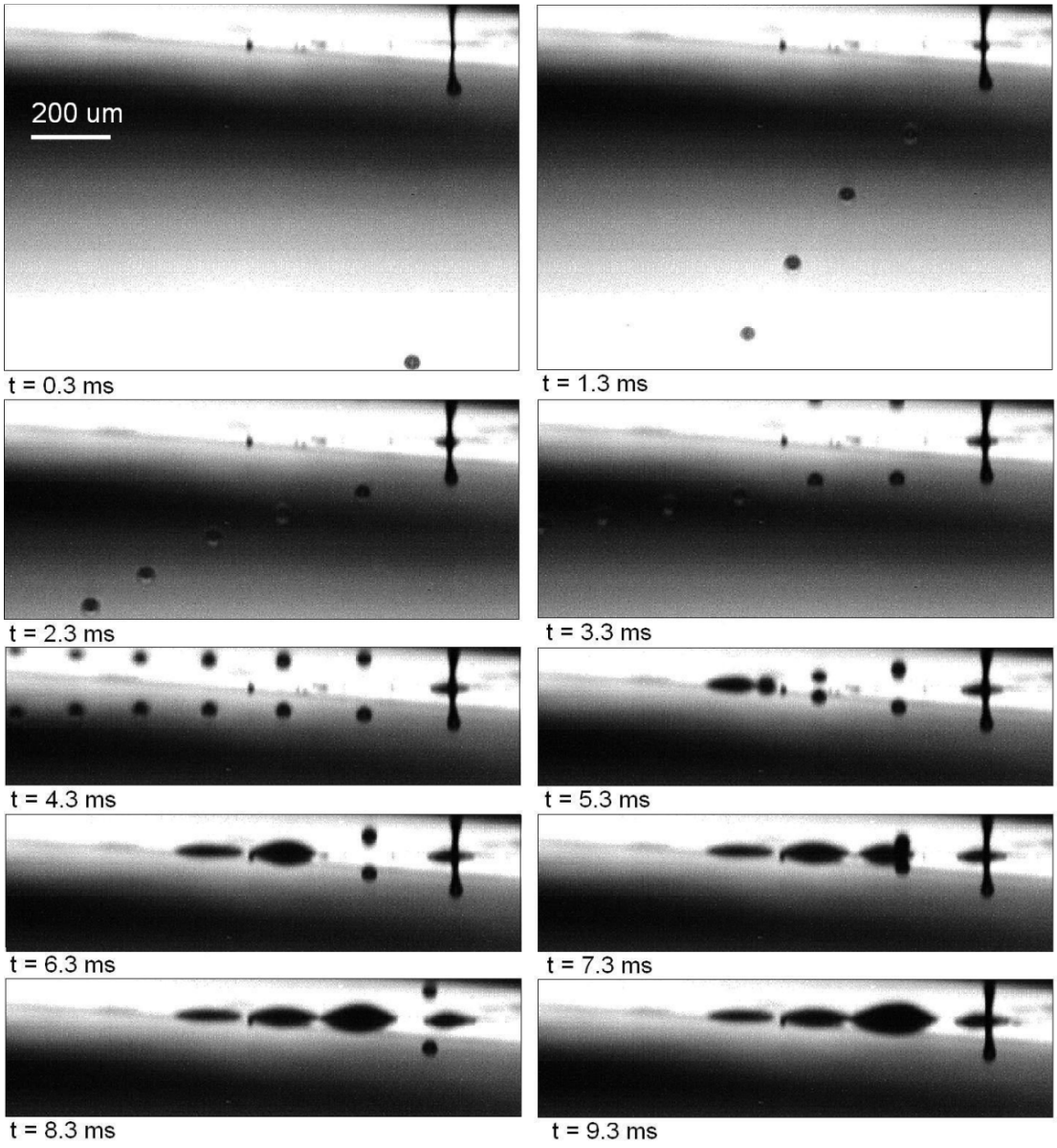

Figure 6-25 Jet failure over time initiated from a trajectory error in a trial with the catalyst mixture (4 ml, 17.5 V, Set 3)

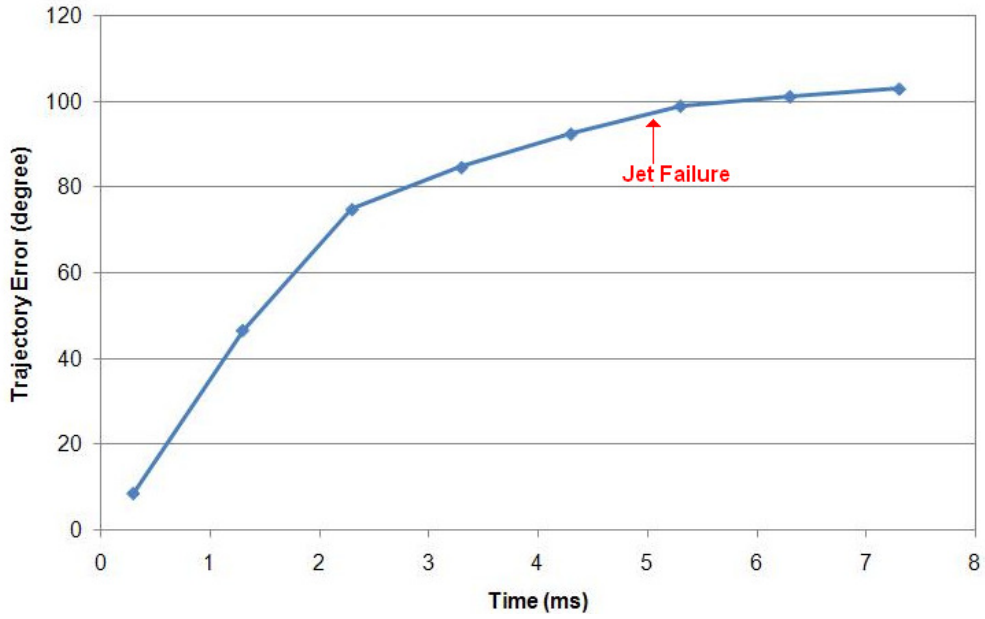

Figure 6-26 Rapid increase of the trajectory error over a short time compared with Figure 6-24 (4 ml, 17.5 V, Set 3)

It was found that jet instability could occur from the first droplet ejected when inappropriate jetting parameters were selected. With too low a jetting voltage, formation of droplets with low kinetic energy occurred. Figure 6-27 shows such a case where after ejection of the first droplet (D1) at t = 0.1 ms, the second droplet (D2) was generated at t = 0.4 ms and was separated from the meniscus with such a low kinetic energy (as inferred from the limited displacement of the droplet between t = 0.4 ms to 0.6 ms) that it seemed to be suspended around the actuating nozzle. The pressure wave oscillated the meniscus only enough to form a droplet and there was no energy left to cause displacement. Therefore, when the third actuation occurred at t = 0.7 ms, the expanded meniscus hit the second droplet and merged with it (D2-D3). When the meniscus was retracting into the nozzle, necking occurred which could attract (pull) the merged droplet towards the nozzle (t = 0.8 ms), and therefore the (merged D2-D3) droplet touched the nozzle at t = 0.9 ms. However,

with the fourth nozzle actuation, the meniscus expansion generated a bigger droplet (D4) at t = 1.1 ms with such a high kinetic energy that it overtook the first droplet (D1) at t = 2.0 ms (see frames t = 1.1 ms to 2.1 ms). After the fourth actuation, no more droplets were formed and the meniscus oscillation from following actuations resulted in the local nozzle wetting during the next 500 ms as seen in Figure 6-27.

Merging of first droplets leading to the jet failure (and the consequent nozzle wetting) was also observed with the activator mixture when a low jetting voltage was used. As seen in Figure 6-28, the low jetting voltage resulted in formation of the first droplet (D1) with very low kinetic energy. The droplet was only displaced a few micron from t = 0.1 to 0.2 ms. Therefore, with the second nozzle actuation at t = 0.3 ms, the expanded meniscus merged with D1 and formed a bigger droplet (D2) which had just enough kinetic energy to be expelled from the nozzle with a very low velocity. However, from the third nozzle actuation afterwards (t = 1.0 ms), no droplet was expelled. The coalescence of the oscillating meniscus with the previous merged droplets upon actuation, resulted in further merging of droplets D3 to D5 until t = 1.5 ms. The meniscus oscillation finally attracted the merged droplets towards the nozzle (when forming D6). This resulted in asymmetric nozzle wetting to the left of the nozzle as seen at t = 1.6 ms and finally led to the failure of droplet generation.

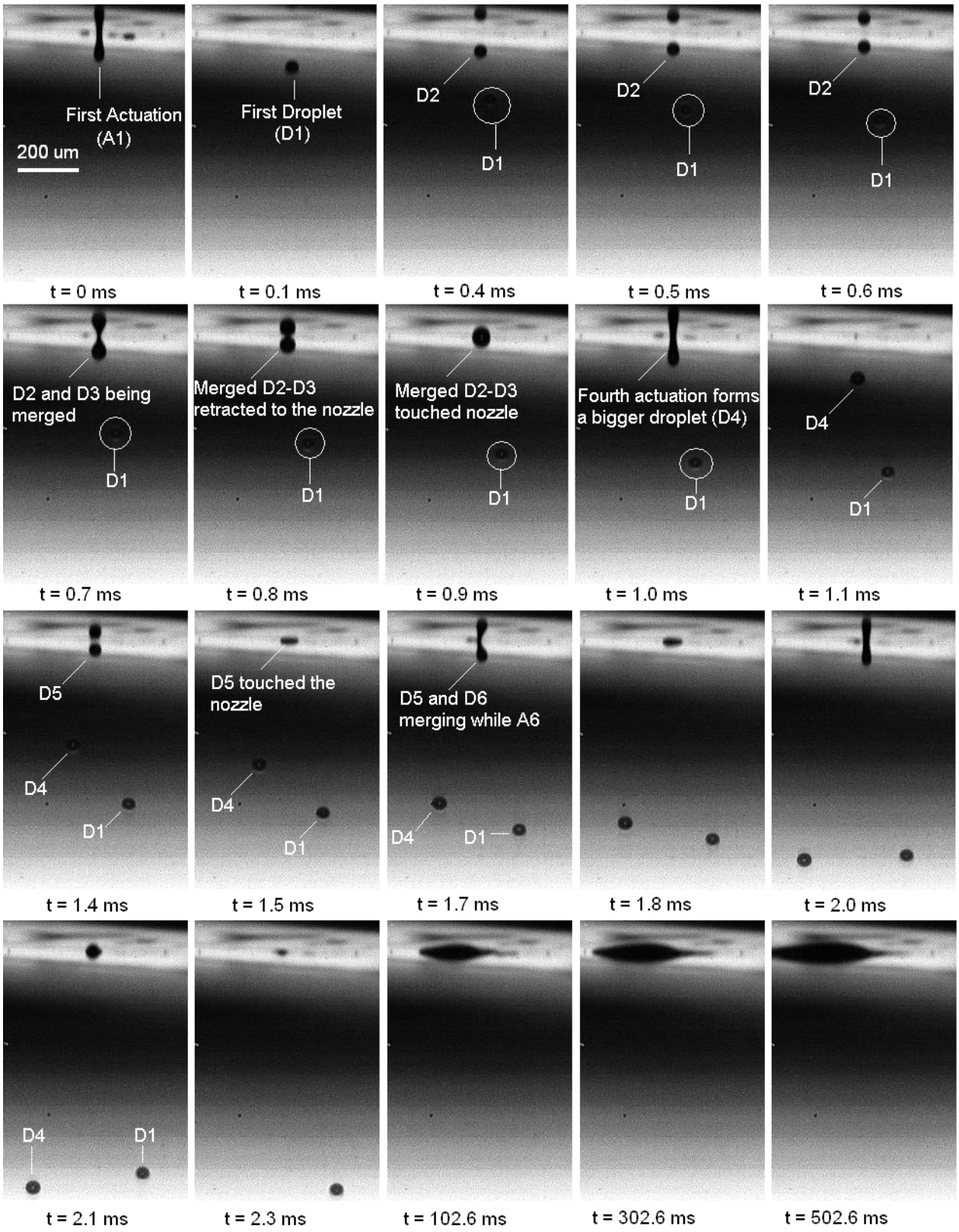

Figure 6-27 Wetting of the nozzle plate by a jet failure in a trial with catalyst mixture due to improper setting of the parameters (3 ml, 17.5 V, Set 3)

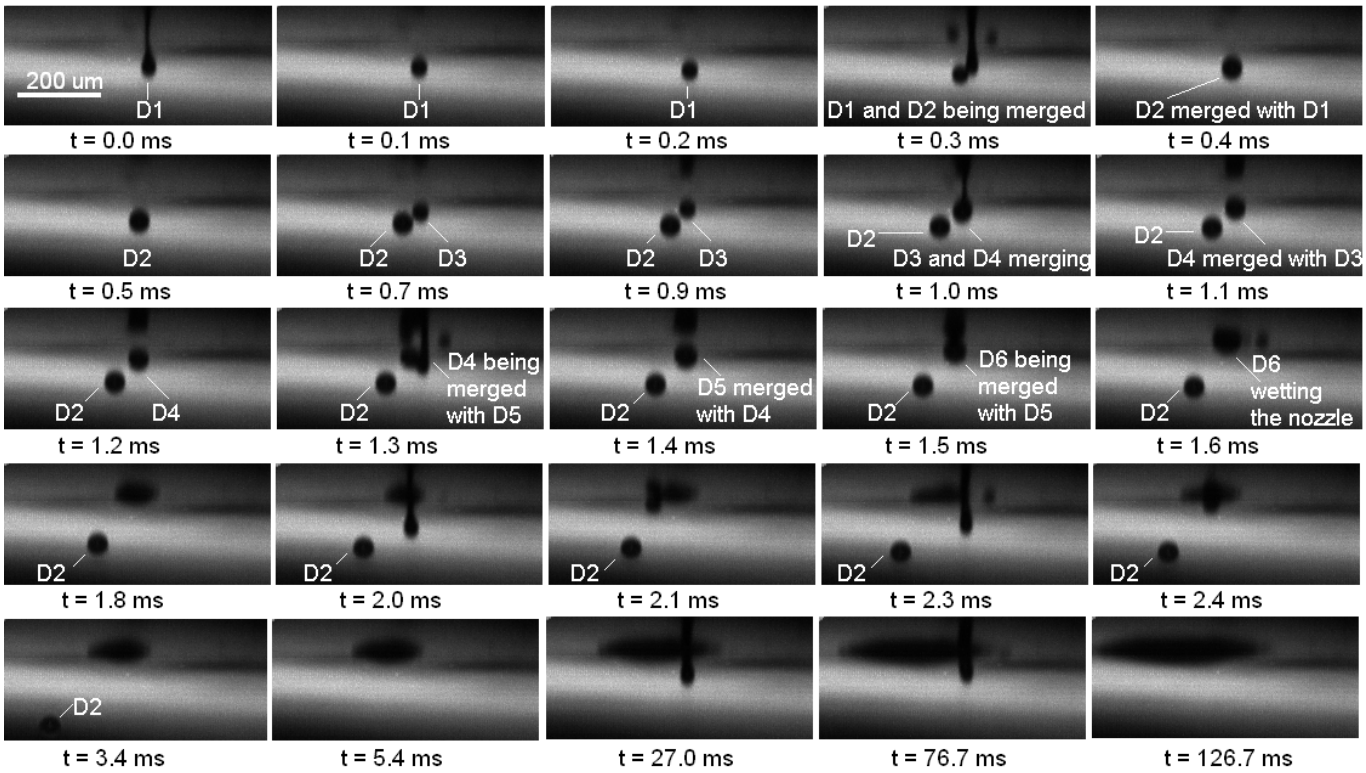

Figure 6-28 Jet failure and nozzle wetting of a trial with the activator mixture due to improper setting of the parameters (17.5 V, 15 mbar, Set 4)

Chapter 7. Deposition of Materials

This chapter reports on the phenomena associated with the material behaviour during the deposition stage. Three main situations discussed are: droplet/surface interactions, microcrystal content within deposited droplets of the catalyst mixture, and mixing of droplets.

7.1 Requirements and Approach

From the results reported in chapters 3 to 5, the following considerations were taken into account for the research into deposition.

Reference Material: As with the previous research, this work also used caprolactam to study deposition before using the reactive mixtures.

Limitation on Jetting Stability: Greater reliability had been seen with a single jet rather than with multiple jets. Therefore, it was decided to keep the situation simple and observe deposition with a single jet.

Narrowing the Range of Jetting Parameters: It was also decided to use a small range of parameters from the process window to avoid jet trajectory errors due to low droplet kinetic energy and also formation of satellite droplets which could influence the droplet placement.

This work investigated several aspects of deposition:

Caprolactam Droplets/Surface Interactions: The impact behaviour of caprolactam droplets onto a static and moving surface was investigated before using the mixtures. The droplets kinetics and surface temperature would vary the impact behaviour (Yarin 2006). To ensure that the caprolactam droplets had suitable kinetic energy to generate spreading and not splashing, the spreading regime was initially investigated onto the static room temperature (cold) and heated surface. Then the formation and stability of a uniform bead onto a moving cold/heated surface was monitored.

Microcrystal Content of Catalyst Mixture Droplets: This was to look at individually deposited droplets of the catalyst mixture at different melt supply levels (1~4 ml) to study the microcrystal dispersion/agglomeration and consistency. The objective was to limit this parameter for further experiments. In addition, the microcrystal content was investigated when multiple droplets coalesced (by the droplets impact kinetics) to compare the agglomeration behaviour with the individually deposited droplets.

Drop-on-Drop Mixing: This step investigated the mixing outcome of the chosen deposition approach. The reactive mixtures were used for this and were monitored by dye tracing and fluorescent imaging.

7.2 Caprolactam Droplets/Surface Interactions

7.2.1 Experiments

Molten caprolactam at 80℃ was jetted at 17.5 V, 5 kHz and 25 mbar. A microscope glass slide (76 mm x 26 mm x 1 mm, Gerhard Menzel GmbH) was used as the deposition surface. Backlight lateral high speed imaging (section 3.5.2) captured the droplet impact behaviour and images were analysed with an edge definition accuracy of better than 2 µm. The glass slide was fixed to the thermally controlled

aluminium substrate as described in section 3.6.2. The surface temperature was at 20±1℃ or 80±3℃. Initial experiments on bead formation were undertaken by moving the surface at 100 mm/s giving a droplet spacing of 20 µm. The results would suggest whether further experiments would be required for research of stable bead deposition.

7.2.2 Results for Droplet Impact on a Static Surface

Splashing was not observed for both the cold and heated surfaces. This confirmed the predictions made by the calculated Reynolds and Weber numbers reported in section 6.3.3 and showed that the jetting parameters were suitable for other deposition trials. Figure 7-1 shows a smooth spreading of the first few droplets deposited onto the heated surface. The number of droplet being deposited, total number of accumulated droplets and also the time from the first impingement are shown in the sequence. No splashing was observed from the impingement of consecutive droplets for both the cold and heated surface.

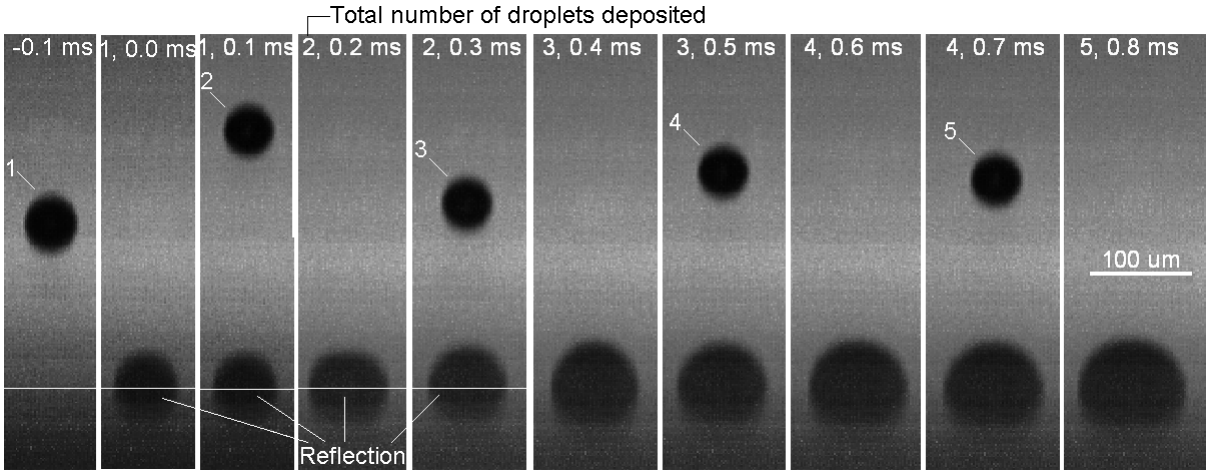

Figure 7-1 Spreading of caprolactam droplets onto heated static glass surface

7.2.3 Results for Droplet Spreading on Moving Surface

Bead Stability upon Formation

Figure 7-2 shows the start of a bead formation on a heated moving surface. Due to the droplet impact kinetics, the surface energy and the droplet spacing, there was coalescence of the droplets. For the first few droplets, the coalescence resulted in the bead having a greater height at the start (left side) compared with the advancing front where new droplets were impinging. This was still visible after the tenth droplet was deposited. A similar situation was recorded with the cold surface. This bulge formation has also been observed by other researchers (Derby 2010).

When depositing a pattern, uniform beads are preferred and therefore the bulge formation at the start of the bead could affect the accuracy of the layer edge definition. However, it is more important to investigate the bead stability until solidification by polymerisation which could occur seconds after the deposition. Although it was shown in Figure 7-2 that the leading edge of the bead was stable and uniform during the initial 2.0 ms, it was necessary to investigate the stability for a longer period.

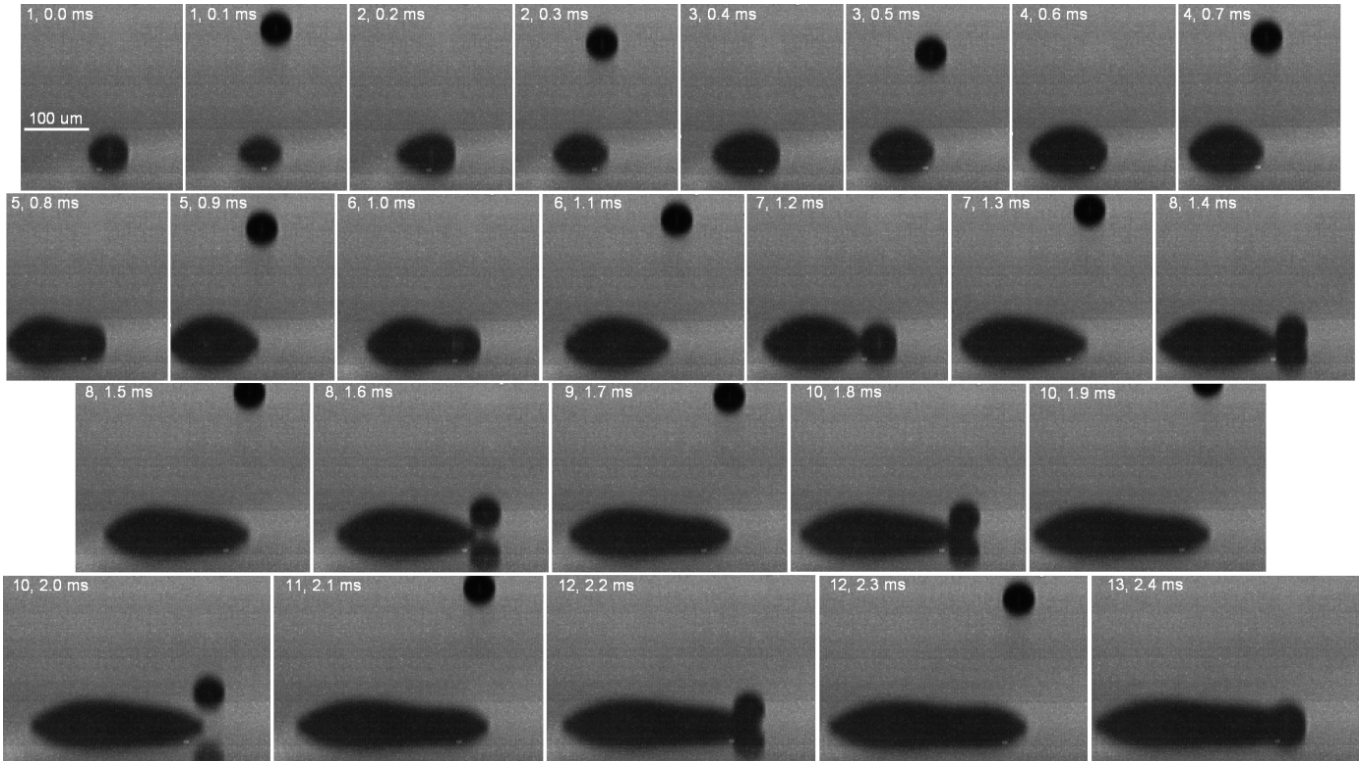

Figure 7-2 Spreading of molten caprolactam droplets onto the heated moving surface forming a bead

Bead Stability over an Extended Period

The caprolactam bead was monitored after 1 sec of deposition and during deposition of a second bead on top. Figure 7-3 shows the lateral view of bead-on-bead deposition onto the cold surface. The bead and its reflection on the surface are seen. Contamination on the surface demonstrates the substrate movement in the sequence shown. It is seen that the first deposited bead had a uniform height of 25 µm. The bead-on-bead deposition produced a uniform total height of 40 µm. The bead-on-bead deposition was repeated so that four beads of caprolactam were deposited on top of each other. There was a 1 sec elapsed time between each of the four bead depositions. A final uniform bead was formed from this process.

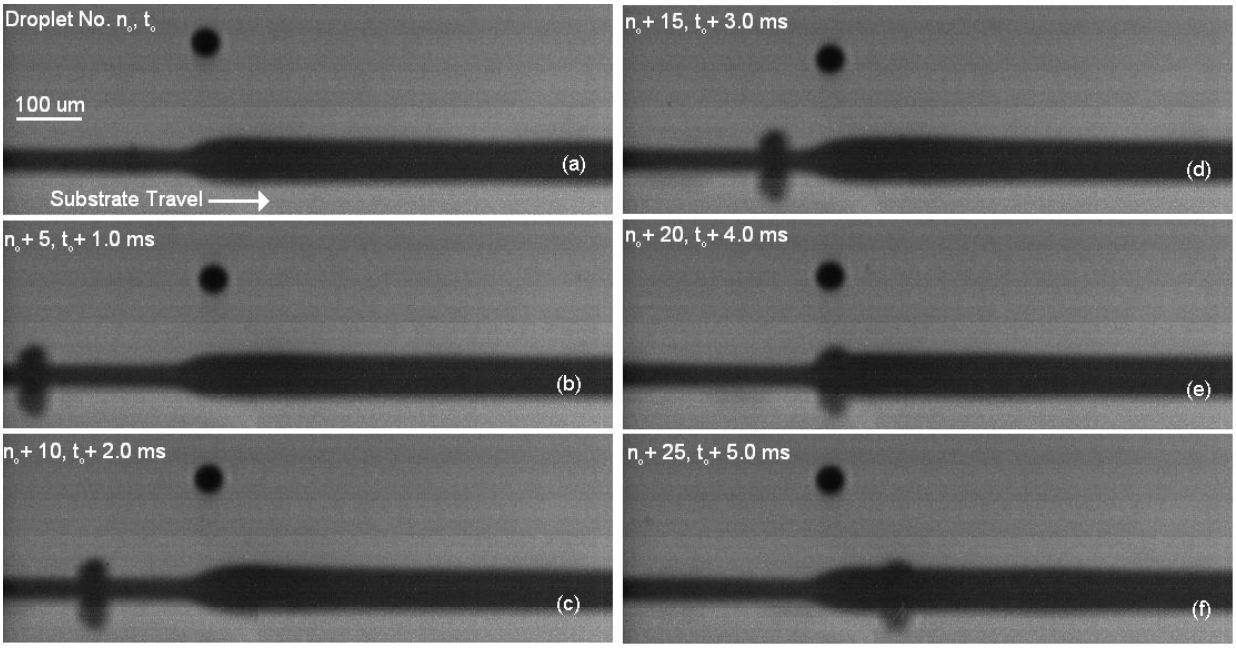

Figure 7-3 Monitoring the stability of a deposited bead of caprolactam on the cold surface (bead-on-bead deposition)

Figure 7-4 shows deposition of a second bead with a heated surface with a 1 second interval between them. The images show that bulge/ridge features and also separated sections of about 300 µm were formed with the first bead as seen to the left side of the droplet impact point in Figure 7-4. With the heated surface, a second bead-on-bead deposition cycle (a total of four beads) was undertaken. Figure 7-5 shows a top view image of the final bead which indicates some parts of the bead with considerable non-uniformity.

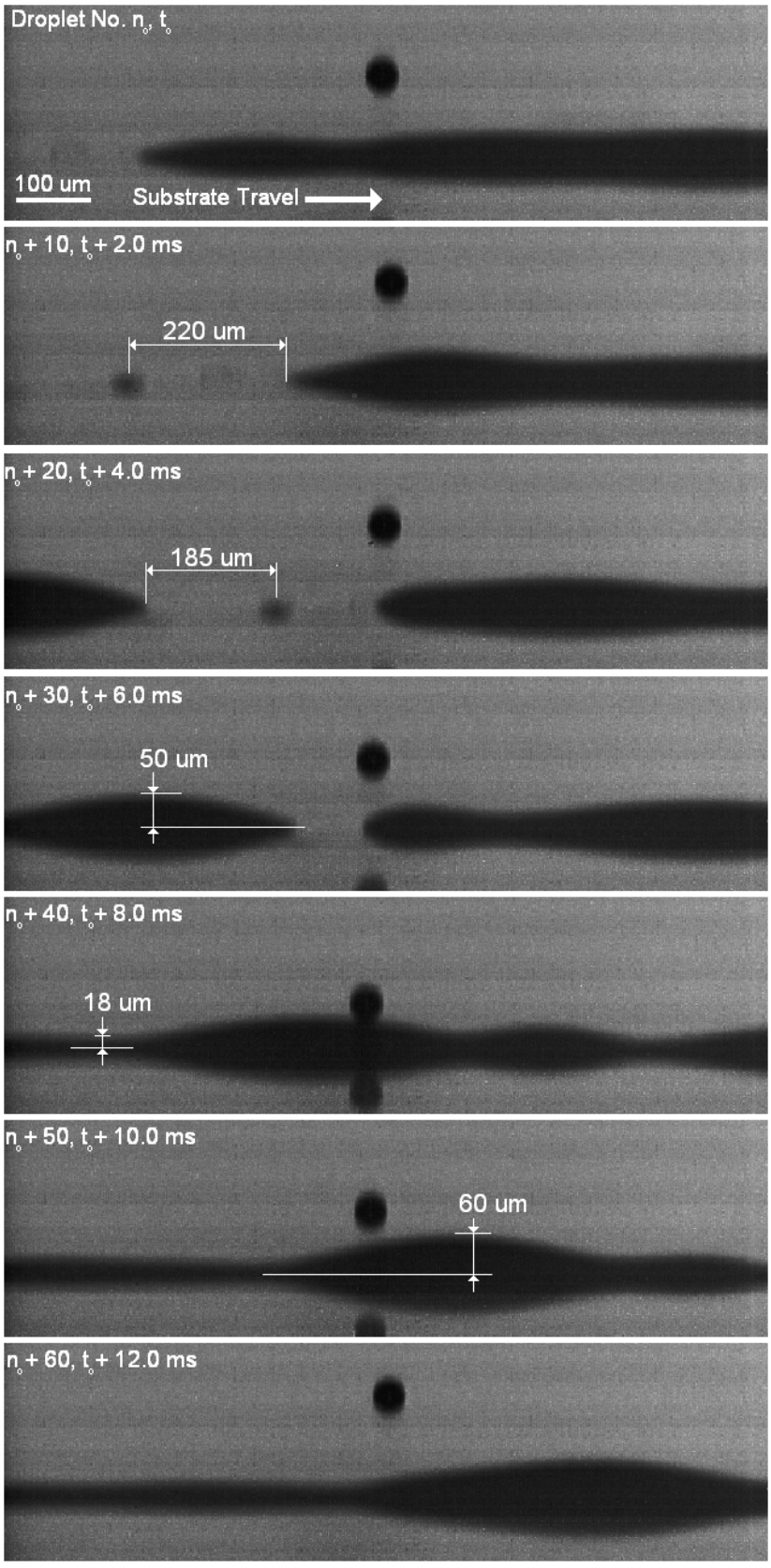

Figure 7-4 Non-uniformity of a deposited bead onto the heated surface during deposition of the second bead (look at the left side of the impact point)

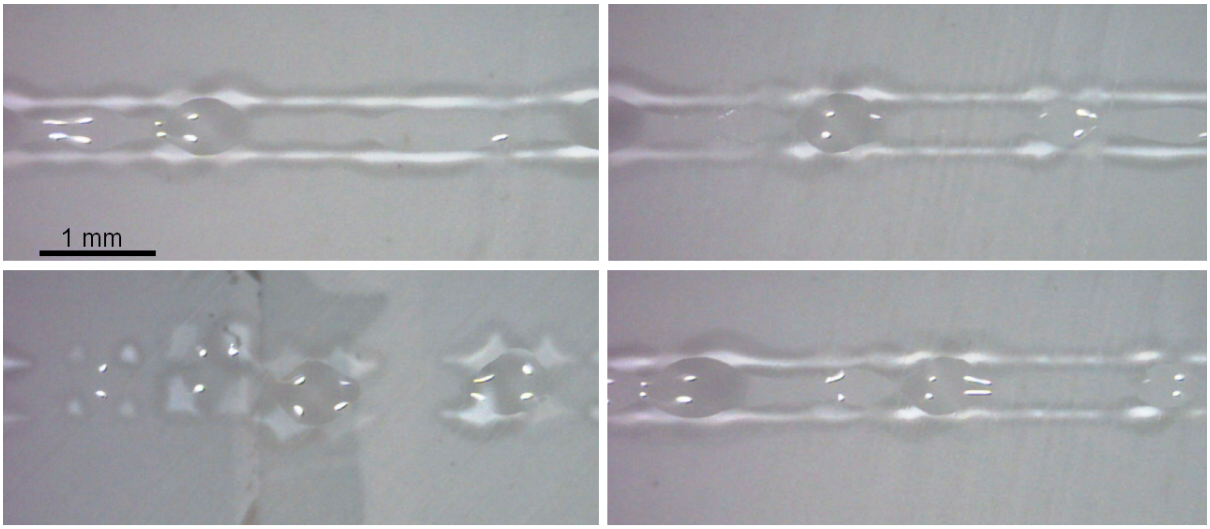

Figure 7-5 Non-uniformity in the deposited beads onto the heated surface (after depositing four beads)

7.2.4 Further Experiments on Droplet/Surface Interactions

Initial uniformity assessment of the deposited caprolactam bead onto the heated surface suggested that an instability occurred within the first second. This irregular bead formation would lead to a variable mixing ratio of the reactive mixtures when a heated surface was used. These irregular beads could be caused by the surface tension forces and would require further investigation of droplet spacing and surface temperature to give a uniform bead (Duineveld 2003, Derby 2010).

The main priority was to investigate the possibility of producing nylon by jetting the reactive mixtures and a suitable sample size was required for DSC analysis. The accumulative drop-on-drop sample deposition was decided to be undertaken directly into a DSC pan. This required a sample size between 3 and 20 mg. A stable single jet of the reactive mixtures was recorded for up to 30 sec in several trials. Therefore, jetting via a single nozzle for 10 sec at 5 kHz was feasible and would produce 50,000 droplets (for each mixture) and a drop-on-drop sample size of about 4 mg in total. However, it was necessary to determine the melt level at which the mixtures were to

be deposited to ensure the microcrystal content of droplets and then study the mixing of droplets inside a DSC pan.

7.3 Microcrystals of Deposited Catalyst Mixture Droplets

7.3.1 Experiments

Multiple droplets were deposited to analyse the agglomeration behaviour upon coalescence (by impact kinetics), and then, individual droplets at different melt supply levels were studied. The results from these two situations were compared with the purged samples (reported in section 4.7) to understand microcrystal agglomeration behaviour when small volumes of melt were deposited.

For the accumulated situation, samples of 100 droplets were jetted with a single nozzle at 20.0 V, 1 kHz and 25 mbar onto the heated static glass slide at different melt supply levels (1, 2, 3 and 4 ml). Although a much greater number of accumulated droplets was to be used later in the reaction stage, it was found that using 1000s of accumulated droplets could lead to inaccuracies in analysing the microcrystal content due to some imaging limitations which will be discussed later.

Individual droplets of the catalyst mixture were deposited via a single nozzle (20.0 V, 1 kHz and 25 mbar) onto a heated glass slide (80℃) at different melt supply levels (1, 2, 3 and 4 ml) to give an array of droplets with 1 mm spacing as shown in Figure 7-6. This was repeated for each melt level to check repeatability.

Similar to microscopy of the purged samples reported in section 4.7, polarised light was employed to detect the microcrystals in the deposited samples. However, no cover slip was placed on top. This was to retain the dispersion of the microcrystals made by the deposition process. Two magnifications of 10X and 50X were used to study the dispersion and size of the microcrystals.

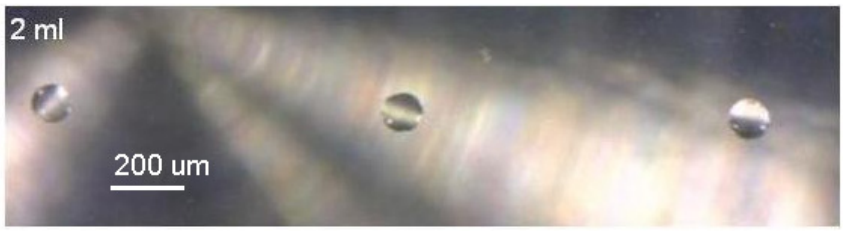

Figure 7-6 Individual catalyst mixture droplets on the heated glass slide at 2 ml melt supply level

7.3.2 Microcrystal Content of Coalesced Droplets

Figure 7-7 shows the results of hot stage microscopy for the accumulated droplets produced at the 4 ml melt supply level. Figure 7-7(a) shows images taken at 10X magnification whereas Figure 7-7(b) details a selected area with the higher magnification of 50X. The microcrystals of the catalyst mixture were seen as bright spots due to their crystalline structure. The images demonstrate how the microcrystals were dispersed. This behaviour was observed for all the melt supply levels. As no cover slip was used on the sample, it was assumed that the dispersion was due to the droplet impact kinetics and mixing.

The microcrystals, after passing through the jetting system, were expected to be less than 5 µm due to the pore size used in both the filters (in the filtration unit and inside the printhead). However, bright spots as large as 10 µm were detected within the samples as seen in Figure 7-7(b). This suggests that the microcrystals had agglomerated during the accumulative deposition. The level of agglomeration was much less however, when compared with the results of purged samples (section 4.7.3). In addition, with the accumulated droplets, the small agglomerations occurred in several (dispersed) positions whereas with the purged samples, agglomeration occurred in large and continuous areas of the samples resulting in large peaks in the microcrystal content graphs as shown in Figure 4-18. This could be due to the use of

a cover slip in the purged samples which could induce a melt shear flow providing a chance for the particles to collide and agglomerate. This could be similar to the turbulent shear agglomeration as reported in literature (Allen *et al.* 2001).

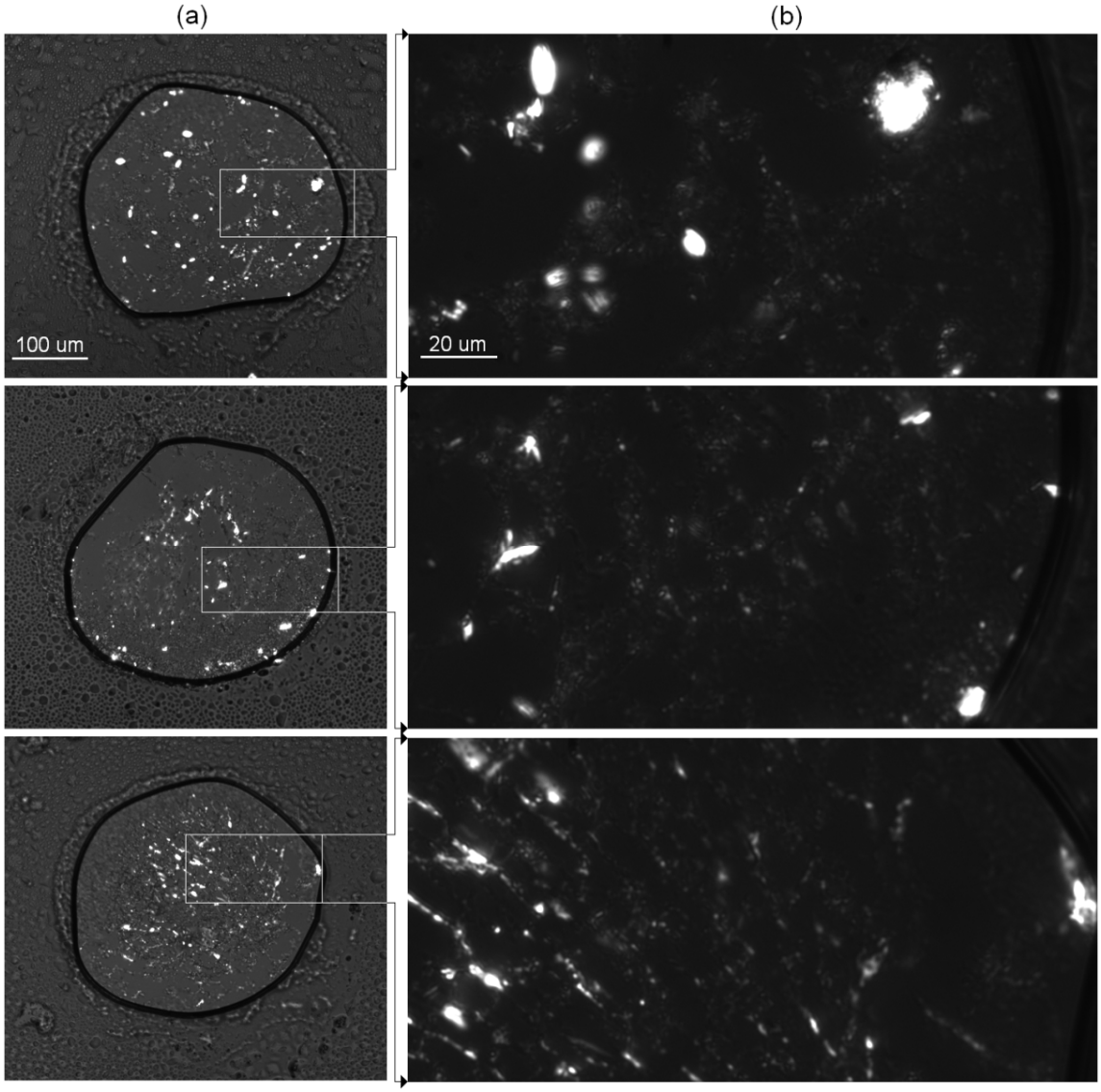

Figure 7-7 Microcrystals within samples of coalesced droplets of the catalyst mixture on the glass slide. Three samples at the 4 ml melt supply level are shown, (a) 10X, (b) selected areas with 50X

The bright spots in Figure 7-7(b) are seen with different grey levels. This could affect the quantification of the microcrystal content by the grey-binary transformation method. Two possibilities could have caused the grey level variation:

1) There was variable agglomeration throughout the accumulatively deposited samples. This could cause the less agglomerated microcrystals to be detected with lower grey level by the microscope camera (due to its limited sensitivity).

2) Microcrystals could exist at different heights of the accumulated deposition which formed a meniscus of about 100 µm in height. It was found that by varying the focal length of the microscope, the microcrystals out of focus in the other levels were recorded with a different grey level. This possibility was investigated in the microscopy of individual droplets.

7.3.3 Microscopy of an Individual Droplet

A catalyst mixture droplet formed a meniscus (of below 25 µm in height) on the heated glass surface. The microscope focal length was controlled with 1 µm resolution for better observation of the microcrystal dispersion at different heights of the spread droplet. Figure 7-8 shows a schematic of setting the focal length. The height (h) was considered as the distance between the top surface of the glass slide and the plane at which the microscope camera was focused. The top surface of the glass (h = 0 µm) was found by focusing on the micron size surface contamination (added during glass slide sample handling). By decreasing the focal length in 1 µm amounts, h was increased until h > 16 µm, where all the bright spots turned grey and then faded away when h > 20 µm. Images of droplets were produced at three different heights (1, 8 and 16 µm) as shown in Figure 7-9(a) and (c). Image processing then was used with a threshold grey level of 128 for better comparison of microcrystal detection as shown in Figure 7-9(b) and (d).

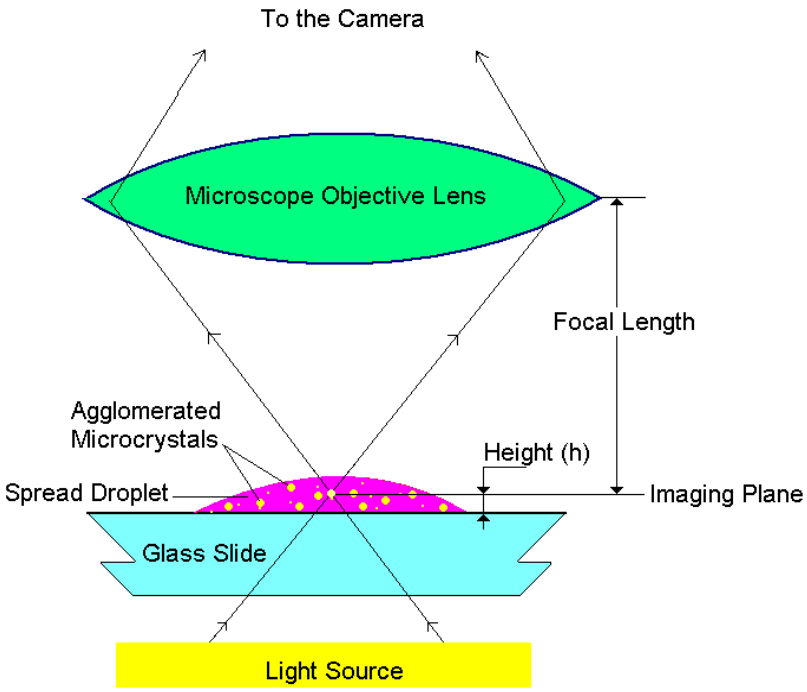

Figure 7-8 Schematic of controlling the focal length for microscopy of microcrystals in a spread droplet

From Figure 7-9 it was found that the microcrystals agglomerated at different positions and heights. However, the level of agglomeration observed was lowest near to the glass surface (h = 1 µm) compared with the middle and top. Therefore, to ensure consistency during microscopy of individual droplets at different melt supply levels, the focal length was set at h = 8 µm.

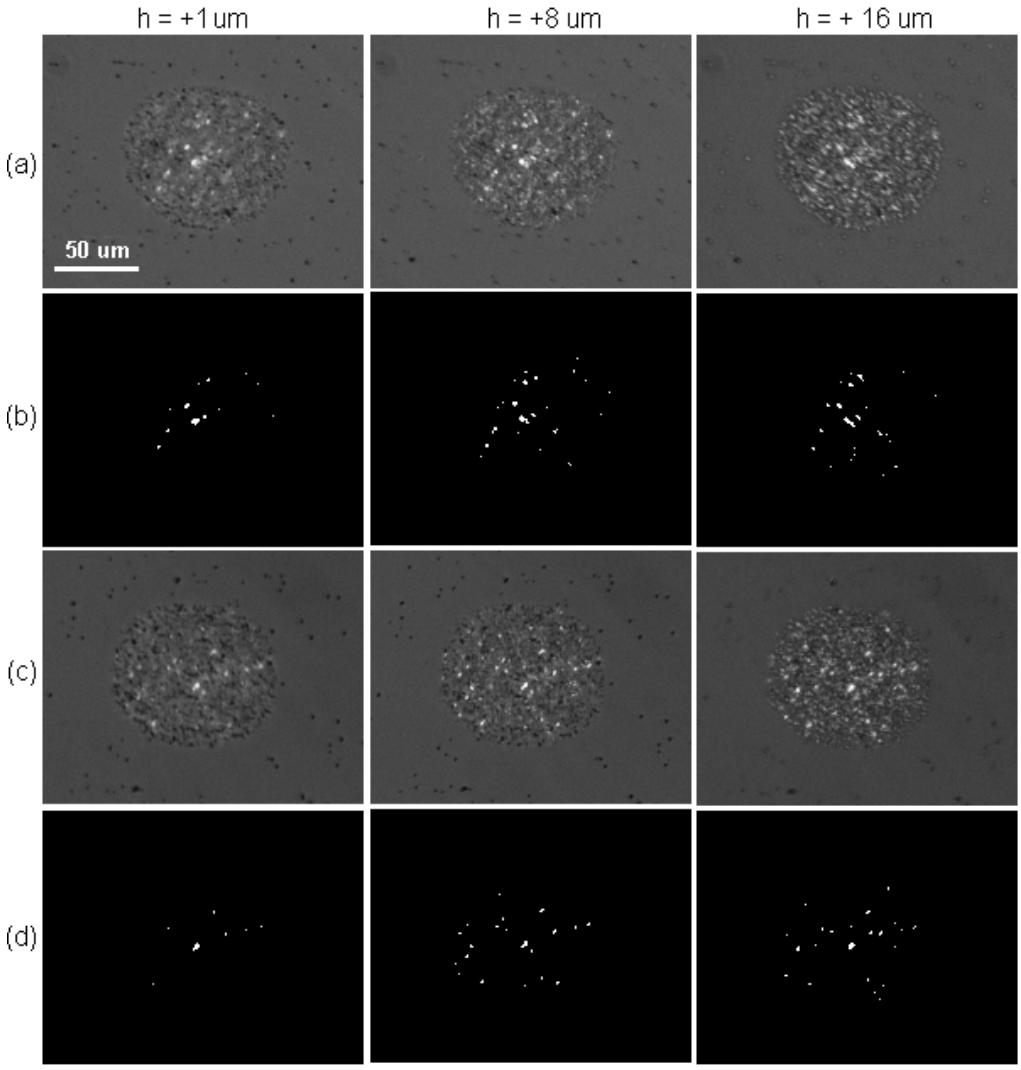

Figure 7-9 Microscopy of the microcrystals in two individual droplets (4 ml melt supply level) at different focal lengths (10X), (a) droplet 1 original image, (b) droplet 1 processed image (threshold grey level: 128), (c) droplet 2 original image, (d) droplet 2 processed image

7.3.4 Microcrystals in Individual Droplets at various Melt Supply Levels

Figure 7-10 shows microscopic images of five droplets deposited from two different arrays with different melt supply levels. The images demonstrate (qualitatively) that the microcrystals existed in all melt supply levels and were well dispersed within individually spread droplets. When comparing the two series of samples in Figure 7-10, it is seen that the microcrystal content was similar when repeating the trials. The images also show that when microcrystals agglomerated, they were recorded as

a brighter spot. However, the level of agglomeration was much less than the coalesced droplets.

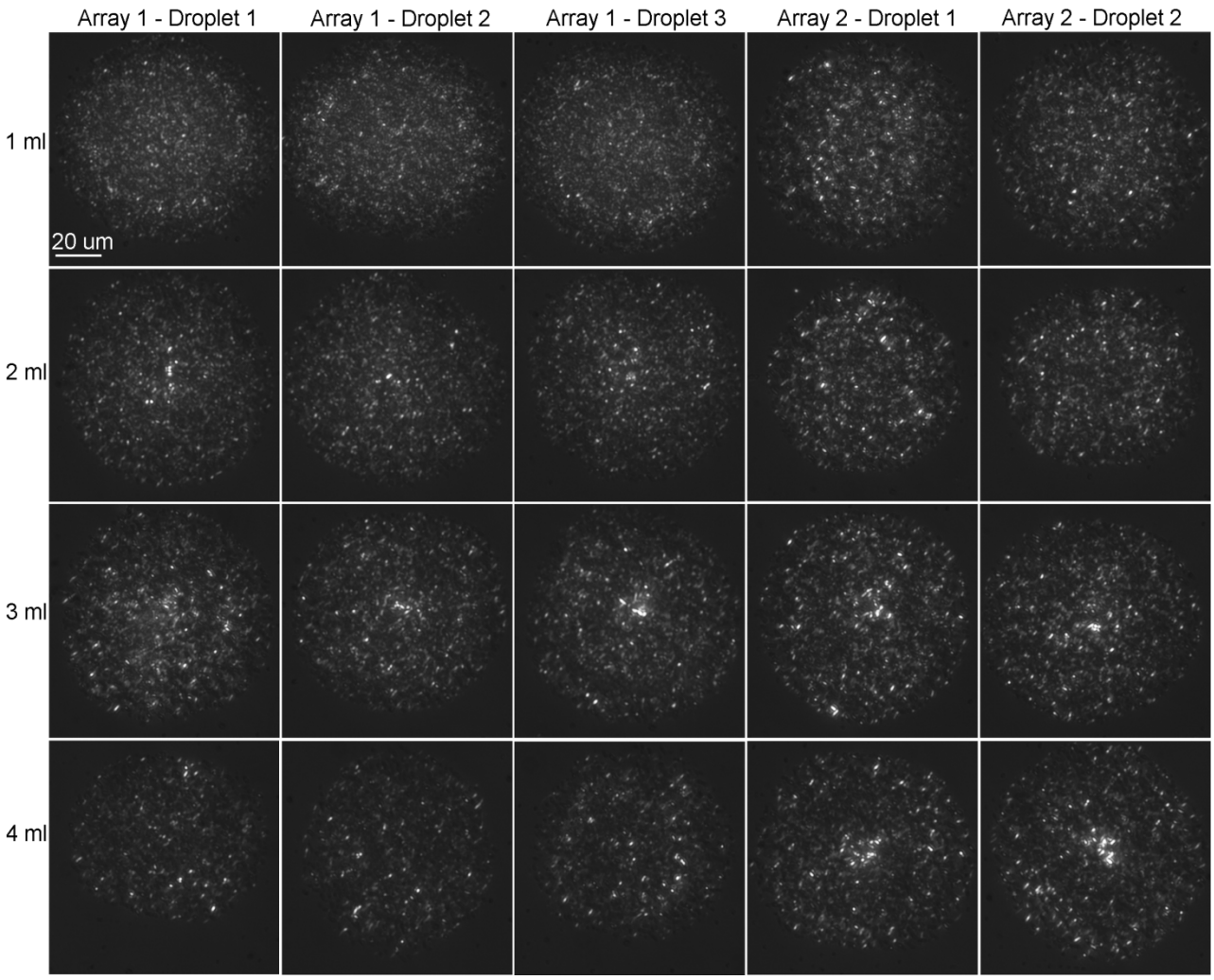

Figure 7-10 Microcrystal content within individual droplets in two arrays at different melt supply levels

7.3.5 Quantification of Microcrystal Content

Image processing was used to give an indication of the microcrystal content at different melt supply levels. The accuracy of the results was limited due to the limitations in magnification and sensitivity of the camera for detecting individual microcrystals. In addition, by setting the focal length at h = 8 µm (to limit the number of experiments), the microcrystals at different heights had a lower grey level.

Figure 7-11 shows an image of the catalyst mixture droplet before and after image processing at different threshold grey levels of 32, 64 and 128. The pixels with grey levels below these numbers were transformed into black and above these numbers into white to detect the bright spots representing the agglomerated microcrystals. When comparing Figure 7-11(a) and (b), it is seen that the threshold level of 32 could not provide a delineation of the microcrystals. This was because over 90% area of the image (Figure 7-11(b)) had white pixels and could not possibly represent the microcrystals. This was because the catalyst mixture was a dilution of 80% pure caprolactam with 20% of C10. As C10 was constituted from 17~19% of NaCL complex in pure caprolactam, the total catalyst complex content supplied for jetting was expected to be less than 4%. Therefore, it seemed that thresholds of 64 and 128 could better represent the microcrystal content.

Figure 7-12 shows the content of the detected agglomerated microcrystals for the two series (arrays) of samples. A threshold grey level of 64 detected microcrystals over about 1.5 to 2.5% of the image area and no distinct variation could be seen where increasing the melt supply level. The droplets deposited at the 4 ml melt supply level in Series 1 gave an exception. With the threshold grey level set at 128, fewer areas were detected. Again the content of agglomerated microcrystals was generally unaffected by the melt supply level. It was therefore assumed that the melt supply level would not affect the reaction outcome. In addition, it was discussed in section 5.5.2 that jet stability was not affected by the melt supply level. Therefore, it was decided to limit this parameter for all further experiments with the reactive mixtures and choose a melt level of 4 ml (as being in the middle of the range for the melt supply before the filter was blocked) to keep the consistency of the experimental conditions.

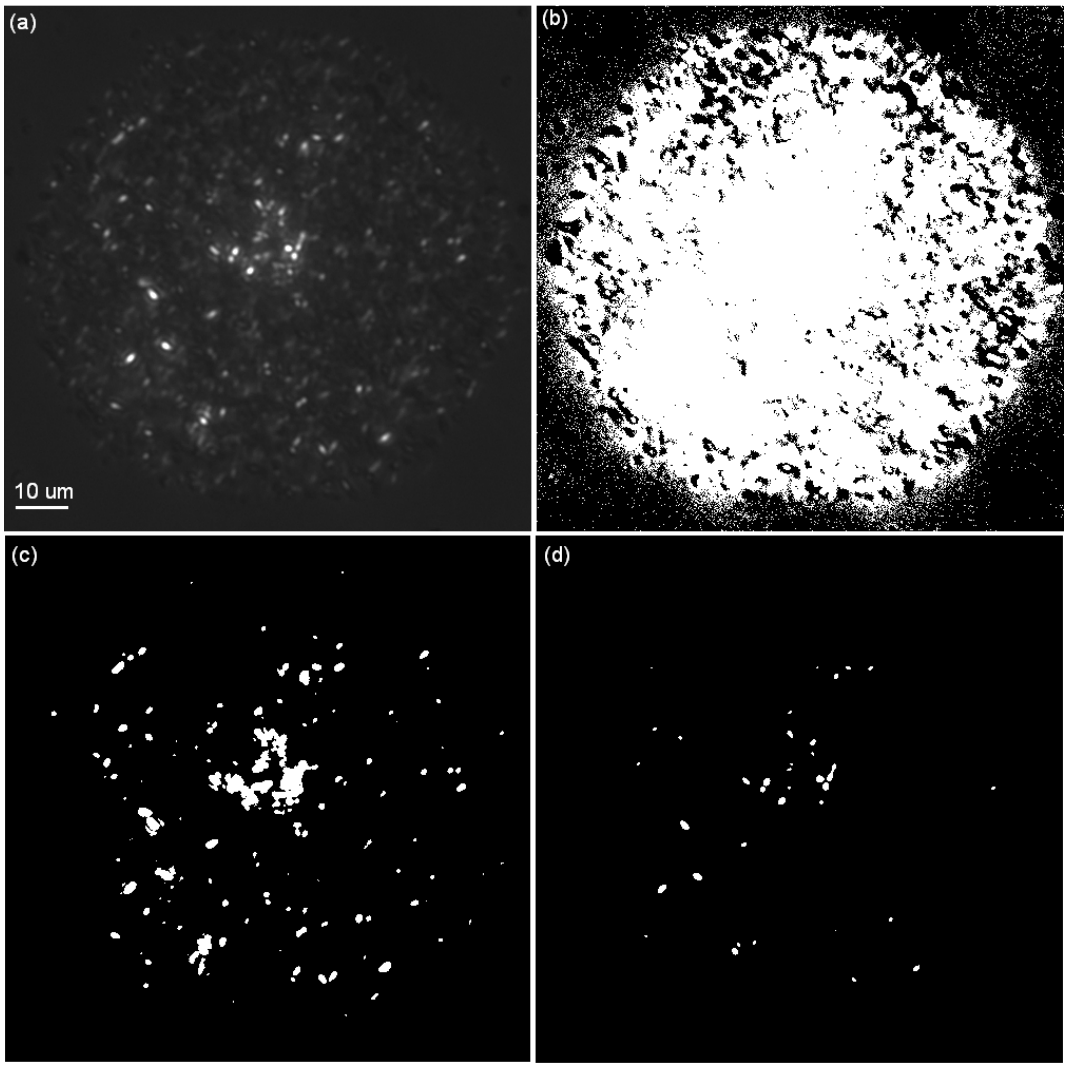

Figure 7-11 Analysis of the microcrystal content of a deposited droplet (4 ml melt supply level) by processing the original image, (a) original image, (b) processed image with threshold grey levels of 32, (c) 64, and (d) 128

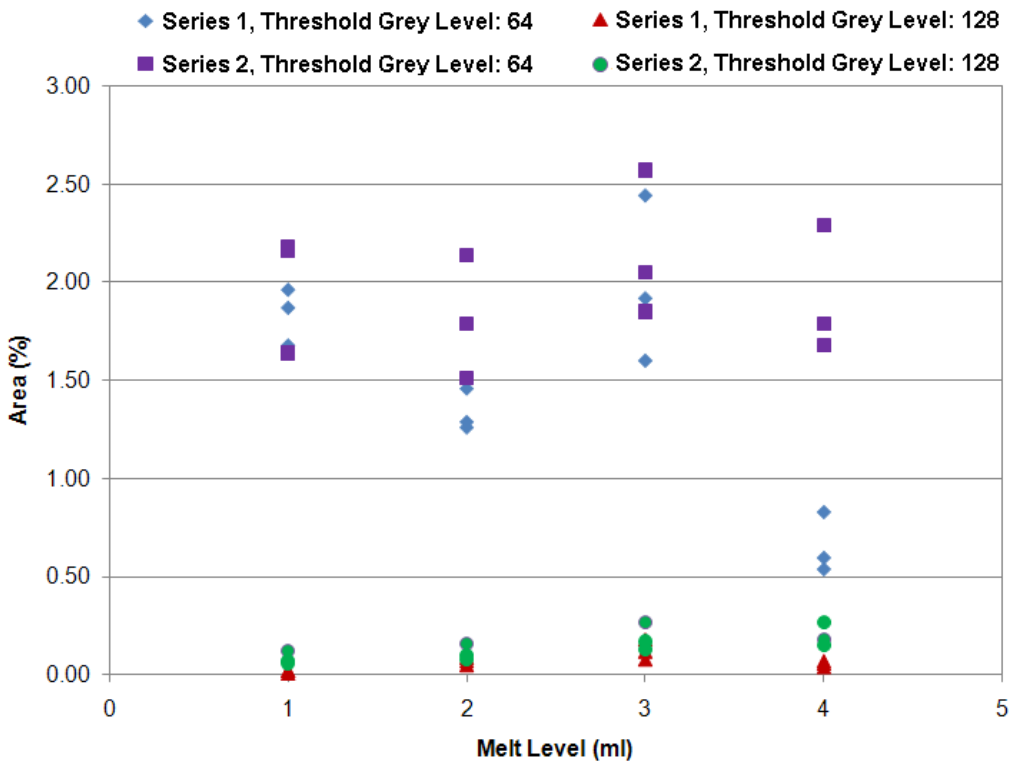

Figure 7-12 Total white pixel area as a proportion of the image size representing the agglomerated microcrystal content of the catalyst mixture at different melt supply levels

7.4 Drop-on-Drop Mixing

7.4.1 Experiments

The reactive mixtures were deposited inside an aluminium DSC pan (Shimadzu DSC-60). Fluorescent dye (Fluorescent Brilliant Yellow R supplied from James Robinson Ltd.) was stirred well into the molten activator mixture at a rate of 0.1% (volumetric) whereas the catalyst mixture was used without a dye.

Mixing was investigated by jetting from a single nozzle at 20.0 V, 5 kHz, 25 mbar and 4 ml. These settings were chosen according to the previous results (for the jet stability, droplet characteristics, and the catalyst concentration) and were considered to be also used for the research of drop-on-drop reaction. Experiments were repeated to give three sets of three DSC pans seated onto the heated aluminium substrate (80℃). In each sample, 50,000 droplets of the transparent catalyst mixture

were deposited via a single nozzle. Then, within 10 sec, 50,000 droplets of the activator mixture were deposited onto the previously deposited catalyst mixture. They were then viewed with the in-line microscope camera where a fluorescent light source showed the mixing outcome.

7.4.2 Mixing inside a DSC pan

The images of one sample for drop-on-drop mixing inside the DSC pan are seen in Figure 7-13. Figure 7-13(a) show the pan after the deposition of the catalyst mixture into the empty pan and then Figure 7-13(b) shows the dyed activator mixture on top of the catalyst. By comparing these two images with Figure 7-13(c), taken with fluorescent lighting, no unmixed area was seen with the deposition into the DSC pan.

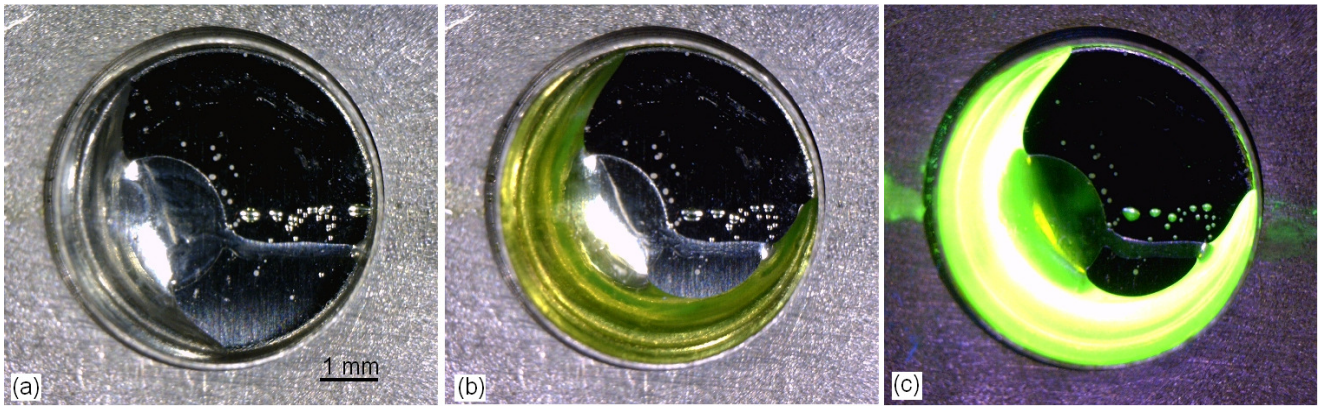

Figure 7-13 Drop-on-drop mixing inside a heated DSC pan, (a) catalyst mixture only, (b) dyed activator mixture deposited onto the catalyst mixture with normal white light and (c) fluorescent light

The droplet impact kinetics and surface tension forces provided mixing inside the pan. In addition, the pan wall could have restricted the escape of the catalyst mixture melt upon consequent impingement of the dyed activator mixture. As a consequence, the deposition formed a ring on the corner of the pan. This behaviour was repeated with the other samples as seen in Figure 7-14.

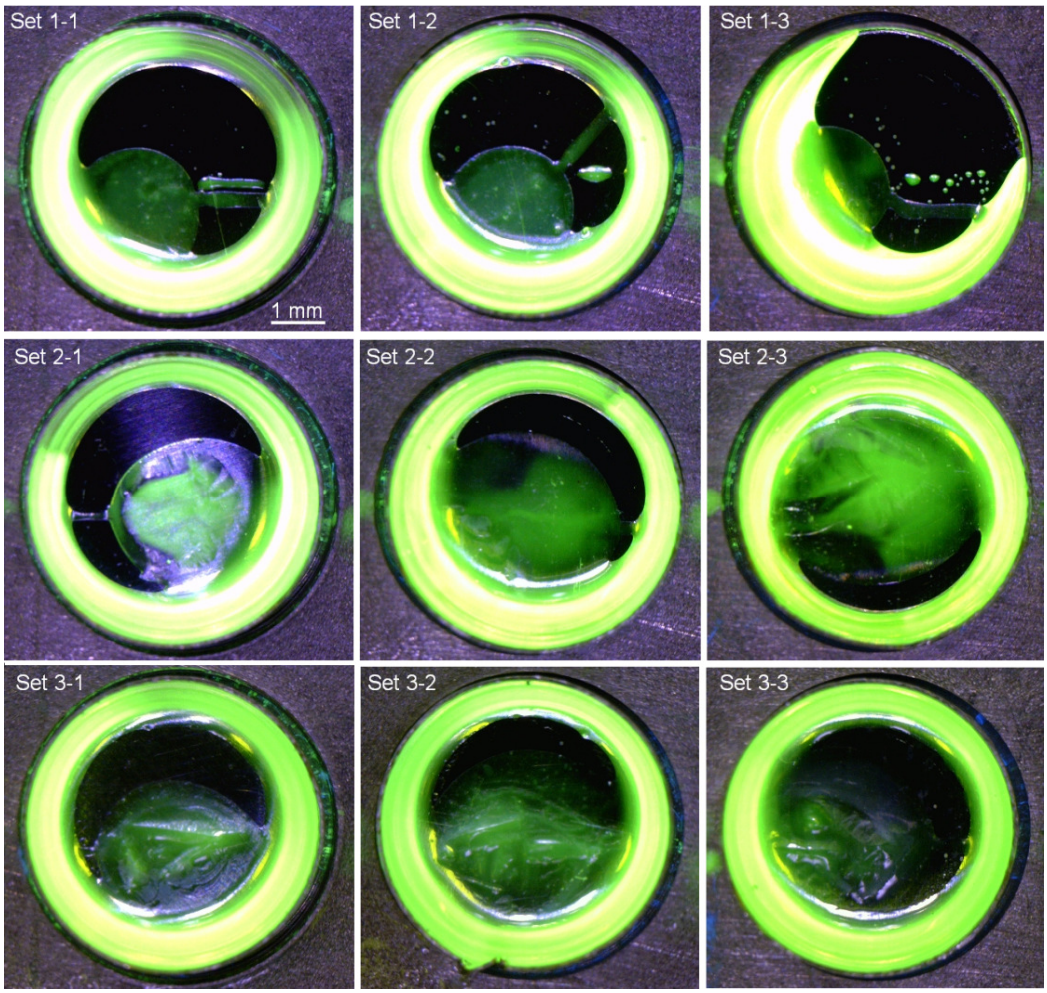

Figure 7-14 Fluorescent imaging of the drop-on-drop deposited dyed activator mixture onto transparent catalyst mixture inside heated DSC pans

Chapter 8. Drop-on-Drop Reaction

This chapter reports on different heating conditions for the drop-on-drop polymerisation reaction.

8.1 Requirements and Approach

From Chapter 7, it was decided to undertake this research using the accumulative drop-on-drop deposition of the two mixtures into a DSC pan on a heated substrate set at 80°C. Therefore, the mixtures needed to be rapidly heated up to a suitable temperature (e.g. 150°C) to initiate reaction. By developing a heating approach, the effect of different heating conditions on the outcome of the drop-on-drop reaction was investigated. The results of investigating the heating approach are presented first as they were used to develop experiments on the reaction outcome.

8.2 Heating to obtain the Reaction

8.2.1 Heating Approach

An elevated substrate temperature of 150°C was used for the heat-up process but it was observed that evaporation occurred instantly after depositing the activator mixture and before depositing the catalyst mixture. This would change the ratio of reactants and affect the results. In addition, the evaporated melt could influence the jet stability during deposition of the next mixture by condensation onto the nozzle plate.

Surface radiation heating was therefore considered as an alternative. In this, the plan was to deposit the mixtures into the pans on the substrate set at 80℃ followed immediately by moving the substrate underneath a unit to expose the mixtures to radiation heating (a description of the unit was given in section 3.7). By setting the power of the unit, the substrate/reaction unit gap and also the period of time that the deposited samples were exposed to the radiation, the heating conditions could be varied. The outcome of the heating in terms of the sample temperature and evaporation was assessed. Caprolactam was used for the assessment as it constituted over 95% of the mixtures.

8.2.2 Monitoring Temperature upon Radiation Heating

Figure 8-1 shows a schematic of the arrangement for the temperature monitoring. A DSC pan was placed onto the substrate set at 80℃, and filled with about 20 mg of caprolactam flakes. When the caprolactam was molten, a thermocouple tip could be immersed inside the pan. The pan with the thermocouple was exposed to radiation heating at different settings (via the 7-channel temperature controller described in section 3.4.2).

With different power settings as described in section 3.7 and using a reaction unit/substrate gap setting of 5 mm, the maximum temperature was found to be low (below 150℃). Therefore, the gap was reduced to 2 mm which provided suitable temperatures when settings of Power 2, 3, 4 and 6 were used. The experiments of the drop-on-drop reaction were initially aimed to be undertaken with 1 min radiation time according to the bulk polymerisation results (Khodabakhshi 2011). Therefore, temperature readings were initially recorded for up to about 90 sec (to cover 1 min radiation).

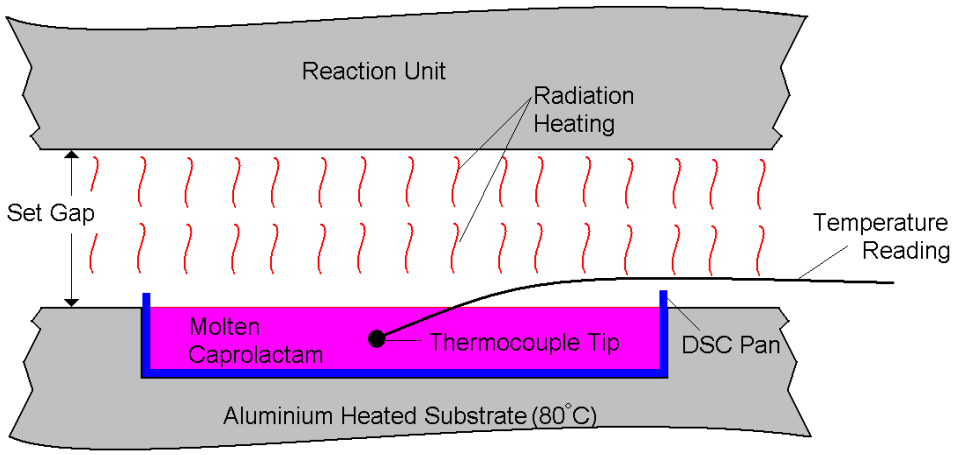

Figure 8-1 Schematic of temperature monitoring inside a DSC pan exposed to the radiation heating

Figure 8-2 presents the first series of temperature monitoring trials. The temperature was recorded from the moment the pan was moved underneath the reaction unit (at t = 0 sec) until a few seconds after it was moved away (at t = 90 sec). It is seen that the temperature increased sharply within the first 20 sec and then increased slowly but constantly. After removing the pan from the heating unit, there was a sharp decrease in temperature within the first 20 sec (t = 90 to 110 sec). This behaviour was similar for all the power settings.

Figure 8-2 shows that high reaction temperatures would be provided using 1 min radiation. However, from the bulk polymerisation results (Khodabakhshi 2011), it was anticipated that a longer heating would be required for the drop-on-drop reaction. Therefore, temperature monitoring was carried out for periods of about 4 min in case an increased time and temperature was required. As with the first series, temperature monitoring was carried out in triplicate to establish repeatability. However, to limit the number of experiments, the temperature for Power 6 was not recorded in the second series as it was thought that such radiation for 4 min would be too high considering the results of the first series (Figure 8-2).

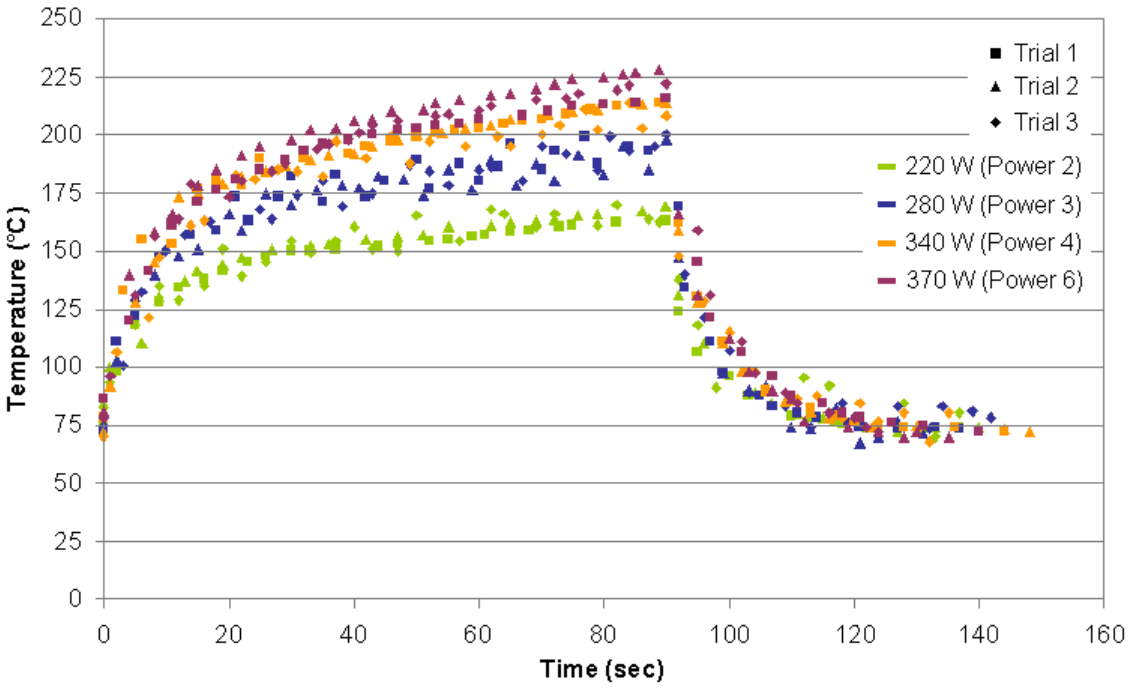

Figure 8-2 First series of temperature monitoring trials within 90 sec of radiation heating at different power settings

Figure 8-3 shows the results for the second series. Similar behaviour was observed, but it was seen that the rate of temperature increase was lower after about the first 90 sec. There were also readings for about 10 sec before the radiation when the sample temperature on the heated substrate (set at 80℃) was observed to be 75±5℃.

It was subsequently found in the reaction experiments that an extended period of radiation heating was required and so a longer heating time of 7 min was employed. However, the results of the first and second series showed that the temperature remained almost constant for radiation longer than 3 min. Therefore, temperature graphs of the two series were used as a reference for the reaction temperature in the drop-on-drop experiments when different radiation heating times and power settings were used.

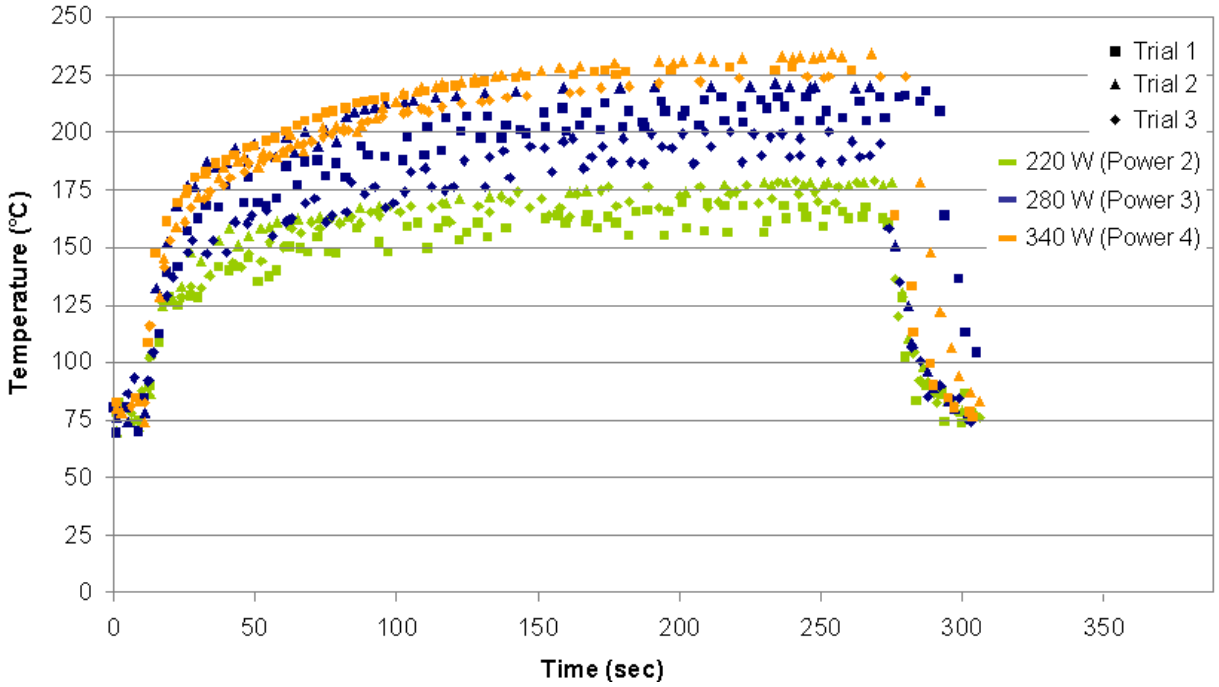

Figure 8-3 Second series of temperature monitoring trials within about 4 min of heating at different power settings

8.2.3 Monitoring Evaporation upon Radiation Heating

To monitor sample evaporation, DSC pans were also used. With small sample sizes (e.g. 5 mg) in a DSC pan, a ring was formed in most cases due to the surface tension as with the experiments reported in section 7.4.2. This could change the sample surface area and subsequently the evaporation rate. Therefore, five pans with different sample weights (within the recommended range for DSC, 3 to 20 mg) were used. The samples were placed on the substrate at 80℃ and radiation times of 1, 4 and 7 min were used with the chosen power settings. Evaporation was also measured when no radiation heating was used and the only heating source was the substrate (80℃).

The pans were measured with a 0.1 mg resolution analytical balance and then placed into the pan seating on the heated aluminium substrate set at 80℃ (see

Figure 3-20). After the caprolactam melted inside the pans (within about 5 sec), the substrate was moved underneath the radiation unit at the required power setting. After each radiation period, the pans were moved away from the unit. They were then removed from the substrate within 2 sec and weighed. It was assumed that the continuation of the evaporation within this time (2 sec) could be neglected as the temperature dropped rapidly upon removing the radiation (Figure 8-2).

Figure 8-4 shows the results for the evaporation in % and the evaporation rate in mg/min calculated by considering the weight loss and the radiation period. When no radiation heating was used (Power OFF, with only the heated substrate at 80℃), no evaporation was detected for samples held for 1 min on the substrate and after 4 and 7 min, the evaporation was still below 4%. Evaporation using Power 2 was below 5% for samples exposed for 1 min and below 10% for the other samples (4 and 7 min). Power 3 produced similar results at radiation times of 1 and 4 min but an evaporation of 15% was recorded with a radiation time of 7 min. A similar trend was also seen with Power 4, but for smaller samples, very high % evaporation was seen as in Figure 8-4(a).

The evaporation rate was less than 0.1 mg/min for the smallest samples whereas with larger samples it was between 0.1 and 0.3 mg/min as seen in Figure 8-4(b). With the smaller samples the melt did not cover the whole pan surface due to the surface tension whereas with higher sample sizes, the whole pan surface was covered with the melt. Therefore, the evaporation rate was higher with the larger samples which had a higher surface area (as evaporation directly depends on the surface area).

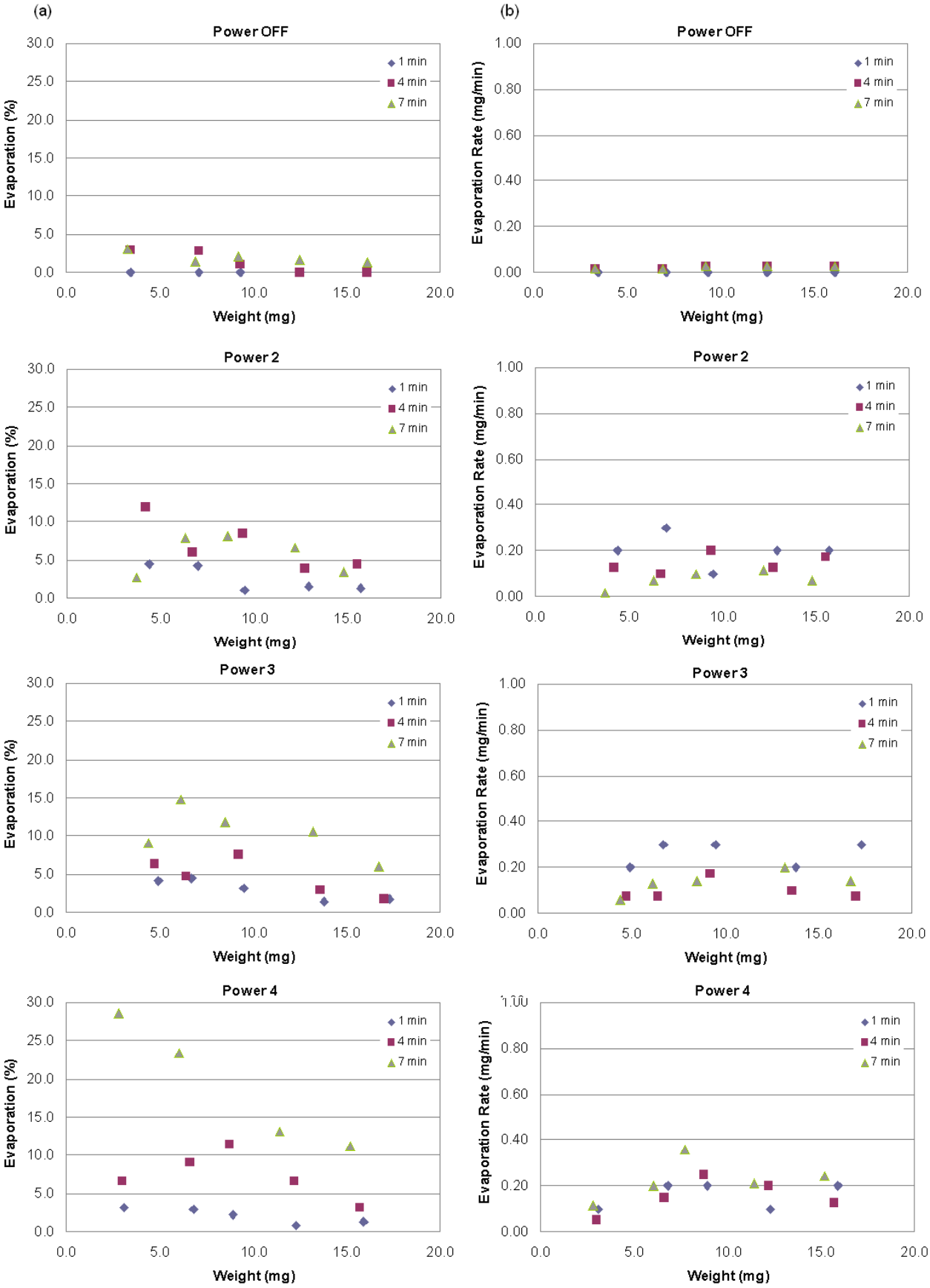

Figure 8-4 Evaporation of caprolactam samples with different weights exposed to different radiation heating conditions (time and power setting)

From an additive manufacturing perspective, evaporation during radiation heating would induce inaccuracies in the amount of material deposition for each layer. A compensation factor could be anticipated for an accurate final volume of drop-on-drop deposition. This however would not be an easy task as evaporation and polymerisation could be occurring simultaneously during the layer fabrication. Polymerisation is expected to be initiated at different points in the deposited mixtures upon radiation heating. This could subsequently affect the evaporation rate across the deposited layer surface and result in uneven evaporation causing surface roughness. However, with a fast reaction, the evaporation of caprolactam would be minimised producing a more uniform surface. This emphasises the importance of rapid reaction upon radiation heating as one of the main aspects in jetting of nylon.

8.3 Drop-on-Drop Reaction

8.3.1 Sample Deposition

The jetting and deposition parameters for the reactive mixtures were selected as with section 7.4.1. The mixtures were jetted at 20.0 V, 5 kHz, 25 mbar and 4 ml, through a single nozzle into a DSC pan at a set melt temperature of 80℃. The sample deposition for drop-on-drop reaction followed a procedure similar to the drop-on-drop mixing where 50,000 droplets of the catalyst mixture were deposited onto the activator in a pan and this was done for three pans in each trial to check repeatability.

The sample deposition process was monitored during each trial to ensure accurate sample deposition. The microscope digital camera observed the nozzle plate (Figure 3-18) for any jet failure just before and after deposition of each mixture into the pans

(observing the jet during the deposition was not possible with the camera). Where jet instabilities were observed, the trial was repeated. In addition, the second digital microscope camera observed inside the pans after deposition (as shown in Figure 3-20) to check the drop-on-drop placement.

8.3.2 Sample Reaction

Table 1 shows the experimental conditions used. It was found that samples of Set 1 had a low monomer conversion. Research on bulk polymerisation suggested that a high ratio of the catalyst to activator, typically 5:1 (10% conc. and 2% conc. respectively) would result in high monomer conversion in air (Khodabakhshi 2011). Therefore, because of the possibilities of reducing the catalyst microcrystals by filtration, the concentration of the catalyst was maintained but the activator concentration was reduced to 4% in Set 2 experiments.

The results for Set 2 showed that the monomer conversion was lower than Set 1. It was concluded that the reaction temperature was not high enough. Therefore, Set 3 was carried out with similar conditions to Set 1 but with a higher substrate temperature of 120℃.

Experimental Settings	Concentration %		Power Setting	Heating Time (min)	Substrate Temperature (℃)
	Catalyst	Activator			
Set 1	20	20	2, 3, 4 ,6	1, 4, 7	80
Set 2	20	4	2, 3, 4 ,6	1, 4, 7	80
Set 3	20	20	2, 3, 4 ,6	1, 4, 7	120

Table 8-1 Sets of experiments for drop-on-drop reaction

8.3.3 Sample Appearance after Radiation Heating

It was assumed that upon radiation heating, a reaction would result in a change of transparency in the deposited molten samples due to the monomer conversion and

formation of solid nylon. In addition, the elevated temperature could result in evaporation and a change in the sample spread geometry. Therefore, the drop-on-drop reaction samples were observed by the second digital camera just after heating.

Figure 8-5 shows a sample in Set 2 before and after the radiation heating. The sample had an increase in area after radiation heating when comparing Figure 8-5(a) and (b). This could be due to the elevated temperatures which could change the wetting contact angle of the molten meniscus and consequently affect the spreading geometry. In addition, some areas with small droplets are seen inside the pan and around the wetting edge in Figure 8-5(b), possibly due to condensation of evaporated caprolactam during radiation heating. These small regions could coalesce with the main body of material and cause further spreading inside the pan.

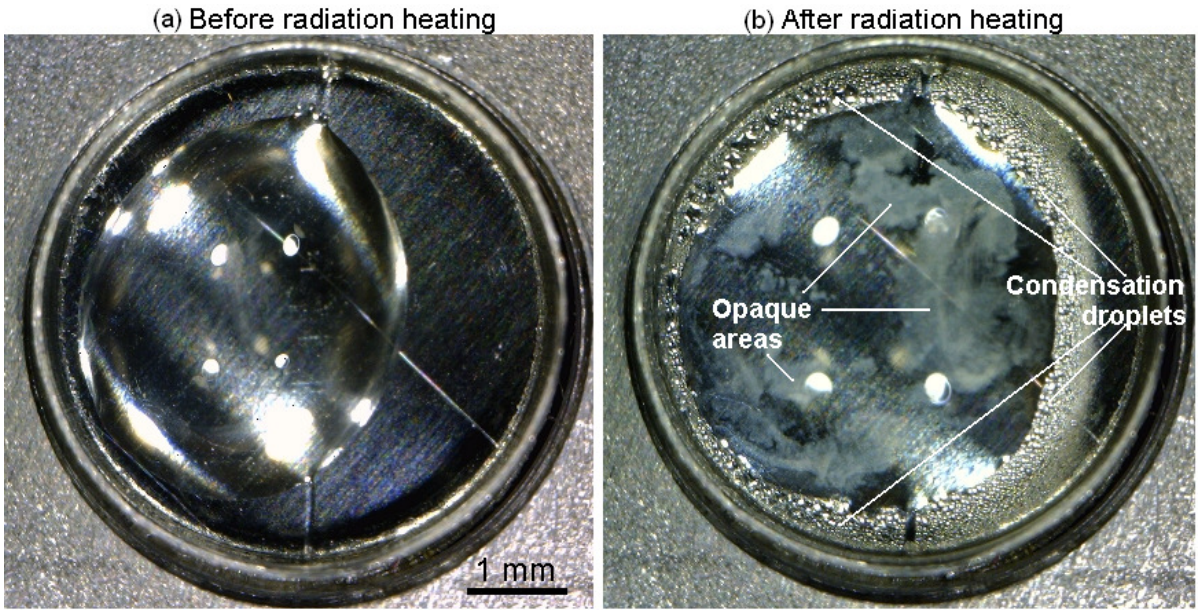

Figure 8-5 Change of spread geometry and transparency in two samples of Set 2 on the heated substrate (80℃) before and after the radiation heating set at Power 2 for 7 min

The drop-on-drop sample after the radiation had some opaque areas as shown in Figure 8-5(b). This could be due to spherulite formation after polymerisation during heating. Khodabakhshi (2011) showed spherulite formation under hot stage optical microscopy and these could have been formed upon crystallisation of the polymer melt (Puffr and Kubanek, 1991). Hot stage microscopy using cross-polarised light can detect spherulites within nylon 6 due to their birefringence (Bower 2002).

The appearance of all samples in Sets 1 and 2 was examined. As there was only limited opaque areas (and samples were largely transparent) after radiation, it was predicted that the monomer conversion was low. The images were taken within 10 sec of being removed from radiation heating during which there was a rapid temperature drop according to section 8.2.2. Therefore, any polymerised melt within the sample would have solidified. However, caprolactam was expected to remain molten due to the heated substrate (80℃). Therefore, the transparent areas in the sample after radiation heating would be unpolymerised molten caprolactam. With high conversions, the samples would have been opaque solid nylon.

To check whether larger deposition volumes would increase the conversion rate and so the opacity, two samples with a greater number of droplets were also deposited for the drop-on-drop reaction and the highest radiation heating conditions (Power 6 for 7 min) were used during Set 2 experiments. However, the samples shown in Figure 8-6 were still molten and the higher amount of opacity seen was possibly because of higher concentration of the spherulites due to the increased sample volume (thicker sample layer) (Figure 8-6(c)). This suggested a considerable amount of unpolymerised monomer existed within the sample, even with the highest radiation heating conditions.

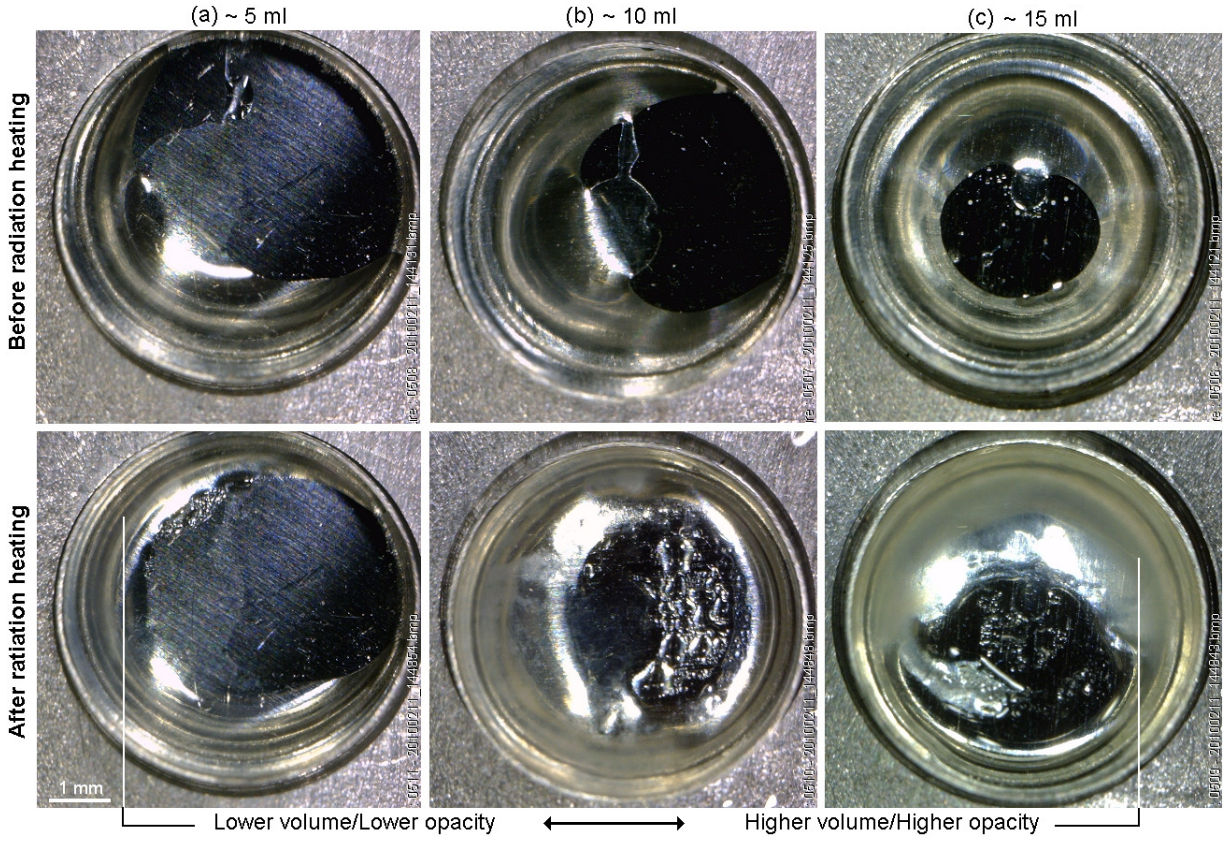

Figure 8-6 Change of transparency in the samples of Set 2 within 10 sec after the radiation heating set at power 6 for 7 min on the heated substrate (80℃)

8.4 Thermal Analysis of Jetting Materials

8.4.1 Thermal Analysis

For thermal analysis of caprolactam, the mixtures and the drop-on-drop reaction samples DSC was used (DSC-60 by Shimadzu Corp.). This technique monitors the flux of heat absorption or release against a reference (empty pan) during heating or cooling at constant rate. Figure 8-7 shows a typical thermogram of a nylon 6 sample made by bulk polymerisation. The synthesised polymer melting endothermic peak is seen with a broad temperature range. The thermogram also shows an exothermic peak due to crystallisation during the cooling stage.

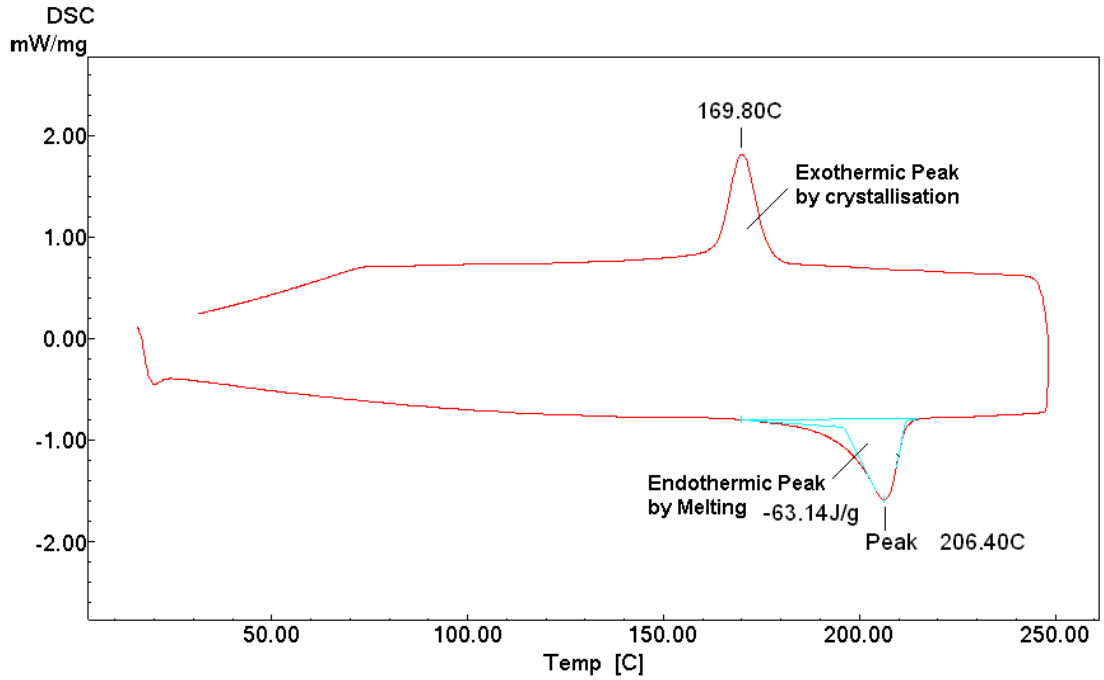

Figure 8-7 DSC Thermogram of a sample of nylon made by bulk polymerisation in air with the mixtures at 5% concentration and a reaction temperature of 160℃ (Khodabakhshi 2011)

For thermal analysis of caprolactam and the mixtures, different sample weights (minimum of five) recommended within the range for DSC (3 to 20 mg) were used to check the repeatability of the results and ensure they were independent of sample weight. For all samples, the pan was crimped with a matching aluminium lid before heating at 10℃/min in the DSC in a thermal cycle of 30-250-30℃ (the lower and upper temperature limits of the cycle were chosen to span the melting temperatures of caprolactam and nylon).

8.4.2 Caprolactam

Figure 8-8 shows a typical thermogram recorded by the DSC for caprolactam. Two endothermic peaks are seen during heating. The first peak corresponds to the melting of caprolactam (Ritz *et al.* 2005). The melting temperature and heat peak for caprolactam were measured using different sample sizes. Results are shown in

Figure 8-9. The average and the standard deviation for the onset and peak temperatures, and the heat peak were respectively 68.7±0.3℃, 73.6±1.1℃ and 140.9±7.0 J/g. It is seen that the results were repeatable with the various sample sizes used. This confirmed that the results were independent of the DSC sample size.

The second broad peak (from about 100℃ to 220℃) was due to evaporation of caprolactam which continued until the pan was empty. This was found by measuring the sample weight before and after the DSC test. This behaviour was also seen for the catalyst and activator mixtures. This showed that the crimped pan was not sealed enough to avoid weight loss by evaporation. The DSC heat chamber was therefore cleaned after each DSC run to remove any condensed caprolactam.

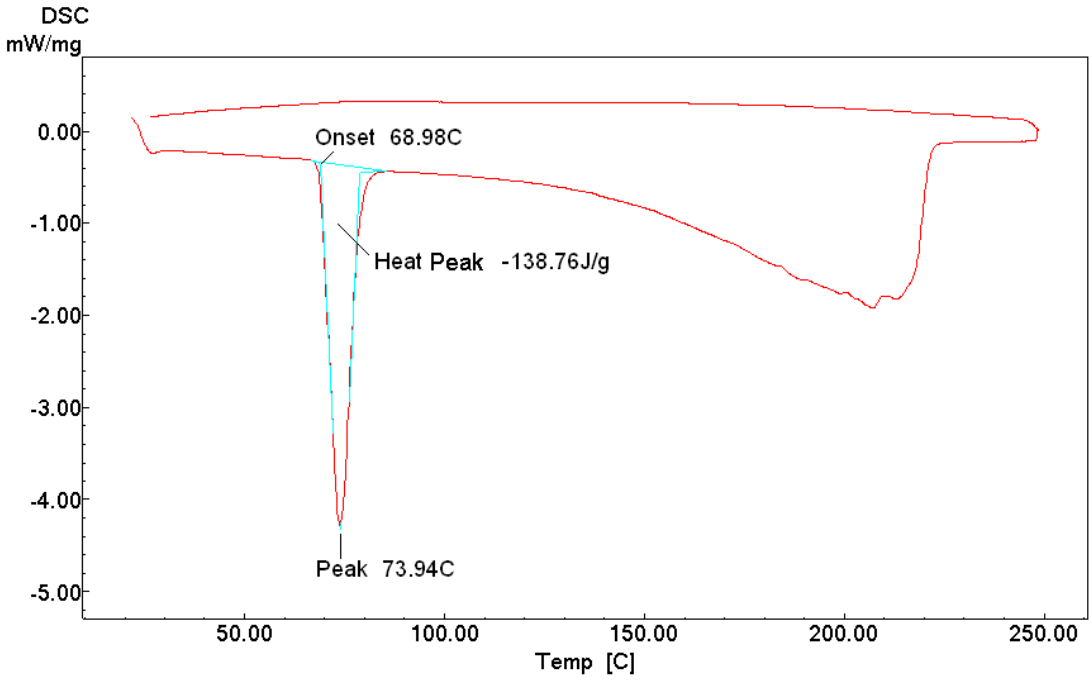

Figure 8-8 Thermal analysis of a caprolactam sample using DSC

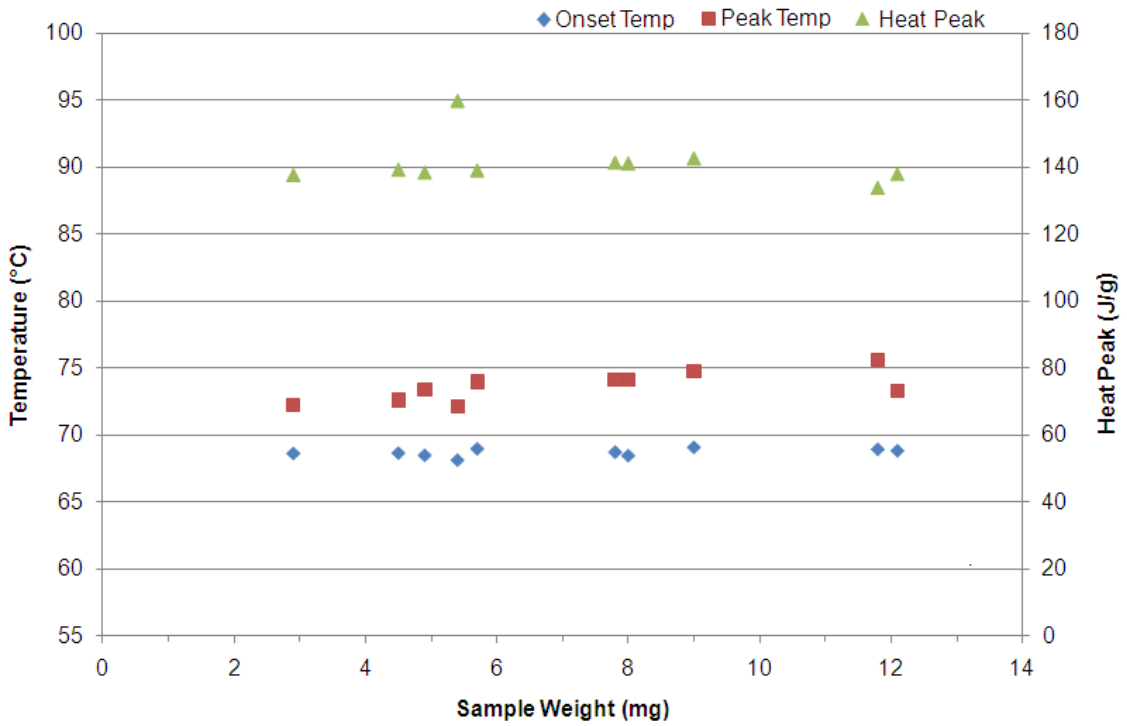

Figure 8-9 Onset and peak temperatures and heat peak of melting caprolactam for different sample weights

8.4.3 Catalyst Mixture

Figure 8-10 shows a typical result of diluted catalyst mixture. A similar endothermic peak is seen for the evaporation of caprolactam. The peak temperature and heat peak, as shown in Figure 8-10, were 72.2±1.0℃ and 126.3±9.4 J/g respectively. The peak temperature was slightly lower than with the pure caprolactam (Figure 8-9). In addition, a decrease was seen in the heat peak with the mixture. These differences could be due to the presence of the microcrystals of caprolactam magnesium bromide complex (CLMgBr) in molten caprolactam which could act as an impurity resulting in a broader onset temperature in the melting peak and reducing the heat required for melting.

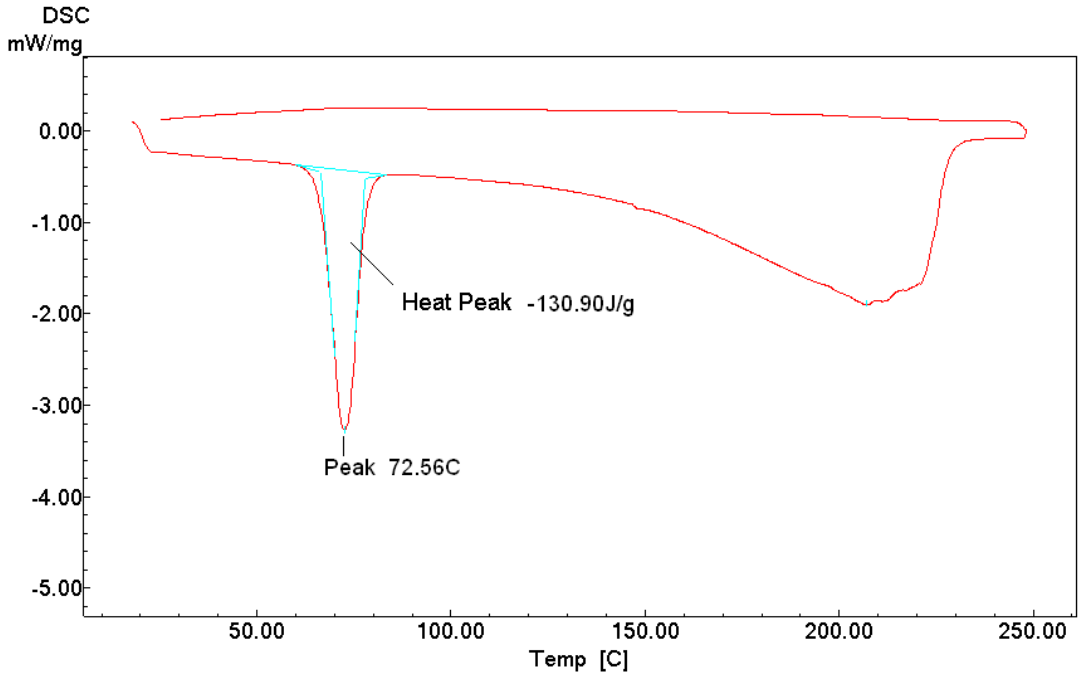

Figure 8-10 Thermal analysis of a catalyst mixture sample

8.4.4 Activator Mixture

With the samples of the diluted activator mixture, two different types of thermal behaviour (Type A and B) were identified as shown in Figure 8-11. The difference was at the start of the endothermic transition, where with Type A samples, a sharp peak was detected whereas Type B samples had a shoulder before the second peak. In addition, Type B had a very low onset melting temperature compared to Type A. With Type A samples, T1, T2 and H_t as shown in Figure 8-11(a), were measured as 55.2±0.5℃, 66.7±0.7℃ and 122.4±4.2 J/g respectively. No T1 was recorded with Type B samples, and T2 and H_t, as shown in Figure 8-11(b), were 64.9±0.2℃ and 107.5±0.7 J/g respectively. The difference in the first endothermic evolution between the two types could have been due to some changes in the content of the activator complex within the samples.

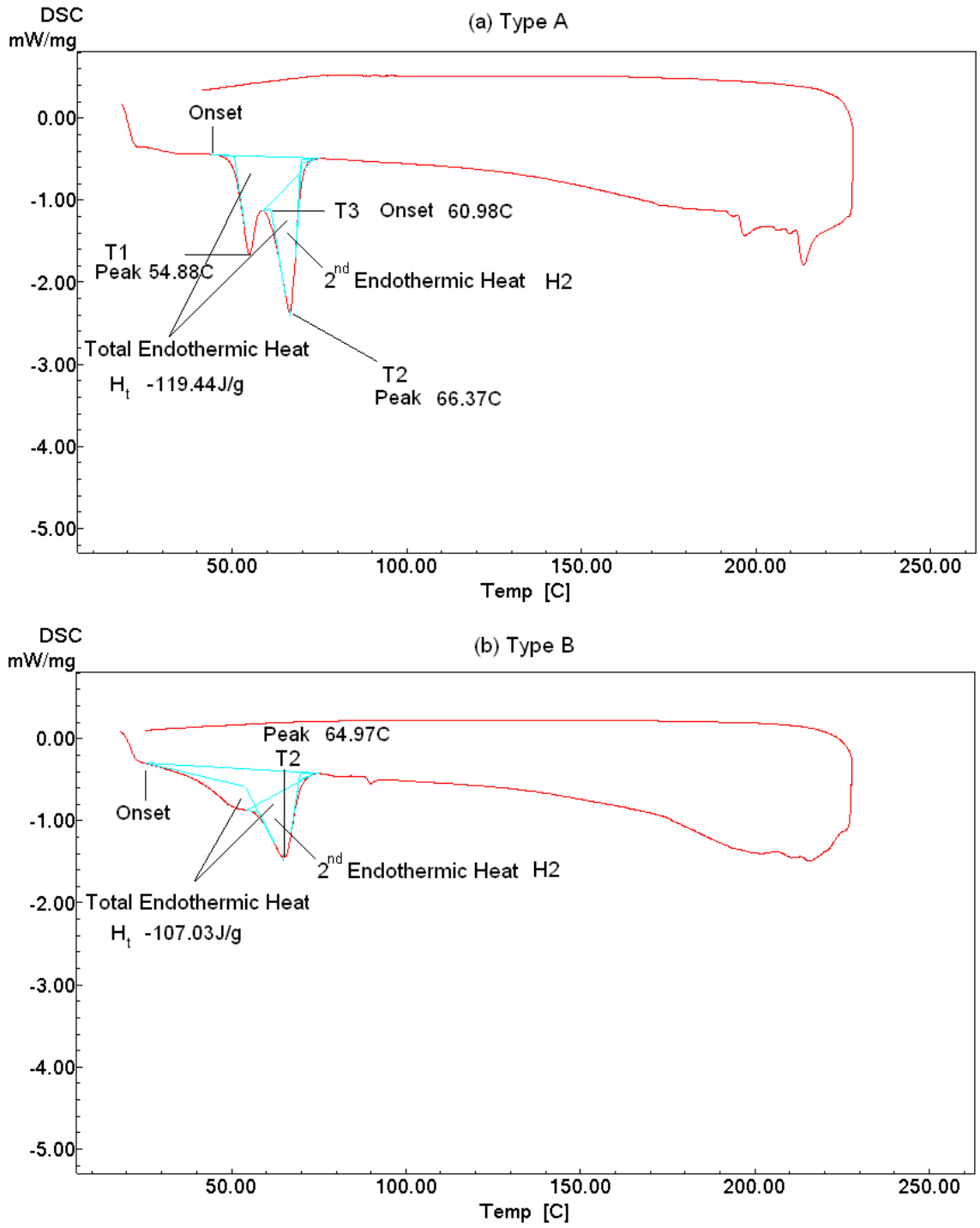

Figure 8-11 Thermal analysis of the activator mixture samples with two melting peak behaviours

8.5 Thermal Analysis of Drop-on-Drop Reaction Samples

This section reports on the thermal analysis of the drop-on-drop reaction samples according to the DSC procedure described in section 8.4.1. The three sets of

samples (Table 1) were analysed to compare with the mixtures. With caprolactam and the mixtures, it was shown that almost all the sample had evaporated after the DSC run. However, with the drop-on-drop samples some material remained. To check whether the remaining material was nylon, a second DSC run was also undertaken with similar DSC settings.

8.5.1 Set 1 Experiments: Effect of Heating

Figure 8-12 shows typical thermal behaviour of the samples from Set 1. The thermogram clearly indicates the sample contained a significant amount of monomer as a large caprolactam melting peak is observed. The first endothermic peak occurred at about 52℃, similar to Type A samples of the activator mixture shown in Figure 8-11(a). Therefore, it is assumed that the activator mixture contributed this peak. The second endothermic peak is due to unreacted caprolactam. The broad endothermic peak which occurred after melting of caprolactam was typical of the caprolactam evaporation as also seen with the mixtures. Measuring the sample weight after the DSC test confirmed that a considerable amount of evaporation (typically 70%) had occurred.

Figure 8-12 also shows a small exothermic peak during the cooling stage at about 160℃. This could have been due to crystallisation of the polymer which had been produced. The evaporation resulted in weight loss during the heating stage of the DSC run and so, the thermogram under-recorded the rate of energy given by crystallisation in mW/mg. This exothermic peak was typical of that for nylon 6, so suggested that some polymer existed in the sample during the cooling stage of the DSC run.

It is not clear whether reaction occurred during the DSC run or during radiation heating. This uncertainty is because the endothermic heat of evaporation of unpolymerised monomer could have dominated any heat released by a possible reaction during the DSC run. Similarly, if radiation heating produced some nylon in the sample, its melting could not be detected due to the large heat absorption by the monomer evaporation. However, the change of transparency (discussed in section 8.3.4), could indicate that at least some monomer conversion occurred during radiation heating.

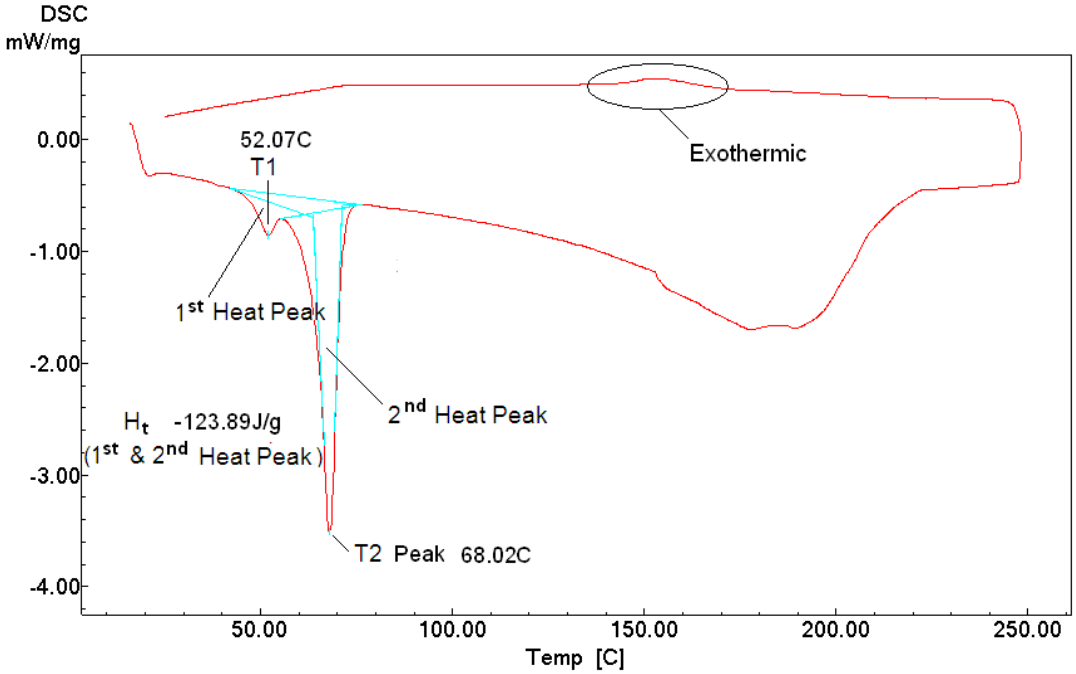

Figure 8-12 DSC thermogram of a sample from Set 1 experiments (Power 3 – 7 min)

A second DSC run was produced as shown in Figure 8-13. There was no weight loss after the second run. Therefore, the endothermic and exothermic peaks in Figure 8-13 are assumed to be respectively due to the melting and crystallisation of the polymer. However, the melting point recorded was about 195℃ which was about 20 to 30℃ lower than that produced with bulk polymerisation (Khodabakhshi 2011).

This could have been due to lower molecular weight of the nylon made in the drop-on-drop reaction samples.

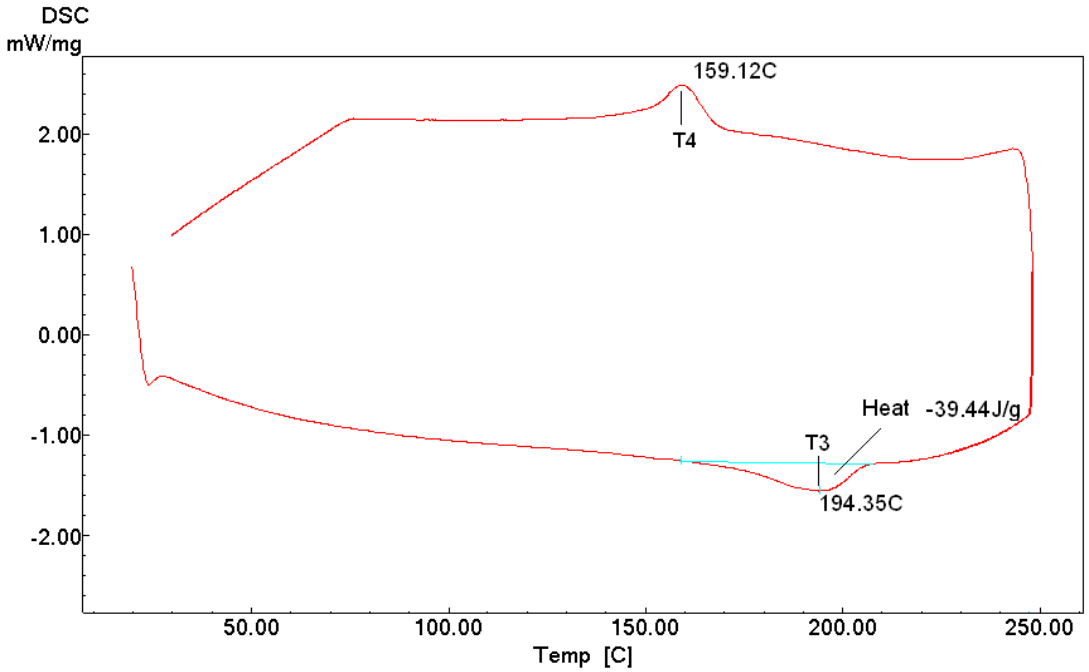

Figure 8-13 Thermogram from second DSC run of the sample corresponding to Figure 8-12 from Set 1 experiments (Power 3 – 7 min)

The thermal analysis for Set 1 samples was to determine whether the radiation heating conditions affected the reaction outcome. Figure 8-14 and Figure 8-15 show the thermal analysis data for peaks from a number of samples. Four temperature values were obtained from the first and second DSC runs for different radiation heating conditions. The first two peak temperatures, T1 and T2, from the first DSC run were not affected by a change in the radiation heating conditions and varied only within ±2℃ as seen in Figure 8-14(a). The peak temperatures in the second run, T3 and T4, varied within a greater range (±7℃) as Figure 8-14(b) shows.

These suggest that the samples were dominated by the unpolymerised mixtures in the first run as they had similar melting endothermic behaviour. However, T3 and T4

in the second DSC run which represented the melting and crystallisation temperatures respectively of nylon 6 would depend on the molecular weight and crystallisation of the polymer. A higher monomer conversion could result in higher melting and crystallisation temperatures (Khodabakhshi 2011). However, no trends in variation of T3 and T4 were seen with the radiation heating conditions. This may suggest some polymerisation occured upon radiation and then further polymerisation could have occured during the first DSC run.

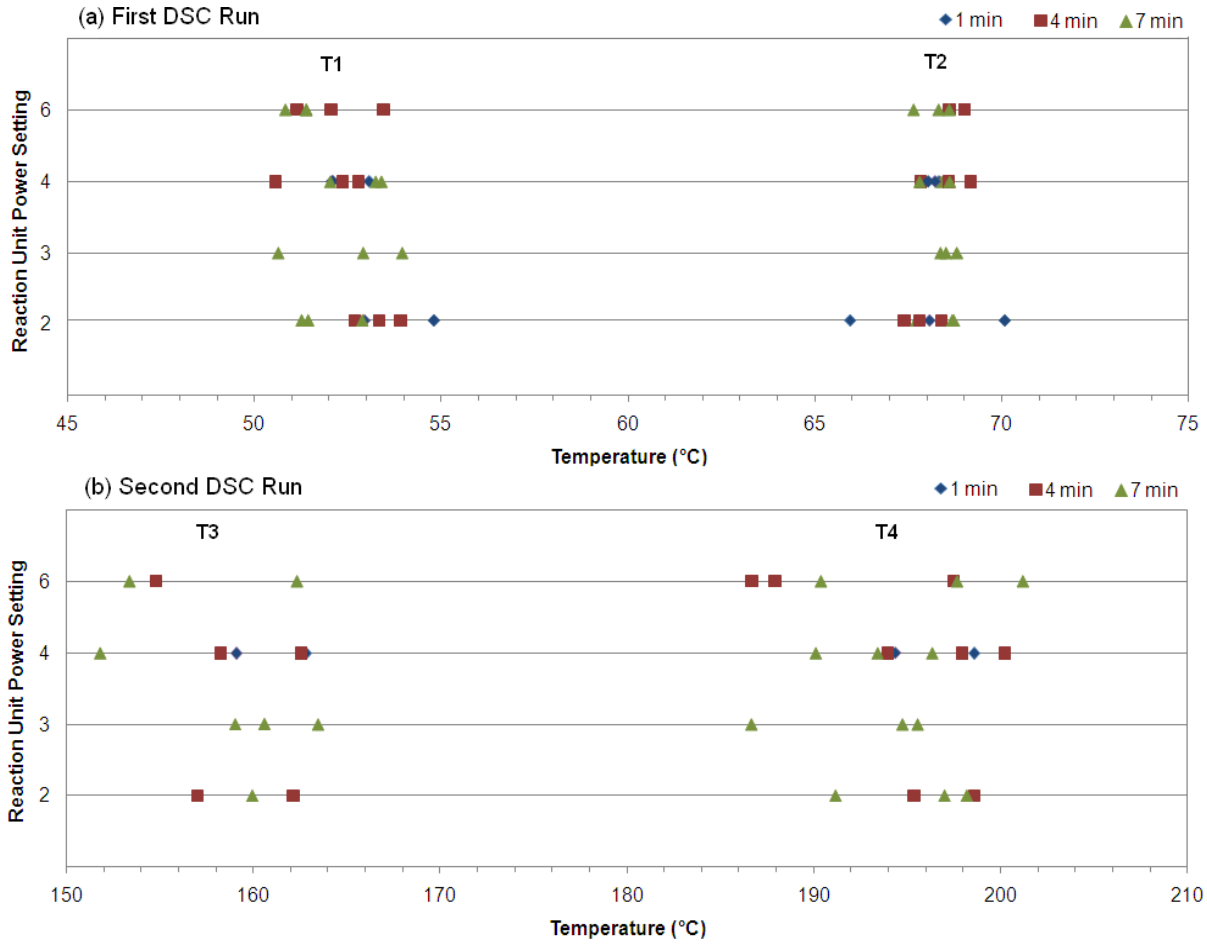

Figure 8-14 Temperature peaks from the thermograms obtained from the first and second DSC runs of samples in Set 1 experiments

Figure 8-15 shows the total heat absorbed during the first DSC run of the samples in Set 1 (H_t as shown in Figure 8-12). No systematic variation of the heat peak values was observed with the radiation heating conditions similar to the peak temperatures. H_t varied from 100 to 130 J/g. This was lower than that of pure caprolactam (140.9±7.0 J/g) suggesting that some polymerisation had occurred. As the proportion of the sample made of polymer did not contribute in the caprolactam melting peak, reducing the heat peak required.

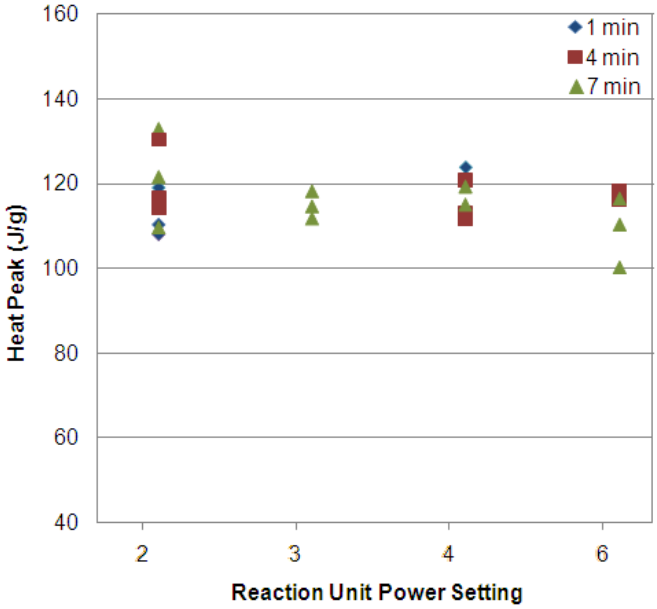

Figure 8-15 Variation of the peaks (H_t) from the thermograms obtained from the first DSC run of samples in Set 1 experiments

No further weight loss was seen during the second DSC run which showed a thermal behaviour similar to nylon. Therefore, dividing the sample weight after the first DSC run by the original drop-on-drop reaction sample weights, the monomer conversion rates were calculated. Figure 8-16 shows the results of the % monomer conversion for different radiation heating conditions. The range of monomer conversion was

between 10% and 30%. The results showed no particular effect due to the radiation heating conditions.

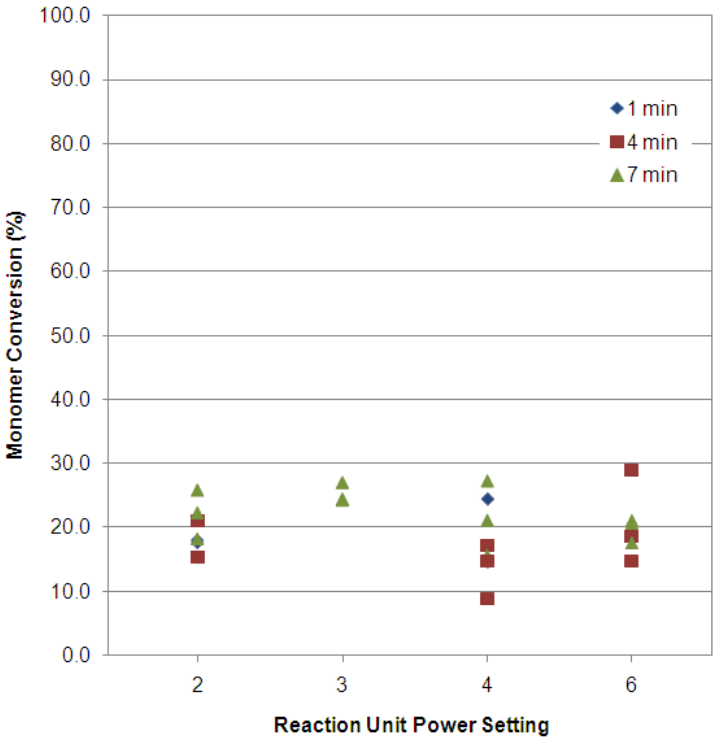

Figure 8-16 Monomer conversion of drop-on-drop reaction samples in Set 1 experiments

8.5.2 Set 2 Experiments: Reduced Activator Concentration

A typical result for thermal analysis of Set 2 samples is shown in Figure 8-17. The figure shows two types of DSC thermograms. As seen in Figure 8-18, T1 was only observed in a limited number of samples as in Figure 8-17(a). Most samples produced results similar to the DSC trace shown in Figure 8-17(b). This difference between the two types of thermal behaviour was similar to the difference seen for the previous activator mixture samples.

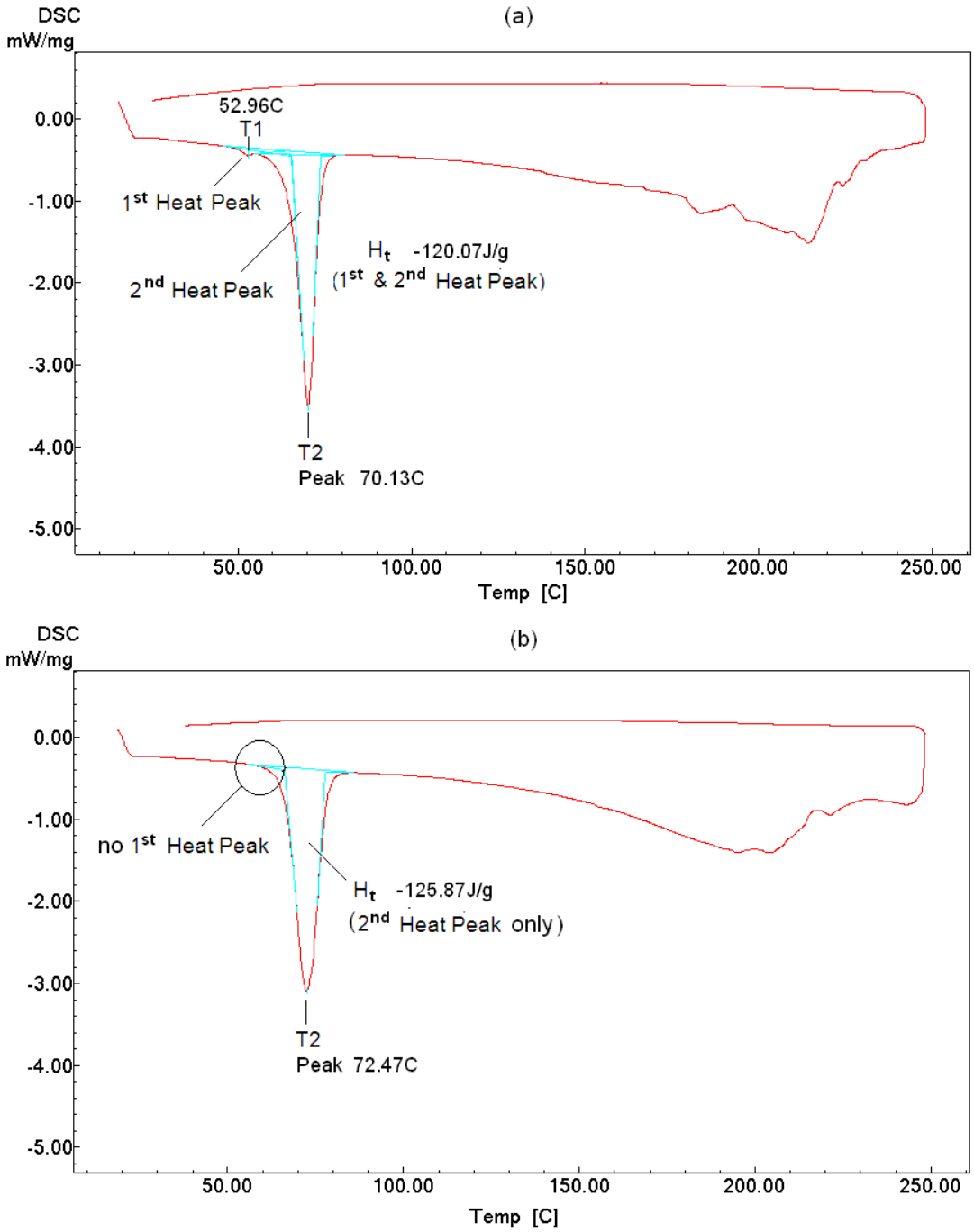

Figure 8-17 DSC thermograms of two samples from Set 2 experiments, (a) 1st and 2nd heat peaks (Power 6 - 4 min), (b) no 1st heat peak (Power 6 – 7 min)

The main peak temperature, T2, was about 5℃ higher than the similar peak in Set 1 when comparing Figure 8-18 with Figure 8-15(a). Figure 8-19 shows that the range of melting heat peak of the samples in Set 2 (120 to 130 J/g) was narrower than in Set 1 (100 to 130 J/g). In addition, the range in Set 2 was closer to caprolactam

(140.9±7.0 J/g). These comparisons suggest that the samples of Set 2 had thermal behaviour closer to the catalyst mixture (Figure 8-10) and were likely to have very low monomer conversion rates. As Figure 8-20 shows, the range of monomer conversion was between 0 to 10%, with the majority below 5%. This showed that the activator concentration and consequently the mixture ratio used for Set 2 experiments were not appropriate for the drop-on-drop reaction.

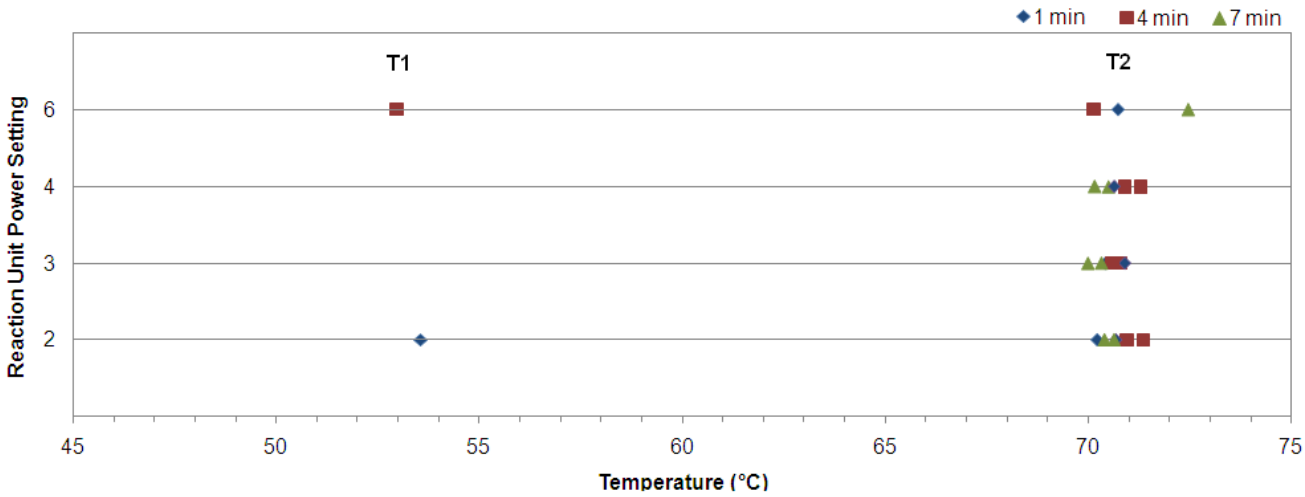

Figure 8-18 Variation of temperature points from the thermograms obtained from samples in Set 2

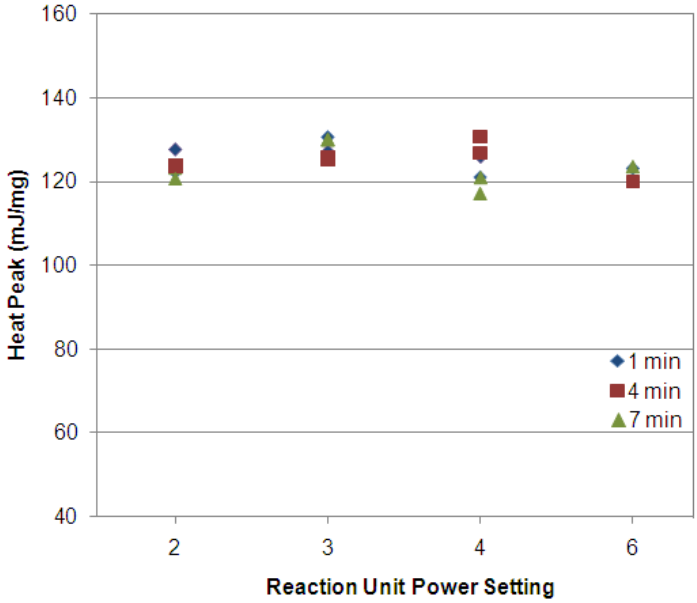

Figure 8-19 Variation of the total heat peak (H_t) in the thermograms obtained from samples in Set 2

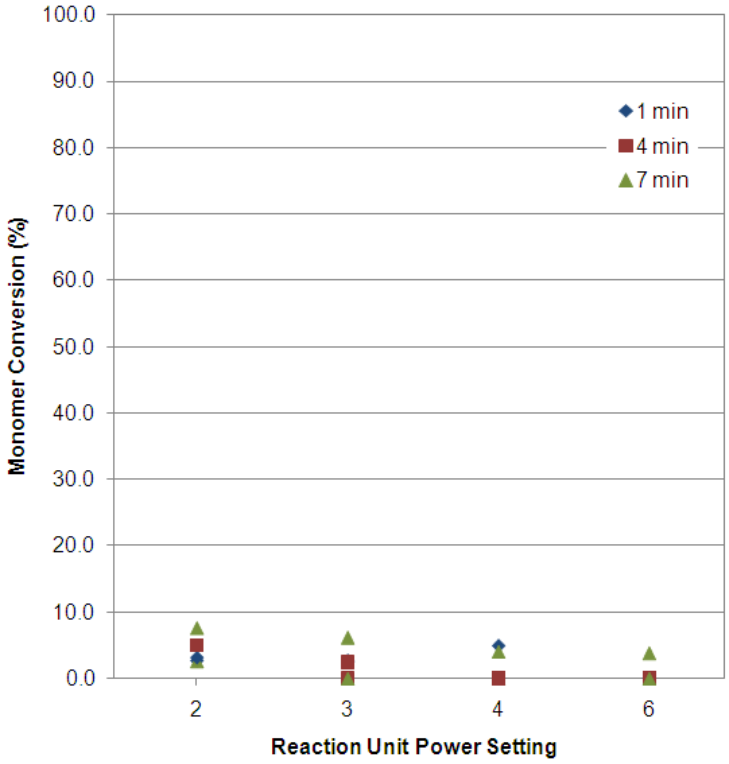

Figure 8-20 Monomer conversion of samples from Set 2 experiments

8.5.3 Alternative Process Variables

The results of Sets 1 and 2 showed that the 1:1 deposition ratio of the mixtures provided a higher monomer conversion than the 5:1 ratio (despite the results with the bulk polymerisation). However, the conversion rates were still too low to solidify the deposited samples upon radiation heating. In addition, the radiation heating conditions had little effect on the reaction outcome which suggests that the results were considerably independent of the heating conditions.

Two reasons could be considered for the lack of monomer conversion: (1) inappropriate heating condition and (2) the effect of environment. The use of an inert gas (e.g. nitrogen) as the alternative moisture/oxygen-free environment would have required additional work on the experimental setup and due to the time restrictions in

the research, it was decided to further investigate the heating conditions and in specific the reaction temperature.

Temperature monitoring via a thermocouple tip (Figure 8-1) suggested that the radiation heating would provide the required heat for the drop-on-drop samples to react. However, after the results from samples in Sets 1 and 2, it was thought that the radiation absorption of the thermocouple (1 mm diameter spherical) tip could have been considerably different from the transparent molten mixtures and also the pan surface. This means that the thermocouple reading might not have been representing the actual melt temperature. In addition, the aluminium pan may not heat up at the same rate as with the thermocouple tip due to its reflective bright surface.

Therefore, at this stage, it was decided to reassess the temperature reached by radiation heating. However, instead of direct temperature reading using a thermocouple tip, an indirect method was to be used. Two approaches were considered. The first was to calculate the amount of radiation heat given to the molten caprolactam (considering the heat flux, molten sample surface area and time), the amount of reflectance from the pan surface and also the amount of radiation absorption of the molten samples (by measuring the samples radiation absorption factor). This was required for each radiation power setting. This approach would have required considerable additional time. Therefore, a second approach was chosen where the melt temperature was determined from the amount of sample evaporation. As evaporation is directly dependent on the sample temperature, it could be compared with a reference chart to find the actual temperature.

8.5.4 Indirect Measuring of Reaction Temperature by Evaporation Rate

As with section 8.2, caprolactam was used for this approach which was undertaken in four steps:

1) Similar to section 8.2.3, the evaporation of caprolactam samples of different weights inside the pans was measured when no radiation heating was involved but instead of one substrate temperature (80℃), several different elevated temperatures between 80℃ to 180℃ with 20℃ increments were used for 1, 4 and 7 min. This was to simulate radiation conditions which could provide this range of reaction temperatures at the given heating times. Therefore, a reference graph of evaporation rates versus substrate temperatures without radiation heating was produced.

2) The evaporation rates using different radiation heating conditions with the substrate at 80℃ (Figure 8-4) was compared with the reference graph from Step 1. This comparison could help to evaluate the accuracy of the temperature monitoring by the thermocouple as reported in section 8.2.2.

3) From the comparison in Step 2, it was found that the thermocouple did not give the sample's actual temperature when radiation heating was used (with the substrate set at 80℃) as the results suggested that the actual temperature was much lower. Therefore, it was decided to use a higher substrate temperature in combination with radiation heating to obtain higher reaction temperatures. The evaporation rates of samples were measured for this new combination and compared with the reference graph (from Step 1) to obtain more accurate sample temperatures. The results would indicate whether the new higher substrate temperature would be high enough to increase the monomer conversion rates.

Figure 8-21 shows the results for Step 1. Heating times had little effect on the evaporation rate suggesting that the substrate heated the sample quickly (in less than 1 min). It is seen in Figure 8-4 that the evaporation rate recorded was below 0.3 mg/min when Power 4 was used with a substrate temperature of 80℃ whereas Figure 8-21 shows that without radiation heating, the substrate set at below 120℃ would provide such evaporation rates. This suggested that the combination of Power 4 radiation and substrate temperature of 80℃ had actually provided reaction temperatures below 120℃. However, the thermocouple recorded values over 200℃ when such combination was used for just over 1 min (Figure 8-3).

This mismatch of the results between the direct thermocouple reading and indirect temperature assessment supported the fact that the thermocouple tip did not provide the actual sample temperature reading. Assuming that molten samples would absorb a certain amount of radiation heat, a higher substrate temperature could produce the required reaction temperature and consequently a higher monomer conversion. Therefore, for a new set of drop-on-drop reaction experiments, an increase in the substrate temperature from 80℃ to 120℃ was expected to provide sufficient reaction temperatures using similar radiation heating conditions. However, this was to be evaluated using the procedure in Steps 1 and 2.

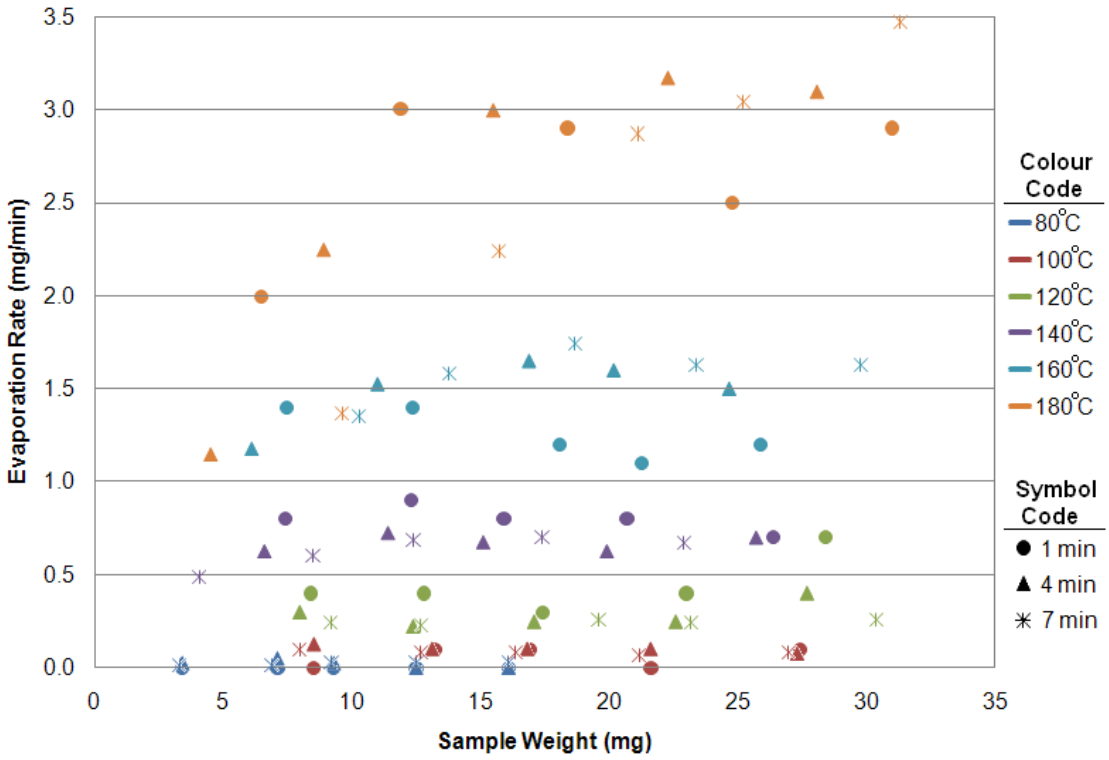

Figure 8-21 Evaporation rates of caprolactam samples inside DSC pan with heated substrate at various temperatures after different periods of times

Figure 8-22 shows the results for evaluating the reaction temperature when substrate temperature at 120℃ was used. The reference graph in Figure 8-21 was presented in temperature zones as shown in Figure 8-22(a). Figure 8-22(b), (c) and (d) show the results of evaporation rates using different radiation power settings after 1, 4, and 7 min respectively. The results of evaporation rates at different reaction unit settings (Power 2, 3, 4 and 6) were superimposed onto the reference temperature zones for the evaluation.

It is seen that the evaporation rate decreased slightly over time (compare Figure 8-22(b) and (d)). This could be due to the decrease of molten sample surface area especially for smaller samples which formed a ring at the pan corner. The sample surface area has a direct influence on the evaporation rate as with larger area there would be more surface from which evaporation could occur.

There were some fluctuations in the evaporation rates as seen in Figure 8-22. However, an estimation of the sample temperature was possible according to the overall trend seen when comparing the temperature reference zones. Table 8-2 shows such estimation which was considered as the reference reaction temperatures for different radiation heating conditions used in Set 3 experiments.

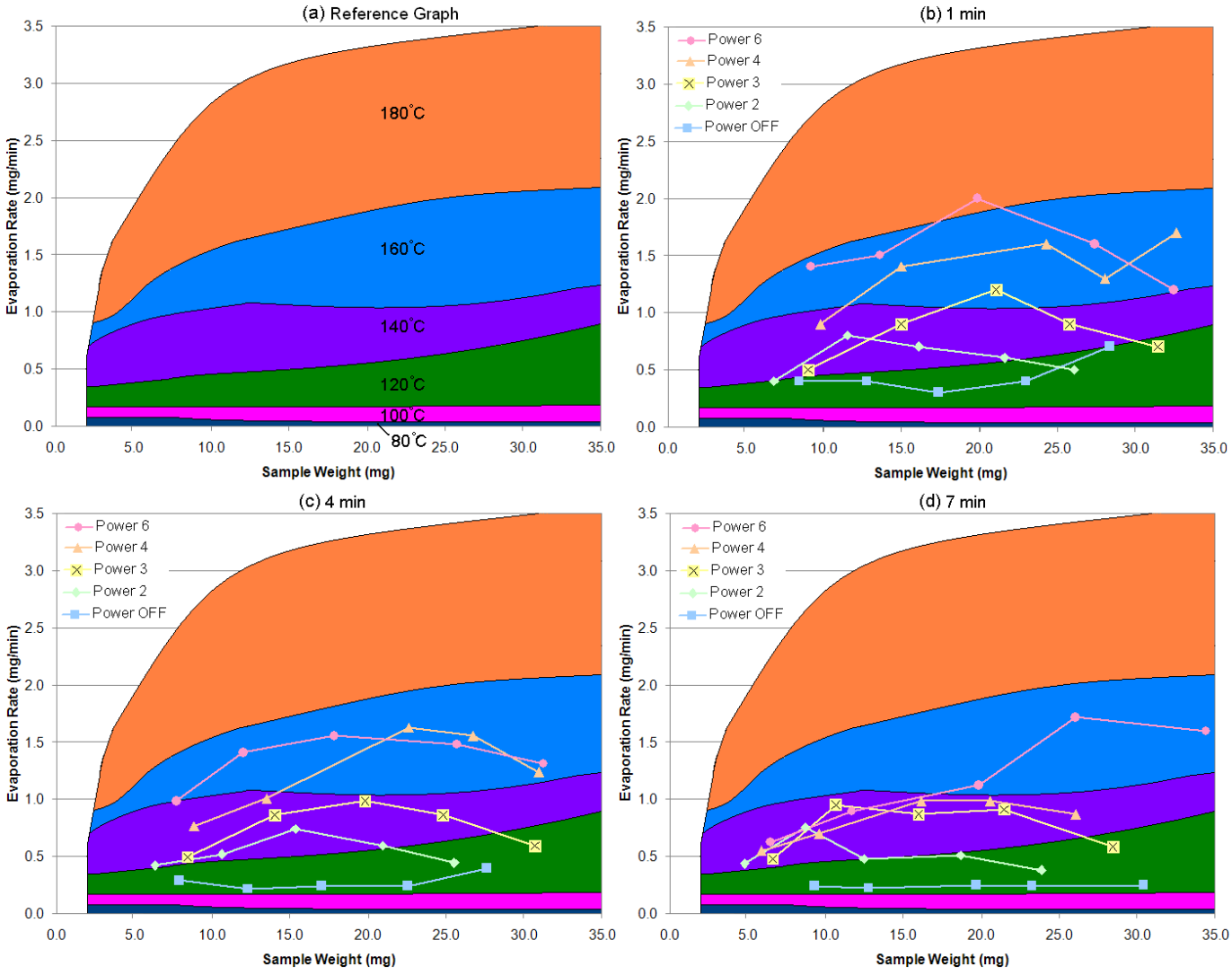

Figure 8-22 Assessing the radiation heating for temperature using the evaporation rate of caprolactam when setting the substrate at 120℃. (a) temperature reference zones based on Figure 8-21, (b) to (d) evaporation rates/temperature zones superimposition when samples were exposed to the radiation heating at different power settings and after different heating timings

Power Setting	Power 2	Power 3	Power 4	Power 6
Estimated Temperature Range (℃)	120 - 140	130 – 150	140 - 160	150 – 170

Table 8-2 Estimation of reaction temperature for Set 3 of drop-on-drop experiments when setting the substrate at 120℃ with the radiation heating according to the assessment shown in Figure 8-22

8.5.5 Set 3 Experiments: Elevated Substrate Temperature

Set 3 experiments were undertaken as with Set 1 but with the higher substrate temperature. A typical result for thermal analysis of Set 3 samples is shown in Figure 8-23. The thermogram shows similar behaviour as seen with Set 1 (Figure 8-12).

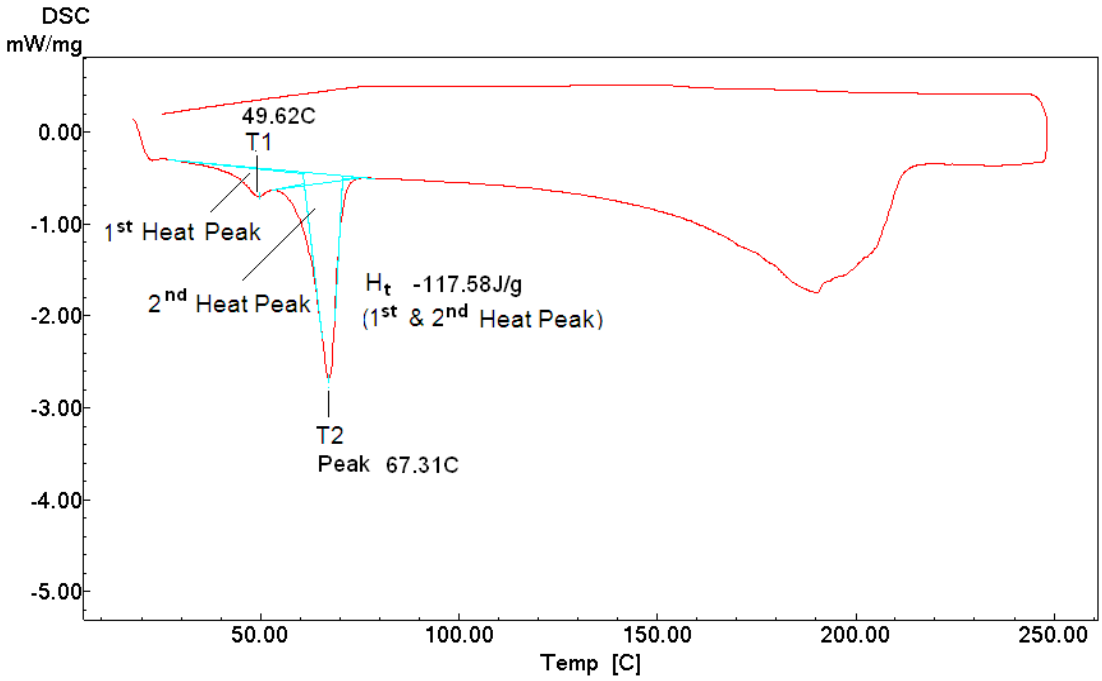

Figure 8-23 Thermogram of a sample from Set 3 experiments (Power 4 - 1 min)

The two peak temperatures in the thermogram, T1 and T2, are shown for all Set 3 samples in Figure 8-24. It is seen that T1 varied from about 45 to 55℃. Similarly, T2 of the second peak had fluctuations within a range just over 5℃. These fluctuations were however less with Set 1 and much less with Set 2 (about 2℃) when comparing

Figure 8-24 with Figure 8-14 and Figure 8-18. This suggested that the variations in the content of the reaction samples in Set 3 were higher than Set 1 and much higher than Set 2.

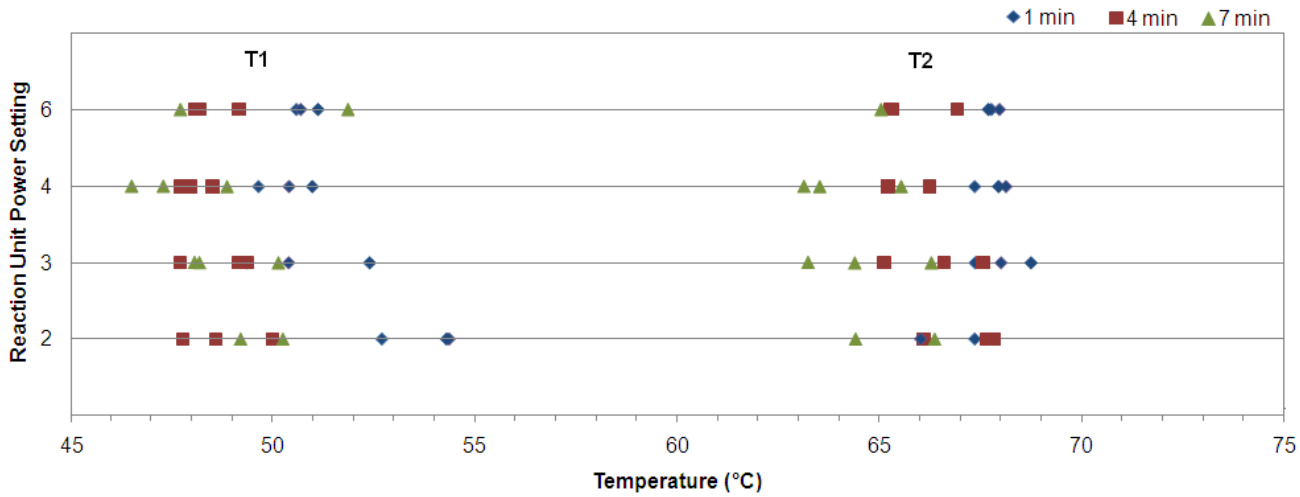

Figure 8-24 Temperature variations in the thermograms peaks obtained from thermal analysis of samples in Set 3

Figure 8-25 shows a similar scenario to the temperature with the heat peak variation for Set 3 when comparing to Sets 1 and 2. Larger fluctuations are seen with Set 3. In addition, with longer radiation time (i.e. 4 and 7 min), a lower heat peak was recorded especially when using a higher power radiation setting (see Power 6 – 7 min in Figure 8-25(b) for example). This may suggest that a higher monomer conversion occurred during the higher radiation heating conditions as the recorded heat peak per unit sample weight was related to the proportion of caprolactam present in the sample.

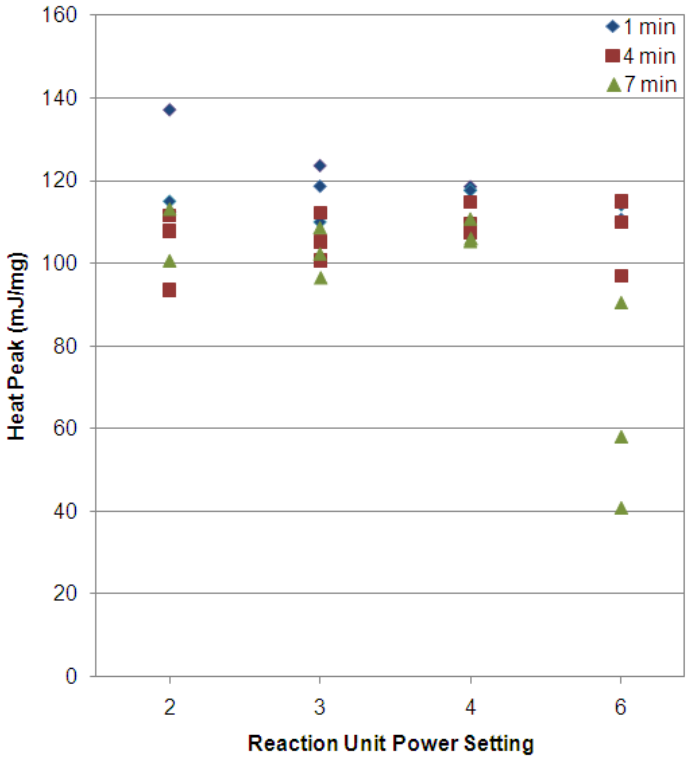

Figure 8-25 Variation of the heat peak (H_t) from the thermograms (as labelled in Figure 8-23) obtained from thermal analysis of samples in Set 3 experiments on drop-on-drop reaction

Figure 8-26 shows the results for monomer conversion of samples for Set 3 experiments (obtained from procedure as with Sets 1 and 2). An overall increase in the conversion rate with power setting is observed. This could be due to the extra radiation heating given to the samples. However, the effect of the extra heating on the evaporation of unconverted monomer (during the radiation) should also be considered. The evaporation rates were expected to be 3 to 5 times higher with the conditions of Set 3 compared with the conditions of Sets 1 and 2 (compare Figure 8-4(b) with Figure 8-22). This higher evaporation could consequently result in samples with a higher concentration of polymer for the thermal analysis and therefore enhanced monomer conversion results. For a practical point of view, the evaporation could be considered by a compensation factor in the process. This

means a higher amount of deposition could be made so that the radiation heating could generate a final required volume of synthesised polymer.

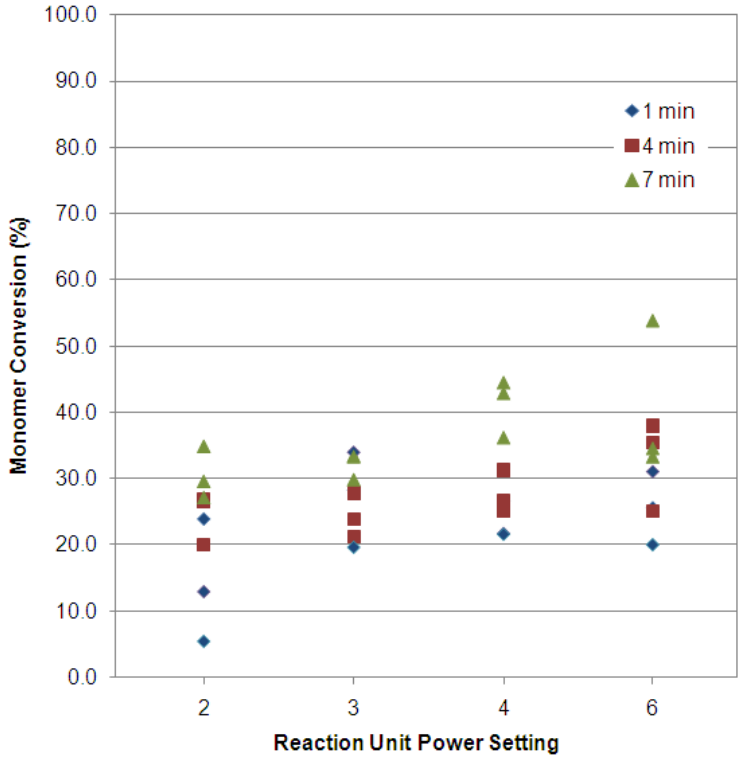

Figure 8-26 Monomer conversion of samples from Set 3 experiments

8.6 Other Parameters in Drop-on-Drop Reaction

The results of Set 3 confirmed that optimising the heating conditions could affect monomer conversion, but as Figure 8-26 shows, the majority of samples had conversion rates below 40%, much lower than the rates using bulk polymerisation (Khodabakhshi 2011). In addition, from the sample appearance observation just after the drop-on-drop reaction, no form of bulk solidification due to reaction was seen in any of the three sets of experiments. These indicate that despite varying a range of heating parameters (radiation power, timing and substrate temperature), it is possible that other factors had a major effect on the results. The results for the drop-on-drop reaction to date did not produce adequate conversion rates for jetting of

nylon which would require a high conversion in a short time to solidify a layer before the next layer was deposited.

It needs to be established why the monomer conversion in the drop-on-drop reaction was not as high as the bulk polymerisation method. The environment was assumed to be a likely reason. However, the atmosphere in the glove box used for drop-on-drop reaction was the same as with the bulk polymerisation using normal atmosphere conditions. Therefore, the focus in this discussion should be on the differences in the influence of environment on the samples between the two methods.

A main difference between bulk polymerisation and the drop-on-drop reaction was the total surface of molten mixture exposed to air. This could have the following effects:

1) Droplets were hundreds of millions of times smaller than the bulk polymerisation samples (30 ml) and during drop-on-drop deposition, 100,000 droplets of about 50 μm in diameter were individually exposed to the environment.

2) The entire spherical surfaces of the droplets were in contact with the environment which gave them extra exposure to oxygen and moisture due to the high surface to volume ratio. However, with bulk polymerisation, the sample's top surface in the beaker was exposed to air.

3) Upon deposition, droplets in flight were exposed to the environment in a similar way as blowing air with 1 m/s speed for about 1 ms (based on the droplet velocity and the nozzle to surface distance of 1 mm). This could give the droplets surface molecules extra chance for contact with oxygen and moisture.

All of these situations with the drop-on-drop reaction could have deactivated the molten mixtures on the surface of the droplets before the reaction stage and therefore limited the polymerisation outcome.

The results of this chapter along with the above discussion suggest the importance of researching the effect of environment on the drop-on-drop reaction. Some work was carried out on the initial design and fabrication to introduce pure nitrogen gas into the glove box, however, it was not possible to continue the work due to lack of time.

Chapter 9. Conclusions and Future Research

This research investigated the use of inkjet technology for drop-on-drop deposition of reactive mixtures to produce nylon 6 by anionic polymerisation. Molten mixtures of caprolactam with activator and catalyst were used and several aspects of material processing were investigated. An experimental setup was developed to study the melt supply behaviour, jetting stability, droplet formation, spreading and mixing, and finally formation of nylon upon radiation heating. This chapter presents the conclusions of the five research stages undertaken and describes the remaining challenges for future work.

9.1 Conclusions

9.1.1 Material Characterisation for Jetting

In addition to caprolactam, different sets of synthesised and commercial reactive mixtures for AP-Nylon were investigated for their physical properties and melt supply behaviour in the jetting system. The surface tension and viscosity of all materials were found to be within the range suitable for inkjet technology. However, with the synthesised catalyst mixture, the jetting system became blocked in the filtration unit during the melt supply start-up process due to the catalyst particles. The particles were assumed to have originated from agglomeration of undissolved salt of caprolactam magnesium bromide (CLMgBr) in molten caprolactam as seen in the form of microcrystals. An elevated temperature of 150°C was found to dissolve the

microcrystals; however, in addition to the limitation with the printhead's operating temperature, this could result in very high evaporation in the system.

There were similar filter blocking issues with the commercial catalyst mixture based on CLMgBr. The sodium caprolactamate (NaCL)-based catalyst mixture however, was purged though the system for up to about two third of the level supplied to the system before the filter was completely blocked and therefore was selected to continue the research. It was found that there was a concentration of microcrystals in all melt levels for the samples produced by purging through the system. However, it was also found that the microcrystals in the samples purged through the system had a tendency to randomly agglomerate (which could originate the filter blocking).

9.1.2 Jetting of Caprolactam and Reactive Mixtures

A stable single jet in trials with caprolactam and the reactive mixtures was achieved. Successful trials with an array of 126 jets were also performed. A processing window for stable jetting was recommended for each material. Jetting frequency had no significant effect on the jetting stability. However, the jets were sensitive to the voltage and vacuum level. Too low or too high values of these parameters induced instability in the form of a trajectory error and in some cases jet failure. With high vacuum levels, air ingestion occurred during nozzle actuation especially when accompanied with higher voltages, and resulted in individual jet failures. It was also found that jetting of the reactive mixtures required higher voltages than caprolactam for stable jets due to their higher viscosity. The melt supply level was found to have no visible effect on the jet stability.

With the molten caprolactam, jet array instabilities occurred occasionally within the stable range of parameters and this was mainly due to the particles left in the

printhead from the functionality test. Most of the instabilities were in the form of an individual jet trajectory error. In some cases, a stable jet with incorrect trajectory was observed which could have been a result of partial blocking of the nozzle by the particles. Jet array failure occurred in a manner similar to falling dominos where the nozzle actuations after the failure of a jet could result in nozzle bleeding and unbalancing the molten layer thickness locally, and as a consequence disturbing the adjacent jets.

Jet array stability was found to be considerably more sensitive with the catalyst mixture than with caprolactam and the activator mixture within the normal stable range of parameters. The instability occurred randomly in the repeated trials with similar conditions. This was assumed to be due to the random microcrystal agglomeration. It was found that there was a flow field in the thin molten layer on the nozzle plate during jetting. This was visualised by tracing particles which were attracted towards the actuating nozzles at velocities up to 2 mm/s as soon as jetting started. The particles were either taken into the nozzle or repelled. A complex velocity profile was assumed to be generated across the thickness of the melt layer as also reported by Beulen *et al.* (2007) for normal ink with a single jet trial. With the multiple jetting of caprolactam though, the flow generated by each nozzle could result in a combined flow pattern. This was because the overall flow field pattern was found to be radial and symmetric to the middle of the multiple jets.

9.1.3 Droplet Formation Characteristics

With high jetting voltages, a tail was formed with all droplets which disintegrated into satellite droplets whereas with lower voltages, it rejoined the main droplet. It was found that the mixtures required an additional 5 V to obtain similar droplet shape and

kinetics to caprolactam due to the mixtures having a 50% higher viscosity. The droplet characteristics were unaffected by the melt supply level with the reactive mixtures.

Jetting frequency had no significant effect on the droplet formation characteristics. However, it affected nozzle wetting behaviour. For the first thousand droplets, it was found that the nozzle wetting developed over a wider area when a lower jetting frequency was used. This suggested a higher jetting frequency could lead to a more reliable deposition if a dry nozzle plate was to be used. However, jetting instabilities were observed in some trials due to asymmetric wetting of the actuating nozzle. These were originated by contamination on the nozzle plate or air motion by convection. Therefore, it was decided to continue the research with a wet nozzle plate for the next stages for which a set of jetting parameters giving satellite-free droplets were chosen.

9.1.4 Deposition of Materials

The investigation showed that with the chosen jetting parameters, there was spreading upon droplet impact. Consecutive impingement of the droplets onto previously spread droplets also did not cause splashing. With a moving surface, a stable bead was obtained with a cold surface whereas with the heated surface, instability was observed in the form of formation of bulges. Maintaining a stable and uniform bead for bead-on-bead deposition of the mixtures would have required further investigations on the droplet spacing and surface temperature and therefore it was decided to deposit multiple droplets into a DSC pan to pursue the research of drop-on-drop reaction.

It was found that a generally consistent content and dispersion of the microcrystals existed within the individual droplets deposited at different melt supply levels. When accumulating droplets, microcrystals had a higher level of agglomeration in different positions in the sample. The agglomeration however was much less than with the purged samples which had a very high level of agglomeration (due to possibly the use of a cover slip onto the molten samples for microscopy).

Dye tracing showed that the use of DSC pan for the accumulative drop-on-drop deposition approach gave good mixing. The consecutive impingement and also surface tension resulted in collection of the sample melt at the pan corner which was thought to further assist the mixing.

9.1.5 Drop-on-Drop Reaction

To initiate reaction of the drop-on-drop deposited mixtures, an elevated substrate temperature at 150℃ was found to result in rapid evaporation and unbalancing the mixtures ratio which could affect the reaction. Therefore, surface radiation was used to heat up the samples after the two mixtures were deposited onto each other.

With the initial sets of experiments, a very low monomer conversion was achieved irrespective of the radiation heating conditions used. The appearance of the drop-on-drop samples was transparent before the reaction, however, after the radiation, limited areas were found to have monomer conversion. This was based on the observed opacity in the samples which was assumed to be nylon spherulites. With a higher substrate temperature, a higher monomer conversion was achieved but the rates were still less than half the results with the bulk polymerisation approach. The biggest difference between the two approaches were the deposition method where jetting of thousands of tiny droplets in air instead of a large volume of sample inside

a beaker (as with the bulk polymerisation) could have resulted in a very high monomer deactivation. Therefore, the effect of environment on the jetting of nylon was thought to be significant.

9.2 Further Research Challenges and Recommendations

Researching into the concept of “Jetting of Nylon” required integration of different technologies and an understanding of several aspects of material processing. To develop the concept into a layer fabrication process, several material and process considerations should be taken into account. This research explored some of the main aspects to provide a fundamental understanding of the parameters involved. However, the agglomeration behaviour of the catalyst mixture microcrystals resulted in time-consuming challenges affecting the progress of the research to the stage where the effect of environment on the drop-on-drop reaction could not be explored. Therefore, the recommendation for immediate future work would be to investigate the effect of using a nitrogen environment in the glove box on the monomer conversion.

One of the most important aspects of the future research will be to develop the understanding of the catalyst mixture microcrystals and their interaction with the jetting system. The main objective will be to obtain stable jetting with high reliability. Two research topics are proposed for this objective. The first is to investigate a method to visualise the mechanism of jet disturbance by the agglomerated microcrystals. This could provide an understanding of the role of the catalyst microcrystals agglomeration on the system reliability. The second topic is to research the agglomeration mechanism and to develop a methodology for dispersing the microcrystals in molten caprolactam. Possibilities could be to charge microcrystals

electrostatically or use a vibration mechanism similar to ultrasonics. Other possibilities could be chemical surfactants which would not affect the reaction.

With an accurate and reliable droplet placement, it will be possible to research bead-on-bead deposition. For bead stability, the main parameters will be the droplet spacing and the surface energy of the substrate. The latter could be controlled by melt and surface temperature and possibly chemical surfactants. This could provide the required conditions to research layer fabrication.

By undertaking the above research, it is hoped that the drop-on-drop reaction outcome is increased to a high monomer conversion level where nylon solidification could be achieved in the form of a layer. Then the solidification time and strength will be important topics. This requires varying parameters such as the mixture compositions and heating parameters with different environments. A research of multiple layers will then be feasible towards additive layer manufacturing of nylon parts.

A challenging future is anticipated for the concept of “Jetting of Nylon”. The success though will be very rewarding as this approach in a reliable and economical process will have a huge commercial impact because of the on-demand deposition and additive manufacturing features in addition to the demand of nylon 6 due to its functionality.

References

Allen, E., Henshaw, J. and Smith, P. (2001), “A review of particle agglomeration”, US Department of Energy, Report AEAT/R/PSEG/0398

Anilkumar, A. V., Lee, C. P. and Wang, T. G. (1991), “Surface tension induced mixing following coalescence of initially stationary drops”, *Physics of Fluids A*, **3(11**), pp. 2587-2591

ASTM (2009), “ASTM WK24055 - New Terminology for additive manufacturing”, Retrieved from: http://www.astm.org/commit/committee/F42.htm

Beaman, J. J. (1997), "*Rapid Prototyping in Europe and Japan - JTEC/WTEC panel report - Chapter 3: Historical Perspective*", published by Society of Manufacturing Engineers (SME), Baltimore, MD, ISBN 1883712440

Beulen, B., de Jong, J., Reinten, H., van den Berg, M., Wijshoff, H. and van Dongen, M. E. H. (2007), “Flow on the nozzle plate of an inkjet printhead”, *Experiments on Fluids*, **42(2)**, pp. 217-224

Bogy, D. B. and Talke, F. E. (1984), “Experimental and theoretical study of wave propagation phenomena in drop-on-demand inkjet devices”, *IBM Journal of Research Development*, **28(3)**, pp. 314-321

Bower, D. I., *An introduction to polymer physics*, Cambridge University Press, 2002, ISBN 052163721X

Brueggemann Chemical GmbH (2009), “AP-Nylon® Materials”, Retrieved from http://www.brueggemann.com/english/ap-nylon-produkte.html

Brunahl, J. (2003), “Physics of Piezoelectric Shear Mode Inkjet Actuators“, PhD thesis, Royal Institute of Technology, Stockholm, Sweden

Bruner, S., Xu, D. and Phillips, C. (2007), “Drop Landing Accuracy Improvements in Inkjet Printed OLED Displays”, *SID International Symposium Digest of Technical Papers*, **38(1)**, pp. 1611-1612

Calvert, P. (2001), “Inkjet Printing for Materials and Devices”, *Chemistry of Materials*, **13**, pp. 3299-3305

Chen, Y., Au, J., Kazlas, P., Ritenour, A., Gates, H. and McCreary, M. (2003), “Electronic paper: Flexible active-matrix electronic ink display”, *Nature*, **423**, pp. 136-137

Chovancova-Lovell, V., Pekarovicova, A. and Fleming III, P. D. (2006), “Novel Phase Change Inks for Printing Three-Dimensional Structures”, *Journal of Imaging Science and Technology*, **50(6)**, pp. 550-555

Courbin, L., Bird, J. C. and Stone, H. A. (2006), “Splash and anti-splash: observation and design”, *Chaos*, **16**, p. 041102

Crawford, R. J. (1998), “Plastics Engineering”, Published by Elsevier Butterworth-Heinemann, Oxford, UK, ISBN 0750637641

Creagh, L. T. and McDonald, M. (2003), “Design and performance of inkjet printheads for non graphic arts applications”, *Materials Research Society Bulletin*, **28**, pp. 807-811

Das, S., Hollister, S. J., Flanagan, C., Adewunmi, A., Bark, K., Chen, C., Ramaswamy, K., Rose, D. and Widjaja, E. (2003), “Freeform fabrication of Nylon-6 tissue engineering scaffolds”, *Rapid Prototyping Journal*, **9(1)**, pp. 43-49

Dave, R. S., Kruse, R. L., Stebbins, L. R. and Udipi, K. (1997), “Polyamide from Lactams via Anionic Ring-Opening Polymerization: 2. Kinetics”, *Polymer*, **38(4)**, pp. 939-948

Dave, R. S., Kruse, R. L., Udipi, K. And Williams, D. E. (1997), “Polyamide from Lactams via Anionic Ring-Opening Polymerization: 3. Rheology”, *Polymer*, **38(4)**, pp. 949-954

de Gans, B. J. and Schubert, U. S. (2003), “Inkjet Printing of Polymer Micro-Arrays and Libraries: Instrumentation, Requirements, and Perspectives”, *Macromolecular Rapid Communications*, **24(11)**, pp. 659-666

de Gans, B. J., Duineveld, P. C., Schubert, U. S. (2004), "Inkjet printing of polymers: State of the art and future developments", *Advanced Materials*, **16(3)**, pp. 203-213

de Jong, J., de Bruin, G., Reinten, H., van den Berg, M., Wijshoff, H., Versluis, M. and Lohse, D. (2006), “Air entrapment in piezo-driven inkjet printheads”, *Journal of Acoustic Society of America*, 120(3), pp. 1257-1265

de Jong, J., Reinten, H., Wijshoff, H., van den Berg, M., Delescen, K., van Dongen, R, Mugele, F., Versluis, M., Lohse, D., (2007), “Marangoni flow on an inkjet nozzle plate”, *Applied Physics Letters*, **91(20)**, p. 204102

Duineveld, P. C. (2003), “The stability of inkjet printed lines of liquid with zero receding contact angle on a homogeneous substrate”, *Journal of Fluid Mechanics,* **477**, pp. 175-200

Elsner, P., Dreher, S., Ederer, I., Voit, B., Gudrun, J. and Stephan, M. (2010), “Method and device for production of a three-dimensional article”, United States Patent No. 7767130, Filed: May 2005, Published: March 2010

Enginger (2010), “Polyamides: TECAGLIDE Green”, Retrieved from: www.ensinger-online.com/en/materials/high-temperature-plastics/polyimides/

Fathi, S., Dickens, P. and Fouchal, F. (2010), “Regimes of droplet train impact on a moving surface in an additive manufacturing process”, *Journal of Material Processing Technology*, **210**, pp. 550-559

Fouchal, F. and Dickens, P. (2006), “Anionic Polymerisation of Caprolactam for Additive Manufacturing Application”, Internal Report, Loughborough University, UK

Frohn, A. and Roth, N. (2000), “*Dynamics of Droplets*”, Published by Springer-Verlag, Berlin, Germany, ISBN 3540658874

Frunze, T. M., Kurashev, V. V., Kotelnikov, V. A. and Volkova, T. V. (1979), “Activators of the Anionic Polymerisation of Lactams”, *Russian Chemical Reviews*, **48(10)**, pp. 991-1005

Gao, F. and Sonin, A. A. (1994), “Precise Deposition of Molten Microdrops: The Physics of Digital Microfabrication”, *Proceeding of Royal Society, London Serial A: Mathematical and Physical Sciences*, **444**, pp. 533-554

Gebhardt, A. (2003), ”*Rapid Prototyping*”, Published by Carl Hanser Verlag, Munich, Germany, ISBN 156990281X

Gibson, I., Rosen, D. W. and Stucker, B. (2009), “*Additive Manufacturing Technologies: Rapid Prototyping to Direct Digital Manufacturing*”, Published by Springer, New York, NY, ISBN 1441911197

Gregory, P. (1991), “*High-Technology Applications of Organic Colorants*”, Published by Plenum Press, New York, NY, ISBN 030643637X

Hanford, W. E. and Joyce, R. M. (1948), “Polymeric amides from epsilon-caprolactam”, *Journal of Polymer Science*, **3(2)**, pp. 167-172

Hon, K. K. B., Li, L. and Hutchings, I. M. (2008), “Direct writing technology-Advances and developments”, *CIRP Annals - Manufacturing Technology*, **57**, pp. 601-620

Hopkinson, N. and Erasenthiran, P. E. (2004), “High speed sintering – early research into a new rapid manufacturing process”, *Proceedings of the 15th Solid Freeform Fabrication Symposium (SFF2004)*, Austin TX, August 2nd – 4th 2004, pp. 312-320

Hopkinson, N., Hague, R.J.M. and Dickens, P.M. (2006) "*Rapid Manufacturing: An Industrial Revolution for the Digital Age*", Published by John Wiley and Sons Ltd., West Sussex, UK, ISBN 04700160132

Hsiao, W. K., Chun, J. H. and Saka, N. (2006), "Effect of Surface Roughness on Droplet Bouncing in Droplet-Based Manufacturing Processes", *CIRP Annuals - Manufacturing Technology*, **55(1)**, pp. 209-212

Hutchings, I. M., Martin, G. D. and Hoath, S. D. (2007), "High Speed Imaging and Analysis of Jet and Drop Formation", *Journal of Imaging Science and Technology*, **51(5)**, pp. 438-444

Hutchings, I. M. (2009), "Inkjet printing in micro-manufacturing: opportunities and limitations", *Proceeding of International Conference on Multi-Material Micro Manufacture (4M/ICOMM 2009)*, Karlsruhe, Germany, September 2009, pp. 47-57

Jeng, J. Y., Wang, J. C. and Lin, T. T. (2000), "Fast interior filling of Model Maker models using a spraying nozzle to accelerate build speed", *Rapid Prototyping Journal*, **6(4)**, pp. 235-243

Johnson, D. R., Kynaston-Pearson, A. W. and Damarell, W. N. (2003), "Inkjet printer which deposits at least two fluids on a substrate such that the fluids react chemically to form a product thereon", Patent No. GB2382798(A), Filed: December 2001, Published: June 2003

Kelly, J. S. and Lindblom, B. S. (2006) "*Scientific Examination of Questioned Documents*", Published by CRC Press, Boca Raton, FL, ISBN 0849320445

Khodabakhshi, K., Gilbert, M., Dickens, P. M., Hague, R., Fathi, S. "Optimized Polymerization Conditions for Inkjetting of Caprolactam to Produce Polyamide Parts", *Proceeding of 19th International Symposium on Solid Freeform Fabrication (SFF2008)*, Austin TX, August 4th – 6th 2008

Khodabakhshi, K., Gilbert, M., Dickens, P. M., Hague, R. and Fathi, S. "New Polymerization/Mixture Formulation for Jetting: An Approach to Production of Polyamide 6 Parts", *Proceeding of 20th International Symposium on Solid Freeform Fabrication (SFF2009)*, Austin TX, August 3rd – 5th 2009

Khodabakhshi, K. (2011), "Anionic polymerisation of caprolactam; an approach to optimise the polymerisation conditions to be used in a jetting process", PhD Thesis, Loughborough University, UK

Kim, H.-Y., Cherng, J.-P., and Chun, J.-H. (2002) "Recent Progress in Droplet-Based Manufacturing Research", *Innovation in Manufacturing Systems and Technology (IMST)*, Droplet-Based Manufacturing Laboratory, MIT, Retrieved from: http://dspace.mit.edu/handle/1721.1/4039

Kim, B. H., Kim, T. G., Lee, T. K., Kim, S., Shin, S. J., Kim, S. J. and Lee, S. J. (2009), "Effects of trapped air bubbles on frequency responses of the piezo-driven inkjet printheads and visualization of the bubbles using synchrotron X-ray", *Sensors and Actuators A: Physical*, **154(1)**, pp. 132-139

Kipphan, H. (2001), "*Handbook of print media: technologies and production methods*", Published by Springer-Verlag Berlin Heidelberg, Germany, ISBN 3540673261

Kohan, M. I. (1995), "*Nylon Plastics Handbook*", Published by Hanser, New York, NY, ISBN 1569901899

Krebs, F. C. (2009), "Fabrication and processing of polymer solar cells: A review of printing and coating techniques", *Solar Energy Materials and Solar Cells*, **93**, pp. 394-412

Kriz, J., Dybal, J., Kurkova, D., Arnoldova, P., Prokopova, I., Brozek, J., Hroch, Z. (2001), “Molecular structure of the complex of hexano-6-lactam with magnesium bromide”, *Macromolecular Chemistry and Physics*, **202 (7)**, pp. 1194-1199

Kröber, P., Delaney, J. T., Perelaer, J. and Schubert, U. S. (2009), “Reactive inkjet printing of polyurethanes”, *Journal of Materials Chemistry*, **19**, pp. 5234-5238

Kwon, K. S. and Kim, W. (2007), “A waveform design method for high-speed inkjet printing based on self-sensing measurement”*, Sensors and Actuators A: Physical*, **140(1)**, pp. 75-83

Kwon, K. S. (2009), “Methods for detecting air bubble in piezo inkjet dispensers”, *Sensors and Actuators A: Physical*, **153(1)**, pp. 50-56

Le, H. P. (1998), “Progress and Trends in Inkjet Printing Technology”, *Journal of Imaging Science and Technology*, **42(1)**, pp. 42-69

Lee, F. C., Mills, R. N. and Talke, F. E. (1984), “The Application of Drop-on-Demand Ink Jet Technology to Color Printing”, *IBM Journal of Research Development*, **28(3)**, pp. 307-313

Lejeune, M., Chartier, T., Dossou-Yovo, C. and Noguera, R. (2009), “Inkjet printing of ceramic micro-pillar arrays”, *Journal of the European Ceramic Society*, **29**, pp. 905-911

Leneweit, G., Koehler, R., Roesner, K. G. and Schaefer, G. (2005), “Regimes of drop morphology in oblique impact on deep fluids”, *Journal of Fluid Mechanics*, **543**, pp. 303-331

Leu, T. S. and Lin, J. H. (2008), “Experimental Studies of Meniscus Dynamic Behaviors in a Squeeze-Mode Piezoelectric Inkjet Printhead”, *Materials Science Forum*, **594**, pp. 155-162

Liu, Q. and Orme, M. (2001), "On precision droplet-based net-form manufacturing technology", *Proceedings of the IMECHE-Part B: Journal of Engineering Manufacture*, **215**, pp. 1333-1355

Lombardi, J. L. and Calvert, P. (1999), "Extrusion freeforming of Nylon 6 materials", *Polymer*, **40**, pp. 1775-1779

Lu, Y., Shi, W., Qin, J. and Lin, B. (2010), "Fabrication and Characterization of Paper-Based Microfluidics Prepared in Nitrocellulose Membrane by Wax Printing", *Analytical Chemistry*, **82**, pp. 329-335

Majewski, C. E., Oduye, D., Thomas, H. R. and Hopkinson, N. (2008), "Effect of infra-red power level on the sintering behaviour in the high speed sintering process*", Rapid Prototyping Journal,* **14(3)**, pp. 155-160

Michaelis, A. J., Paton, A. D., Temple, S. and Bartky, W. S. (1989), "Droplet deposition Apparatus", US Patent No. 4887100, Filed: January 1988, Published: December 1989

MicroFab Technologies$_1$ (1999), "MicroFab Technote 99-02: Fluid Properties Effects on Inkjet Device Performance", Microfab Technologies, Inc., Plano, TX, Retrieved from: http://www.microfab.com/equipment/technotes/technote99-02.pdf

MicroFab Technologies$_2$ (1999), "MicroFab Technote 99-03: Drive Waveform Effects on Inkjet Device Performance", Microfab Technologies, Inc., Plano, TX, http://www.microfab.com/equipment/technotes/technote99-03.pdf

MicroFab Technologies (2010), "Solder Jet Technology", MicroFab Technologies, Inc., Plano, TX, retrieved from: http://www.microfab.com/technology/electronics/electronics.html

Millipore Corporation (2009), "Mitex^{tm} Membrane Filter**",** Retrieved from http://www.millipore.com/catalogue/module/C254

Mironov, V., Boland, T., Trusk, T., Forgacs, G. and Markwald, R. R. (2003), “Organ printing: computer-aided jet-based 3D tissue engineering”, *Trends in Biotechnology*, **21(4)**, pp. 157-161

Mironov, V., Reis, N., and Derby, B. (2006), “Bioprinting: A Beginning”, *Tissue Engineering*, **12(4)**, pp. 631-634

Mundo, C., Sommerfeld, M. and Tropea, C. (1995), “Droplet-Wall Collisions: Experimental Studies of the Deformation and Breakup Process”, *International Journal of Multiphase Flow*, **21(2)**, pp. 151-173

Okawa, T., Shiraishi, T. and Mori, T. (2008), “Effect of impingement angle on the outcome of single water drop impact onto a plane water surface”, *Experiments in Fluids*, **44**, pp. 331-339.

Orme, M. (1991), "On the Genesis of Droplet Stream Microspeed Dispersions", *Physics of Fluids*, **3(12)**, pp. 2936-2947

Pandey, P.M., Reddy, N.R. and Dhande, S.G. (2003), “Slicing procedures in layered manufacturing: a review”, *Rapid Prototyping Journal*, **9(5)**, pp. 274-288

Pan K. L. and Law, C. K. (2007), “Dynamics of droplet-film collision”, *Journal of Fluid Mechanics*, **587**, pp.1-22

Pan, K. L., Cheng, K. R., Chou, P. C. And Wang, C. H. (2008), “Collision dynamics of high-speed droplets upon layers of variable thickness”, *Experiments in Fluids*, **45(3)**, pp. 435-446

Perelaer, J., Smith, P. J., Mager, D., Soltman, D., Volkman, S. K., Subramanian, V., Korvink, J. G. and Schubert, U. S. (2010), “Printed electronics: the challenges involved in printing devices, interconnects, and contacts based on inorganic materials”, *Journal of Material Chemistry*, **20**, pp. 8446-8453

Pique, A. and Chrisey, B. (2002), "*Direct-Write Technologies for Rapid Prototyping Applications*", Published by Academic Press, San Diego, CA, ISBN 0121742318

Puffr, R. and Kubanek, V., *Lactam-based Polyamides: Polymerization, structure, and properties*, Volume 1, CRC Press, 1991, ISBN 0849349656

Raman, G. (1999), "Reduced Crosstalk Inkjet Printer Printhead", United State Patent No. 5,912,685

Rayleigh (1878), "On the Instability of Jets", *Proceedings of the London Mathematical Society*, **10(4)**, pp. 4-13

Rein, M. (1993), "Phenomena of liquid drop impact on solid and liquid surfaces", *Fluid Dynamics Research*, **12(2)**, pp. 61-93

Rein, M. (2002), "Drop-Surface Interactions", Published by Springer-Verlag, New York, NY, ISBN 3211836926

Reis, N., Ainsley, C. and Derby, B. (2005), "Inkjet delivery of particle suspensions by piezoelectric droplet ejectors", *Journal of Applied Physics*, **97**, p. 094903

Ritz, J., Fuchs, H., Kieczka, H. and Moran W. C. (2005), "Caprolactam" in "*Ullmann's Encyclopedia of Industrial Chemistry*", Published by Wiley-VCH Verlag GmbH & Co. KGaA, Weinheim, Germany, doi:10.1002/14356007.a05_031

Sachs, E., Cornie, J., Brancazio, D., Bredt, J., Curodeau, A., Fan, T., Khanuja, S., Lauder, A., Lee, J. and Michaels, S. (1993), "Three dimensional printing: the physics and implications of additive manufacturing", *CIRP Annals – Manufacturing Technology*, **42(1)**, pp. 257-260

Saunders, R., Gough, J. and Derby, B. (2008), "Delivery of human fibroblast cells by piezoelectric drop-on-demand inkjet printing", *Biomaterials*, **29**, pp.193-203

Schiaffino, S. and Sonin, A.A. (1997), "Formation and stability of liquid and molten beads on a solid surface", *Journal of Fluid Mechanics*, **343**, pp. 95-110

Schubert, S. B. and Werner, J. H. (2006), “Flexible solar cells for clothing”, *Materials Today*, **9(6)**, pp. 42-50

Sele, C. W., von Werne, T., Friend, R. H. and Sirringhaus, H. (2005), “Lithography-Free, Self-Aligned Inkjet Printing with Sub-Hundred-Nanometer Resolution”, *Advanced Materials*, **17(8)**, pp. 997-1001

Singh, M., Haverinen, H. M., Dhagat, P. and Jabbour G. E. (2010), “Inkjet Printing - Process and Its Applications”, *Advanced Materials*, **22**, pp. 673-685

Sirringhaus, H., Kawase, T., Friend, R. H., Shimoda, T., Inbasekaran, M., Wu, W. and Woo, E. P. (2000), “High-Resolution Inkjet Printing of All-Polymer Transistor Circuits”, *Science*, **290**, pp. 2123-2126

Sirringhaus, H. and Shimoda, T. (2003), “Inkjet Printing of Functional Materials”, *MRS Bulletin*, **28(11)**, pp. 802-803

Soltman, D. and Subramanian, V. (2008), “Inkjet-printed line morphologies and temperature control of the coffee ring effect”, *Langmuir*, **24(5)**, pp. 2224-2231

Stringer, J. and Derby, B. (2010), “Formation and Stability of Lines Produced by Inkjet Printing”, *Langmuir*, **26(12)**, pp. 10365-10372

Tay, B. Y., Evans, J. R. G. and Edirisinghe, M. J. (2003), “Solid freeform fabrication of ceramics”, *International Materials Reviews*, **48(6)**, pp. 341-370

Tomeckova, V. and Halloran, J. W. (2010), “Critical energy for photopolymerization of ceramic suspensions in acrylate monomers”, *Journal of the European Ceramic Society*, **30**, pp. 3273-3282

Udipi, K., Dave, R. S. and Kruse, R., L. and Stebbins, L. R. (1997), “Polyamides from lactams via anionic ring-opening polymerization: 1. Chemistry and some recent findings”, *Polymer*, **38(4)**, pp. 927-938

Uhlmann, E. and Elsner, P. C. (2005), "New printing technology for fully graduated material properties", *Proceeding of 16th Solid Freeform Fabrication Symposium (SFF2005)*, Austin TX, August 1st – 3rd 2005, pp. 13-18

van Rijswijk, K., Bersee, H. E. N., Jager, W. F. and Picken, S. J. (2006), "Composites Optimisation of anionic polyamide-6 for vacuum infusion of thermoplastic composites: choice of activator and initiator", *Composites Part A: Applied Science and Manufacturing*, **37(6)**, pp 949-956

Verkouteren, R. M. and Verkouteren, J. R. (2009), "Inkjet metrology: high-accuracy mass measurements of microdroplets produced by a drop-on-demand dispenser", *Analytical Chemistry*, **81(20)**, pp. 8577-8584

Waldvogel, J. M. and Poulikakos, D. (1997), "Solidification phenomena in picoliter size solder droplet deposition on a composite substrate", *International Journal of Heat and Mass Transfer*, **40**, pp. 295-309

Wang, T., Hall, D. and Derby, B. (2004), "Inkjet Printing of Wax-based PZT Suspensions", *Key Engineering Materials*, **264**/**268**, pp. 697-700

Wallace, D. B. and Hayes, D. J. (1998), "Solder Jet Technology Update", *The International Journal of Microcircuits and Electronic Packaging*, **21**, pp. 1-4

Wijshoff, H. (2008) "Structure- and Fluid-Dynamics in Piezo Inkjet Printheads", PhD Thesis, University of Twente, the Netherlands

Wikipedia (2010), "Halftone", retrieved from: http://en.wikipedia.org/wiki/Halftone

Wohlers, T. (2007), "*Wohlers Report 2007*", Wohlers Associates Inc., Colorado, US, ISBN 0975442937

Xaar plc, (2008), "Xaar 126 product datasheet", Retrieved from http://www.xaar.com/uploads/xaar126datasheet_final.pdf

Xiang-hui, Z., Le-hua, Q., Hua, H., Xiao-shan, J. and Yuan, X. (2010), “Experimental Research of Pneumatic Drop-on-Demand High Temperature Droplet Deposition for Rapid Prototyping”, *Key Engineering Materials*, **419-420**, pp 405-408

Xu, D., Sanchez-Romaguera, V., Barbosa, S., Travis, W., de Wit, J., Swan, P. and Yeates, S. G. (2007), “Inkjet printing of polymer solutions and the role of chain entanglement”, *Journal of Materials Chemistry*, **17**, pp. 4902-4907

Yarin, A. L. (2006), “Drop Impact Dynamics: Splashing, Spreading, Receding, Bouncing”, *Annual Review of Fluid Mechanics*, **38**, pp. 159-192